PULSAR OBSERVATIONS AT MOLONGLO.

by

Alan E. Vaughan B.Sc.(Hons).

A Thesis submitted for the Degree
of Doctor of Philosophy at the
University of Sydney.

May, 1974.

Summary of Thesis.

The Molonglo radio telescope played an important role in the early days of pulsar astronomy, being used to discover over 30 pulsars. This thesis describes nearly all facets of pulsar work at the observatory with which the author was involved.

The first chapter is a brief review of pulsar astronomy highlighting important features of pulsars and the present understanding of their nature.

Many different types of pulsar observations were carried out at Molonglo and these are discussed in Chapter 2.

Specific details of the pulsar searches made using the telescope are given in Chapter 3, attention being focussed on the search sensitivities and their degree of completeness.

A new method of determining pulsar declinations was designed and developed by the author and used to measure precise declinations for many southern (and a few northern) pulsars. The technique is described in Chapter 4, giving details of the equipment and computing methods used. The declination measurements are listed and discussed in Chapter 5.

Chapter 6 gives the results of period measurements of pulsars which also arise from the technique described in Chapter 4. Also the results of some pulsar flux density measurements from the same technique are given.

In Chapter 7 the question of pulsar-supernova associations is raised, particularly the association suggested by some position measurements made by the author on a pulsar near a supernova remnant.

In a similar way Chapter 8 reviews the present situation regarding the association of pulsars with optical objects, especially the search for optical pulsations associated with radio pulsars. As a preliminary step the optical fields of some southern pulsars, whose declinations have been measured precisely, are illustrated.

The final chapter of the thesis contains an analysis of pulsar distributions in luminosity, period and height above the galactic plane. Implications are drawn from the results of this analysis which are relevant both to theoretical consideration of pulsars and to future pulsar surveys.

Preface.

This thesis is based on work carried out in the Astrophysics Department of the School of Physics in the University of Sydney. The thesis covers much of the pulsar work carried out by the School, since the author has been involved in almost every aspect of this work from its inception in early 1968.

A large proportion of the work was done in conjunction with other people as follows:

a) during 1968, early pulsar searches were carried out by Dr. A. J. Turtle and the author (leading to the discovery of two pulsars).

b) during the same period the author was engaged in the design and construction of the East-West Multibeaming unit under the supervision of Dr. M. I. Large.

c) later pulsar searches (Oct. 1968 - early 1970) were carried out together with and under the direction of Dr. Large (and occasionally Dr. R. Wielebinski) (27 pulsars).

From that time the author was engaged in research of his own choosing and design aimed at making accurate and precise measurements of the positions, periods and flux densities of pulsars. As a result of this, some collaborative work was undertaken with Dr. M. J. Disney of Mt. Stromlo Observatory on the optical fields of some Southern pulsars. Data obtained from the measurements was combined with the results of the pulsar searches to continue the analysis of pulsar distribution functions in luminosity, period and z-distance begun by Dr. Large, taking into account any correlations which might

exist within the data.

The thesis reviews some important aspects of pulsar astronomy in Chapter 1, while the specific work carried out at the Molonglo Radio telescope is detailed in Chapter 2. The pulsar searches carried out at Molonglo are discussed in Chapter 3. Chapters 4, 5 and 6 describe the techniques and the results of the precise measurements of position, period and flux density for pulsars. Chapter 7 reviews some suggested pulsar-supernova remnant associations with particular reference to a proposed association arising from the position measurements at Molonglo. Optical observations of the fields of radio pulsars are discussed in Chapter 8, with particular mention of the field of the Vela pulsar, studied by the author in collaboration with Dr. W. B. McAdam. The analysis of pulsar distribution functions is contained in Chapter 9 together with some discussion of the implications of the results.

Acknowledgements.

I wish to thank Prof. H. Messel for the use of the facilities of the School of Physics of the University of Sydney and its field station at the Molonglo Radio Observatory. I acknowledge the support provided by grants from the Australian Research Grants Committee, the Sydney University Research Grants Committee and the Science Foundation for Physics within the University of Sydney.

I further acknowledge personal financial support received from a Commonwealth Postgraduate Research Studentship for four

years, and from Teaching Fellowships granted by the University of Sydney for the past three years.

I have enjoyed the support of many members of the staff of the Astrophysics Department, including Mr. A. Little, Dr. W. B. McAdam and Dr. A. J. Turtle who were always ready to discuss matters related to my work. I particularly wish to thank Dr. D. F. Crawford for his assistance in matters to do with computing.

It has also been my pleasure to have worked under Professor B. Y. Mills as Head of the Department, and I have appreciated the assistance he has given me over the years.

I have been privileged to have Dr. M. I. Large as my supervisor for the past six years and I owe much to him for his guidance and encouragement as the work continued. Under his direction pulsar work at Molonglo won wide acclaim and it is to him that a large measure of its success is due.

I wish also to acknowledge the support of my family during my period of study, particularly thanking my mother for typing this thesis, my sister for help with the diagrams, and my wife, Elaine, not only for assistance in proof-reading, but also for her unfailing encouragement and help during the past three years.

I humbly acknowledge the providence of Almighty God in guiding my hand and lighting my path, through the knowledge of His Son and the power of His Spirit.

[redacted]

May, 1974.

List of Published Papers.

1. Turtle, A. J., and Vaughan, A. E., "Discovery of two Southern Pulsars", Nature, 219, 689 (1968).

2. Turtle, A. J., and Vaughan, A. E., "Positions of Four Pulsars", Nature, 219, 845 (1968).

3. Large, M. I., and Vaughan, A. E., "Dispersion and Pulse Length of Pulsating Radio Source PSR1749-28". Nature, 220, 43 (1968).

4. Large, M. I., Vaughan, A. E., and Mills, B. Y., "A Pulsar Supernova Association?" Nature, 220, 340 (1968).

5. Large, M. I., Vaughan, A. E., and Wielebinski, R., "Pulsar Search at Molonglo Radio Observatory", Nature, 220, 753 (1968).

6. Wielebinski, R., Vaughan, A. E., and Large, M. I., "Clustering of Pulsars along the Galactic Plane", Nature, 221, 47 (1969).

7. Vaughan, A. E., and Large, M. I., "Pulsar Observations at Molonglo", Proc. Astron. Soc. Austral., 1, No. 5, 220 (1969).

8. Large, M. I., Vaughan, A. E., and Wielebinski, R., "Some Further Pulsar Observations at the Molonglo Radio Observatory", Astrophys. Lett., 3, 123 (1969).

9. Vaughan, A. E., Large, M. I., and Wielebinski, R., "Three New Pulsars", Nature, 222, 963 (1969).

10. Large, M. I., Vaughan, A. E., and Wielebinski, R., "Highly Dispersed Pulsar & Three Others", Nature, 223, 1249 (1969).

11. Vaughan, A. E., and Large, M. I., "Five New Pulsars". Nature, 225, 167 (1970).

12. Large, M. I. and Vaughan, A. E., "A Search of the Galactic Plane for High Dispersion Pulsars", Mon. Not. R. astr. Soc., 151, 277 (1971).

13. Vaughan, A. E., and Large, M. I., "Improved Data for Eight Molonglo Pulsars", Mon. Not. R. astr. Soc., 156, 25P (1972).

14. Vaughan, A. E., and Large, M. I., "Discovery of Three Pulsars", Mon. Not. R. astr. Soc., 156, 27P (1972).

15. Large, M. I., and Vaughan, A. E., "A New Pulsar-Supernova Association", Nature Phys. Sci., 236, 117 (1972).

16. Vaughan, A. E., and McAdam, W. B., "Position of PSR0833-45". Nature Phys. Sci., 241, 138 (1973).

17. Vaughan, A. E., Disney, M. J., and Nicholson, P., "Accurate Positions and Optical Studies in Nine Southern Pulsar Fields", Mon. Not. R. astr. Soc., (in the press) (1974).

Table of Contents.

Chapter 1

PULSAR ASTRONOMY.

1.1 Introduction.

All branches of science progress by a series of steps as important breakthroughs or discoveries are made, each step being followed by a period of time during which the discovery is investigated, extended and either understood, or at least modelled, for ease of description. A phenomenon of our times is the increasing frequency of the steps and the subsequent flurry of activity as new techniques and ideas are tested, a new field of specialization being founded in the process.

Astronomy is no exception to this. For a long time, "astronomy" implied optical astronomy, then radio astronomy arrived, followed by infra-red, x-ray and γ-ray astronomy. Within radio astronomy the highlights so far have been the detection of galactic emission, radio sources, quasars and pulsars.

It is the last of these which form the basis of this thesis. This chapter aims at providing a brief outline of the main characteristics of pulsars and an indication of current speculation as to their nature.

1.2 Initial Discovery.

In the course of an investigation of interplanetary scintillation of radio sources being carried out by researchers at the Mullard Radio Astronomy Observatory in Britain, signals similar to interference but of non-terrestrial origin were detected[1]. Absence of any parallax ruled out space probes as the sources of the signals and it was soon clear that the signals were of natural origin. They had remained undetected until this time because most radio astronomers had used long

post-detector time constants in their receivers to increase the signal to noise ratio for continuous radio sources, effectively integrating out any pulsed signals.

The features of pulsars which were immediately obvious were the stable pulsar period, the variability of the pulse amplitudes, and the frequency dispersion of the pulses due to passage through the ionized interstellar medium.

1.3 Further Discoveries.

After the initial discoveries were announced[1,2] there was little progress for about six months as various observatories around the world commenced pulsar searches. During this period there was much theoretical speculation, but since it was based on little data no detailed discussion was possible. It was at this time that a model was suggested which, in general terms, still stands as that which best fits the data. That is, that a pulsar is a rotating neutron star[3].

At this point new pulsars began to be announced at the rate of about five per month until over thirty had been discovered, [4-22] the majority of them at Molonglo. In particular, the Molonglo discoveries clearly indicated that pulsars were galactic objects since they were clustered along the galactic plane. During this period also the rotating neutron star model came to be widely accepted and attempts began to refine the model to account for the details of the observed emission from the pulsars. This was given further impetus by the discovery of the optical pulsar in the Crab Nebula[23].

Since then pulsars have been discovered at irregular intervals until the present when the total stands at about

115[24-39]. The distribution of discoveries among various observatories is given in Table 1.1, and illustrated in Figure 1.1 is the discovery rate.

Table 1.1

Observatory	Number discovered
Jodrell Bank	40
Molonglo	31
Arecibo	15
Parkes	9
Greenbank	7
Cambridge	6
Bologna	5
Puschino	1
Ooty	1

The searches at Molonglo (see Ch. 3), Cambridge[2] and Bologna[40] were carried out by searching for individual pulses on analogue records, while most of the others used pulse integration techniques. As a result most of the pulsars initially found were discovered at the above observatories, since pulse integration techniques were not very successful on erratic pulsars, while analogue records were sensitive to occasional large pulses. However, after most of the strong pulsars had been found, pulse integration searches using on-line computers became more important as sensitivity limits were extended, particularly when some searches were carried out at frequencies higher than 408MHz, where pulsars tend to be less erratic.

Figure 1.1 A diagram illustrating the rates at which pulsars were discovered over the period 1968 to 1974. Most of the early discoveries were from analogue chart records. Recent increases have come from searches using on-line computers and pulse integration techniques.

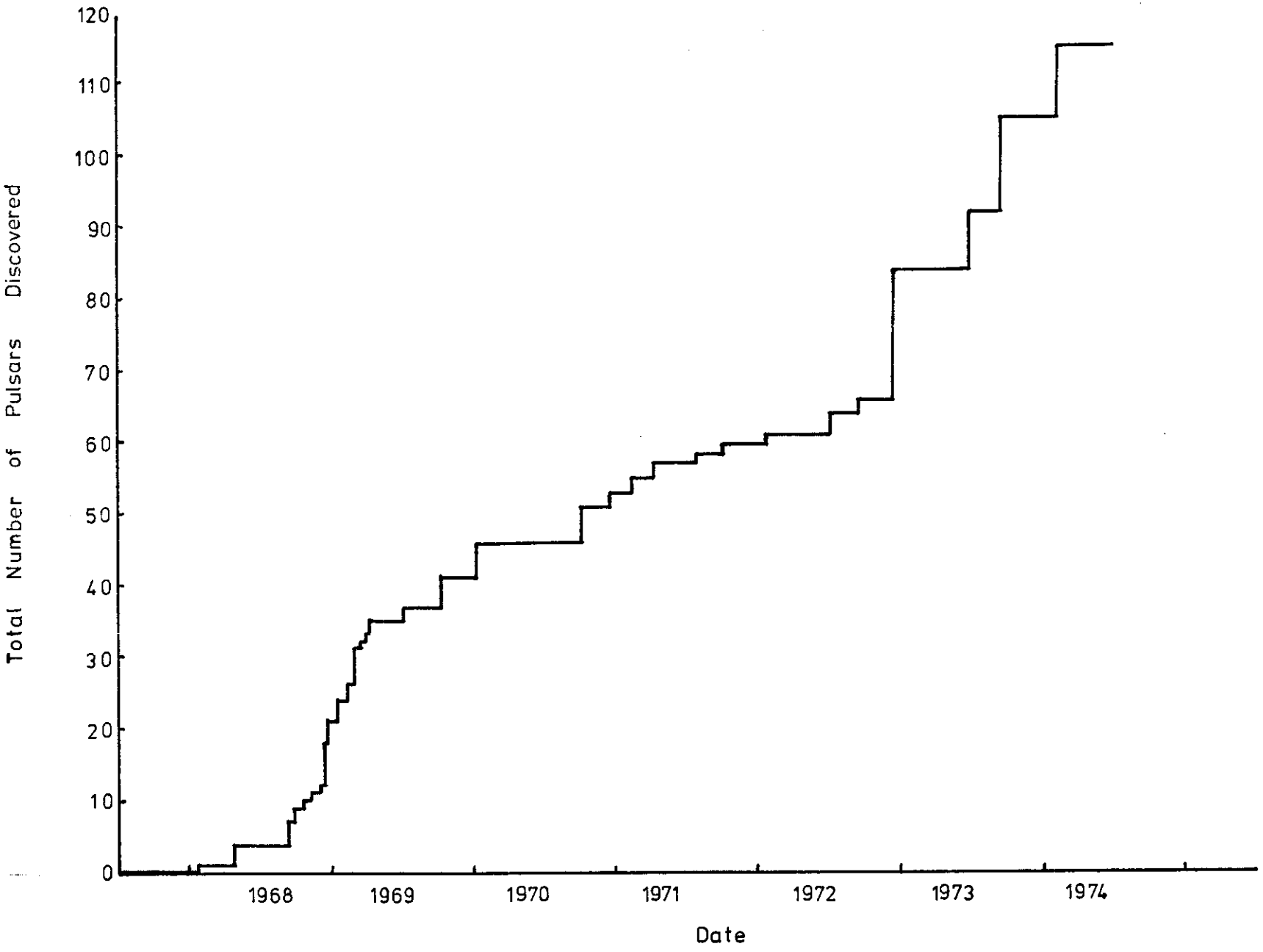
Total Number of Pulsars Discovered
120
110
100
90
80
70
60
50
40
30
20
10
0
1968
1969
1970
1971
1972
1973
1974
Date

1.4 Observed Properties of Pulsars.

The observed properties of pulsars can be divided into two classes:

a) those arising at the pulsar itself, revealing something of the nature of the pulsar eg. periodicities, pulse widths and shapes, polarization and spectra,

b) those caused by the passage of the pulses through the ionised interstellar medium. These properties carry information about the matter lying between the observer and the pulsar. Examples are dispersion measure, rotation measure and scintillation.

1.4.1 Periodicities.

Several different periodic phenomena have been observed in pulsar signals. The principal period, P_1, is that property which sets pulsars apart from other known radio sources[1]. P_1 ranges from ~0.033 seconds to ~3.7 seconds and is illustrated in the records shown in Figure 3.4. Most pulsars show a secular increase in P_1 of about $10^{-15} \times P_1$ sec per sec[41], though for the two pulsars with low values of P_1 (Crab pulsar and Vela pulsar) the increase is about $10^{-13} \times P_1$ sec per sec[41]. For these two pulsars discontinuous changes in P_1 have also been observed[42,43,44], these "glitches" possibly arising from mechanical alterations of the pulsar surface.

Four other periodicities have been observed for some pulsars as follows:

P_2 -- the separation of drifting subpulses[45].

Generally $P_2 \quad w_p$

P_3 -- the time taken for the sub-pulse phase to drift by P_2

relative to the phase of P_1. P_3 lies in the range 2 to 20 sec[46] and may correspond to short term pulse amplitude variations as pulses of similar structure recur. However P_3 is not as stable as this phenomenon[47,48] so the question is still open.

P_4 -- this can be expressed as a function of P_1, P_2 and P_3 and is the time taken for the sub-pulse phase to drift by P_1 relative to the phase of P_1. It may explain longer term variation of pulse intensity ($\sim$2 to 6 minutes)[47] but its relevance is not certain[48].

P_5 -- the time over which the drift rate of the sub-pulses with respect to the phase of P_1 varies[49]. This is possibly related to various sub-pulse modes which have been observed[50].

The interest in these periodicities derives from the belief that they may be fundamentally related to the emission mechanisms of pulsars.

1.4.2 Pulse Shapes.

For a given pulsar, the integrated pulse profile is constant[51], except in a few cases[52], and can be thought of as a pulsar signature. In fact it has been suggested[53,54] that the integrated profile may be used to classify pulsars.

The integrated pulse profile is open to several interpretations[55]. It may represent the probability distribution function for the occurrence of individual pulses at given longitudes within the pulse window, individual pulses being in general simple gaussian shaped. For pulsars with

drifting sub-pulses the integrated profile may represent the relative strengths of the sub-pulses as they occur at different positions within the pulse window.

The integrated profile generally occupies less than 20° of pulsar longitude ($360^{\circ} = P_1$), and is only weakly dependent on radio frequency, variations $\propto \nu^{-0.25}$ having been reported[56]. This has suggested to some that the radiation is due to relativistic beaming of electrons rather than something analogous to a simple aerial[57] ($\propto \nu^{-1}$).

Observed integrated pulse profiles can be classified as follows:[55]

-- single pulse (+ precursor pulses, interpulses, outriders)

-- double pulse

-- triple and more complex

1.4.3 Pulse Height Variations.

Pulsars are known to vary in intensity on timescales ranging from less than a millisecond[58] (still unresolved down to 10 microseconds[60]) up to several months[59]. Those variations attributable to the pulsar itself are as follows:

a) Microstructure[58]

This is a wideband phenomenon, though there is sharp structure in its spectrum[60]. It requires precise de-dispersing of the signal for it to be observed and is accompanied by fast changes of polarization, suggesting its origin at the pulsar.

b) Periodic Phenomenon with $\tau \sim 2$ - 10 pulsar periods.

For some pulsars this is explicable in terms of drifting sub-pulses[45] though this is not clear in all cases.

c) Pulse Nulling -- Type II[61]

Similar to the above except that P_2 is longer than the integrated pulse profile so that several pulses are absent every 10 pulses or so. A broadband phenomenon.

d) Pulse Nulling -- Type I[61] ($\tau \sim 1$ - 10 minutes).

Led to the introduction of P_4[47] and is semi-periodic. That it is not due to the medium has not yet been clearly established.

e) Very Long Term Variations[62,63] ($\tau \sim$ several months)

These variations are correlated over a large frequency range and in some cases are as large as several orders of magnitude.

f) Large Pulses from the Crab Pulsar

It has been observed that about 1 in 10^4 pulses from the Crab pulsar is about 1000 times stronger than the average pulse[64,65].

1.4.4 Polarization.

Polarization studies are likely to give valuable information about the emission mechanisms of pulsars. Comprehensive studies have been made[66] and the results are complex. Early studies showed that the linear polarization angle is variable through the pulse on a short timescale[67], being continuous[68] and repeatable from pulse to pulse, with occasional 90° changes of position angle at a given longitude in the pulse[69]. Circular polarization has also been observed[58] often at a high level[70], though with a variable handiness, to that the integrated value is low[71]. It has been found that polarization features are attached to the

sub-pulses where they drift--suggesting that they may represent the basic emission[69]. Polarization features have been observed throughout the radio spectrum, at microwave frequencies[72], and in the optical region[73] for the Crab pulsar, such studies showing that, after correction for Faraday rotation in the interstellar medium and the ionosphere, the features are correlated over the whole spectrum[74]. This may[75] give information about the position of the magnetic pole of the pulsar and the disposition of fields around the pulsar.

1.4.5 Spectra.

1.4.5.1 Mean Spectra.

Because of the long timescales on which pulsars are known to vary, it is difficult to specify a mean flux density at one particular frequency, let alone specify a spectrum over a wide range of frequencies. Spectra that have been obtained, however, show a peak in the emission at about 100-500MHz with a sharp low frequency cut-off and a steep power law spectrum, $\overline{S} \propto \nu^{\alpha}$, α varying from -1 to -4, above these frequencies.[76,77] At higher frequencies some different emission mechanism evidently becomes important since for the Crab pulsar the infra-red, optical and x-ray spectra are related[78,79,80,81] while differing from the radio spectrum.

1.4.5.2 Dynamic Spectra.

Early observations[82] showed that pulsars had fine structure in their spectra and it was found[83] that this was related to amplitude variations, due to scintillation by the interstellar medium, which had timescales considerably longer

than the pulsar period. By defining, and measuring, characteristic bandwidths which reduced the fluctuation index of pulsars by 50% compared to a narrow bandwidth receiver, it was found that the characteristic bandwidth varied as $(dm)^{-2}$, leading to the conclusion that the scintillation was caused by scattering along the whole path from the pulsar, rather than at localized points along the path. The dynamic nature of the spectral features is seen in that they persist only for times of the order of 10 - 100 minutes, the timescale for the features increasing with observing frequency. At 408MHz the features are typically 0.1 - 20MHz wide.

1.4.6 Dispersion Measure.

The delay at lower frequencies compared to the pulse arrival times at high frequencies was noticed as soon as pulsars were discovered[1]. An expression and explanation for the effect is given in Appendix 6B. Because of finite receiver bandwidths used in pulsar searches, it was found that many searches suffered a loss in sensitivity due to dispersion broadening[86]. This is described in Appendix 3A.

1.4.7 Scintillation Broadening.

When some very highly dispersed pulsars were discovered [31,36,37] it was found that pulses which travel through a large amount of interstellar medium are broadened by interstellar scattering (scintillation). The broadening occurs because of different travel times for different ray paths at the same frequency through the scattering medium. It has been shown[87] that the exact

shape of the function convolving with the original pulse will depend on the geometrical conditions of the scattering (ie, thin screen, or extended medium). Examples of both these cases have been found[88,89].

1.5 Pulsar Positions.

Pulsar positions have been measured by two fundamentally different methods. As with other radio sources, interferometric measurements[1,90,91] have been made giving positions to about ± 3 arc sec. Among these are the results given in Chapter 5 of this thesis. The alternate method is the measurement of the ecliptic coordinates of a pulsar by recording the phase and amplitude of the annual variation of pulse arrival times as the earth moves around the sun[92]. The phase of the variation gives the ecliptic longitude of the pulsar while its amplitude gives the ecliptic latitude. Positions obtained by this method[93,94] are at least an order of magnitude more precise than the interferometric positions. However both methods give results consistent with each other, except for PSR0833-45, where there is some discrepancy. See Chapter 8 for a discussion of this.

1.6 Associations With Other Objects.

A fuller discussion of this is given in Chapter 7. The situation at the moment is that there is one certain association, the Crab pulsar with the Crab Nebula, and several other possible associations. This question is of interest for models describing the possible history of pulsars.

1.7 A Summary of Theoretical Models for Pulsars.

This section will only follow the main lines of thought concerning the nature of pulsars. Many other subsidiary ideas have been discussed, but have lapsed as the body of data increased.

It was clear at the outset[1] that pulsars must be very dense objects. The lack of optical identifications ruled out white dwarfs[95] and this was confirmed when the Vela and Crab pulsars were found, their periods being too short to be due to vibrations of a white dwarf star model. The idea of a rotating neutron star[3] soon came to be widely accepted as the basic starting point for describing a pulsar. It was shown[96] that a rotating neutron should possess a dense co-rotating magnetosphere, the outer layers of which would be moving at velocities near the speed of light.

The question of how pulses were emitted, led to several different models at this point.

One view[97] was that the emission came from electrons spiralling along curved field lines at the velocity of light cylinder. Observed polarization characteristics provide some problems for this model, particularly the occasional fast position angle changes[69].

Further observations led to the suggestion[68] that an oblique rotator model may be more successful, with the characteristics of the radiation being governed by the geometric configuration of the rotation and magnetic axes and the line of sight. This model was developed further[98,75] with the actual emission mechanism[99,100] arising from γ-rays

annihilating to form e^--- e^+ pairs giving a two stream instability leading to charge bunching and coherent radio emission.

A third important emission mechanism suggested is that of relativistic beaming from a bunch of charged particles within or near the velocity of light cylinder[101,55,102]. While this model accounts for the frequency independent pulse widths that are observed and gives reasonable results for the polarization characteristics, it suffers from the problem of how to contain dense bunches of energetic electrons for long periods of time (as suggested by pulsar sub-pulse structure memory).

In short it can be said that no model satisfactorily explains all the observed properties of pulsars and further observations and calculations are obviously required.

1.8 References.

1. Hewish, A., Bell, S. J., Pilkington, J. D. H., Scott, P. F., and Collins, R. A., Nature, 217, 709 (1968).

2. Pilkington, J. D. H., Hewish, A., Bell, S. J., and Cole, T. W., Nature, 218, 126 (1968).

3. Gold, T., Nature, 218, 731 (1968).

4. Cole, T. W., and Pilkington, J. D. H., Nature, 219, 574 (1968).

5. Huguenin, G. R., Taylor, J. H., Goad, L. E., Hartai, A., Orsten, G. S. F., and Rodman, A. K., Nature, 219, 576 (1968).

6. Turtle, A. J., and Vaughan, A. E., Nature, 219, 689 (1968).

7. Craft, Jr., H. D., Sutton, J. M., Comella, J. M., and Lovelace, R. V. E., Nature, 219, 1237 (1968).

8. Craft, Jr., H. D., Lovelace, R. V. E., and Sutton, J. M., I. A. U. Circ. No. 2100 (1968).

9. Large, M. I., Vaughan, A. E., and Mills, B. Y., Nature, 220, 340 (1968).

10. Davies, J. G., I. A. U. Circ. No. 2107 (1968).

11. Staelin, D. H., and Reifenstein, 111, E. C., I. A. U. Circ. No. 2110 (1968).

12. Large, M. I., Vaughan, A. E., and Wielebinski, R., Nature, 220, 753 (1968).

13. Taylor, J. H., and Huguenin, G. R., I. A. U. Circ. No. 2120 (1968).

14. Alekseev, Yu. I., Vitkevitch, V. V., Zhuraviev, V. F., and Shitov, Yu., I. A. U. Circ. No. 2123 (1968).

15. Huguenin, G. R., and Taylor, J. H., I. A. U. Circ. No. 2128 (1969).

16. Wielebinski, R., Vaughan, A. E., and Large, M. I., Nature, 221, 47 (1969).

17. Taylor, J. H., and Huguenin, G. R., Nature, 221, 816 (1969).

18. Huguenin, G. R., and Taylor, J. H., I. A. U. Circ. No. 2135 (1969).

19. Lang, K. R., and Bosque, B., I. A. U. Circ. No. 2137 (1969).

20. Vaughan, A. E., and Large, M. I., Proc. Astron. Soc. Austral., 1, 220 (1969).

21. Large, M. I., Vaughan, A. E., and Wielebinski, R., Astrophys. Lett., 3, 123 (1969).

22. Lovelace, R. V. E., and Sutton, J. M., I. A. U. Circ. No. 2135 (1969).

23. Cocke, W. J., Disney, M. J., and Taylor, D. J., Nature, 221, 525 (1969).

24. Vaughan, A. E., Large, M. I., and Wielebinski, R., Nature, 222, 963 (1969).

25. Large, M. I., Vaughan, A. E., and Wielebinski, R., Nature, 223, 1249 (1969).

26. Vaughan, A. E., and Large, M. I., Nature, 225, 167 (1970).

27. Vaughan, A. E., and Large, M. I., Mon. Not. R. astr. Soc., 156, 27P (1972).

28. Davies, J. G., Lyne, A. G., and Sieradakis, J. H., Nature, 240, 229 (1972).

29. Davies, J. G., Lyne, A. G., and Sieradakis, J. H., Nature Physical Science, 244, 84 (1973).

30. Davies, J. G., and Large, M. I., Mon. Not. R. astr. Soc., 149, 301 (1970).

31. Davies, J. G., Large, M. I., and Pickwick, A. C., Nature, 227, 1123 (1970).

32. Laboratorio Nazionale di Radioastronomia, Bologna, I.A.U.Circ. No. 2287 (1971)

33. Salter, C. J., I. A. U. Circ. No. 2295 (1971).

34. Colla, G., Salter, C., and Sutton, J., I. A. U. Circ. No. 2374 (1971).

35. Sutton, J., Salter, C., Colla, G., I. A. U. Circ. No. 2386 (1972).

36. Komesaroff, M. M., Hamilton, P. A., McCulloch, P. M., Ables, J. G., Cooke, D. J., I. A. U. Circ. No. 2505 (1973).

37. Komesaroff, M. M., Hamilton, P. A., McCulloch, P. M., Ables, J. G., Cooke, D. J., I. A. U. Circ. No. 2563 (1973).

38. Swarup, G., Mohanty, D. K., Balasubramanian, V., I. A. U. Circ. No. 2356 (1971).

39. Taylor, J. H., Private Communication (1974).

40. Bonsignori-Facondi, S. R., Salter, C. J., and Sutton, J. M., Astron. and Astrophys., 27, 67 (1973).

41. Hunt, G. C., Mon. Not. R. astr. Soc., 153, 119 (1971).

42. Radhakrishnan, V., and Manchester, R. N., Nature, 222, 228 (1969).

43. Reichley, P. E., and Downs, G. S., Nature, 222, 229 (1969).

44. Boynton, P. E., Groth, 111, E. J., Partridge, R. B., and Wilkinson, D. T., I. A. U. Circ. No. 2179 (1969).

45. Drake, F. D., and Craft, Jr. H. D., Nature, 220, 231 (1968).

46. Sutton, J. M., Staelin, D. H., Price, R. M., and Weimer, R., Ap. J. Letters, 159, L89 (1970).

47. Staelin, D. H., Ewing, M. S., Price, R. M., and Sutton, J. M., Ap. J. Letters, 160, L7 (1970).

48. Slee, O. B., and Mulhall, P. S., Astrophys. Lett., 8, 5 (1971).

49. Cole, T. W., Nature, 227, 788 (1970).

50. Huguenin, G. R., Taylor, J. H., and Troland, T. H., Ap. J., 162, 727 (1970).

51. Lyne, A. G., and Rickett, B. J., Nature, 219, 1339 (1968).

52. Lyne, A. G., Mon. Not. R. astr. Soc., 153, 27P (1971).

53. Taylor, J. H., and Huguenin, G. R., Ap. J., 167, 273 (1971).

54. Huguenin, G. R., Manchester, R. N., and Taylor, J. H., Ap. J., 169, 97 (1971).

55. Lyne, A. G., Smith, F. G., and Graham, D. A., Mon. Not. R. astr. Soc., 153, 337 (1971).

56. Craft, Jr., H. D., and Comella, J. M., Nature, 220, 676 (1968).

57. Smith, F. G., Nature, 223, 934 (1969).

58. Craft, Jr. H. D., Comella, J. M., and Drake, F. D., Nature, 218, 1122 (1968).

59. Cole, T. W., Hesse, H. K., and Page, C. G., Nature, 225, 712 (1970).

60. Hankin, T. H., Ap. J., 169, 487 (1971).

61. Backer, D. C., Nature, 228, 42 (1970).

62. Hesse, K. H., Nature, 231, 54 (1971).

63. Hesse, K. H., Nature, 235, 27 (1972).

64. Graham, D. A., Lyne, A. G., and Smith, F. G., Nature, 225, 526 (1970).

65. Heiles, C., Campbell, D. B., and Rankin, J. M., Nature, 226, 529 (1970).

66. Manchester, R. N., Ap. J. Supp. No. 199., 23,283 (1971).

67. Lyne, A. G., and Smith, F. G., Nature, 218, 124 (1968).

68. Radhakrishnan, V., Cooke, D. J., Komesaroff, M. M., and Morris, D., Nature, 221, 443 (1969).

69. Manchester, R. N., Paper given at Stanford Pulsar Conference, January 1974.

70. Ekers, R. D., and Moffett, A. T., Ap. J. Letters, 158, L1 (1969).

71. Graham, D. A., Nature, 229, 326 (1971).

72. Gardner, F. F., and Whiteoak, J. B., Nature, 224, 893 (1969).

73. Cocke, W. J., Disney, M. J., and Gehrels, T., Nature, 223, 576 (1969).

74. Smith, F. G., Nature, 228, 913 (1970).

75. Radhakrishnan, V., and Cooke, D. J., Astrophys. Lett., 3, 225 (1969).

76. Smith, F. G., Rep. Prog. Phys., 35, 399 (1972).

77. Hewish, A., Ann. Rev. Astr. Astrophys., 8, 265 (1970).

78. Fishman, G. J., Harnden, F. R., Haymes, R. C., Ap. J. Letters, 156, L107 (1969).

79. Oke, J. B., Ap. J. Letters, 156, L49 (1969).

80. Neugebauer, G., Becklin, E. E., Kristian, J., Leighton, R.B., Snellen, G., Westphal, J. A., Ap. J. Letters, 156, L115 (1969).

81. Fritz, G., Henry, R. C., Meekins, J. F., Chubb, T. A., and Friedman, H., Science, 164, 709 (1969).

82. Komesaroff, M. M., McCulloch, P. M., Hamilton, P. A., and Cooke, D. J., Nature, 220, 358 (1968).

83. Saltpeter, E. E., Nature, 221, 31 (1969).

84. Rickett, B. J., Nature, 221, 158 (1969).

85. Rickett, B. J., Mon. Not. R. astr. Soc., 150, 67 (1970).

86. Large, M. I., and Vaughan, A. E., Mon. Not. R. astr. Soc., 151, 277 (1971).

87. Williamson, I. P., Mon. Not. R. astr. Soc., 157, 55 (1972).

88. Ables, J. G., Komesaroff, M. M., and Hamilton, P. A., Astrophys. Letters, 6, 147 (1970).

89. Counselman, C. C., and Rankin, J. M., Ap. J., 166, 513 (1971).

90. Turtle, A. J., and Vaughan, A. E., Nature, 219,845 (1968).

91. Huguenin, G. R., Taylor, J. H., Hjellming, R. M., and Wade, C. M., Nature, 234, 50 (1971).

92. Davies, J. G., Hunt, G. C., and Smith, F. G., Nature, 221, 27 (1969).

93. Reichley, P. E., Downs, G. S., and Morris, G. A., Ap. J. Letters, 159,L35 (1970).

94. Manchester, R. N., and Peters, W. L., Ap. J. Letters, 173, L221 (1972).

95. Bailey, J. A., and Mackay, C. D., Nature, 218, 129 (1968).

96. Goldreich, P., and Julian, W. H., Ap. J., 157, 869 (1969).

97. Gold, T., Nature, 221, 25 (1969).

98. Komesaroff, M. M., Nature, 225, 615 (1970).

99. Sturrock, P. A., Nature, 227, 465 (1970).

100. Sturrock, P. A., Ap. J., 164, 529 (1971).

101. Smith, F. G., Nature, 231, 191 (1971).

102. Smith, F. G., Nature, 232, 165 (1971).

Chapter 2

PULSAR OBSERVATIONS AT MOLONGLO.

2.1 Introduction.

This chapter describes the various types of pulsar observations carried out at Molonglo in which the author had some part. A detailed description of some specific measurements made by the author is given in Chapters 4, 5, 6.

2.2 The Telescope.

The Molonglo Radio Telescope[1] is a Cross-type instrument. Each arm of the cross is approximately 1.6Km long, the East-West arm being 12.8m wide and the North-South arm 11.6m wide. The East-West arm, consisting of two separate 0.8Km aerials, is mechanically steerable in declination from about $\delta = +19^{\circ}$ to the South Pole. The North-South arm is steered in declination by the introduction of phase gradients along the arms[2], so that it covers the same declination range as the East-West arm, though it can in fact be steered to $\delta = +30^{\circ}$ with considerable loss of efficiency. The telescope cannot be steered in hour angle as it is a transit instrument.

Over the period covered by this thesis, the telescope has operated at a basic frequency of 408MHz, with a maximum available bandwidth of 4MHz on the East-West arm and 2.5MHz on the North-South arm.

Table 2.1 gives the sensitivities and beam dimensions for various modes of operation of the telescope and the purpose for which each mode was used. A simplified block diagram of the system is given in Figure 2.1.

The North-South aerial has been phased to produce 11 beams separated in declination by 1.4 sec (z) arc min while the East-West aerial has been phased to produce 3 beams separated

Figure 2.1 Block diagram of the overall system at the Molonglo Radio Telescope, illustrating the various beams available. Since the pulsar searches began, further multipliers have been added, making it possible to form 33 pencil beams (11 early, 11 centre, 11 late) for observations on ordinary radio sources.

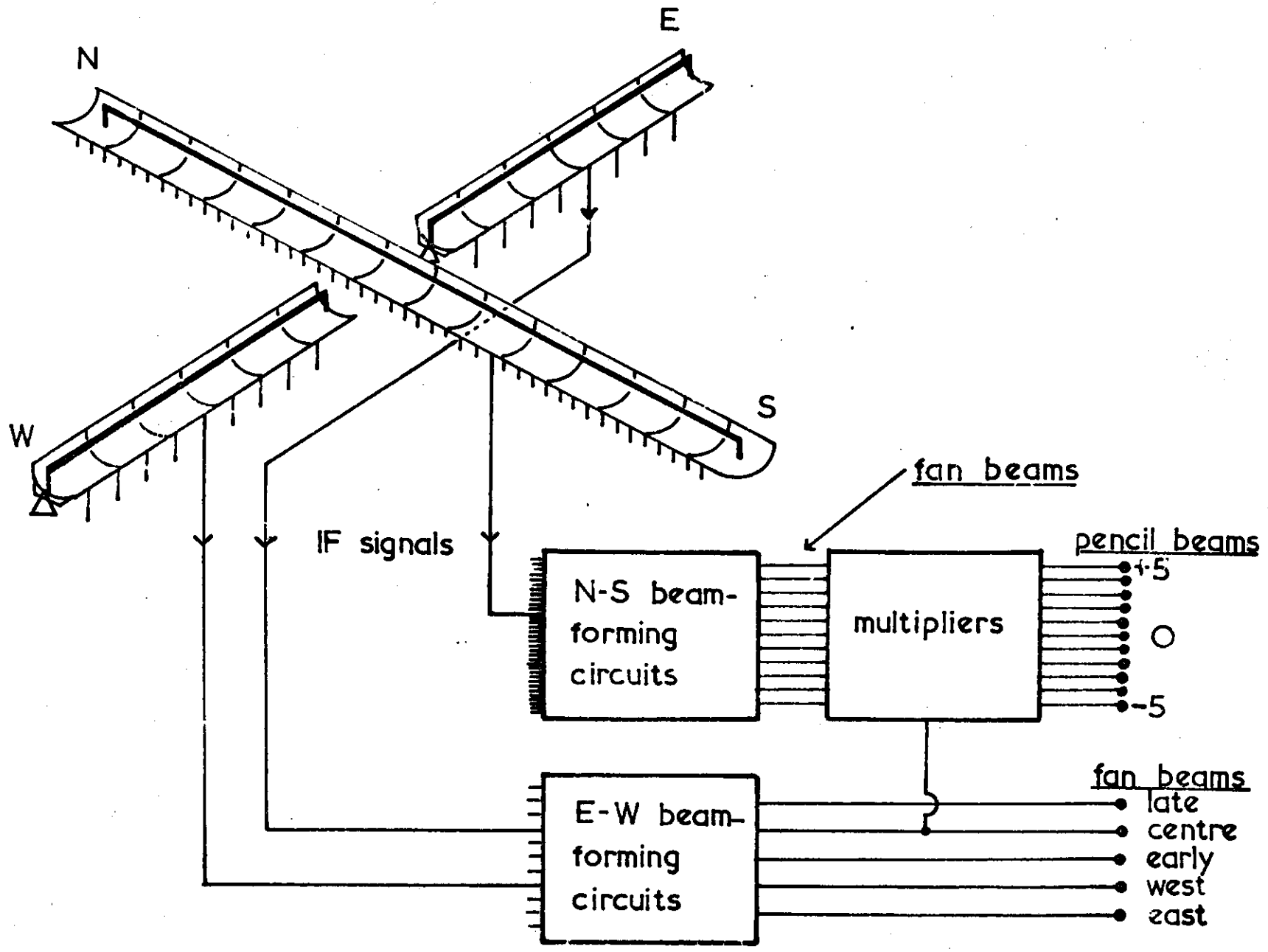
N
E
S
W
IF signals
fan beams
N-S beam-forming circuits
multipliers
pencil beams
+5
0
-5
E-W beam-forming circuits
fan beams
late
centre
early
west
east

Table 2.1

System	Relative Sensitivity	Beam Dimensions*	Purpose
E-W fan beams	1	4° N-S	Search; measurement
		1'.5 E-W	of P, α, dm.
E arm	0.5	4°N-S	Approx. measurement
W arm		3' E-W	of δ
N-S fan beams	0.2	1'.5 sec(z)N-S	Accurate measurement
		4° E-W	of δ, P
Cross Pencil		2'.8 sec(z)N-S	Accurate measurement
Beams	0.4	2'.8 E-W	of α, δ.

* z is zenith angle

by 1.4 arc min in hour angle. This means that the telescope can be operated with up to 11 simultaneous North-South total power beams, 3 simultaneous East-West total power beams, and 33 simultaneous cross pencil beams.

Calibration for the aerial gain is obtained by injecting the noise signal from a saturated diode into the centre module of the North-South, and East-West, arms.

2.3 Pulsar Searches at Molonglo.

2.3.1 Initial Aerial Configurations.

Several weeks after the discovery of pulsars was announced,[3] observations of pulsars were commenced at Molonglo, and search programmes were initiated. Construction of the East-West Multibeaming system was only just being started,

so only one beam from the full East-West arm was available, while the North-South arm, being much less sensitive, was less suitable for pulsar work at the time.

The following factors were considered in deciding how to use the East-West arm for pulsar searching:

a) the high sensitivity of the full East-West arm and the low flux density of the known pulsars,

b) the narrow beamwidth of the full East-West arm and the erratic nature of the known pulsars,

c) the difficulty in discriminating between interference and variable amplitude pulses from a pulsar.

The options available for pulsar searching are given in Table 2.2, together with inherent advantages and disadvantages of each system. The multibeamed system is included for completeness, though it was not initially available.

The failure of the system using the summation after detection of signals from N small sections of the aerial can be attributed to the loss in sensitivity, since N was sometimes equal to 5 but more often equal to 11. In the latter case the sensitivity to single pulses was about 5.2db ($=\sqrt{11}$) below the sensitivity for the full East-West arm.

The pulsars discovered using the separate East and West arms set 2^{o} apart in declination were quite strong[4], thus overcoming the 3db loss in sensitivity of this system compared to the full East-West arm. Using this system, approximate declinations could be obtained (see later 2.4.1) assisting in later position measurements.

Table 2.2

System	Advantages	Disadvantages	Pulsars Discovered
Full E W arm single beam	High sensitivity	Narrow beam-pulsars erratic No discrimination between pulsars and interference	None - not used.
Addition of detected signals from small sections of aerial.	Wide beam (XN) Thorough cover of sky (~1 minute at each point of sky). Good for erratic pulsars	Sensitivity reduced $\sqrt{N}$ where N = No. of small sections. No discrimination between pulsars and interference.	None - though used extensively.
Separate E and W arms, set 2° apart in declination	Beam 2x width of full aerial beam. Large coverage. Initial value for . Partial discrimination against interference.	Sensitivity reduced by 0.5 for individual pulses.	PSR1749-28 PSR2045-16
'Early' and 'late' EW beams Multibeamed system.	High sensitivity Two independent observations-helpful for erratic pulsars. Good discrimination against interference	None-for pulsars of moderate period and dispersion measure	PSR0031-07, MP0254, PSR0450-18, PSR0628-28, PSR0736-40, PSR0818-13, PSR0833-45, PSR0835-41, MP0940, MP0959, PSR1055-52, MP1359, PSR1426-66, PSR1449-64, PSR1451-68, PSR1530-53, PSR1556-44, MP1604, PSR1642-03*, MP1700, PSR1706-16, PSR1727-47, PSR1747-46, PSR1818-04, PSR1857-26, PSR1911-04, PSR1929+10, PSR1944+17. *PSR1642-03 was announced in ref.(20). It was found independently during the Molonglo searches.

2.3.2. The Multibeamed East-West Configuration.

During 1968 a Multibeaming system was added to the East-West arm. Signals from each of the 22 bays of the East-West aerial were combined into pairs (adjoining bays) and the 11 signals were then combined in such a way as to produce 3 different phase gradients along the aerial. The phase gradients were produced using different lengths of cable.

The centre beam of the three was equivalent to the normal beam of the East-West arm, the other two being separated from it by 1.4 arc min in hour angle.

The two outside beams, called "early" and "late" beams, were essentially independent of each other (ie. no overlap in hour angle) when used as total power beams. They were used in the main pulsar search carried out at the Molonglo Observatory from October 1968 till 1972.[5-13]

The advantages of searching with the early and late beams are given in Table 2.2. Discrimination against interference was provided by the delay in hour angle between the two beams as they swept across the sky. Celestial objects appeared with a known time delay between the two beams, while interference occurred simultaneously.

The search using this aerial configuration led to the discovery of 28 pulsars, listed in Table 3.2. A detailed discussion of this search is to be found in Chapter 3.

2.3.3 The Search in the Galactic Plane.

Early Molonglo discoveries demonstrated conclusively that pulsars were galactic objects, since they were clustered near

the galactic plane[6]. It was expected that more pulsars would be found close to the galactic plane[9], but that they would probably have high dispersion measures because of high electron densities in the interstellar medium and because they might be at large distances compared to local pulsars. Since dispersion measure imposed limits on the sensitivity of the "early-late" beam search, it was clear that the sensitivity for high dispersion measure pulsars could be increased by a system which "de-dispersed" the pulsar signal.

The effects of dispersion measure and receiver bandwidth on the detectibility of pulsars is discussed in Appendix 3A. The main effect, however, is pulse broadening as the dispersed pulse passes through the aerial bandwidth. A de-dispersing system would need to sweep the receiving frequency at a rate equal to the frequency sweep rate of the dispersed pulse. A technique, however, which is almost equivalent, is to split the aerial band into narrow bandwidth channels and sum the detected outputs of the narrow bands after graded delays have been applied to them. The two methods are strictly equivalent in sensitivity improvement when the dispersion is such that the instantaneous bandwidth of the pulsar $Wp\dot{\nu}$ is greater than the bandwidth of the narrow bands (Wp is the actual pulse width of the pulsar and $\dot{\nu}$ is the frequency sweep rate due to dispersion). (See Appendix 3A).

In the first "dispersion remover" built[9], the 4MHz bandwidth was split into two 2MHz bands separated by 2MHz, the detected signals from each band being added after a delay

of 45 m sec had been introduced into the signal from the band of higher received frequency. Depending on the pulse width of the pulsar the sensitivity to pulsars with dispersion measure 200 $cm^{-3}pc$ was increased by up to $\sqrt{2}$. In the second case the 4MHz band was split into twenty 200KHz bands separated by 200KHz, the detected signals from each band being progressively delayed before being added. The dispersion measure of maximum sensitivity could be varied but was usually set at 400 $cm^{-3}pc$. The increase in sensitivity was up to $\sqrt{20}$.

The search system consisted of the two dispersion removers operating in parallel with a normal beam of the East-West arm[14]. The two highly dispersed pulsars PSR1154-62 and PSR1240-64 were discovered during this search.

This technique for pulsar searching was used at Molonglo in 1969. Recently (1973), by de-dispersing the output from the 64M dish in a computer using a two-dimensional Fourier analysis, observers at Parkes have discovered more pulsars near the galactic plane[15,16].

A more detailed account of the galactic searches at Molonglo is given in Chapter 3.

2.4 Measurement of Pulsar Parameters.

2.4.1 Position.

2.4.1.1 Right Ascension.

The right ascensions of pulsars were generally measured from transits through the total power fan beams of the East-West arm. In most cases the right ascensions were obtained by fitting the pulses to the beamshape, effects of

pulse height variations being averaged out by repeated observations.(5-13,18)

For a few pulsars, the pulses during several transits were strong enough to be seen in both the early and centre, or centre and late beams of the East-West arm where these beams overlapped. The right ascension could be measured by taking ratios of pulse heights on the overlapping beams.

A computer programme was written which effectively applied both these methods to a transit of a pulsar through the early, centre and late beams using an iterative process. The results are listed in Table 5.1 in Chapter 5.

2.4.1.2 Declination.

Since the width in declination of the East-West fan beams is 4°, the initial precision with which the declination of pulsars discovered at Molonglo could be specified was $\pm 2^{\circ}$. Using the split East-West configuration, with the East and West arms separated by 2° in declination, the precision could be increased to about $0^{\circ}.5$ if a relatively strong pulse happened to occur during the transit, and to $0^{\circ}.2$ for some strong pulsars.

More precise declinations could only be achieved using the fan beams of the North-South arm.

The procedure adopted initially was to search for individual pulses in the outputs of five adjacent fan beams using an ultraviolet recorder. The declination of the North-South arm was stepped in increments of 7 arc min at intervals of approximately 30 seconds. If pulses were detected on one of the outputs during the long fan beam transit the precision in declination for the pulsar increased to about 1 arc min.

This was a tedious technique, particularly if the initial precision was low, since many beams had to be searched, often requiring many transits of the pulsar. The method also suffered because of the lower sensitivity of the North-South arm to individual pulses compared with the full East-West arm, even after low noise 408MHz preamplifiers were installed. Figure 2.2 shows the sensitivity of the North-South arm, as a function of declination, compared to the East-West arm. The curve includes a cos (z) term (z=zenith angle) due to aerial foreshortening, and an oscillatory term due to the back radiation patterns of the dipoles.

For some pulsars an initial declination measurement from another observatory narrowed the search in declination (particularly from the Parkes Radiotelescope in the case of several Southern pulsars[18]). However, for many pulsars the precision in the periods was not sufficient for the standard pulse integration techniques (superposed epoch) used by other observatories, and other methods had to be used.

A system for measuring pulsar declinations to high precision ($\sim$ 5 arc sec) without a very precise knowledge of the pulsar period, and which was also matched to the data handling system at Molonglo, was developed and is described fully in Chapter 4. The method is called Beat Period Integration (BPI).

2.4.2 Measurement of Parameters other than Position.

2.4.2.1 Period.

Pulsar periods were initially measured at Molonglo from the separation between pulses on a paper chart record of an East-West fan beam transit. The precision obtained was about

Figure 2.2 The sensitivity of the North-South Fan beams to individual pulses, compared to the East-West Fan beams, as a function of declination. The precise value for the sensitivity of the East-West Fan beams is indicated only approximately by the dotted line.

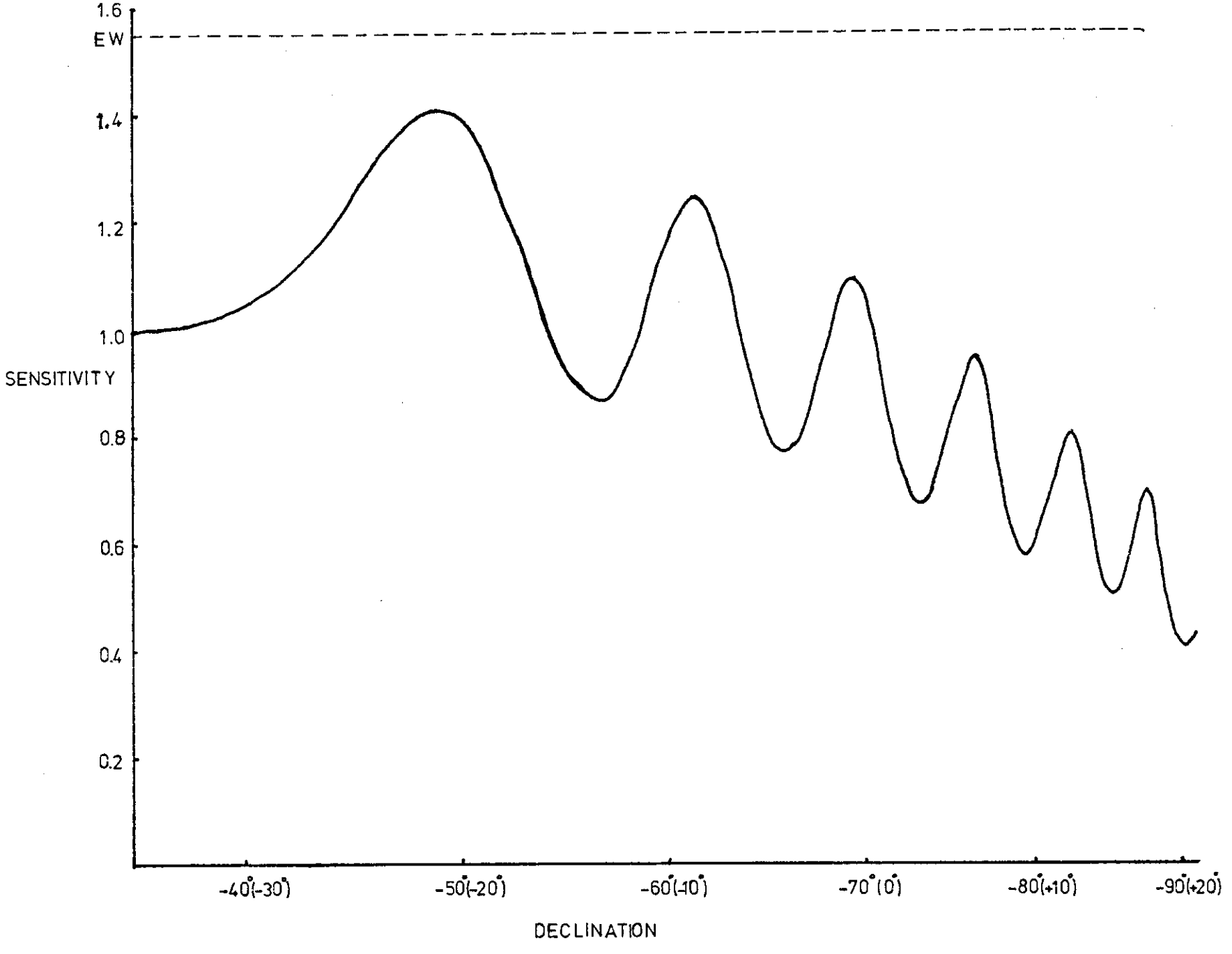
1.6
EW
1.4
1.2
1.0
SENSITIVITY
0.8
0.6
0.4
0.2
-40°(-30°)
-50°(-20°)
-60°(-10°)
-70°(0°)
-80°(+10°)
-90°(+20°)
DECLINATION

1%, depending on the number of pulses visible.

By recording the pulses on a fast recorder, together with a 50Hz reference signal, the precision could be increased to about 0.1 - 0.5%, the improvement being mainly due to the better resolution of the pulse shapes.

Strong pulsars whose declinations were known precisely enough could often be observed as individual pulses on a fan beam of the North-South arm. Chart measurements of these transits gave periods precise to 0.01%, the improvement being due to the long transit time.

More precise periods were obtained, even for weak pulsars, by BPI as described in Chapter 4.

2.4.2.2. Dispersion Measure.

By measuring the time of arrival of a pulsar pulse at different observing frequencies the dispersion usually attributed to the interstellar medium can be measured. At Molonglo the range of frequencies for measuring dispersion measure is limited to 406 - 410MHz. By splitting this band into two 2MHz bands centred on 407MHz and 409MHz, approximate values for dispersion measure were obtained from the difference between arrival times of individual pulses in the two bands.

Since the difference in arrival times was generally less than 50 msec the precision of this measurement was low. Later measurements at other observatories revealed large errors in values of dispersion measure obtained at Molonglo, probably caused by the complex dynamic spectra of individual pulses due to scintillation, as well as the narrowness of the

observing bandwidth.

2.4.2.3 Pulse Width.

Recordings of individual pulses were averaged to determine values of pulse widths. Large uncertainties were present in the measurements due to poor resolution, poor signal to noise, uncertainties in dispersion measure, effects due to the dynamic spectra of pulses, and scintillation broadening. Also since the telescope is linearly polarized, errors arose due to the variable polarization within the pulses.

2.4.2.4 Flux Densities or "Typical Pulse Energies".

Because of the erratic nature of pulsars, and the great variability of pulse amplitudes, it is difficult to specify pulsar flux densities. Integration times over 20 minutes in length overcome most scintillation effects for most pulsars[19], though for many pulsars there appear to be intrinsic luminosity changes on a time scale much longer than 20 minutes.

For most pulsars observed at Molonglo the best that could be done was to assign an energy to "typical strong pulses" observed whenever the pulsar was visible during an East-West arm fan beam transit. An approximate calibration was obtained from a switched attenuator in signal path.

The pulse energy so derived was rounded and put into one of the following categories: 0.01, 0.02, 0.05, 0.1, 0.2, 0.5, 1.0, 2.0 x 10^{-26} $Jm^{-2}Hz^{-1}$. More accurate specification could not be justified.

Later measurements using BPI obtained values for pulsar flux densities averaged over about 20 minutes. The results are discussed in Chapter 6.

2.5 References.

1. Mills, B. Y., Aitchison, R. E., Little, A. G., and McAdam, W. B., Proc. I. R. E. Aust., 24, 156 (1963).

2. Large, M. I., and Frater, R. H., Proc. I. R. E. E. Aust., 30, 227 (1969).

3. Hewish, A., Bell, S. J., Pilkington, J. D. H., Scott, P. F., and Collins, R. A., Nature, 217, 709 (1968).

4. Turtle, A. J., and Vaughan, A. E., Nature, 219, 689 (1968).

5. Large, M. I., Vaughan, A. E., and Mills, B. Y., Nature, 220, 340 (1968).

6. Large, M. I., Vaughan, A. E., and Wielebinski, R., Nature, 220, 753 (1968).

7. Wielebinski, R., Vaughan, A. E., and Large, M. I., Nature, 221, 47 (1969).

8. Vaughan, A. E., and Large, M. I., Proc. astron. Soc. Austral., 1, 220 (1969).

9. Large, M. I., Vaughan, A. E., and Wielebinski, R., Astrophys. Lett., 3, 123 (1969).

10. Vaughan, A. E., Large, M. I., and Wielebinski, R., Nature, 222, 963 (1969).

11. Large, M. I., Vaughan, A. E., and Wielebinski, R., Nature, 223, 1249 (1969).

12. Vaughan, A. E., and Large, M. I., Nature, 225, 167 (1970).

13. Vaughan, A. E., and Large, M. I., Mon. Not. R. astr. Soc., 156, 27P (1972).

14. Large, M. I., and Vaughan, A. E., Mon. Not. R. astr. Soc., 151, 277 (1971).

15. Komesaroff, M. M., Hamilton, P. A., McCulloch, P. M., Ables, J. G., Cooke, D. J., I. A. U. Circ. No. 2505 (1973).

16. Komesaroff, M. M., Hamilton, P. A., McCulloch, P. M., Ables, J. G., Cooke, D. J., I. A. U. Circ. No. 2563 (1973).

17. Turtle, A. J., and Vaughan, A. E., Nature, 219, 845 (1968).

18. Private Communications from M. M. Komesaroff, and J. G. Ables.

19. Smith, F. G., Rep. Prog. Phys., 35, 399 (1972).

20. Huguenin, G. R., and Taylor, J. H., I. A. U. Circ. No. 2135 (1969).

Chapter 3

THE MOLONGLO PULSAR SEARCHES.

3.1 Introduction.

The methods of pulsar searching used at Molonglo have been described in Chapter 2. The purpose of this chapter is to examine in detail the extent and sensitivity of the searches and to discuss the results of the searches. Later searches carried out from other observatories are used to demonstrate the degree of completeness of the Molonglo searches within certain defined limits.

3.2 Multibeamed East-West Search.

3.2.1 The Search Area.

The extent of the search carried out using the early and late beams of the East-West arm is illustrated in Fig. 3.1 and summarized in Table 3.1.

Table 3.1

Total Observable Area	8.7 steradians
Area *Observed more than once	68%
Area *Observed only once	22%
Area not *Observed	10%

*A point was regarded as observed if it lay within $\pm 2^{\circ}$ in declination of the declination setting of the East-West beams during a search.

It should be noted that 58% of those parts of the sky not observed at all lie North of $\delta = +12^{\circ}$ and South of $\delta = -60^{\circ}$, ie. in an area constituting 20% of the total observable sky. This reflects the fact that the search tended to be more intense near the galactic plane, as well as the time-consuming

Figure 3.1 A map showing the extent of the search using the multibeamed East-West arm of the Molonglo Radio Telescope. Areas observed once are designated by , while areas observed more than once by . The area north of $\delta = +21^{\circ}$ was not searched since it lies outside the range of observable sky. The galactic plane and the $\pm 10^{\circ}$ parallels of galactic latitude are also shown.

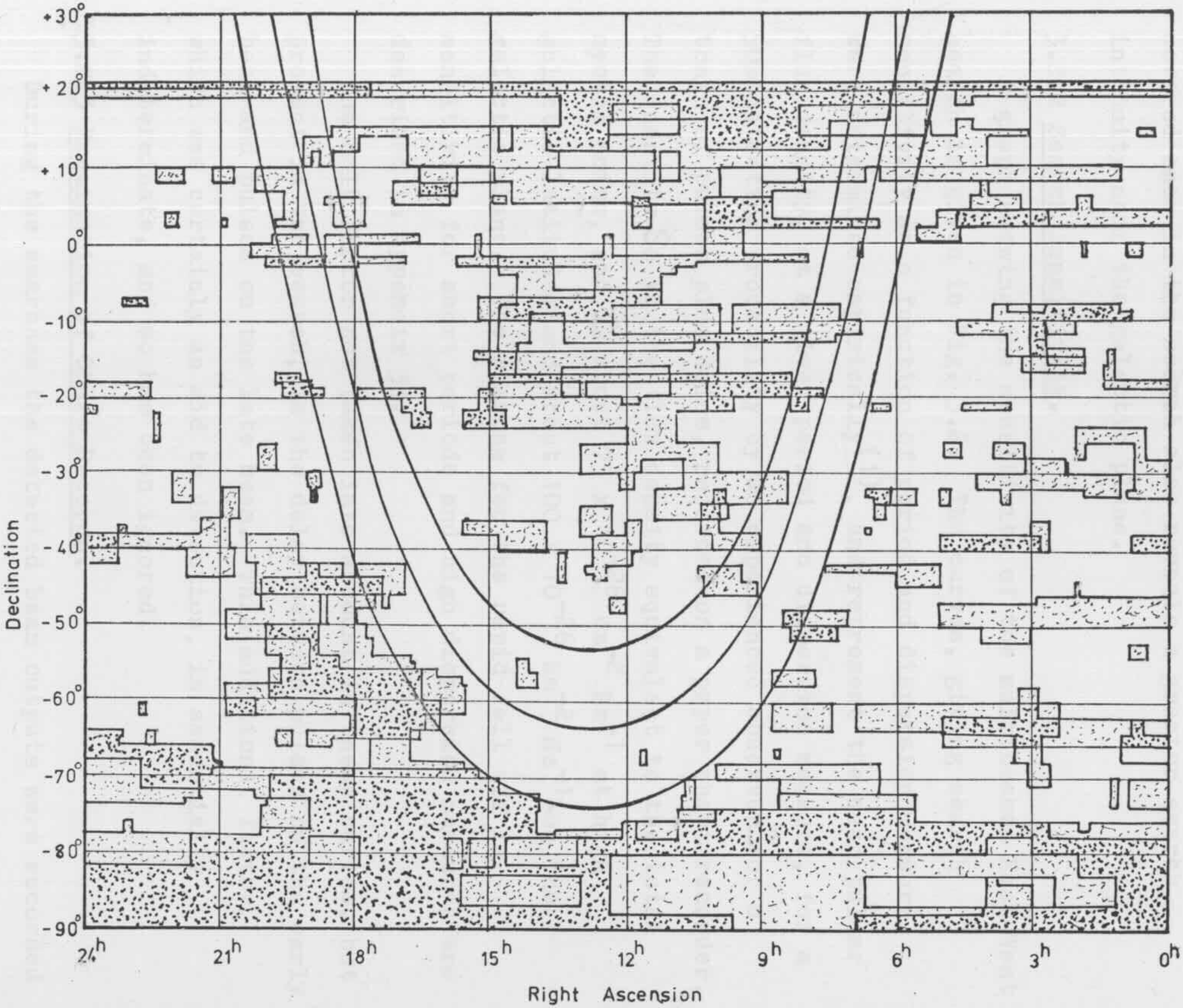
+30°
+20°
+10°
0°
-10°
-20°
-30°
-40°
-50°
-60°
-70°
-80°
-90°
Declination
24h
21h
18h
15h
12h
9h
6h
3h
0h
Right Ascension

nature of searches using a transit instrument at declinations further South than about -70°. The distribution of areas only covered once in the search also reveals a greater search intensity near the galactic plane.

3.2.2 Search Sensitivity.

A graph showing the sensitivity of the multibeamed East-West search is given in Fig. 3.2. The curves, giving search sensitivity as a function of period and dispersion measure, were determined empirically[1], and represent the mean pulsar flux density, at a given period and dispersion measure, for a 50% detection probability by an experienced observer for a train of pulses plus noise, recorded on a paper chart recorder. The quantity S_o is the flux density equivalent to the total system noise, and is about 75×10^{-26} Wm^{-2} Hz^{-1} at high galactic latitudes and about 100×10^{-26} Wm^{-2} Hz^{-1} on the galactic plane. The reasons for the rapid fall off in sensitivity for short periods and high dispersion measures are described in Appendix 3A.

The only factor not taken into account in these curves, but present in the search, is the delay between pulses on the early beam and pulses on the late beam. This additional factor, which was certainly an aid to detection, is essentially indeterminate, and so has been ignored.

3.2.3 Examination of Chart Records.

During the searches the detected beam outputs were recorded on paper charts. The most common chart speed was about 8cm min^{-1}, a roll of chart lasting about $2\frac{1}{2}$ hours. Since the signals were a.c. coupled, the records maintained a constant

Figure 3.2 Experimentally derived sensitivity curves for the search using the multibeamed East-West arm. S_o was 100 x 10^{-26} Wm^{-2} Hz^{-1} on the Galactic Plane and about 75 x 10^{-26} Wm^{-2} Hz^{-1} away from the Plane. The parameter on each curve is the period in seconds.

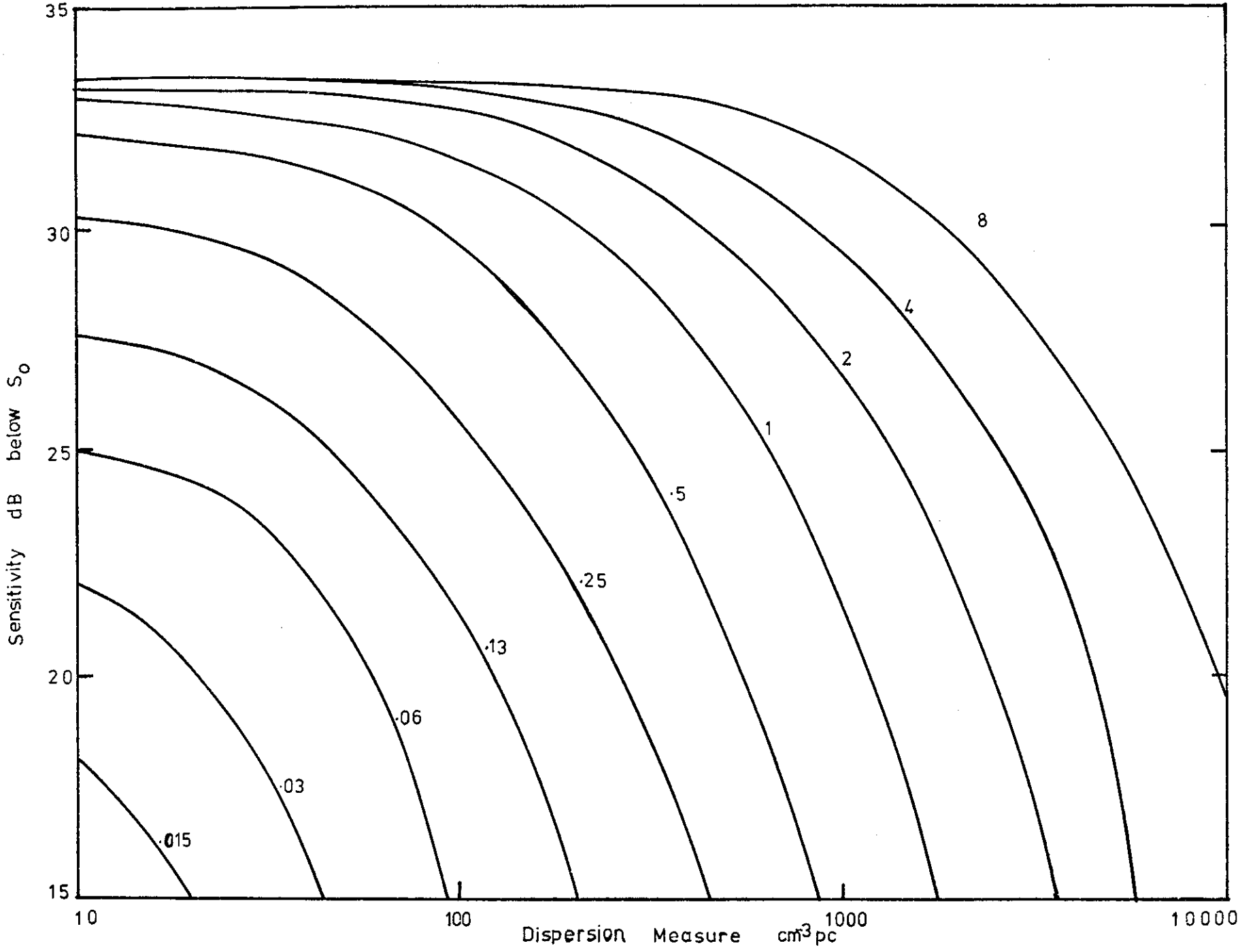
35
30
25
20
15
Sensitivity dB below S_o
8
4
2
1
·5
·25
·13
·06
·03
·015
10
100
1000
10000
Dispersion Measure $cm^3 pc$

d.c. level, so the charts could be used several times with different zero offsets. To improve the response of the pens to pulses, the signals were passed through pulse lengthening circuits matched to the pen response, before application to the recorder[2].

The charts were generally subjected to cursory examination at the observatory so that "obvious" new pulsars could be confirmed, and their properties measured, the following day. On their return to Sydney the charts were subjected to close scrutiny, a note being made of the positions of suspected pulsars.

Various criteria were used to decide whether a piece of record contained a pulsar signal or not. A regular train of pulses in the early beam, repeated, after a known delay, in the late beam, was a clear pulsar signal. Also erratically spaced pulses in both beams with the appropriate delay, was a fairly clear indication of the presence of a pulsar. The presence of several pulses in only one beam, with no simultaneous pulses in the other, was also regarded as a possible pulsar signal, since interference produced simultaneous responses in both beams.

No objective lower limit was set to the height of pulses which could be classed as coming from suspected pulsars. However, a practical lower limit chosen to produce on the average a suspect every few hours of observing time, was imposed to restrict the number of suspects so that there was a realistic chance of re-observing them.

As an example of this, a well-documented series of chart

examinations by Br. Paul Hough of about 600 hours of recorded data resulted in a suspect list totalling about 300, with 30 "prime" suspects, of which 5 were ultimately confirmed as pulsars[3,4].

A later search for pulsars, carried out using an automated pulsar logger[5], was found to have approximately the same search sensitivity as the search under discussion[6], with discriminators set at about 4σ above zero, where σ was the standard deviation of the noise ripple in time constants in the range of expected pulse widths. Hence the practical limit applied to the Multibeamed search was probably a little less than 4σ, allowing for the non-inclusion of both beams in the sensitivity curves.

A typical section of a search chart record is shown in Fig. 3.3.

3.2.4 Pulsars discovered during the Multibeamed Search.

A total of 25 pulsars were found during the original multibeamed East-West search. A further 3 were discovered using the automated search. All are listed in Table 3.2 together with their periods, dispersion measures and mean flux densities (at 408MHz). Some of the discovery observations are shown in Fig. 3.4.

3.2.5 Pulsars missed during the Multibeamed Search.

At present (Feb. 1974) there are 52 pulsars South of $\delta = +20^{\circ}$ which were not discovered during the multibeamed search. All are listed in Table 3.3, together with their periods, dispersion measures, and mean flux densities (at 408MHz) where measured. The last column in the table notes the reason why the pulsar

Figure 3.3 A copy of a section of a chart made during the search using the multibeamed East-West arm. The signal was a.c. coupled to keep the record moving straight along the chart, permitting the chart to be re-used several times. The time is indicated every 30 seconds. Starting from the lower edge of the diagram the traces are the outputs of the Early beam and the Late beam alternatively.

ART No. H25-1 PRINTED IN AUSTRALIA 7/67

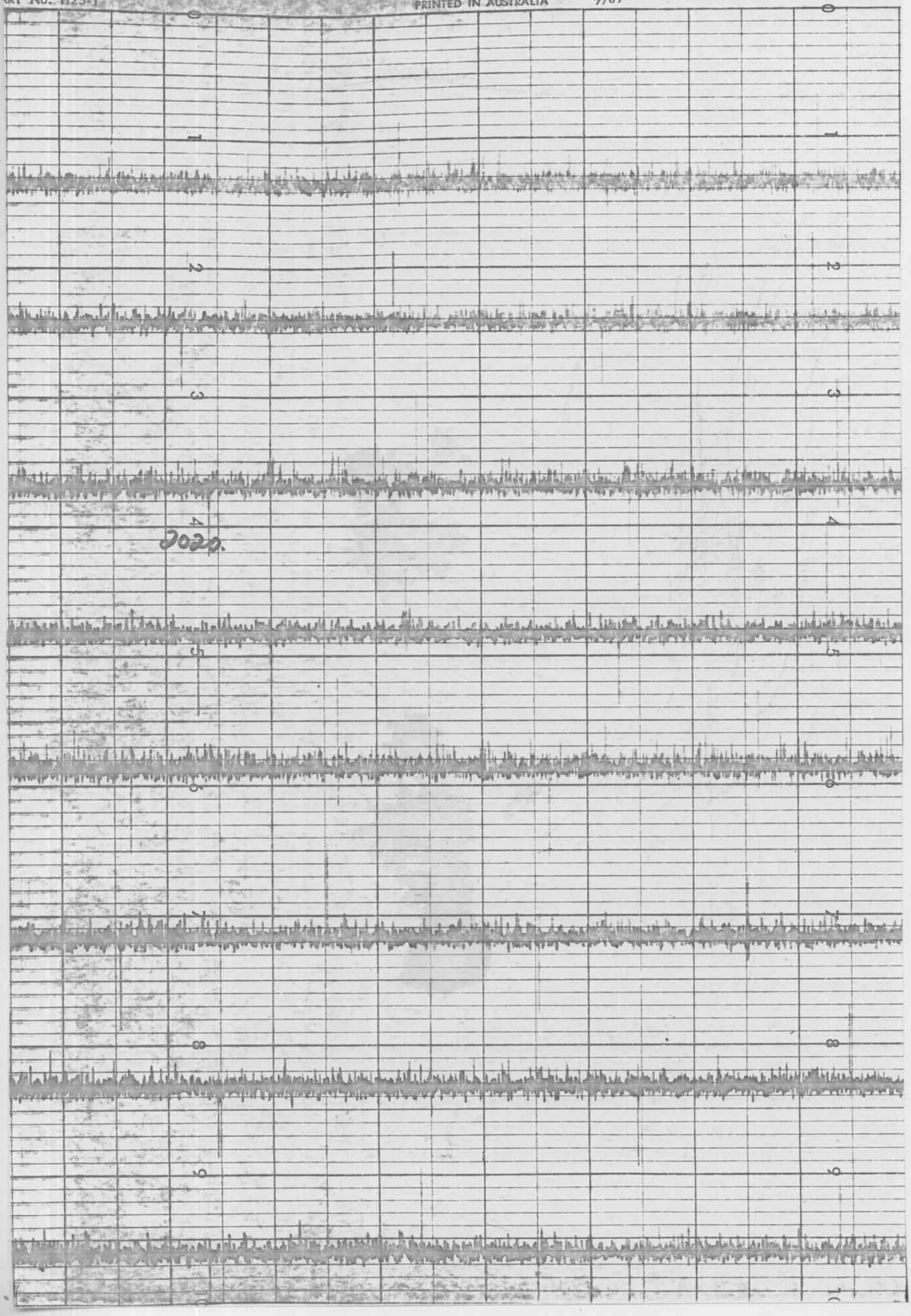

Figure 3.4 Copies of the discovery transits of some Molonglo pulsars found during the search using the multibeamed East-West arm. Note in most cases the pulses appearing in both beams, with an appropriate delay between the beams.

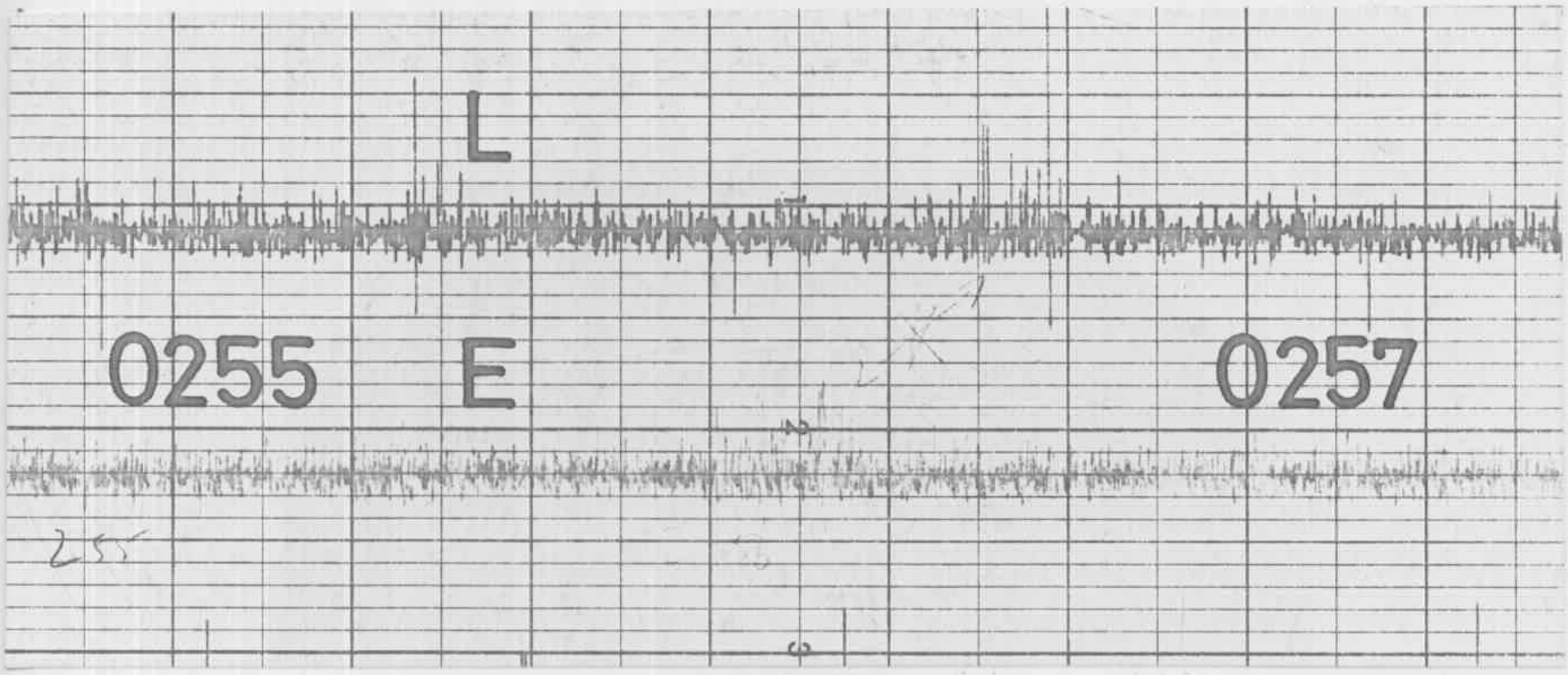

MP0254

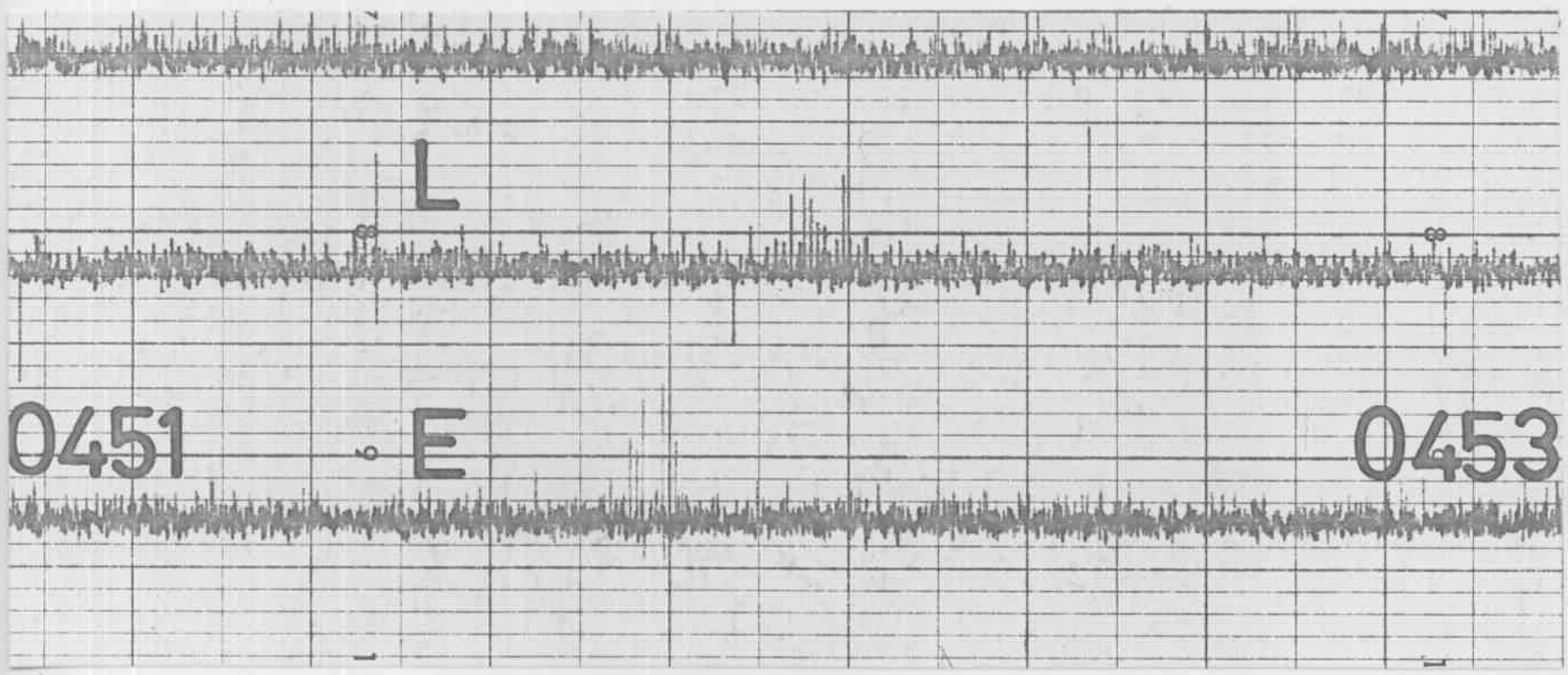

PSR0450-18

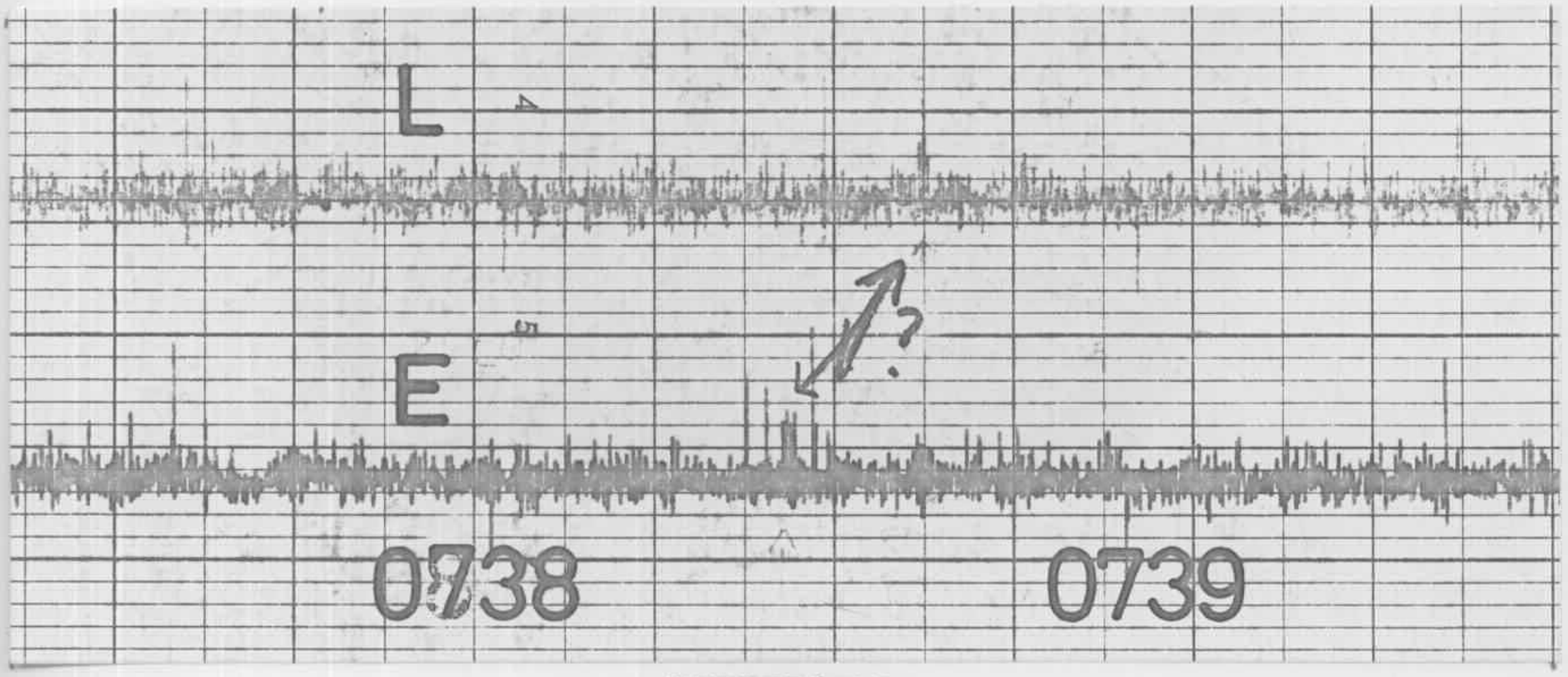

PSR0736-40

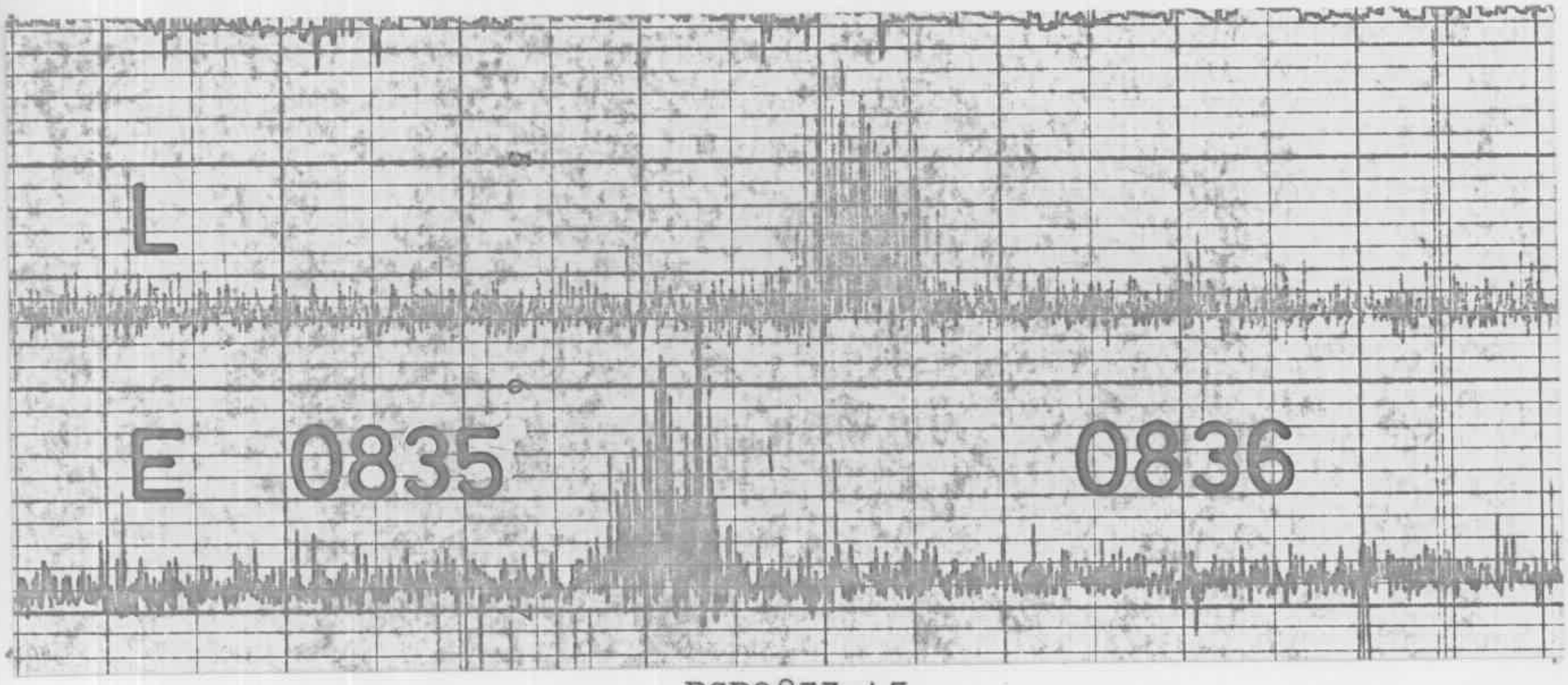

PSR0833-45

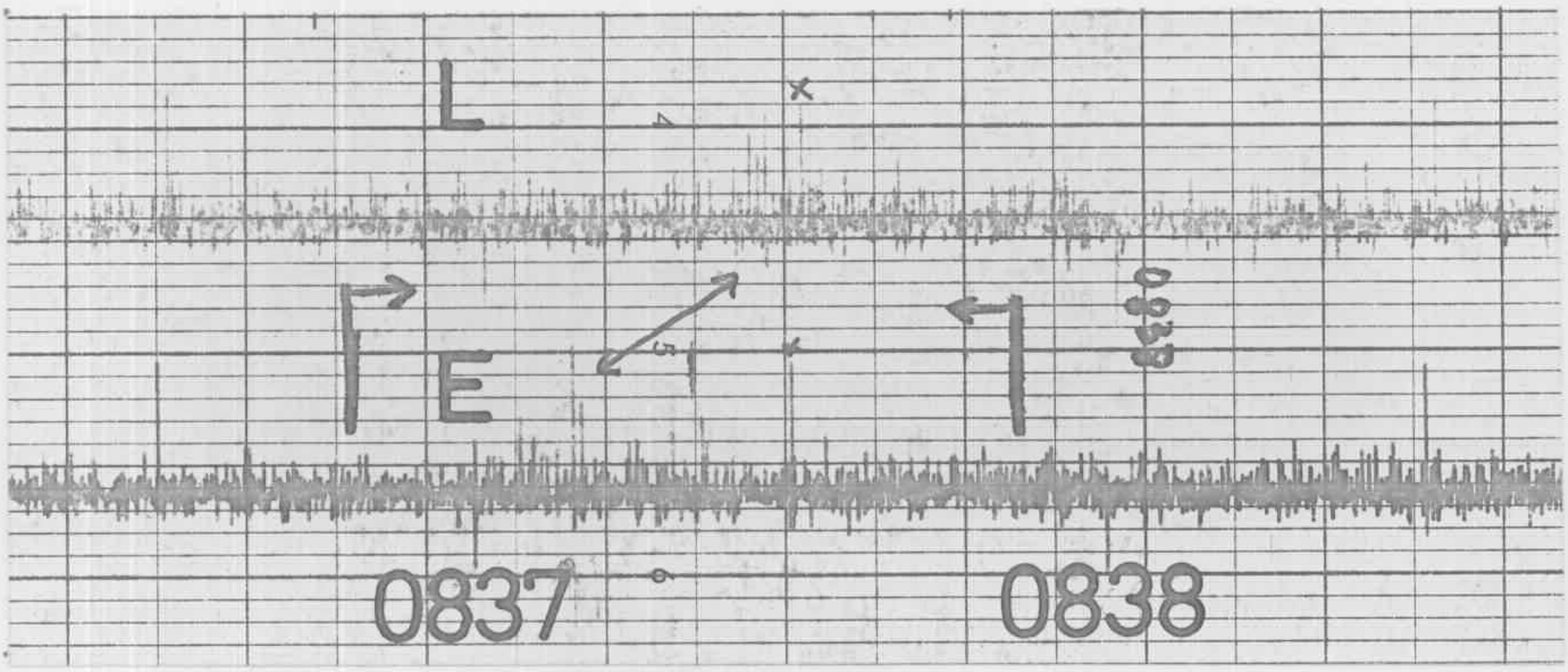

PSR0835-41

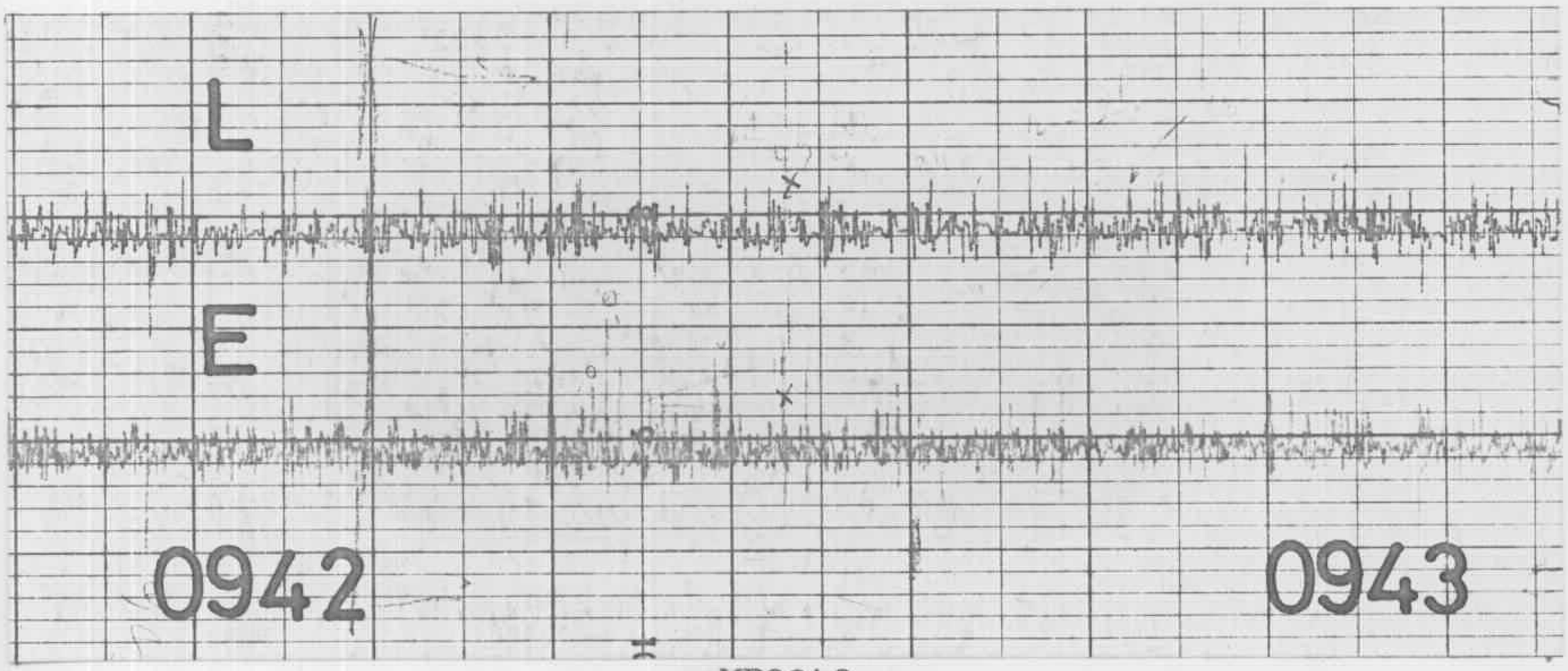

MP0940

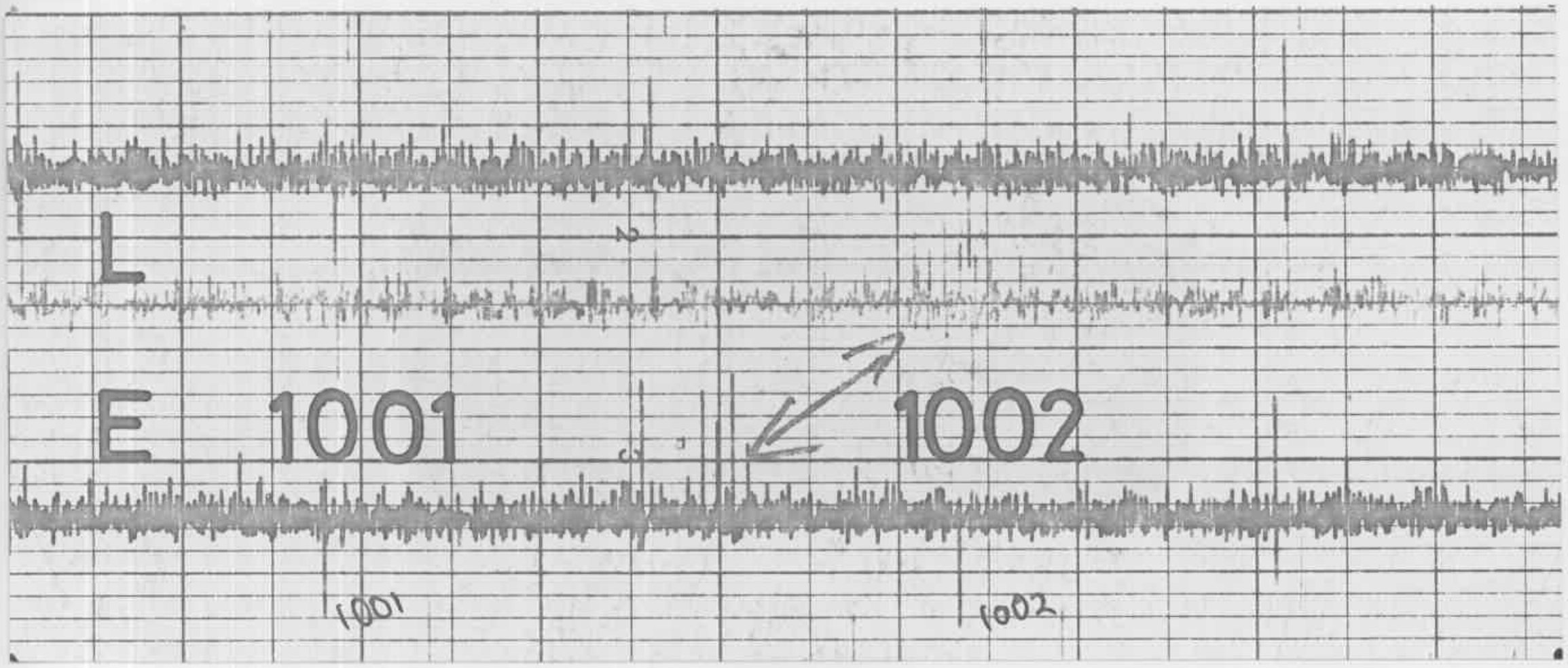

MP0959

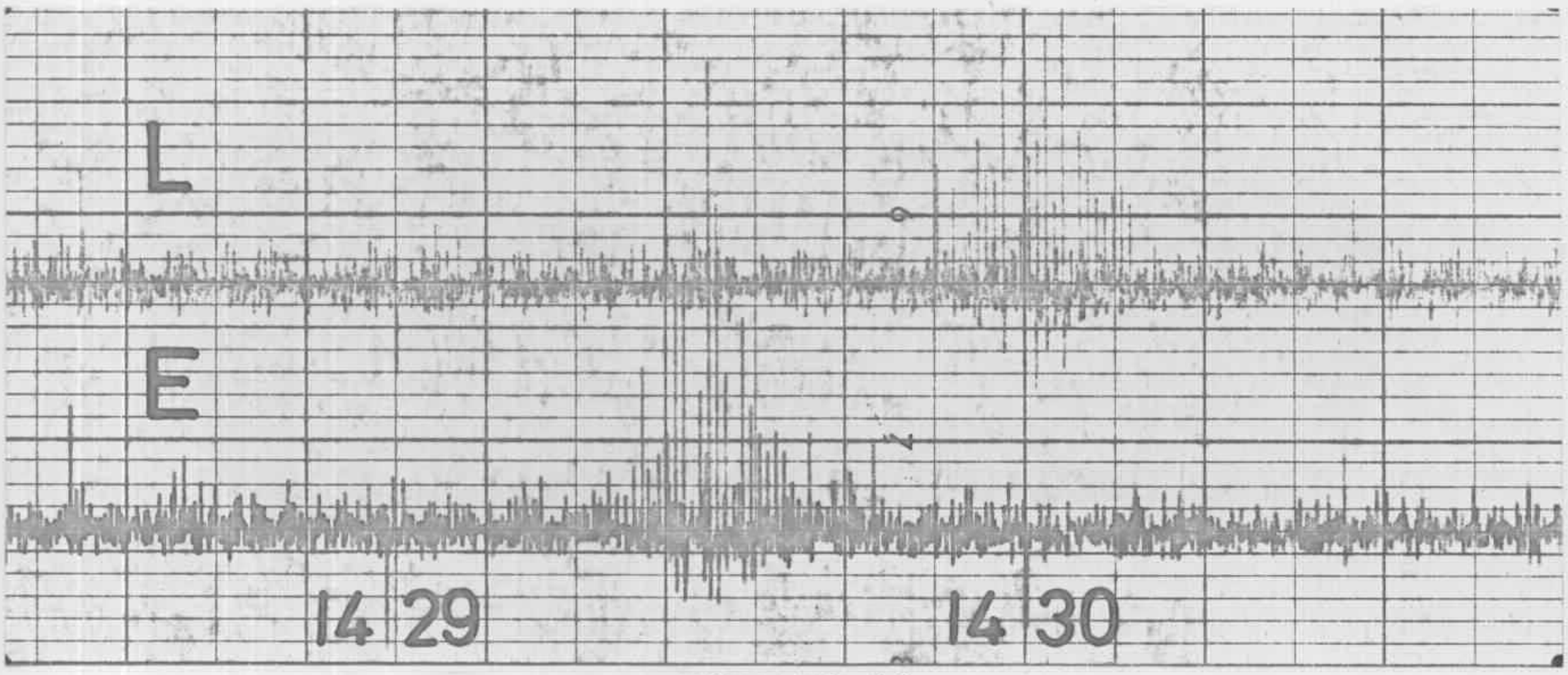

PSR1426-66

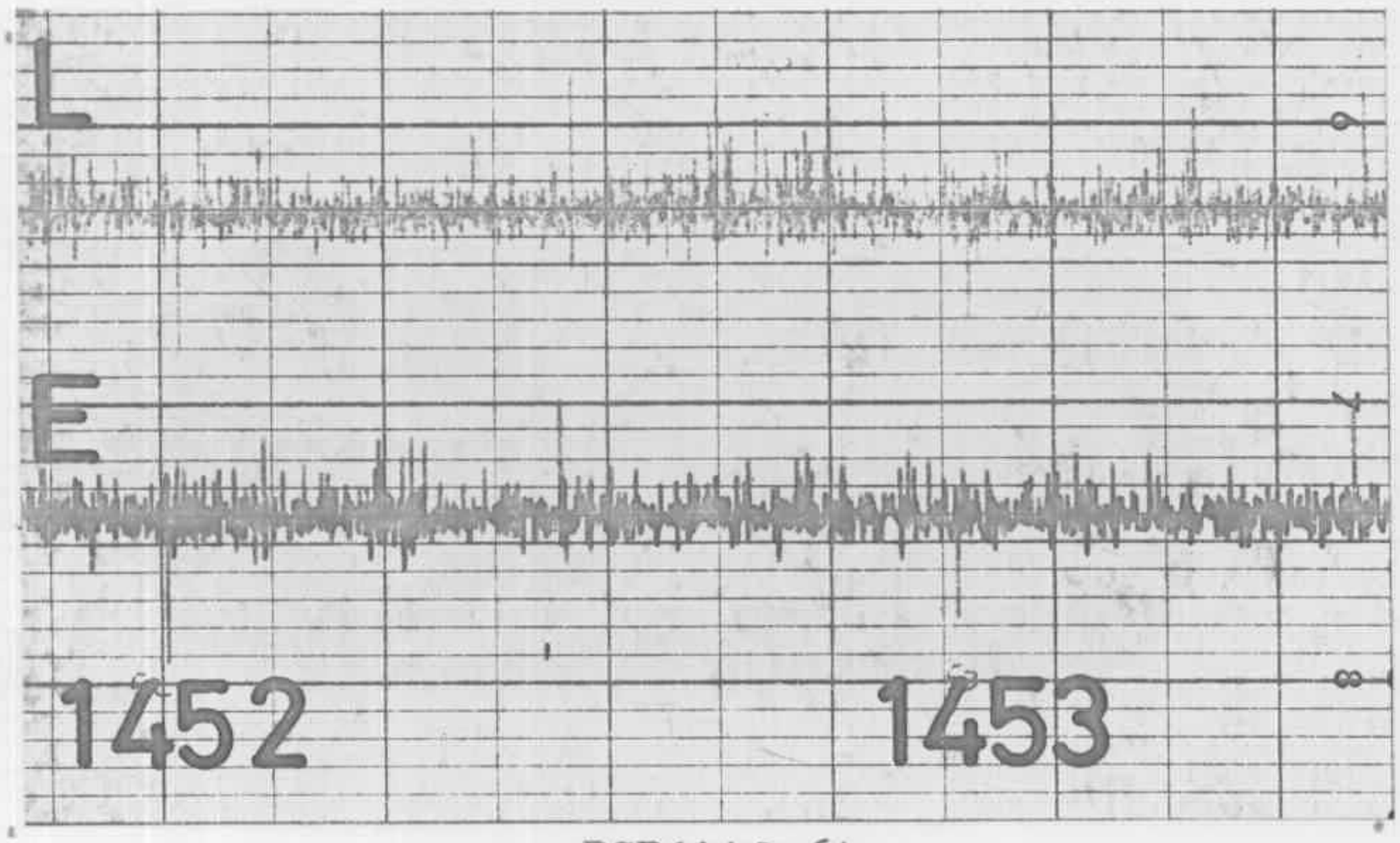

PSR1449-64

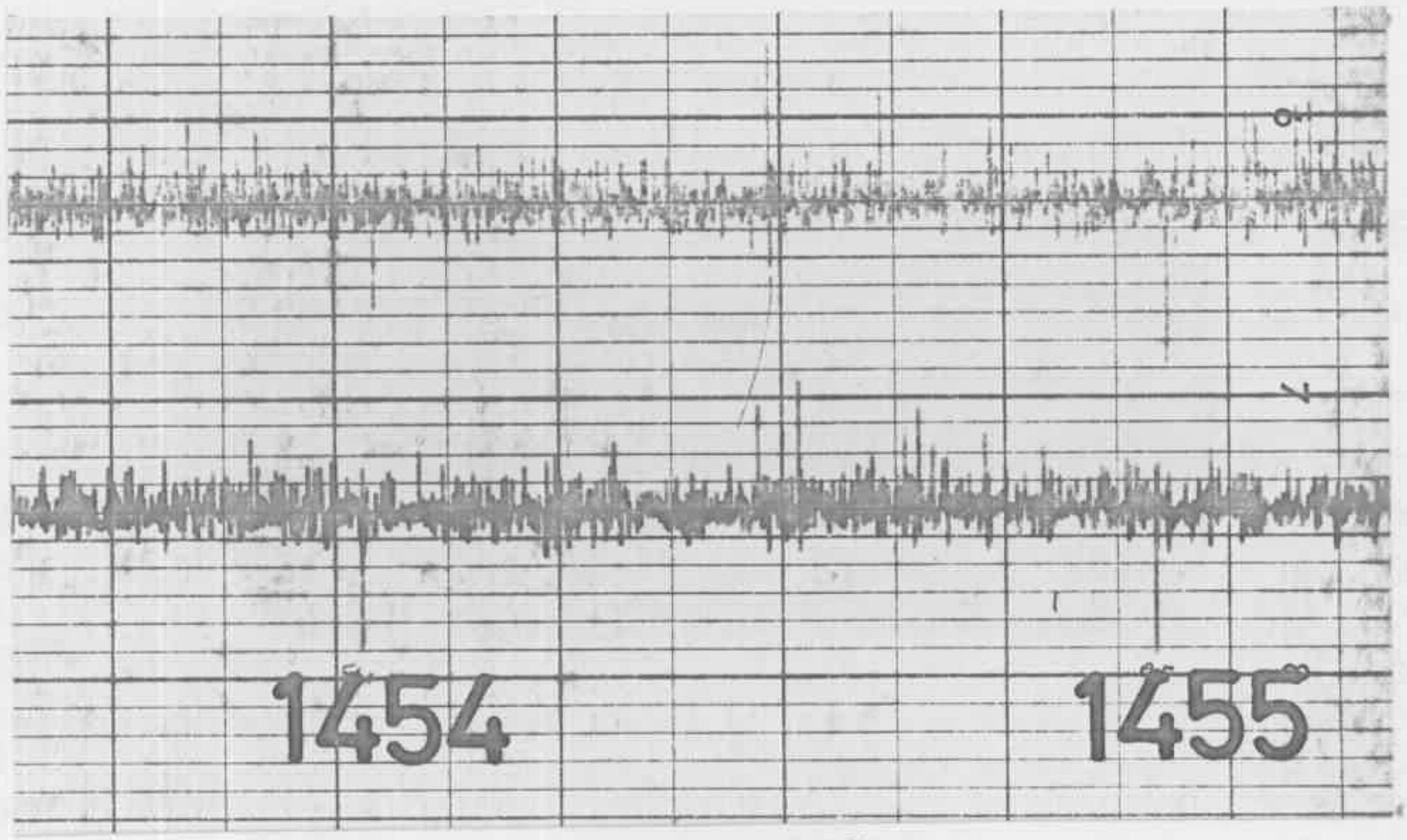

PSR1451-68

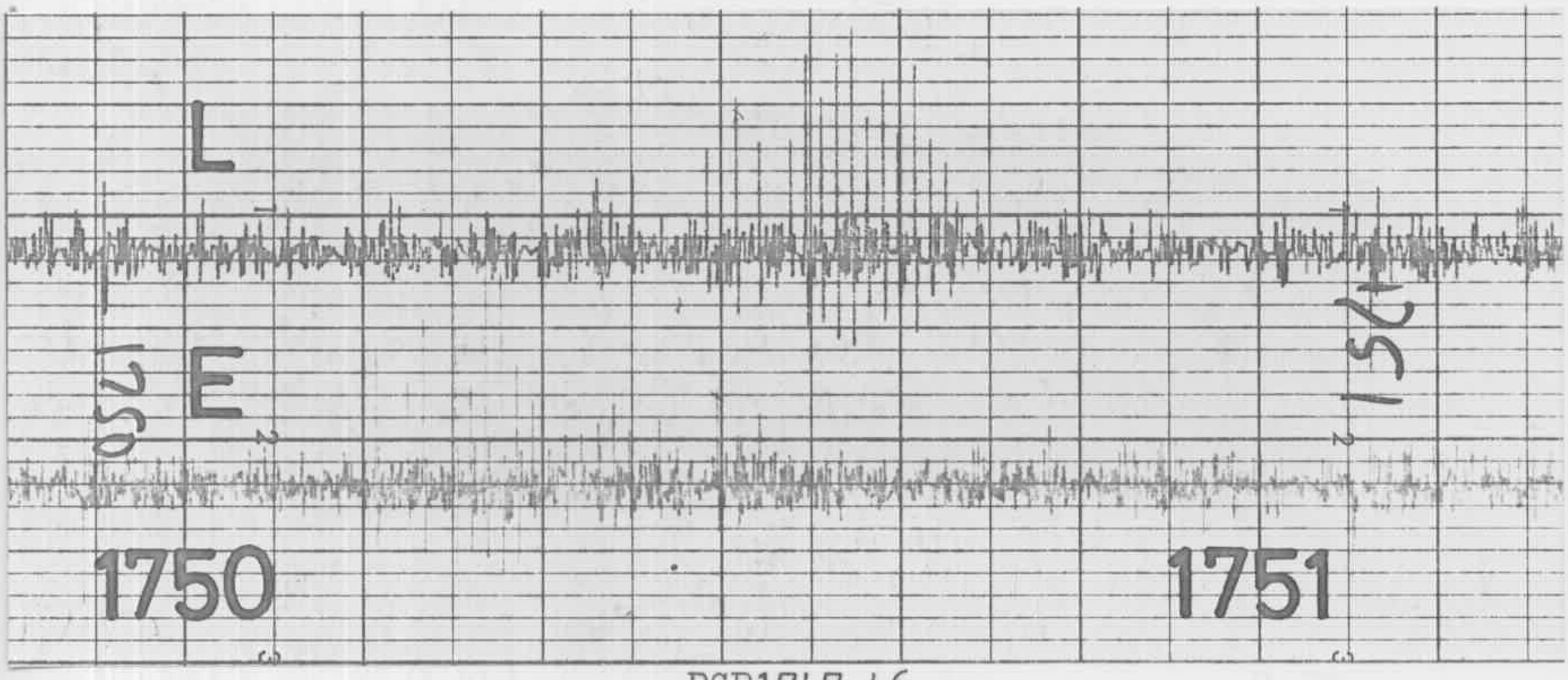

PSR1747-46

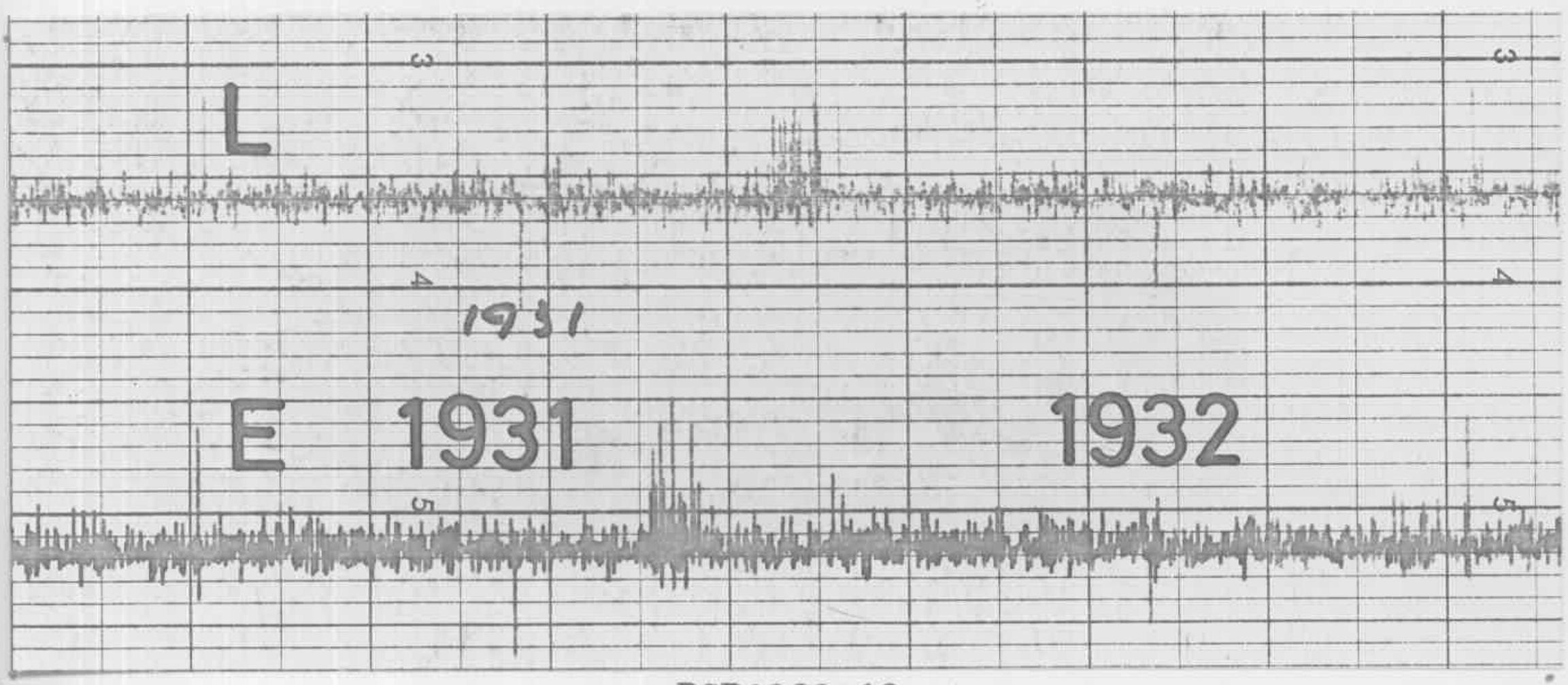

PSR1929+10

Table 3.2

Molonglo Pulsars discovered during Multibeamed Search.

Pulsar	Period (s)	Dispersion Measure* ($cm^{-3}pc$)	S_{408}+ (f.u.)
0031-07	0.943	10.9	0.07
0254-54	0.448	10	0.10
0450-18	0.549	39.9	0.07
0628-28	1.244	34.4	0.23
0736-40	0.375	161	0.15
0818-13	1.238	40.9	0.05
0833-45	0.089	69.2	1.59
0835-41	0.767	147.6	0.16
0940-55	0.664	145	0.15
0959-54	1.437	130.6	0.10
1055-52	0.197	23.8	0.10
1359-50	0.690	20	0.10
1426-66	0.787	65.3	0.15
1449-64	0.180	71.3	0.27
1451-68	0.263	8.6	0.12
1530-53	1.369	24.8	0.08
1556-44	0.257	58.8	0.08
1604-00	0.413	10.7	0.05
1642-03	0.388	35.7	0.63
1700-18	0.802	40	0.10
1706-16	0.653	24.9	0.05
1727-47	0.830	121.9	0.20
1747-46	0.742	20.7	0.07
1818-04	0.598	84.5	0.18
1857-26	0.612	36	0.12
1911-04	0.826	89.4	0.10
1929+10	0.227	3.2	0.50
1944+17	0.441	16.3	0.20

*Accurate dispersion measures determined by other observers[11 - 16].

+Mean flux density used in analysis in Chapter 9. Note that PSR0833-45 has been observed with intensity of 8.0 f.u.[17]

Table 3.3

Pulsars Not Detected during Multibeamed Search.

Pulsar	Period (s)	Dispersion Measure ($cm^{-3}pc$)	S_{408} (f.u.)	Reason for non-discovery
0301+19	1.388	15.7	0.75 0.02	?
0740-28	0.167	80	0.24	Historical
0834+06	1.274	12.9	0.04 0.10	Historical
0943+10	1.098	15.4	0.01	Historical
0950+08	0.253	3.0	0.07 0.50	Historical
1133+16	1.188	4.8	0.22 0.12	Historical
1154-62	0.401	270	0.19	Sensitivity
1221-63	0.216	92	----	?
1240-64	0.389	300	0.14	Sensitivity
1323-62	0.530	313	0.09*	Sensitivity
1354-62	0.456	400	0.04*	Sensitivity
1541+09	0.748	35.0	0.45	Historical
1557-50	0.193	270	----	?
1558-50	0.864	165	0.03*	Sensitivity
1601-52	0.658	35	0.08*	Suspect
1641-45	0.455	449	>1 *	Scintillation broadening
1700-32	1.212	103	0.09	?
1717-29	0.620	45	0.03	Suspect
1718-32	0.477	120	0.10	Sensitivity
1730-22	0.872	45	0.03	Sensitivity
1742-30	0.367	84	----	?
1749-28	0.563	50.9	0.52	Historical

Table 3.3 (contd.)

Pulsars Not Detected during Multibeamed Search.

Pulsar	Period (s)	Dispersion Measure ($cm^{-3}pc$)	S_{408} (f.u.)	Reason for non-discovery
1754-24	0.234	188.1	----	?
1813-26	0.593	90	0.03	Sensitivity
1819-22	1.874	140	0.02	Sensitivity
1822-09	0.769	19.3	0.03	Sensitivity
1826-17	0.307	210	0.09	Sensitivity
1831-04	0.290	68	0.08	Sensitivity
1845-04	0.598	141.9	0.06	Sensitivity
1845-01	0.659	163	0.06	Sensitivity
1846-06	1.451	152	0.06	Sensitivity
1858+03	0.655	402	0.07	Sensitivity
1900-06	0.432	180	0.02	Sensitivity
1900+01	0.729	228	0.10	Sensitivity
1900+05	0.747	166	----	?
1906+00	1.017	111	0.03	Sensitivity
1907+02	0.495	190	0.02	Sensitivity
1907+10	0.284	144	0.06	Sensitivity
1910+20	2.233	84	0.01	Not Searched
1914+13	0.282	230	----	?
1915+09	1.181	40	----	?
1915+13	0.195	97	0.04	Sensitivity
1916+14	0.270	40	----	?
1917+00	1.272	85	0.03	Sensitivity
1918+19	0.821	140	0.04	Not Searched

Table 3.3 (contd.)

Pulsars Not Detected during Multibeamed Search.

Pulsar	Period (s)	Dispersion Measure ($cm^{-3}pc$)	S_{408} (f.u.)	Reason for non-discovery
1919+14	0.618	100	----	?
1924+16	0.580	160	----	?
1929+15	0.314	120	----	?
1930+20	0.268	200	----	Not Searched
1933+15	0.967	160	----	?
1933+16	0.359	158.5	0.40 0.20	Historical
2045-16	1.962	11.5	0.26	Historical

*These are flux densities measured at 750MHz.

was not seen during the search. For 11 pulsars there are "historical" reasons why they were not discovered in the search. In these cases the pulsars were discovered in other searches before the Molonglo search covered their position. Two pulsars also were discovered during the search of the galactic plane (3.3.4). Of the remaining 39 pulsars, 5 were noted as suspects during searches at Molonglo.

The great majority of the 39 pulsars discovered elsewhere were found using Fourier transform search techniques with on-line computers and many minutes of integration time[7,8,9,10]. These techniques are much more sensitive than the Molonglo search, and are relatively unaffected by dispersion measure. Fig. 3.5 demonstrates that the populations of these pulsars in luminosity ($(dm)^2 S$) are similar for the pulsars found in the Molonglo search and the pulsars missed. However from Fig. 3.6 it can be seen that the pulsars missed extend to much higher dispersion measures. Since these pulsars are in general at greater distances, their observed flux densities are lower.

Hence the major reason why these pulsars were missed was the low relative sensitivity of the Molonglo search, particularly for pulsars with high dispersion measures.

To illustrate this, the sensitivity curves of Fig. 3.2 have been re-drawn as contours of equal search sensitivity in period-dispersion measure space and the pulsars missed in the search plotted on the diagram (Fig. 3.7). It can be seen that most were missed for reasons of sensitivity, including three listed as suspects. Four pulsars had a 50% chance of detection and were missed, while three ought to have been found, if flux

Figure 3.5 a) A histogram of the luminosities of pulsars missed by the Molonglo search but found during other searches.

b) A histogram of the luminosities of pulsars discovered during the Molonglo search.

Note that the luminosities in both samples are similar.

a)

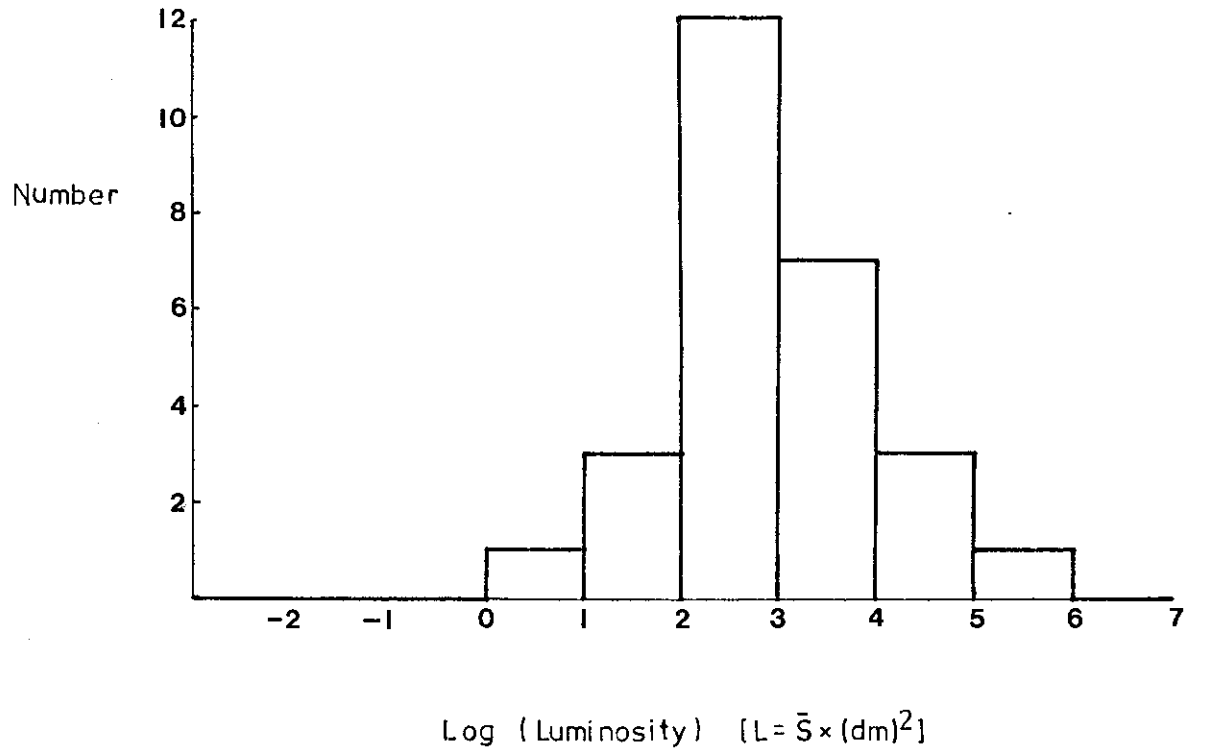
Number
12
10
8
6
4
2
-2
-1
0
1
2
3
4
5
6
7
Log (Luminosity) [L = S̄ × (dm)²]

b)

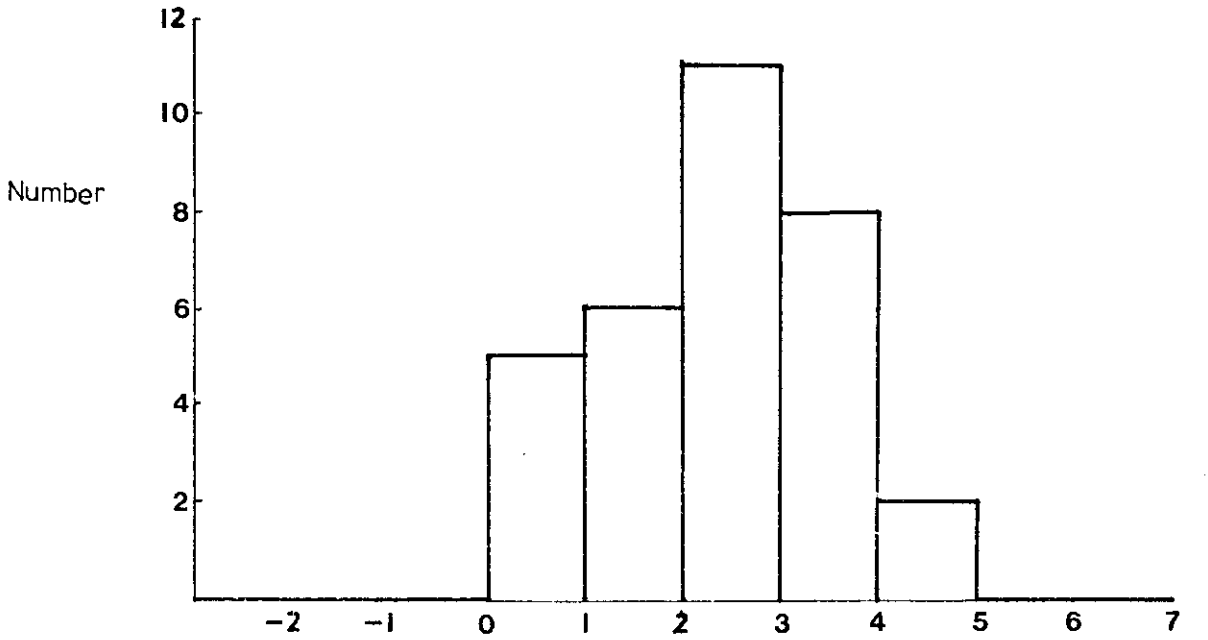
Number
12
10
8
6
4
2
-2
-1
0
1
2
3
4
5
6
7

Figure 3.6 Superimposed dispersion measure distributions for Molonglo pulsars (shaded) and those missed by the Molonglo search. Note the greater extent in dispersion measure of the latter.

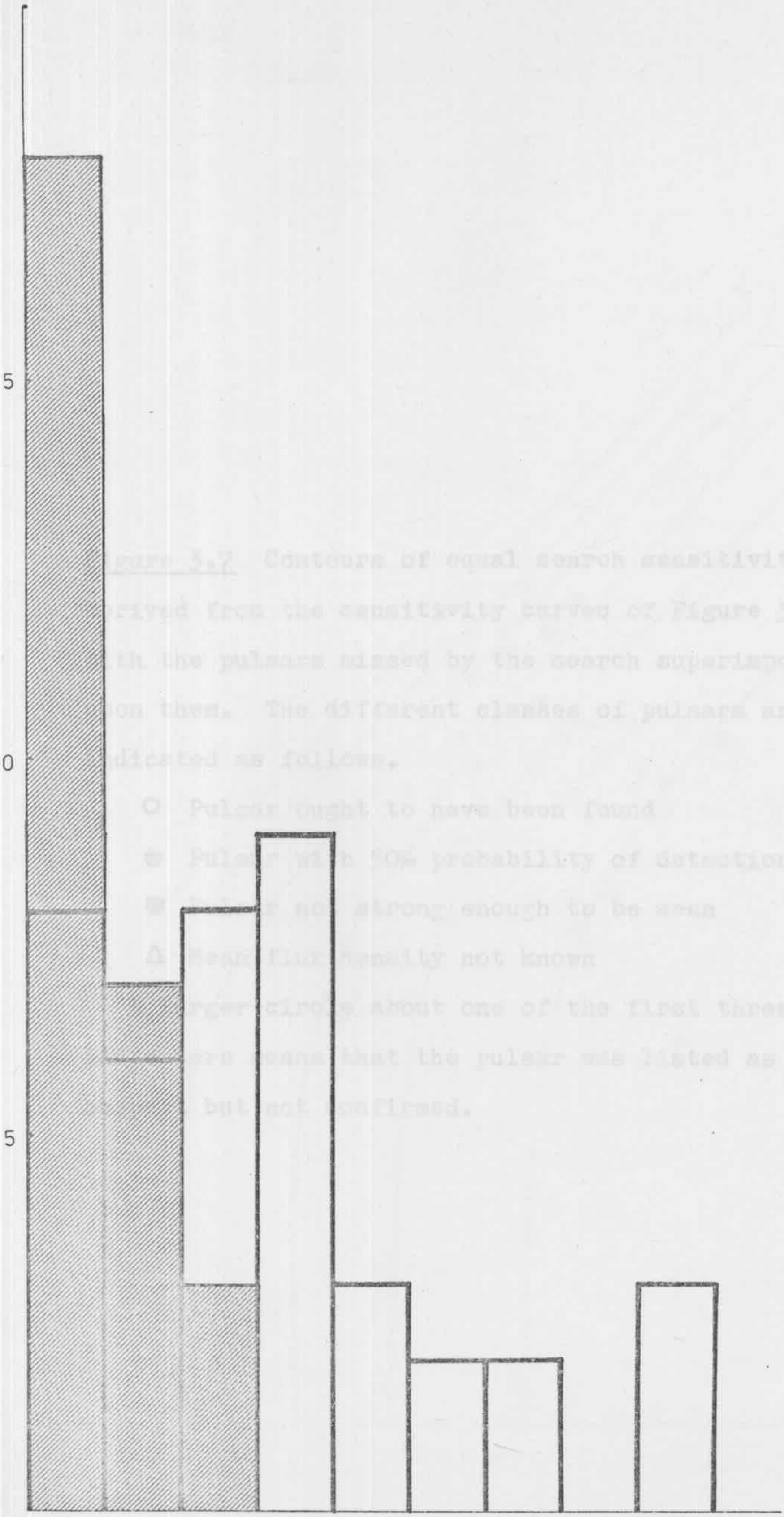
15
Number
10
5
0
50
100
150
200
250
300
350
400
450
Dispersion Measure (cm-3 pc)

Figure 3.7 Contours of equal search sensitivity, derived from the sensitivity curves of Figure 3.2, with the pulsars missed by the search superimposed upon them. The different classes of pulsars are indicated as follows.

- O Pulsar ought to have been found
- ◓ Pulsar with 50% probability of detection
- ● Pulsar not strong enough to be seen
- Δ Mean flux density not known

A larger circle about one of the first three indicators means that the pulsar was listed as a suspect but not confirmed.

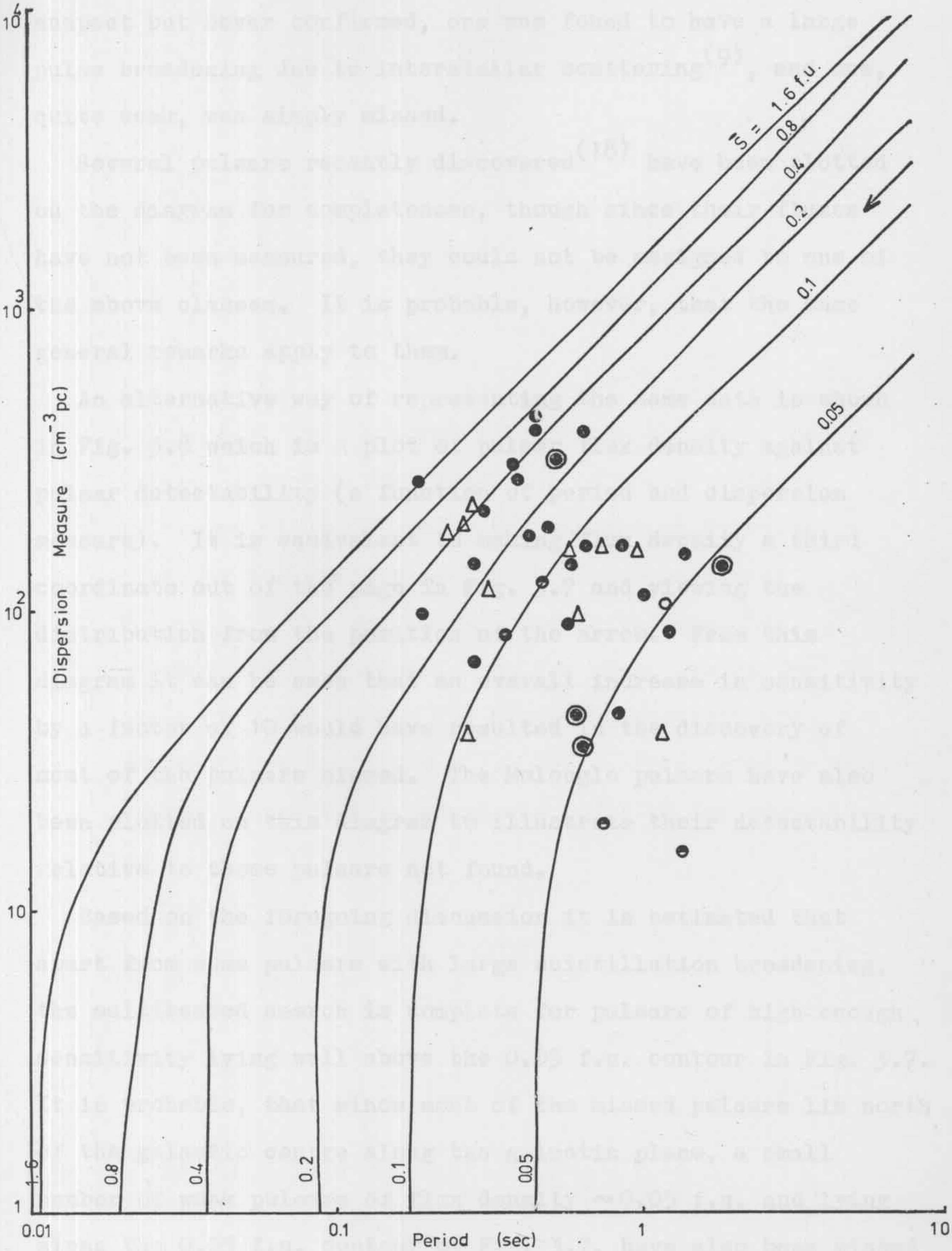
Dispersion Measure (cm^{-3}pc)
10^4
10^3
10^2
10
1
0.01
0.1
1
10
Period (sec)
S = 1.6 f.u.
0.8
0.4
0.2
0.1
0.05
1.6
0.8
0.4
0.2
0.1
0.05

density were the only factor. One of these was listed as a suspect but never confirmed, one was found to have a large pulse broadening due to interstellar scattering[9], and one, quite weak, was simply missed.

Several pulsars recently discovered[18] have been plotted on the diagram for completeness, though since their fluxes have not been measured, they could not be assigned to one of the above classes. It is probable, however, that the same general remarks apply to them.

An alternative way of representing the same data is shown in Fig. 3.8 which is a plot of pulsar flux density against pulsar detectability (a function of period and dispersion measure). It is equivalent to making flux density a third coordinate out of the page in Fig. 3.7 and viewing the distribution from the position of the arrow. From this diagram it can be seen that an overall increase in sensitivity by a factor of 10 would have resulted in the discovery of most of the pulsars missed. The Molonglo pulsars have also been plotted on this diagram to illustrate their detectability relative to those pulsars not found.

Based on the foregoing discussion it is estimated that apart from some pulsars with large scintillation broadening, the multibeamed search is complete for pulsars of high enough sensitivity lying well above the 0.05 f.u. contour in Fig. 3.7. It is probable, that since most of the missed pulsars lie north of the galactic centre along the galactic plane, a small number of weak pulsars of flux density $\sim$0.05 f.u. and lying along the 0.05 f.u. contour of Fig. 3.7, have also been missed south of the galactic centre.

Figure 3.8 This diagram illustrates the relationship between the mean flux densities of pulsars missed by the multibeamed search and the search sensitivity given by the surface defined by the contours of Figure 3.7. It can be regarded as viewing the surface and the pulsars from the direction of the arrow in Figure 3.7. The classes of pulsars are indicated as in Figure 3.7. The pulsars found by the search, indicated as + are also plotted for comparison.

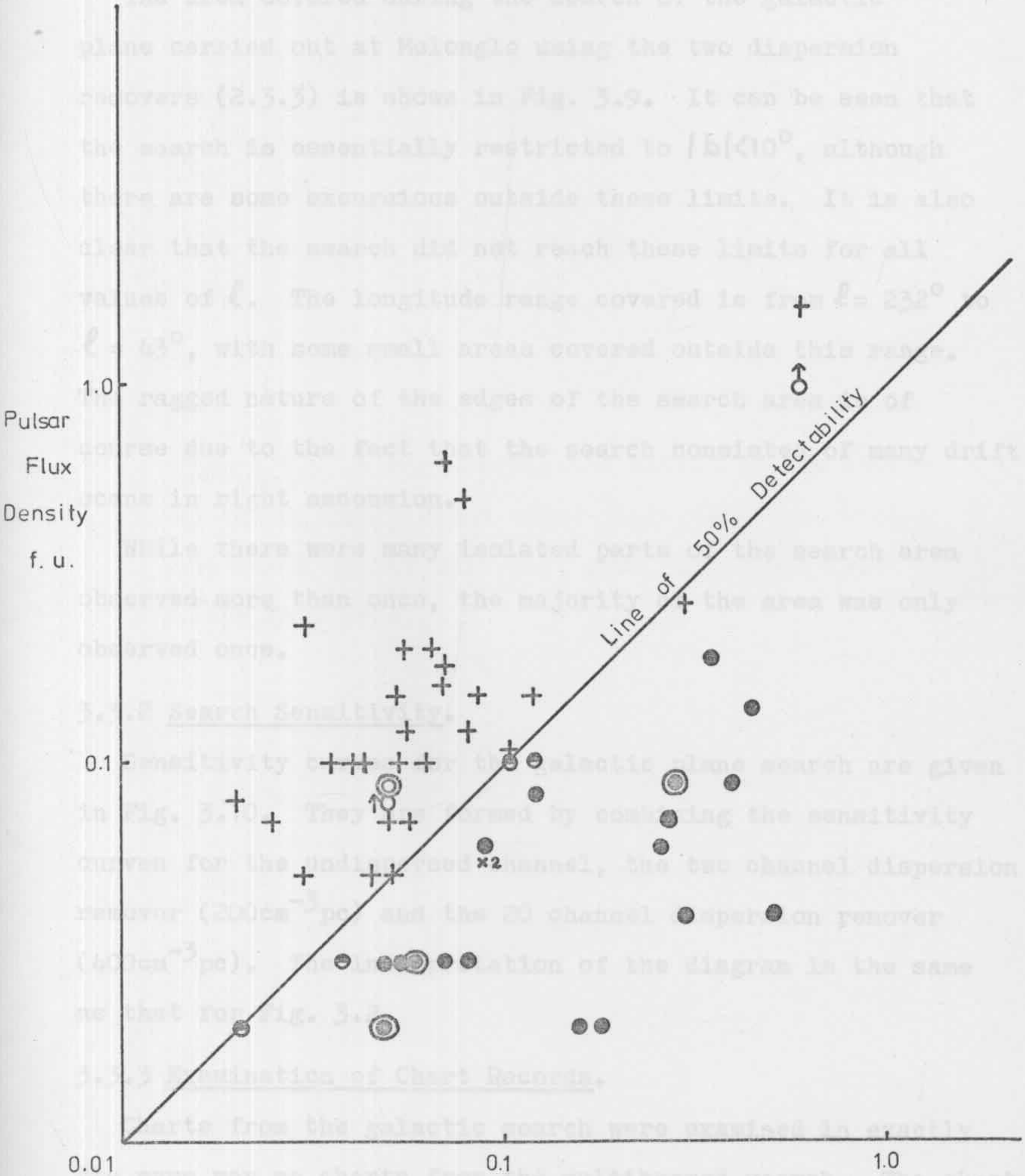
1.0
0.1
Pulsar
Flux
Density
f. u.
Line of 50% Detectability
×2
0.01
0.1
1.0
Pulsar Detectability (50%) f.u.

3.3 The Search of the Galactic Plane.

3.3.1 The Search Area.

The area covered during the search of the galactic[1] plane carried out at Molonglo using the two dispersion removers (2.3.3) is shown in Fig. 3.9. It can be seen that the search is essentially restricted to $|b|<10^{\circ}$, although there are some excursions outside these limits. It is also clear that the search did not reach these limits for all values of ℓ. The longitude range covered is from $\ell = 232^{\circ}$ to $\ell = 43^{\circ}$, with some small areas covered outside this range. The ragged nature of the edges of the search area is of course due to the fact that the search consisted of many drift scans in right ascension.

While there were many isolated parts of the search area observed more than once, the majority of the area was only observed once.

3.3.2 Search Sensitivity.

Sensitivity curves for the galactic plane search are given in Fig. 3.10. They are formed by combining the sensitivity curves for the undispersed channel, the two channel dispersion remover ($200 cm^{-3} pc$) and the 20 channel dispersion remover ($400 cm^{-3} pc$). The interpretation of the diagram is the same as that for Fig. 3.2.

3.3.3 Examination of Chart Records.

Charts from the galactic search were examined in exactly the same way as charts from the multibeamed search. The charts examined by Br. Paul Hough[3] included many from this search, and many of the suspects were found in this search. A typical

Figure 3.9 A map showing the extent of the search of the Galactic Plane using dispersion removers on the beams of the East-West arms of the Molonglo Radio Telescope.

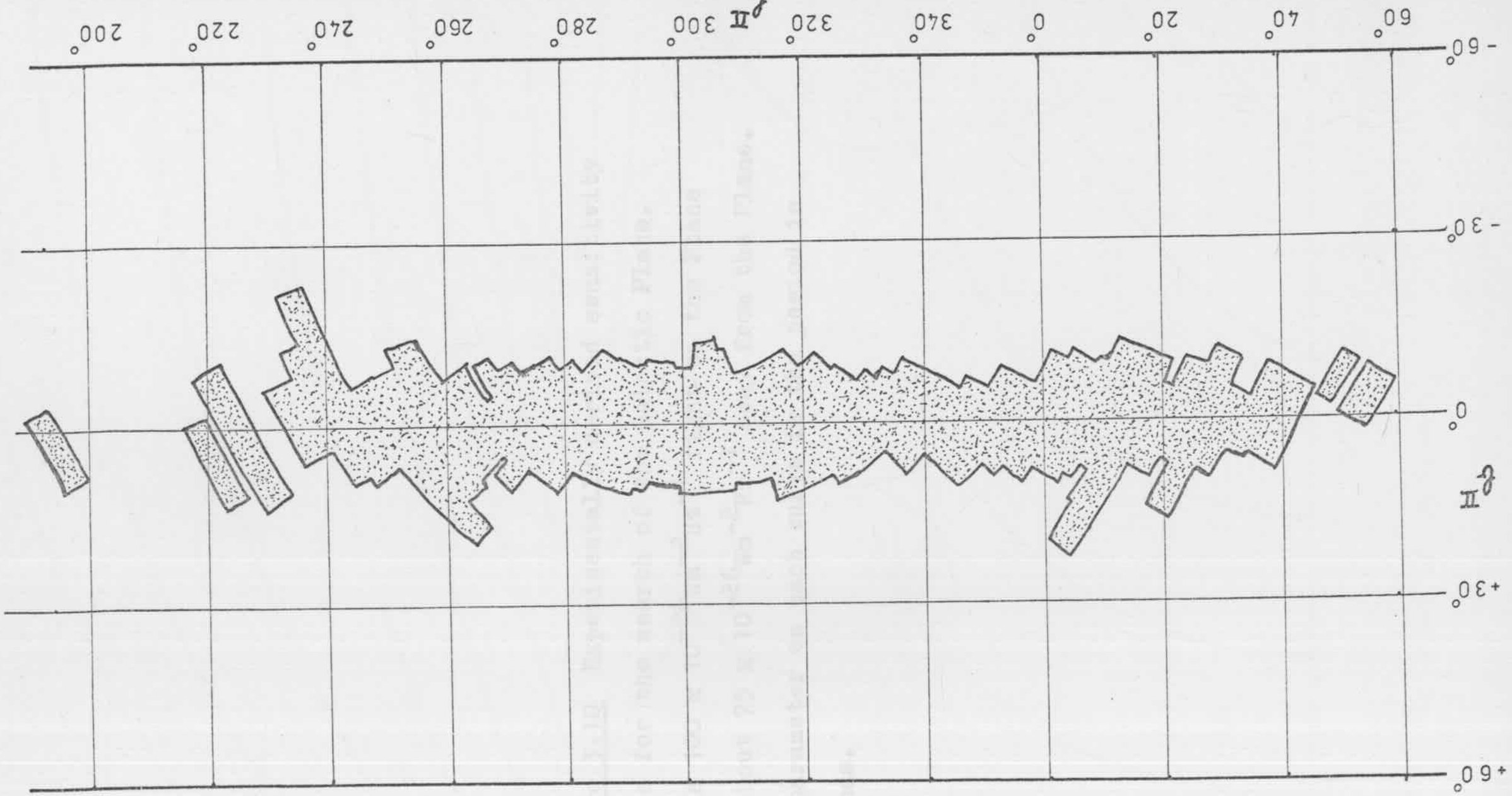
-60°
-30°
0°
+30°
+60°
ρ_{II}
60°
40°
20°
0°
340°
320°
300°
280°
260°
240°
220°
200°
ρ_{II}

Figure 3.10 Experimentally derived sensitivity curves for the search of the Galactic Plane. S_o was 100 x 10^{-26}Wm^{-2}Hz^{-1} right on the Plane and about 75 x 10^{-26}Wm^{-2}Hz^{-1} away from the Plane. The parameter on each curve is the period in seconds.

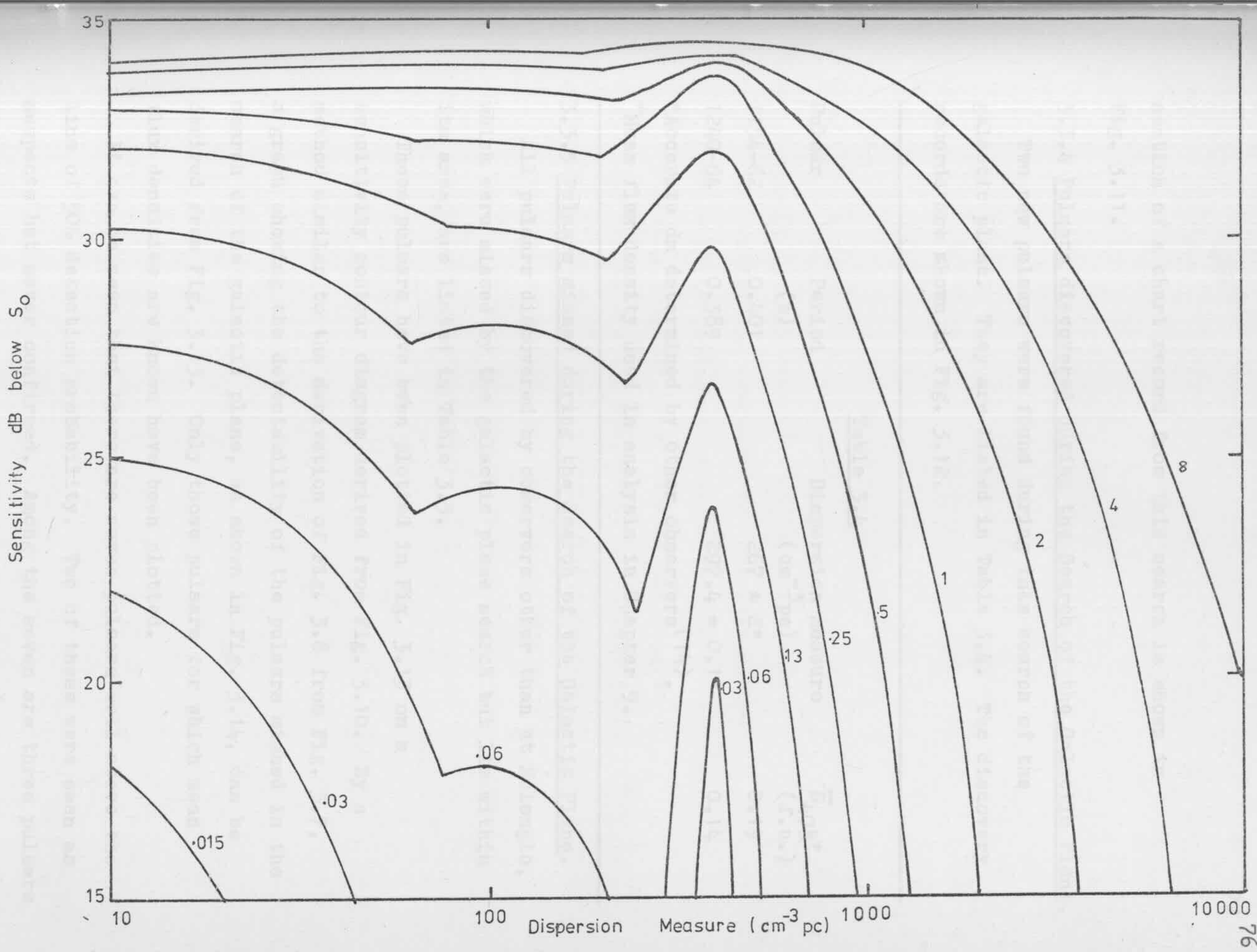
35
30
25
20
15
Sensitivity dB below S_o
10
100
1000
10000
Dispersion Measure (cm^{-3} pc)
·015
·03
·06
·03
·06
·13
·25
·5
1
2
4
8

section of a chart record from this search is shown in Fig. 3.11.

3.3.4 Pulsars discovered during the Search of the Galactic Plane.

Two new pulsars were found during this search of the galactic plane. They are listed in Table 3.4. The discovery records are shown in Fig. 3.12.

Table 3.4

Pulsar	Period (s)	Dispersion measure ($cm^{-3}pc$)	$\bar{S}_{408}$+ (f.u.)
1154-62	0.401	267 ± 2*	0.19
1240-64	0.389	297.4 ± 0.1*	0.14

*Accurate dm determined by other observers[14].

+Mean flux density used in analysis in Chapter 9.

3.3.5 Pulsars missed during the Search of the Galactic Plane.

All pulsars discovered by observers other than at Molonglo, which were missed by the galactic plane search but lie within its area, are listed in Table 3.5.

These pulsars have been plotted in Fig. 3.13 on a sensitivity contour diagram derived from Fig. 3.10. By a method similar to the derivation of Fig. 3.8 from Fig. 3.7, a graph showing the detectability of the pulsars missed in the search of the galactic plane, as shown in Fig. 3.14, can be derived from Fig. 3.13. Only those pulsars for which mean flux densities are known have been plotted.

It can be seen that there are seven pulsars well above the line of 50% detection probability. Two of these were seen as suspects but never confirmed. Among the seven are three pulsars with high dispersion measures (313, 402, 449$cm^{-3}pc$). They

Figure 3.11 A copy of a section of a chart made during the search of the Galactic Plane. The time is indicated every 30 seconds. Starting from the lower edge of the diagram the traces are the outputs of the direct Early beam, the Early beam with the multichannel dispersion remover, and the Centre beam with the two channel dispersion remover, the sequence being repeated twice more.

WARBURTON FRANKI—RIKADENKI CHART No. H25-1 PRINTED IN

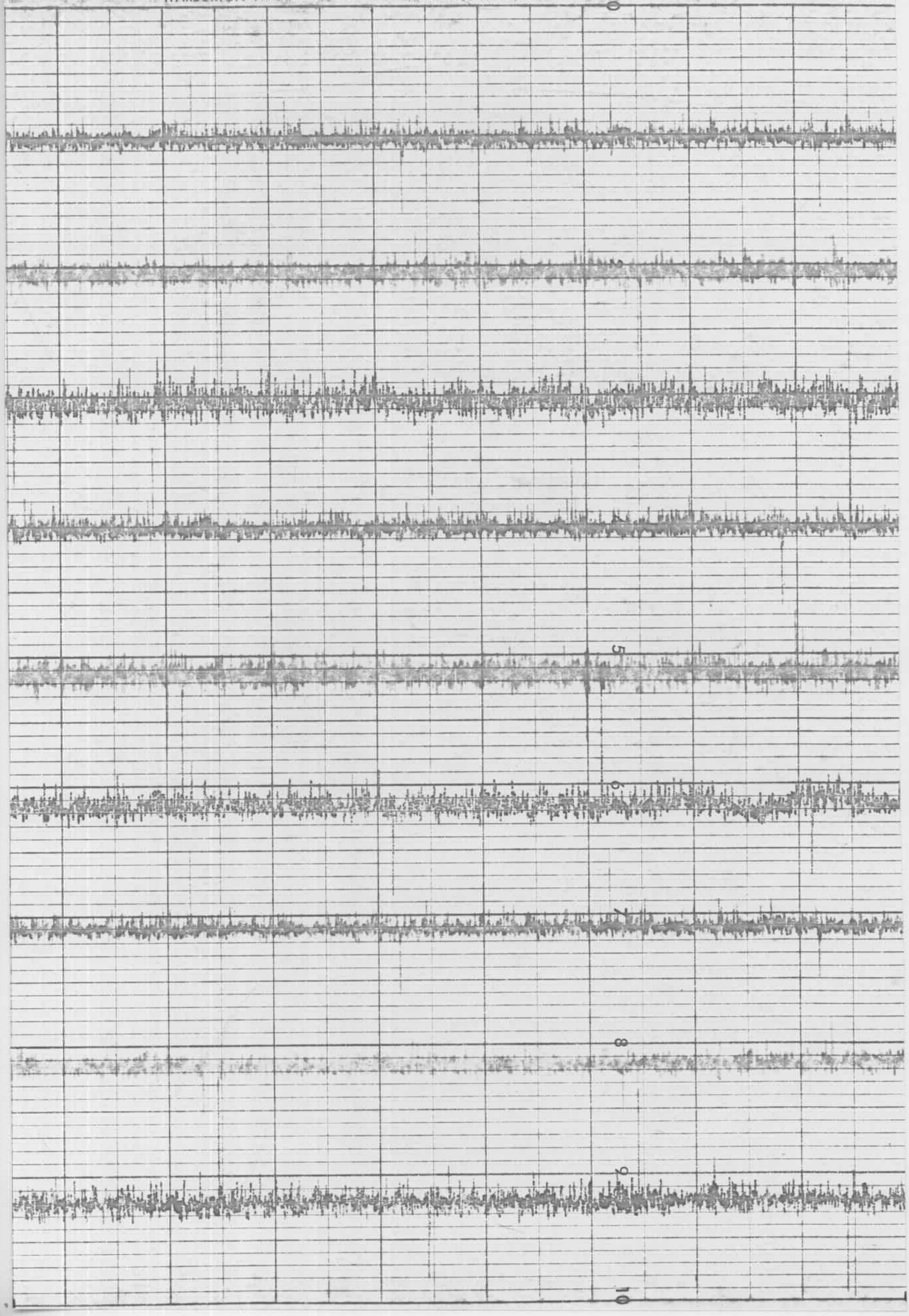

Figure 3.12 Copies of the discovery transits of PSR1154-62 and PSR1240-64. Note the greater response of PSR1154-62 in the dispersion removed channel.

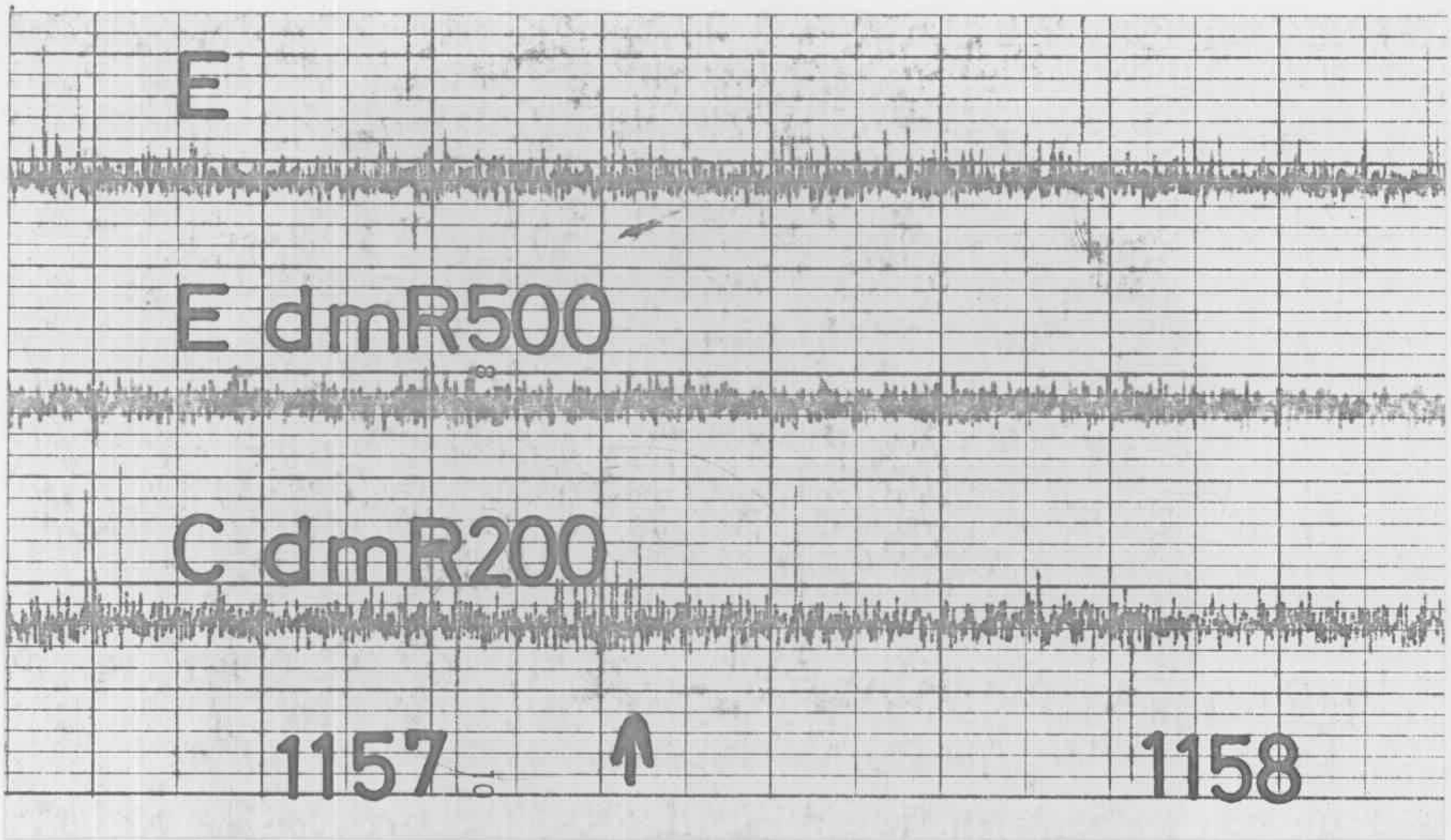

PSR1154-62

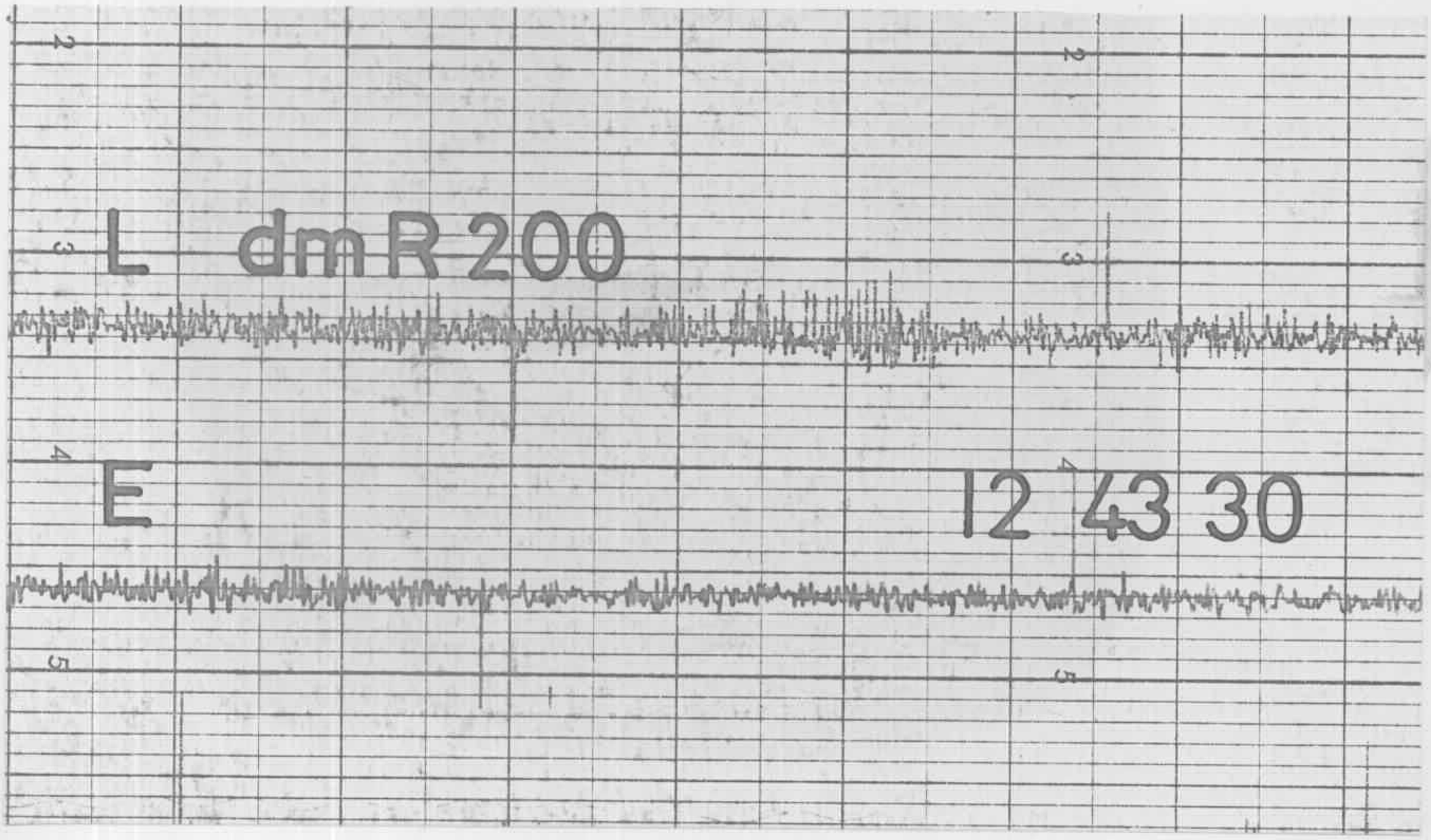

PSR1240-64

Figure 3.13 Contours of equal search sensitivity derived from the sensitivity curves of Figure 3.10, with the pulsars missed by the search superimposed upon them. The different classes of pulsar are indicated as in Figure 3.7.

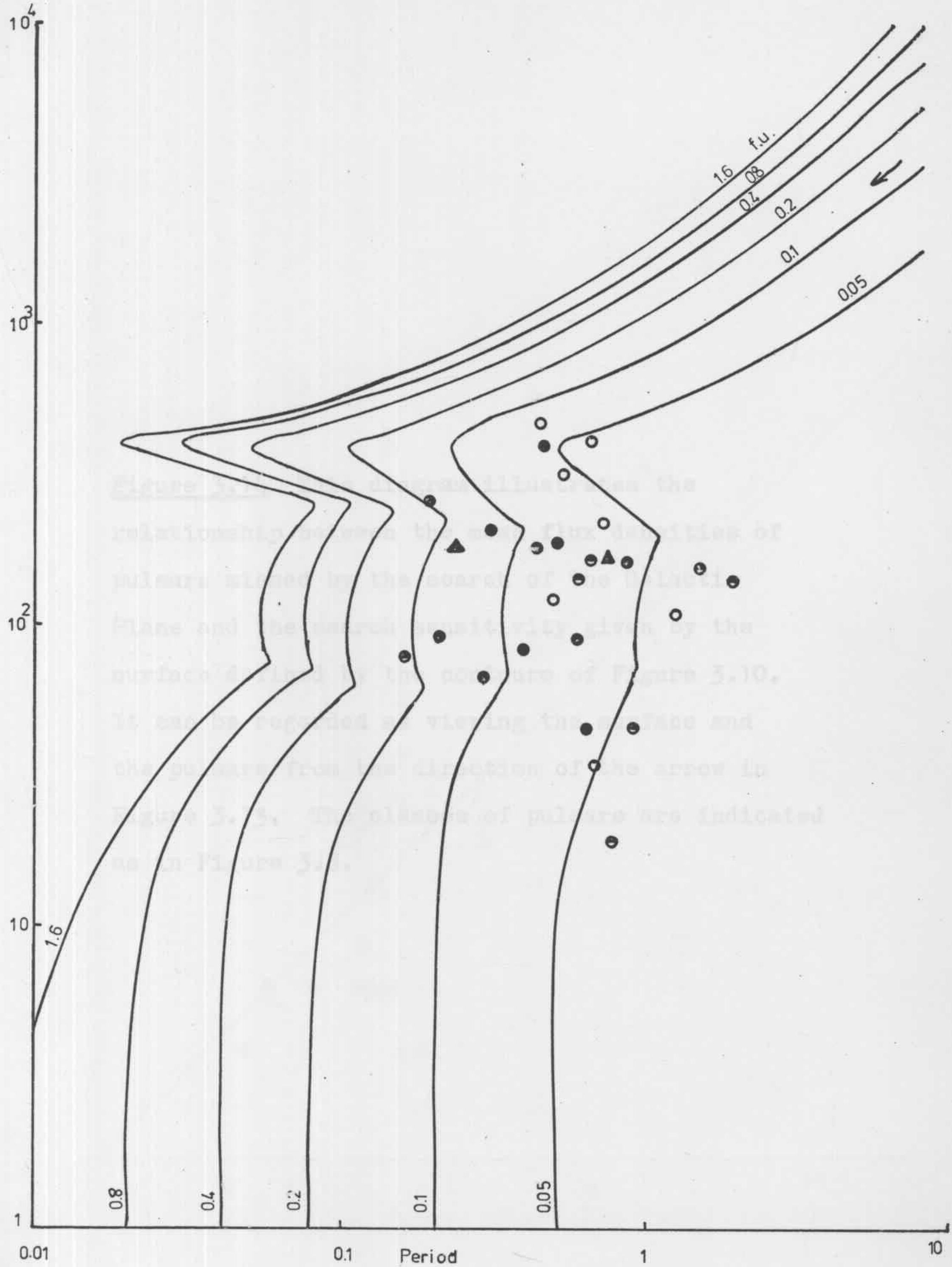
Dispersion Measure
Period
f.u.
1.6
0.8
0.4
0.2
0.1
0.05
10^4
10^3
10^2
10
1
0.01
0.1
1
10

Figure 3.14 This diagram illustrates the relationship between the mean flux densities of pulsars missed by the search of the Galactic Plane and the search sensitivity given by the surface defined by the contours of Figure 3.10. It can be regarded as viewing the surface and the pulsars from the direction of the arrow in Figure 3.13. The classes of pulsars are indicated as in Figure 3.8.

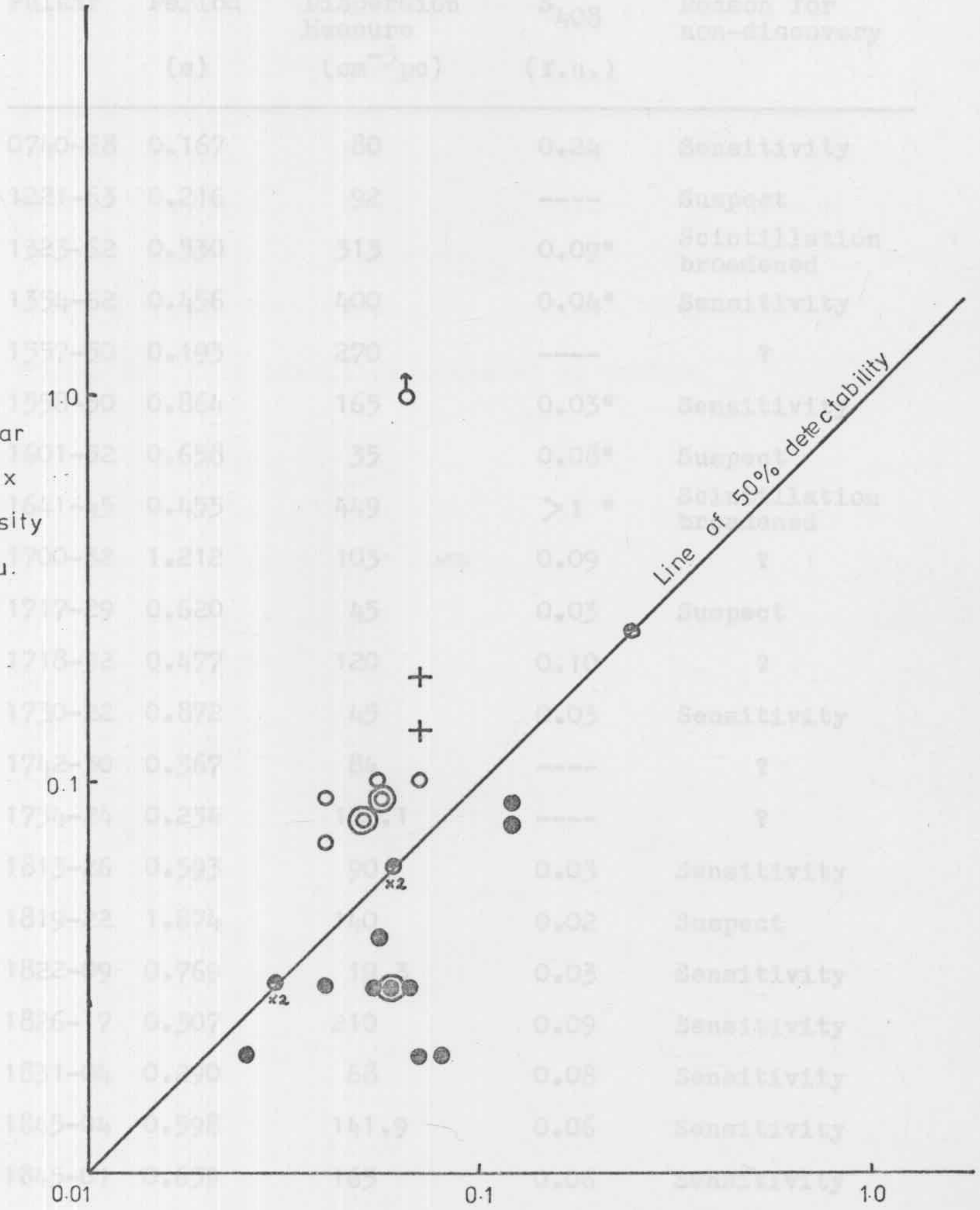
Line of 50% detectability
1.0
0.1
0.01
0.1
1.0
Pulsar flux density f.u.
Pulsar detectability (50%) f.u.
x2
x2

Table 3.5

Pulsars not detected during Search of Galactic Plane.

Pulsar	Period (s)	Dispersion Measure ($cm^{-3}pc$)	S_{408} (f.u.)	Reason for non-discovery
0740-28	0.167	80	0.24	Sensitivity
1221-63	0.216	92	----	Suspect
1323-62	0.530	313	0.09*	Scintillation broadened
1354-62	0.456	400	0.04*	Sensitivity
1557-50	0.193	270	----	?
1558-50	0.864	165	0.03*	Sensitivity
1601-52	0.658	35	0.08*	Suspect
1641-45	0.455	449	>1 *	Scintillation broadened
1700-32	1.212	103	0.09	?
1717-29	0.620	45	0.03	Suspect
1718-32	0.477	120	0.10	?
1730-22	0.872	45	0.03	Sensitivity
1742-30	0.367	84	----	?
1754-24	0.234	188.1	----	?
1813-26	0.593	90	0.03	Sensitivity
1819-22	1.874	140	0.02	Suspect
1822-09	0.769	19.3	0.03	Sensitivity
1826-17	0.307	210	0.09	Sensitivity
1831-04	0.290	68	0.08	Sensitivity
1845-04	0.598	141.9	0.06	Sensitivity
1845-01	0.659	163	0.06	Sensitivity
1846-06	1.451	152	0.03	Sensitivity
1858+03	0.655	402	0.07	Scintillation broadened

Table 3.5 (contd.)

Pulsars not detected during Search of Galactic Plane.

Pulsar	Period (s)	Dispersion Measure ($cm^{-3}pc$)	S_{408} (f.u.)	Reason for non-discovery
1900-06	0.432	180	0.02	Sensitivity
1900+01	0.729	228	0.10	?
1900+05	0.747	166	----	?
1907+02	0.495	190	0.02	Sensitivity

*These are flux densities measured at 750MHz.

were missed because of scintillation broadening of the pulses, so that the pulsed component was a small fraction of the total flux. For example, the detected signal from PSR1641-45 was observed at 408MHz to be approximately a sine wave with a peak to peak flux density only 10% of the total flux density of the pulsar[19].

For three pulsars there are no obvious reasons why they were missed. A close re-examination of search records covering the positions of these three pulsars revealed no trace of any signal which ought to have been, or could possibly be, identified as a pulsar. These pulsars are probably erratic, emitting no detectable pulses during the times of the transits.

These results show that the search of the galactic plane was limited essentially by the sensitivity of the aerial. At high dispersion measures, scintillation broadening was also a major factor in limiting the search sensitivity.

3.4 Conclusion.

Both of the major pulsar searches carried out at Molonglo were limited by the sensitivity of the aerial. If further pulsar searches are to be conducted, the search sensitivity will have to be increased by lower noise preamplifiers or longer integration times.

Within the limits indicated by the sensitivity curves, the multibeamed search was complete apart from the possibility of exceptions due to very erratic behaviour or high scintillation broadening. On the other hand, the search of the galactic plane does not appear to have been complete even after allowing for those pulsars with high scintillation broadening,

and it is likely that a few more pulsars within the sensitivity limits of the galactic search remain to be found.

Examination of the distribution along the galactic plane of pulsars missed by the Molonglo searches, indicates that a significant increase in search sensitivity will lead to the discovery of a significant number of new pulsars.

3.5 References.

1. Large, M. I., and Vaughan, A. E., Mon. Not. R. astr. Soc., 151, 277 (1971).

2. Vaughan, A. E., and Large, M. I., Proc. astron. Soc. Austral., 1, 220 (1969).

3. Internal Report,--Br. P. Hough (1969).

4. Vaughan, A. E., and Large, M. I., Nature, 225, 167 (1970).

5. Vaughan, A. E., and Large, M. I., Mon. Not. R. astr. Soc., 156, 27P (1972).

6. Internal Report,--V. Combe.

7. Davies, J. G., Lyne, A. G., and Seiradakis, J. H., Nature, 240, 229 (1972).

8. Davies, J. G., Lyne, A. G., and Seiradakis, J. H., Nature, 244, 84 (1973).

9. Komesaroff, M. M., Hamilton, P. A., McCulloch, P. M., Ables, J. G., and Cooke, D. J., I. A. U. Circ. No.2505 (1973)

10. Komesaroff, M. M., Hamilton, P. A., McCulloch, P. M., Ables, J. G., and Cooke, D. J., I. A. U. Circ. No.2563 (1973).

11. Goldstein, S. J. Jr., and James, J. T., Ap. J., 158, L179 (1969).

12. Manchester, R. N., Taylor, J. H., and Huguenin, G. R., Nature Physical Science, 240, 74 (1972).

13. Komesaroff, M. M., Ables, J. G., Morris, D., Cooke, D. J., Schwartz, U. J., and Hamilton, P. A., I. A. U. Circ. No. 2201 (1970).

14. McCulloch, P. M., Komesaroff, M. M., Ables, J. G., Hamilton, P. A., and Rankin, J. M., Astrophys. Letters, 14, 169 (1973).

15. Manchester, R. N., Ap. J., 172, 43 (1972).

16. Ables, J. G., Komesaroff, M. M., and Hamilton, P. A., Astrophys. Letters, 6, 147 (1970).

17. Vaughan, A. E., and McAdam, W. B., Nature Physical Science, 241, 138 (1973).

18. Taylor, J. H., Private Communication.

19. Sutton, J. M., and Large, M. I., Private Communication.

Appendix 3A.

The Effects of Pulsar Dispersion Measures and Periods, and the Receiver Bandwidth on Search Sensitivities.

Definition of terms.

$\bar{S}$	mean flux density of pulsar
P	period of pulsar
B	receiver bandwidth (Gaussian)
w_{obs}	observed pulse width
w_p	natural pulse width
$\dot{\nu}$	frequency sweep rate
D	dispersion measure
T	total observing time
τ	observing time constant

Consider the following situation

The r.m.s. uncertainty in determining the level y_1 is

$$\Delta y_1 \propto \left(\frac{B}{\frac{w_{obs}}{P} T} \right)^{\frac{1}{2}}$$

since $\frac{w_{obs}}{P}$. T is that fraction of T for which y_1 is observed.

Similarly $$\Delta y_2 \propto \left(\frac{B}{\left(\frac{P - w_{obs}}{P}\right) T} \right)^{\frac{1}{2}}$$

Hence the r.m.s. uncertainty in $y_1 - y_2$ is

$$\propto B^{\frac{1}{2}} T^{-\frac{1}{2}} P^{\frac{1}{2}} \left[\frac{1}{w_{obs}} + \frac{1}{P - w_{obs}} \right]^{\frac{1}{2}}$$

$$\propto B^{\frac{1}{2}} T^{-\frac{1}{2}} P \left[\frac{1}{(P - w_{obs}) w_{obs}} \right]^{\frac{1}{2}}$$

Now the actual value of $y_1 - y_2$ is

$$\propto \frac{\bar{S}\ P\ B}{w_{obs}}$$

Hence the signal-to-noise ratio for the pulsar is

$$\propto \bar{S}\ B^{\frac{1}{2}}\ T^{\frac{1}{2}}\ w_{obs}^{-\frac{1}{2}}\ (P - w_{obs})^{\frac{1}{2}}.$$

Now $$w_{obs}^2 = w_p^2 + \tau^2 + \left(\frac{B}{\dot{\nu}}\right)^2$$

Hence the signal-to-noise ratio can be written as

$$S/N \propto \bar{S}\, B^{\frac{1}{2}}\, T^{\frac{1}{2}} \frac{\left(\frac{P}{w_p} - \sqrt{1 + \frac{\tau^2}{w_p^2} + \left(\frac{B}{\dot{\nu} w_p}\right)^2}\right)^{\frac{1}{2}}}{\sqrt{1 + \frac{\tau^2}{w_p^2} + \left(\frac{B}{\dot{\nu} w_p}\right)^2}}$$

Now at 408MHz

$$\dot{\nu} = \frac{8180}{D} \qquad \text{(Appendix 6B)}$$

Assuming $P = 20w_p$ for simplicity, we then have

$$S/N \propto \bar{S}\, B^{\frac{1}{2}} T^{\frac{1}{2}} \frac{\left(20 - \sqrt{1 + \frac{1}{p^2}\left[400\tau^2 + \left(\frac{BD}{409}\right)^2\right]}\right)^{\frac{1}{2}}}{\sqrt{1 + \frac{1}{p^2}\left[400\tau^2 + \left(\frac{BD}{409}\right)^2\right]}}$$

This relationship describes the sensitivity as a function of bandwidth, period and dispersion measure for a search procedure consisting of some form of integration.

However the Molonglo search differed in that it was the detectability of individual pulses which was important. This can be approximated by setting T = P in the expression for (S/N).

Two further effects are also present.

Firstly at very long periods, the short transit time of the East-West arm prevents an unlimited increase in sensitivity.

Secondly from a model of pulsar pulse amplitude statistics it is possible to determine the effect on the sensitivity to detection of the number of pulses actually present, related inversely to the period. However, this effect is not significant compared to the overall dependence on period as described above.

Hence, ignoring the effect of limited transit times the (S/N) can be expressed as

$$S/N \propto \bar{S}\, B^{\frac{1}{2}} P^{\frac{1}{2}} \frac{\left(20 - \sqrt{1 + \frac{1}{P^2}\left[400\tau^2 + \left(\frac{BD}{409}\right)^2\right]}\right)^{\frac{1}{2}}}{\sqrt{1 + \frac{1}{P^2}\left[400\tau^2 + \left(\frac{BD}{409}\right)^2\right]}}$$

For the Molonglo search $\tau = 5 \times 10^{-3}$ sec and B = 4MHz, whence

$$S/N \propto \bar{S}\, P^{\frac{1}{2}} \frac{\left(20 - \sqrt{1 + \frac{1}{P^2}\left[0.01 + \left(\frac{D}{102.3}\right)^2\right]}\right)^{\frac{1}{2}}}{\sqrt{1 + \frac{1}{P^2}\left[0.01 + \left(\frac{D}{102.3}\right)^2\right]}}$$

The form of this expression is illustrated in Fig. 3.15. It can be seen that it closely resembles the experimentally derived sensitivity curves shown in Fig. 3.2.

Figure 3.15 Theoretically derived sensitivity curves for a pulsar search sensitive to individual pulses. The parameter on each curve is the period in seconds.

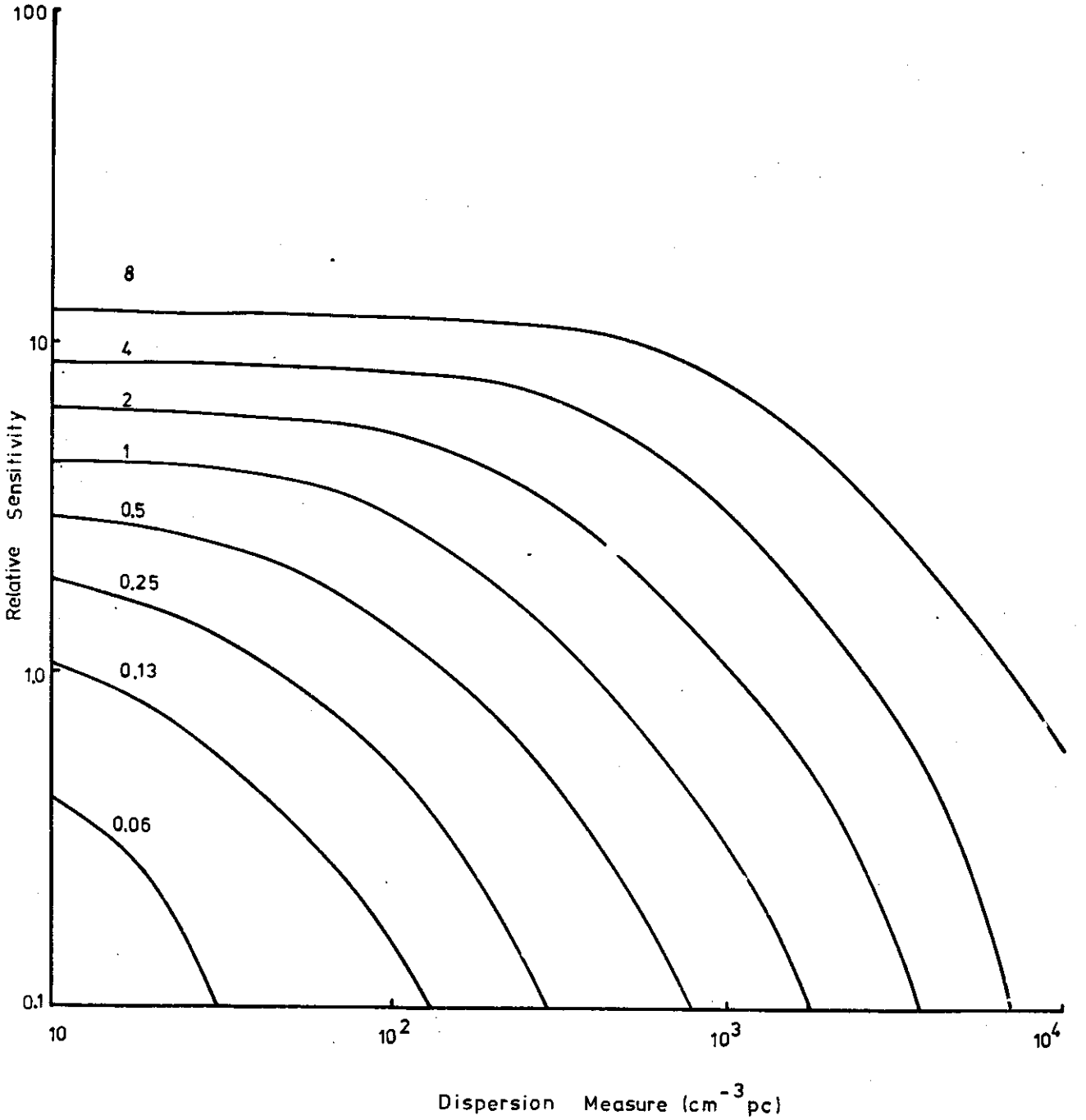
100
10
1.0
0.1
Relative Sensitivity
8
4
2
1
0.5
0.25
0.13
0.06
10
10^2
10^3
10^4
Dispersion Measure (cm^{-3} pc)

Chapter 4

BEAT PERIOD INTEGRATION OF PULSARS.

4.1 Introduction.

A major problem of computerized pulsar data analysis is the amount of computer storage required. For example, one channel of data digitized into 12 bits every millisecond would produce 25 K words (each word = 48 bits) in approximately 100 seconds.

Since the English Electric KDF-9 Computer available for analysis of Molonglo data has a total available storage of 26 K words, a new technique had to be designed so that many channels of pulsar data could be recorded for up to 20 minutes and analysed, space also being allowed for the computer programme. A further constraint imposed was the decision to make the new system compatible with the recording system already available[1] at Molonglo. This involved digitizing the data after integrating for 3 seconds, rather than at a much higher rate. The decision was based on the lack of any immediate prospects for an on site computer and the consideration that the system should interrupt the general running of the telescope as little as possible.

The technique devised with these constraints, which allows pulsar observations with no loss of signal to noise, has been called Beat Period Integration (BPI).

4.2 The Technique of Beat Period Integration.

The basic principle of this method is the gating of the detected output from the aerial at a frequency slightly different to the pulsar repetition frequency using a symmetrical zero-mean gate waveform as shown in Figure 4.1. The output from the gate is integrated over an integral number of gate periods and the integrated output read to magnetic tape. The integration is completed in the computer.

Figure 4.1 The Gating waveform used in the Beat Period Integration system. This can be regarded as the output of the gates for a steady D.C. input. The value for P_g was selected so that $\frac{1}{P_g} - \frac{1}{P_p} = \frac{1}{100 \text{ secs.}}$ where P_p is the pulsar period.

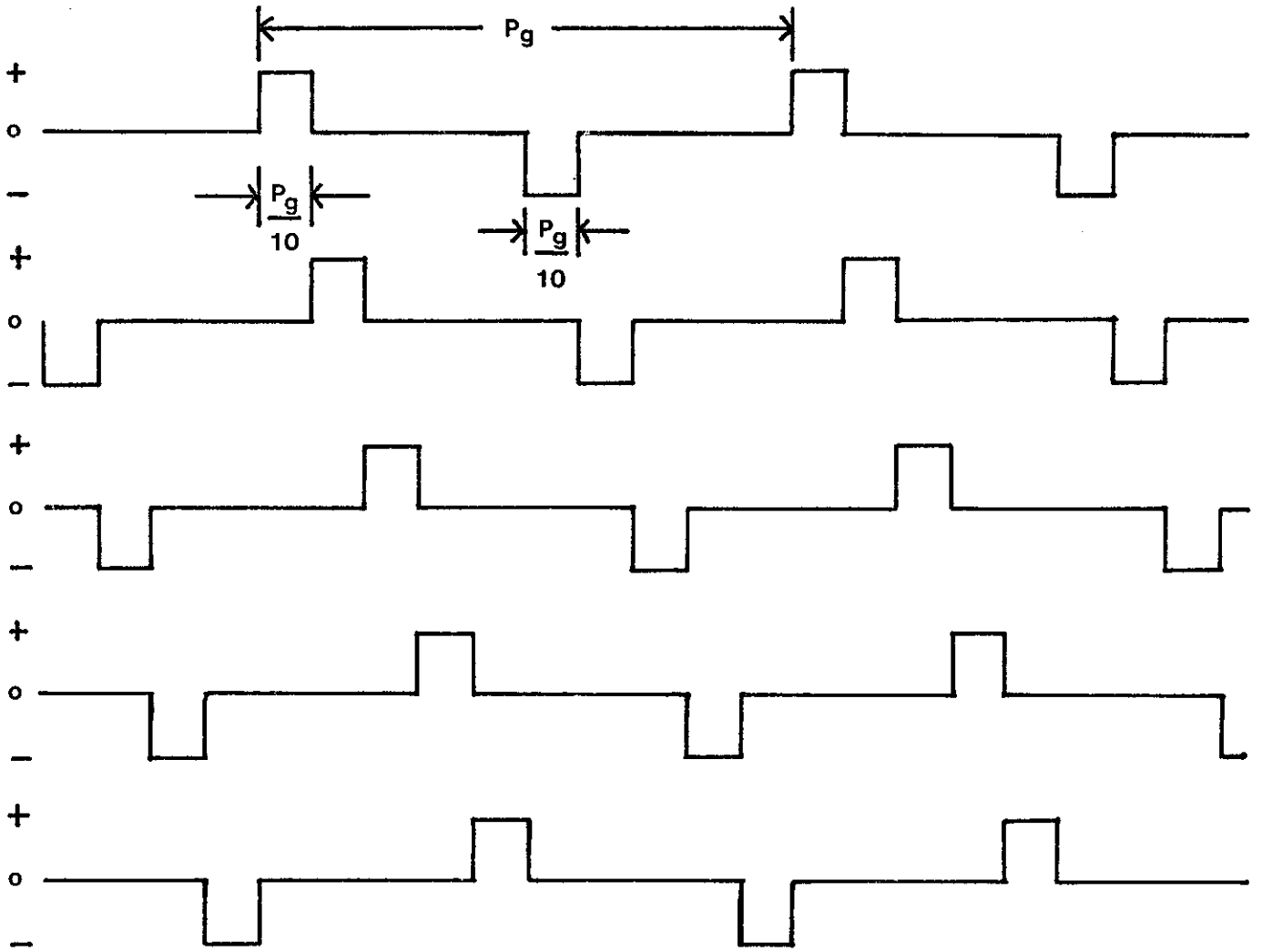
Pg
+
o
–
Pg
10
Pg
10
+
o
–
+
o
–
+
o
–
+
o
–

On each detector there are, in fact, five separate gates offset in phase by steps of 0.1 of the gate period. A steady voltage at the inputs of the five gates would produce the five outputs shown in Figure 4.1.

The output of a gate when a detected signal is applied to its input is shown in Figure 4.2 (a).

The gate is designed to remove effects due to the sky background, or drifting offsets in the detectors, since the positive and negative parts of the gate will cancel, apart from a residual noise signal, when integrated over an integral number of gate periods.

When a pulse is present in the positive part of the gate, the output is as shown in Figure 4.2 (b), and integration over an integral number of gate periods will produce a nett positive voltage.

Similarly, when a pulse is present in the negative part of the gate, the output is as shown in Figure 4.2.(c) and integration will produce a nett negative voltage.

Since the pulsar period P_p is less than the gate period P_g, the relative phase between the pulsar and the gate will slowly change, the pulsar pulse advancing through the gating waveform.

The integrated output from each gate will therefore be as shown in Figure 4.3. The beat period $P = \frac{P_g P_p}{P_p - P_g}$ could be set by an appropriate choice of P_g. It was usually kept near 100 seconds. Since this was much greater than the integration time, which was approximately 3 seconds, there was no loss of sensitivity due to the integration. This output was digitized and read to magnetic tape for analysis in the computer.

Figure 4.2 a) The output of a particular gate with a detected signal on the input.

b) The output of a particular gate with a pulsar present, its pulses being in phase with the + ve part of the gating waveform.

c) The same output with the pulsar pulses in phase with the - ve part of the gating waveform.

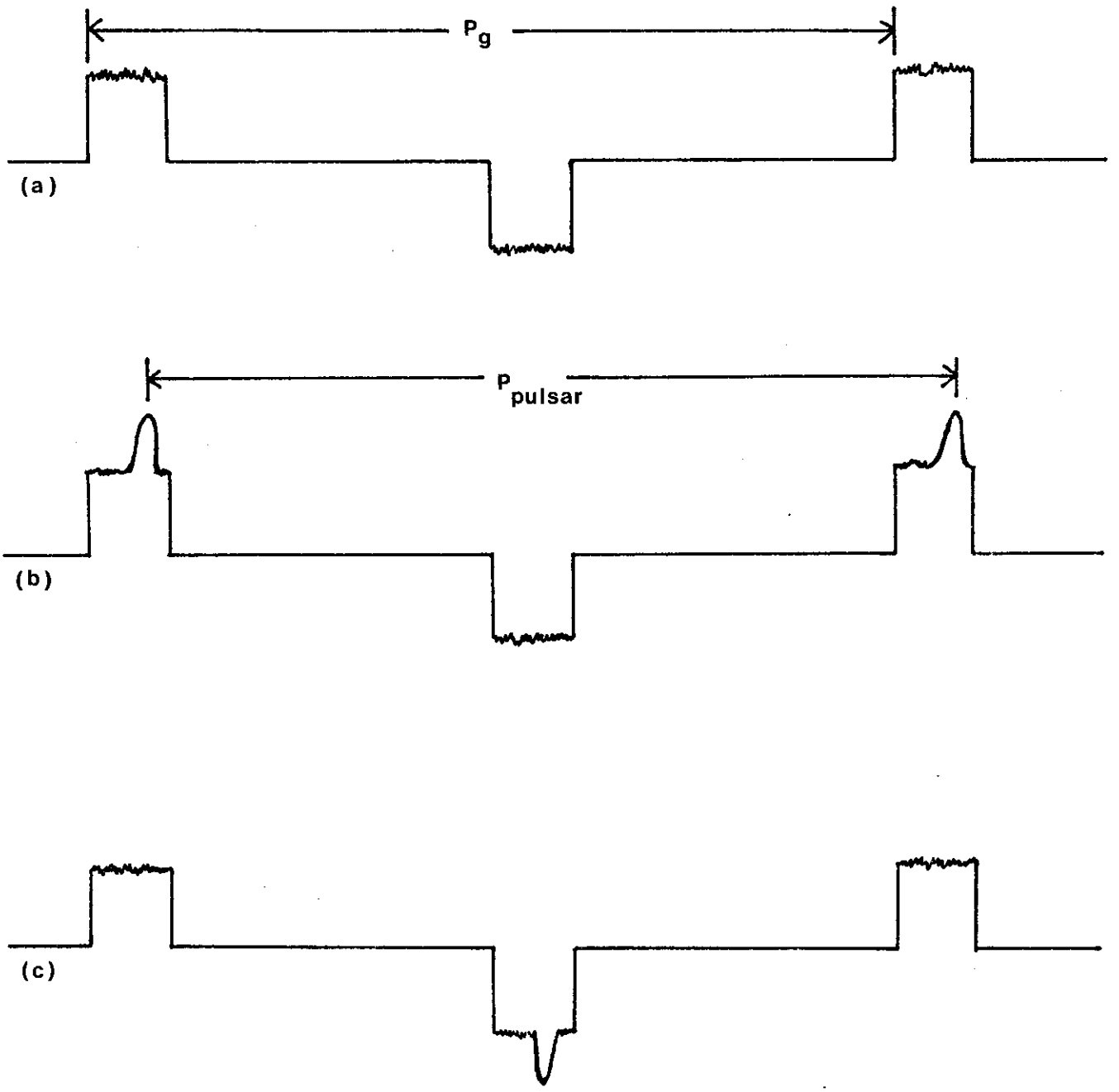
P_g
(a)
P_{pulsar}
(b)
(c)

Figure 4.3 The effect of integrating, for an integral number of gate periods, the outputs displayed in Figure 4.2. b), c). Note the time scale: P ~ 100 seconds. This is the waveform which is digitized for analysis by computer.

$$P = \frac{P_g \; P_p}{|P_p - P_g|}$$

The particular waveform shown has been used before[2] for pulsar work. In this case, however, the phase of the output waveform was measured over 12 hours, and from a knowledge of the motion of the earth, the pulsar position was obtained from the phase variation. This is quite different to the use made of this technique as described in 4.4 for declination measurements.

4.3 Equipment.

4.3.1 Detectors.

The detectors were of the self-multiplication type[3] to give true power linearity (±2%) over a wide dynamic range. A circuit diagram is shown in Figure 4.4. The R.F. signal was the 5.5 MHz 2nd I.F. of the Molonglo Cross. The post-detection time constant was set at 0.1 msec.

4.3.2 The Gating System.

4.3.2.1 The Period Generator.

The period generator, built by Dr. A. J. Turtle, allowed any period from 1 μsec to 1 second, as set up on thumbwheel switches, to be derived from a standard 1 MHz signal from a Hewlett-Packard Counter. As used in this system, the period generator range was equivalent to a range of 10^{-5} sec to 10 seconds in gate period.

4.3.2.2 Control Circuitry.

The control circuitry consisted of a decade counter to control the gates and a setable counter to control the integration time and start the digitizing cycle. A block diagram is shown in Figure 4.5. The setting of the counter (N) was such that $NP_g \sim 3$ seconds.

Figure 4.4 The circuit of the multiplier type detector used on the beams of the North-South arm for pulsar work. The four transistors were mounted on a single chip. The input to the device was the 5.5MHz 2nd I.F. The output was fed to a differential amplifier.

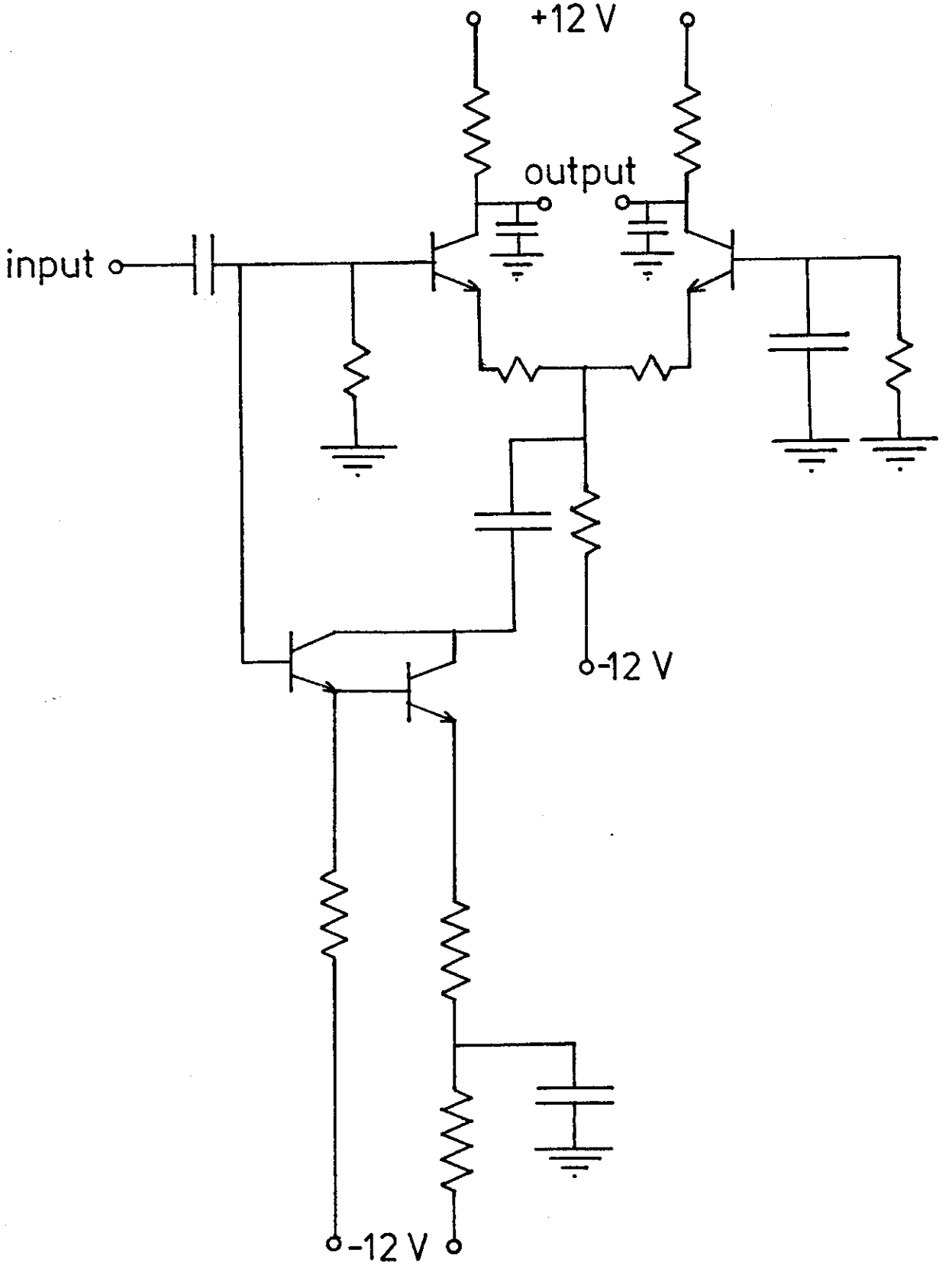
+12 V
output
input
-12 V
-12 V

Figure 4.5 A block diagram of the control circuitry. This generated the gating control signals and the integration time.

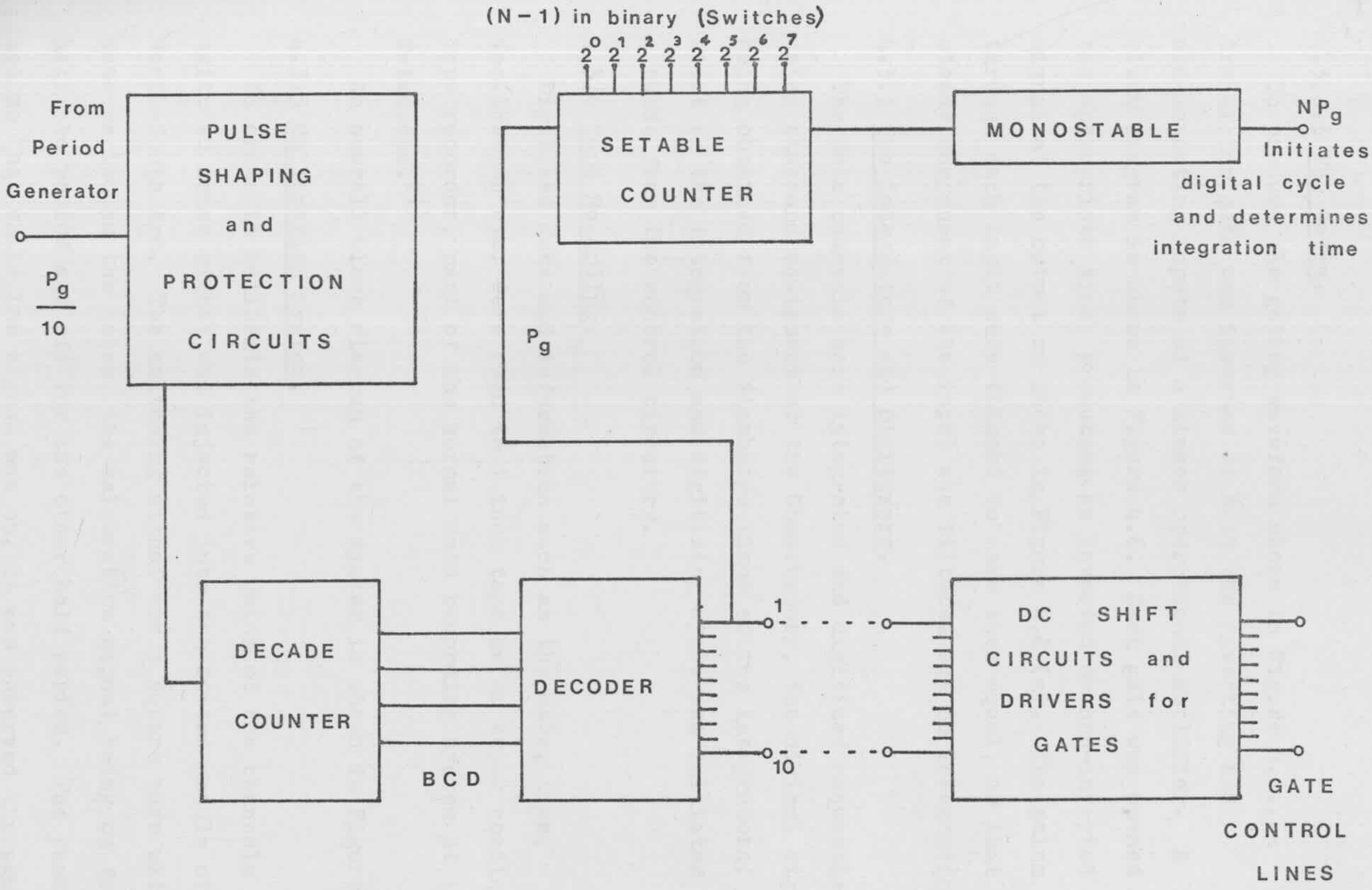
(N – 1) in binary (Switches)
2^0 2^1 2^2 2^3 2^4 2^5 2^6 2^7
From Period Generator
$\frac{P_g}{10}$
PULSE SHAPING and PROTECTION CIRCUITS
SETABLE COUNTER
MONOSTABLE
NP_g
Initiates digital cycle and determines integration time
P_g
DECADE COUNTER
BCD
DECODER
1
10
DC SHIFT CIRCUITS and DRIVERS for GATES
GATE CONTROL LINES

4.3.2.3 The Gates.

To produce the gating waveform shown in Figure 4.1., a transistor gate was inserted at both the inverting and non-inverting inputs of a linear operational amplifier. A block diagram is shown in Figure 4.6. Each gate was opened at the appropriate time, producing an inverted or non-inverted signal at the output as shown in Figure 4.2 (a). The gains through each input were trimmed to make them equal, so that the steady component of the input was filtered out on integration.

4.3.3 The Integrators and Digitizers.

The data channels were integrated and digitized sequentially using standard equipment at the Observatory, the digital signals being obtained from the discharge times of the integrators. The start of the integration and digitizing cycle was initiated by a pulse from the control circuitry.

4.3.4 Tape Recording.

Digitized data and information such as the date, time, declination etc. were read to 1 inch tape on an Ampex continuous tape recorder, part of the normal data recording system at the Telescope.(1)

An overall block diagram of the system is shown in Figure 4.7.

4.3.5 Calibration System.

In order to calibrate the relative gains of the channels a switched noise signal was injected into the centre module of the North-South Arm. The switching signal was a square wave with the same period as the gates, the calibration signal being on for half the period and off for the other half period. The phase was set so that while the signal was on, it was observed through all

Figure 4.6 A block diagram of the gating circuit used to generate the waveform of Figure 4.1.

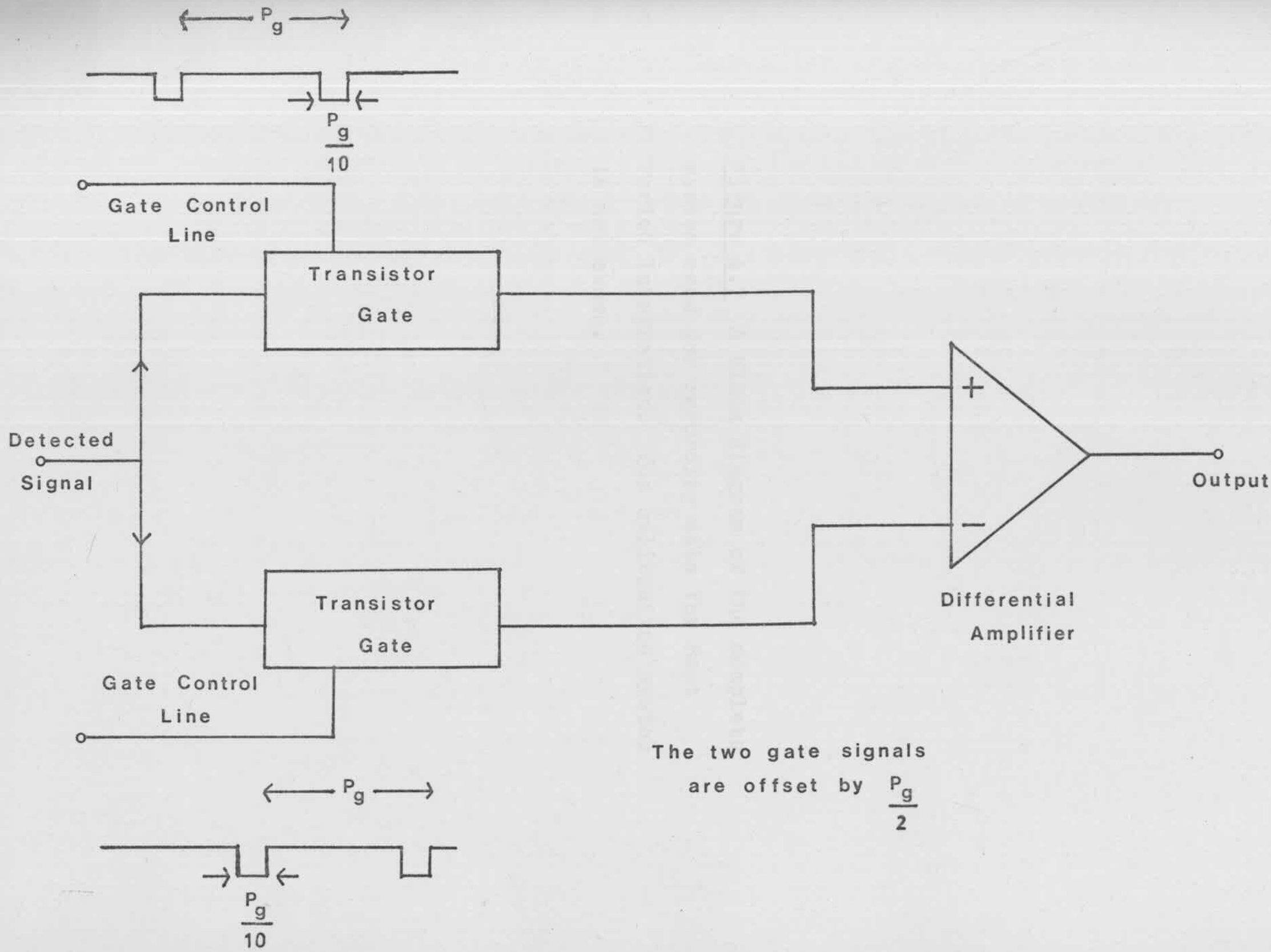

The two gate signals are offset by $\frac{P_g}{2}$

Figure 4.7 A block diagram of the complete system used for recording data for Beat Period Integration. The calibration system is not shown.

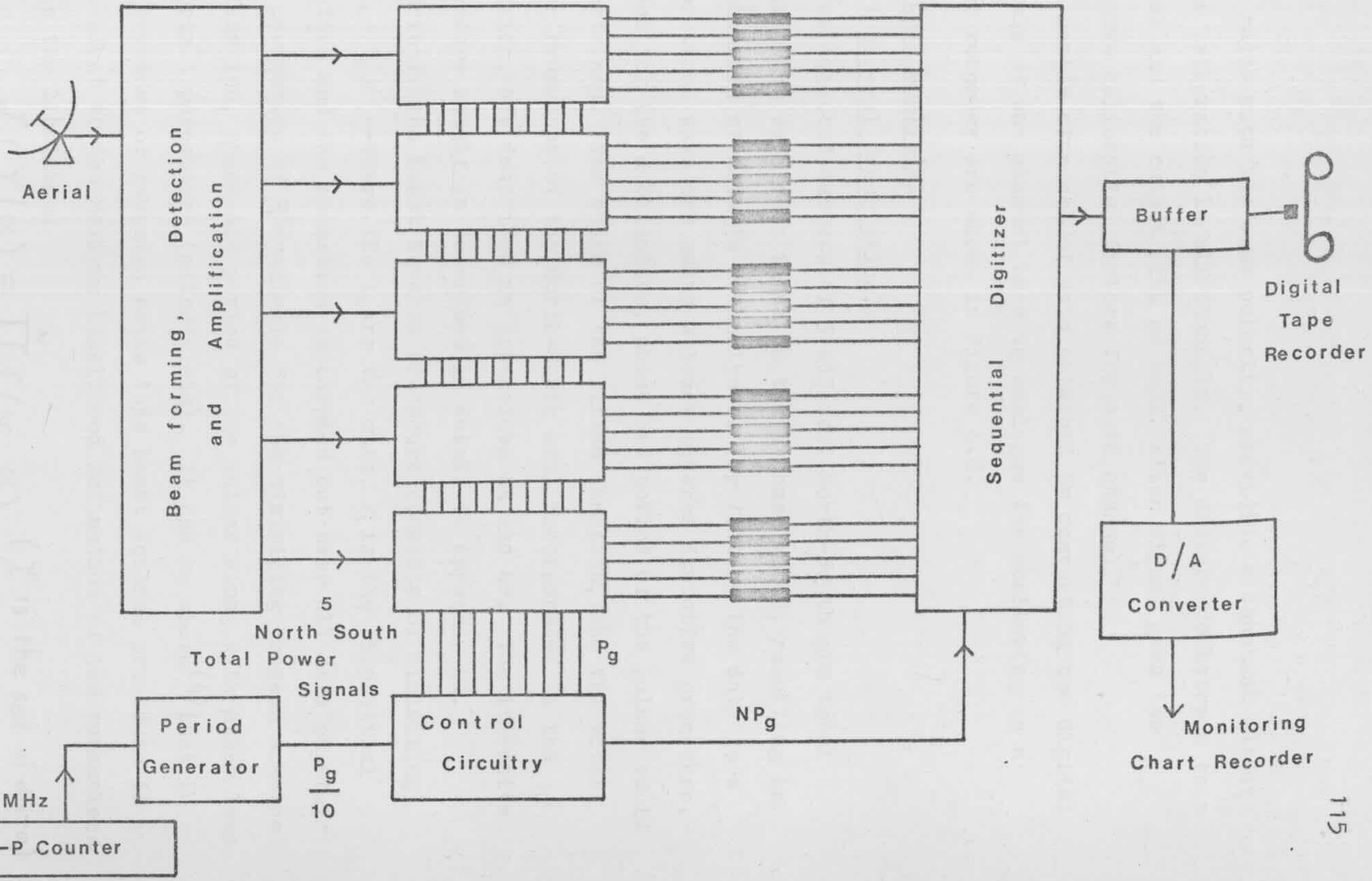
Gate Circuits
Integrators
Aerial
Beam forming, Detection and Amplification
Sequential Digitizer
Buffer
Digital Tape Recorder
D/A Converter
Monitoring Chart Recorder
5
North South Total Power Signals
P_g
NP_g
Period Generator
$\frac{P_g}{10}$
Control Circuitry
1 MHz
H-P Counter

five gates with the same polarity, providing a constant output after integration in all channels. The difference between this signal and the output with no calibration signal gave the relative calibration factors for each channel.

A sample of a set of data obtained by converting the digital signals of one channel back to analogue for monitoring on a chart recorder are shown in Figure 4.8.

4.4 Data Analysis.

4.4.1 General Description.

The detected outputs of 5 adjacent North-South arm total power beams were each input to the 5-phase gates, resulting in 25 channels of data to be analysed. By fitting the data to a theoretical waveform using a least squares iterative procedure, values for the declination, phase and period of the pulsar could be obtained. The shape of the fitted function, and the total power beamshape of the North-South arm, incorporated in the function, are described in Appendices 4A and 4B. The iterative procedure itself is described in detail in Appendix 4E.

Briefly the Least Squares procedure consists of minimizing $\sum_i (Y_i - F_i)^2$ --where the Y_i are the data, F_i is the theoretical waveform and the summation is carried out over all data points. The parameters of F_i available for the minimizing process are the declination, phase and period of the pulsar along with other less important parameters (offsets etc). It can be shown[4] that in the presence of gaussian noise this Least Squares procedure is equivalent to the Maximum Likelihood Estimation of the parameters since the likelihood

$$\mathcal{L}(\underline{Y}|\underline{\alpha}) = \prod_{i=1}^{N} f(Y_i, \underline{\alpha})$$

($\underline{Y}$ is the set of data) ($\underline{\alpha}$ is the set of parameters)

Figure 4.8 For monitoring purposes one of the digital channels was output via a D - A convertor onto a chart recorder. Illustrated is a transit of PSR0833-45. The length of the data itself is about 20 minutes. The record shows a period of several minutes during which the equipment was checked, a calibration period, a period to establish a zero level for the calibration, and lastly the data. The spike at the end of each digital reading was caused by the digital transition appearing through the D - A convertor.

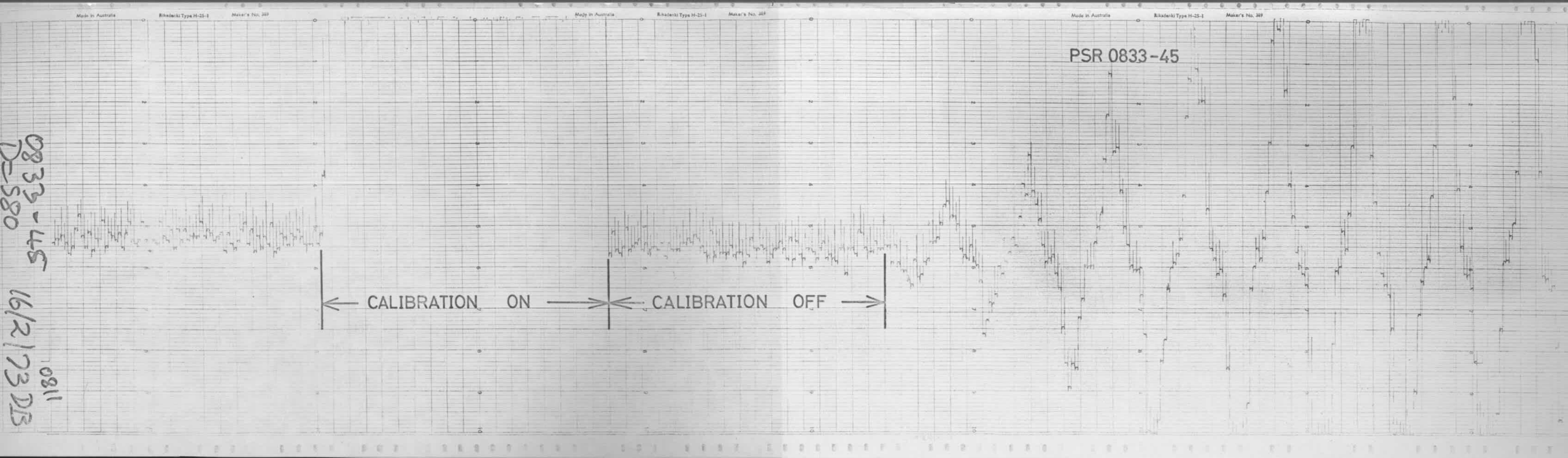
Made in Australia
Rikadenki Type H-25-1
Maker's No. 369
PSR 0833-45
CALIBRATION ON
CALIBRATION OFF

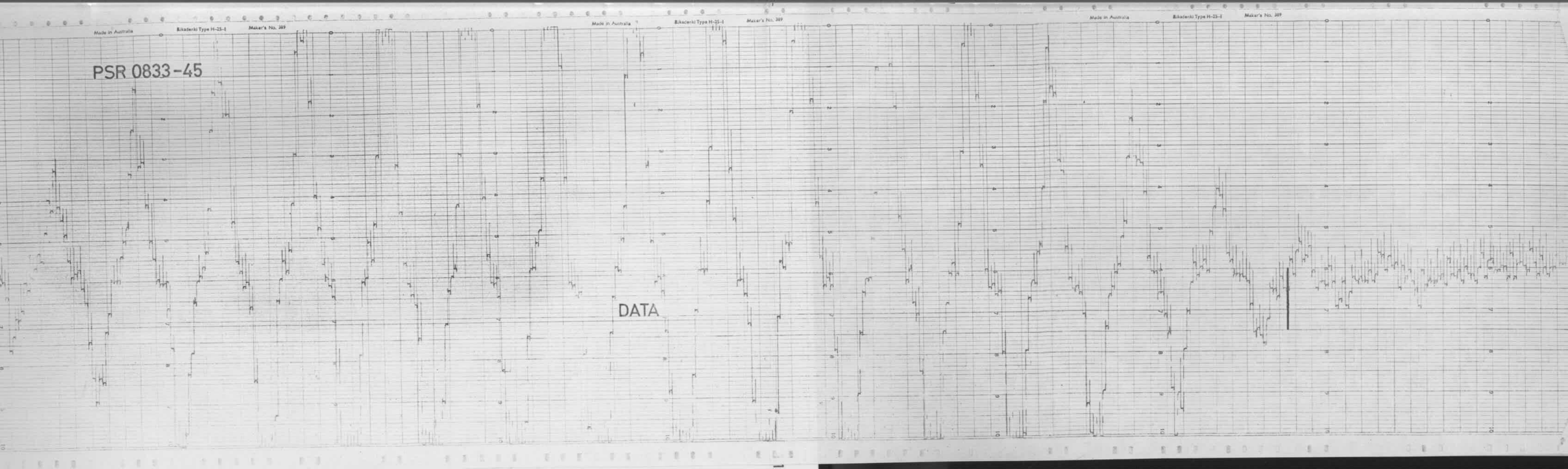
Made in Australia
Bikadenki Type H-25-I
Maker's No. 389
PSR 0833-45
DATA

where $f(Y_i, \underline{\alpha}) = e^{-\frac{1}{2\sigma^2}(Y_i - F_i(\underline{\alpha}))^2}$ (Gaussian probability fn)

ie $\mathcal{L}(\underline{Y}/\underline{\alpha}) = e^{-\frac{1}{2\sigma^2}\sum_1^N (Y_i - F_i(\underline{\alpha}))^2}$

or $\ln \mathcal{L} = -\frac{1}{2\sigma^2}\sum_1^N (Y_i - F_i)^2$

and maximizing ln L (or L) is the same as minimizing $\sum_1^N (Y_i - F_i)^2$.

4.4.2 Initial Parameter Values.

Since the theoretical function depends in a complicated manner on the minimization parameters, there are no explicit solutions to the Least Squares conditions

$$\frac{\partial}{\partial \alpha_j}\left(\sum_i (Y_i - F_i)^2\right) = 0$$

ie $$\sum_i (Y_i - F_i)\frac{\partial F_i}{\partial \alpha_j} = 0 \quad \text{(j equations)}$$

Hence the iteration is necessary, and this implies the provision of initial values to start the procedure. Several methods were applied to obtain these.

a) guessed values were used

b) then better values were determined from the data, before entering the Least Squares procedure.

The guessed values were not completely random in the cases of declination and period. However, since nothing was known about pulsar phase it was eventually found necessary to step the pulsar phase by 0.1 periods until the value of phase was found for which $\sum_i (Y_i - F_i)^2$ was smallest.

Two procedures were used to determine better initial values. They were necessary to reduce the number of iterations in the Least Squares procedure since each iteration occupied about 30sec of computer time. The "Simplex" procedure, described in Appendix 4C, was quite successful though slow in some cases,

while the Convolution procedure, described in Appendix 4D, was always fast and successful. The latter eventually supplanted the "Simplex" procedure despite the drawback that some analysis by hand was necessary before the Least Squares procedure was entered.

4.5 Computing.

4.5.1 The Computing Facility.

The computer used for analysis of the data was the English Electric KDF-9 in the Basser Computing Centre in the Sydney University. The available store for data and programme was 26 K words, each word being 48 bits in length. Full floating point arithmetic was available and a comprehensive subroutine library was stored on a magnetic tape. The analysis programme itself was stored on magnetic tape and facilities were provided for editing and correcting the programme during its development.

4.5.2 The Analysis Programme.

A detailed description and flow chart of the computer programme is to be found in Appendix 4F. The number of 12 bit data points used in each transit analysis was 10,000, being composed of 400 3second samples (=20 minutes, North-South Total Power transit time) on 25 channels. This was stored as quarter words along with other data such as time, date, declination etc, occupying a total of 4000 words of store. The complete analysis, programme and data, used 22 K of store. Most of the computation was done in floating point format for simplicity, and for compatibility with the library subroutines available.

The computing time varied between 5 minutes and 15 minutes,

depending on how many iterations were necessary.

4.5.3 Programme Input/Output.

Observational data was stored on magnetic tape, as was the analysis programme itself. Access to the programme was obtained by reading in a paper tape, while control parameters as described in Appendix 4F were also read in on paper tape. The results of each iteration were output on line printer, as was the final output after the last iteration. The Fourier transform of the Amplitude Function (Appendix 4A) was also printed out to help with the detection of periodicities in the pulsar amplitude. A sample output page is shown in Appendix 4F.

4.6 References.

1. Large, M. I., and McAdam, W. B., C. S. I. R. O. Symposium--The Collection and Processing of Field Data (1966).

2. Ryle, M., and Bailey, Judy A., Nature, 217, 907 (1968).

3. Frater, R. H., The Review of Scientific Instruments, 35, 810 (1964).

4. Parrat, L. G., "Probability and Experimental Errors in Science", p135. John Wiley and Sons, Inc., New York. (1961).

Appendix 4A.

The Fitted Function and its Derivatives.

Notation.

$F_L = F_{cK}$	Fitted Function L = 1,...., 10000 all data points c = 1,..., 25 all channels K = 1,...., 400 all 3sec intervals
A_K	Pulsar Amplitude at time t_K
f_{cK}	The shape of the Fitted Function
B_c	The Background level (offset) for channel c
G_{cK}	The North South Total Power Beam Response
H_{cK}	The Result of convolving the Pulsar signal with the gating system.
W_p	Pulse Width
P	Pulsar Period
P_g	Gate Period
D	Declination Number (See Appendix 4B for Definition)
T	The North South Fan Beam Transit time.
ϕ	The Phase of H_{1K} with respect to T
F	The Difference between the Gate frequency and the Pulsar Repetition frequency (= Beat freq.)
t_K	The time of occurrence of each integration period
ϕ_c	The phase of H_{cK} with respect to T
ϕ_{cK}	The phase of point t_K in H_{cK} with respect to T.

The Function.

The fitting function was given the following form

$$F_L = F_{CK} = A_K f_{CK} + B_C$$

where $f_{CK} = G_{CK} H_{CK}$

The derivation of G_{CK} is given in Appendix 4B.

It is quoted here for completeness

$$G_{CK} = \frac{e^{-\frac{1}{2\sigma_1^2} X_{CK}^2}}{1 + a X_{CK}^6} \cdot e^{-\frac{1}{2\sigma_2^2} Y_K^2}$$

where $$X_{CK} = \frac{\lambda}{40L}(D_C - D) + \frac{(t_K - T)^2}{2} \sin\Delta \cos\delta$$

and $$Y_K = (t_K - T)\cos\delta$$

The function H_{CK} is a series of straight line segments, the slope and position of which depend on the time t_K, the phase ϕ_C of the channel, the pulse width and the period of the pulsar, and the difference between the pulsar and gate frequencies.

Typical forms for H_{CK} are shown in Figure 4.9.

These forms have been derived by making the assumption that the pulsar pulses are rectangular. This is of course not correct. Better approximations would be to regard them as triangular or gaussian shaped, for example. However, the main effect of making these approximations would be to reduce the formal errors of the fit rather than alter the final values of the fitted parameters. Strictly, a different shape should have been used for each pulsar--but even then the pulse shapes are variable from pulse to pulse. It was felt, therefore, that the computational simplicity of the rectangular pulse approximation outweighed the marginal improvement to be gained in the formal errors of the procedure. A further justification for this was the fact that the formal declination errors were, in general, smaller than the uncertainties in the pointing calibration of the aerial.

Figure 4.9 Typical forms for H_{ck}. Initially the slant edges of the waveform decrease their slopes with increasing w_p until the second situation is reached ($w_p = \frac{P}{10}$) at which the slopes remain constant while the widths of the non-zero sections increase. Note that this assumes a rectangular pulsar pulse.

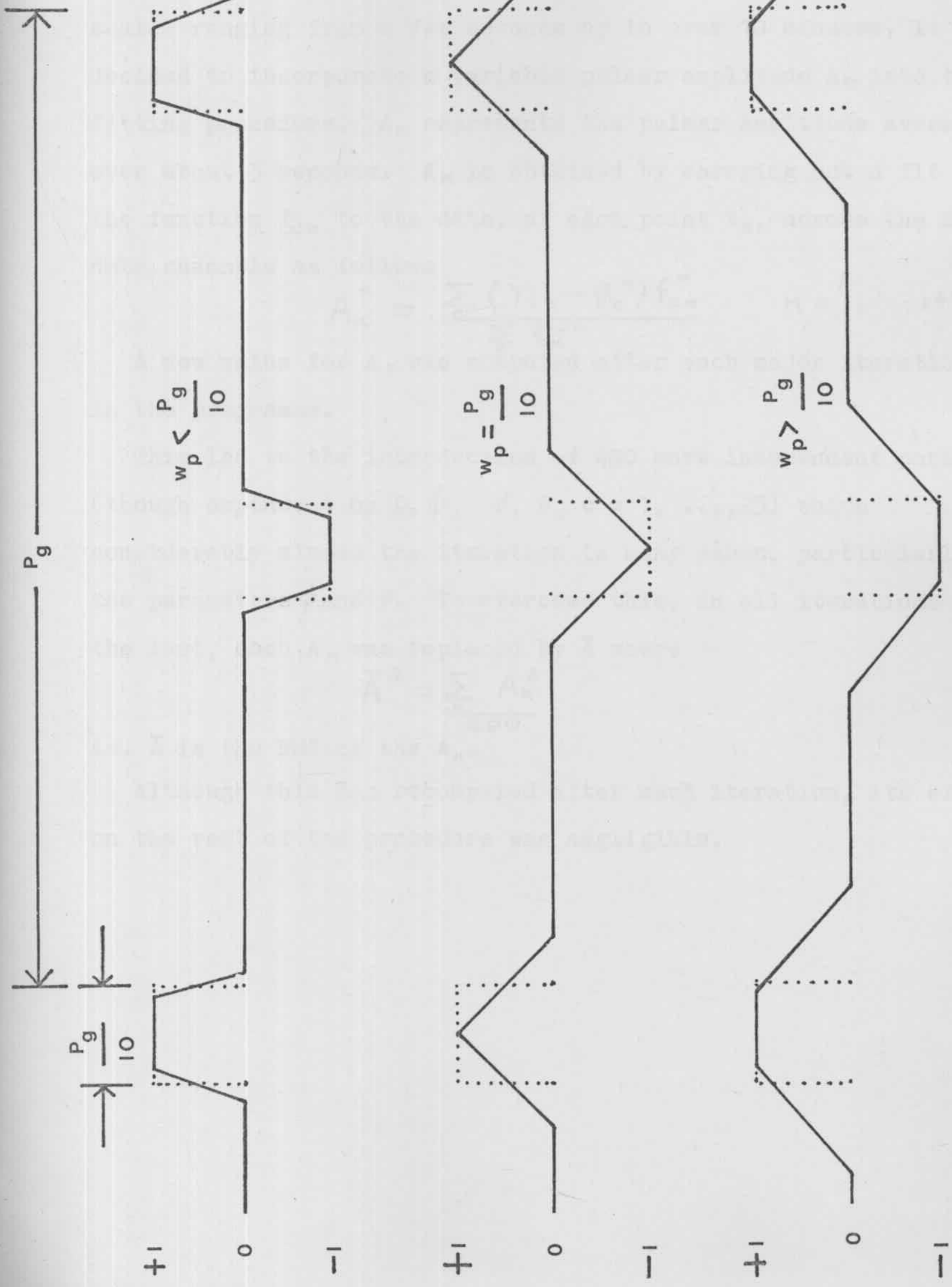
P_g
$\frac{P_g}{10}$
$w_p < \frac{P_g}{10}$
$w_p = \frac{P_g}{10}$
$w_p > \frac{P_g}{10}$
+
0
−

Pulsar Amplitude Function.

Because of the variability of pulsar amplitudes over time scales ranging from a few seconds up to over 10 minutes, it was decided to incorporate a variable pulsar amplitude A_K into the fitting procedure. A_K represents the pulsar amplitude averaged over about 3 seconds. A_K is obtained by carrying out a fit of the function f_{cK} to the data, at each point t_K, across the 25 data channels as follows

$$A_K^\circ = \frac{\sum_c (Y_{cK} - B_c^\circ) f_{cK}^\circ}{\sum_c f_{cK}^{\circ 2}} \qquad K = 1, \ldots, 400$$

A new value for A_K was computed after each major iteration in the programme.

This led to the introduction of 400 more independent parameters (though dependent on D, ϕ, F, B_c c = 1, ...,25) which considerably slowed the iteration in many cases, particularly in the parameters ϕ and F. To overcome this, in all iterations but the last, each A_K was replaced by $\bar{A}$ where

$$\bar{A}^2 = \frac{\sum_K A_K^2}{400}$$

ie. $\bar{A}$ is the RMS of the A_K.

Although this was recomputed after each iteration, its effect on the rest of the procedure was negligible.

Derivatives of the Function.

The parameters of the fitting procedure are D, ϕ, F, and B_c. Derivatives of F_{ck} with respect to these parameters are required in the fitting procedure. They were computed as follows:

(1) $$\frac{\partial F_i}{\partial D} = \frac{\partial F_{ck}}{\partial D} = A_k H_{ck} \frac{\partial G_{ck}}{\partial D}$$

ie $$\boxed{\frac{\partial F_{ck}}{\partial D} = A_k . H_{ck} . \frac{\lambda}{40L} . X . \left[\frac{1}{\sigma_1^2} + \frac{6aX^4}{1+aX^6}\right] . \frac{e^{-\frac{X^2}{2\sigma_1^2}} . e^{-\frac{Y^2}{2\sigma_2^2}}}{1+aX^6}}$$

(2) $$H_{ck} = H_{ck}(\phi_{ck})$$

and $$\phi_{ck} = 2\pi F(t_k - T) - \phi_c$$

$$\frac{\partial H_{ck}}{\partial t_k} = \frac{\partial H_{ck}}{\partial \phi_{ck}} . \frac{\partial \phi_{ck}}{\partial t_k}$$

$$= 2\pi F \frac{\partial H_{ck}}{\partial \phi_{ck}}$$

$$= -2\pi F \frac{\partial H_{ck}}{\partial \phi_c}$$

$$= -2\pi F \frac{\partial H_{ik}(\phi_{ik} - \frac{2\pi n}{10})}{\partial \phi}$$ n is integer part of $\frac{c}{5}$

$$\therefore \frac{\partial H_{ck}}{\partial \phi} = \frac{\partial H_{ik}(\phi_{ik} - \frac{2\pi n}{10})}{\partial \phi}$$

$$= -\frac{1}{2\pi F} \frac{\partial H_{ck}}{\partial t_k}$$

ie $$\boxed{\frac{\partial F_{ck}}{\partial \phi} = -\frac{1}{2\pi F} A_k G_{ck} \frac{\partial H_{ck}}{\partial t_k}}$$

(3) $$\frac{\partial H_{ck}}{\partial t_k} = 2\pi F \frac{\partial H_{ck}}{\partial \phi_{ck}}$$

$$= 2\pi F \frac{\partial H_{ck}}{\partial F} \frac{1}{2\pi(t_k - T)}$$

$$= \frac{F}{t_k - T} \frac{\partial H_{ck}}{\partial F}$$

$$\therefore \frac{\partial H_{ck}}{\partial F} = \frac{\partial H_{ik}(\phi_{ik} - \frac{2\pi n}{10})}{\partial F} = \frac{t_k - T}{F} \frac{\partial H_{ck}}{\partial t_k}$$

ie. $$\boxed{\frac{\partial F_{ck}}{\partial F} = A_k G_{ck} \frac{t_k - T}{F} \frac{\partial H_{ck}}{\partial t_k}}$$

The derivatives of H_{ck} are the slopes of the various line segments composing H_{ck}.

(4) The derivatives with respect to the channel offsets are as follows:

$$\boxed{\begin{aligned} \frac{\partial F_{ck}}{\partial B_d} &= 1 \qquad c = d \\ &= 0 \qquad c \neq d \end{aligned}}$$

Appendix 4B.

The North-South Total Power Beamshape.

The two coordinates of position in the beam of the North-South arm are the cone angle around the North-South arm as axis $(90 - \phi)$, and the cone angle around an axis at right angles to the North-South arm in an East-West direction $(90 - \psi)$.

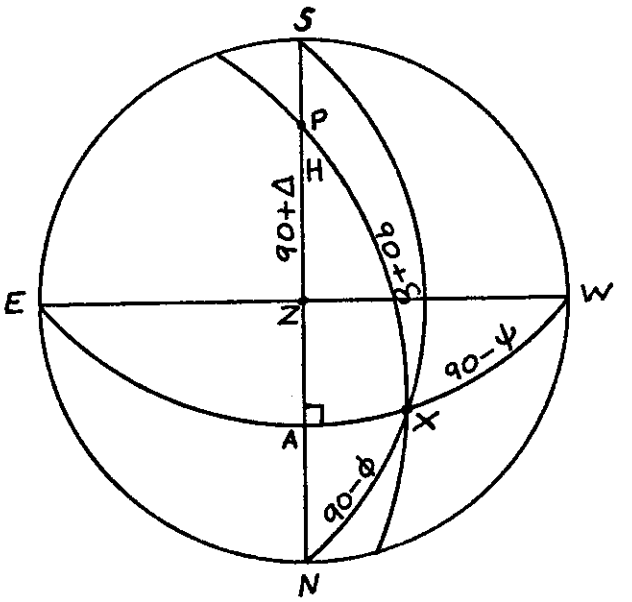

Notation.

δ	declination, - ve South, + ve North
Δ	latitude of observatory = $-35^{\circ}.51$
ϕ	complement of Cone angle around N S axis + ve North of Z, - ve South of Z.
ψ	complement of Cone Angle around E W axis + ve West of Z, - ve East of Z.
H	Hour angle from meridian
T	Transit time of source in North-South beam.
D	Declination number
λ	Wavelength of received signal (0.735 m).
L	Length of Module of North-South arm.

The point P in the diagram is the South Celestial Pole while X represents some point on the beam. Z is the zenith.

In the spherical triangle P. N. X.

$$\cos(90^\circ-\phi) = \cos(180^\circ+\Delta)\cos(90^\circ+\delta) + \sin(180^\circ+\Delta)\sin(90^\circ+\delta)\cos H$$

ie $$\sin\phi \doteq \cos\Delta\sin\delta - \sin\Delta\cos\delta\left(1-\frac{H^2}{2}+\cdots\right)$$

for small H

$$\doteq \sin(\delta-\Delta) + \frac{H^2}{2}\sin\Delta\cos\delta$$

Now let $\delta-\Delta = \phi_0$, the value of ϕ when H = 0

Then $$\boxed{\sin\phi - \sin\phi_0 = \frac{H^2}{2}\sin\Delta\cos\delta}\ .$$

For the spherical triangle P. A. X.

$$\frac{\sin\psi}{\sin H} = \frac{\sin(90^\circ+\delta)}{\sin 90^\circ}$$

$\therefore$ for small H, ψ

$$\psi = H\cos\delta$$

With the tapered illumination of the North-South arm the beamshape in declination can be represented by the modified gaussian

$$\frac{e^{-\frac{1}{2\sigma_1^2}X^2}}{1+aX^6}$$

The denominator in this expression was obtained empirically by fitting to a computed beamshape.

The argument X is given by

$X = (\phi - \phi_B)\cos\phi_B$ where ϕ_B is the complement of the cone angle of the beam and ϕ is the parameter describing position in the beam. The factor $\cos\phi_B$ arises from the foreshortening of the aerial as one moves away from the zenith.

For the North-South arm

$$\sin\phi = \frac{\lambda}{L}\cdot\frac{500-D}{40}$$

which can be regarded as a definition of D.

Now $$\phi - \phi_B = \phi_o - \phi_B + \phi - \phi_o$$
$$\doteq \frac{\sin\phi_o - \sin\phi_B}{\cos\phi_B} + \frac{\sin\phi - \sin\phi_o}{\cos\phi_B}$$
$$\doteq \frac{1}{\cos\phi_B}\left[\frac{\lambda}{40L}(D_B - D_o) + \frac{H^2}{2}\sin\Delta\cos\delta\right]$$

from previous expressions. The subscript B refers to the direction the beam is pointing.

Hence $X = \frac{\lambda}{40L}(D_B - D_o) + \frac{(t-T)^2}{2}\sin\Delta\cos\delta$

as $H = t - T$

D_o is the declination number of the source at meridian transit and is equal to D, the parameter of declination in the fitting programme.

In right ascension, the beamshape of the North-South arm was assumed to be a gaussian with half-power width $4^o.2$.

$$e^{-\frac{1}{2\sigma_2^2}\psi^2}$$

where $\psi = H\cos\delta = (t-T)\cos\delta$

Hence the function used to evaluate the beamshape for the North-South total power fan beams was as follows:

$$G = \frac{e^{-\frac{1}{2\sigma_1^2}X^2} \cdot e^{-\frac{1}{2\sigma_2^2}Y^2}}{1 + aX^6}$$

where $X = \frac{\lambda}{40L}(D_B - D) + \frac{(t-T)^2}{2}\sin\Delta\cos\delta$

and $Y = (t-T)\cos\delta$

The constants were as follows:

$\frac{1}{2\sigma_1^2} = 7878741$ for (t - T) in radians

$a = 1.031630671 \times 10^{19}$ for (t - T) in radians

$\frac{\lambda}{40L} = 0.002078946679$

$\sin\Delta = \sin(-35^\circ.51) = -0.5808450368$

$\frac{1}{2\sigma_2^2} = 516$ for (t - T) in radians

The beam derivative $\frac{\partial G}{\partial D}$ was derived from the above expression as follows: $$\frac{\partial G}{\partial D} = \frac{\lambda}{40L} \cdot X \cdot \frac{e^{-\frac{1}{2\sigma_1^2}X^2} \cdot e^{-\frac{1}{2\sigma_2^2}Y^2}}{1+aX^6}\left[\frac{1}{\sigma_1^2} + \frac{6aX^4}{1+aX^6}\right]$$

Appendix 4C.

The "Simplex" Procedure for Initial Parameter Values.

An initial value for pulsar phase was found by stepping ϕ in increments of $\frac{2\pi}{10}$ till $\sum_i (Y_i - F_i)^2$ was smallest. Using the value ϕ_o from this process and D_o and F_o input to the procedure the set (D_o, ϕ_o, F_o) was obtained. From this, three other sets $(D_o + 1, \phi_o, F_o)$, $(D_o, \phi_o + 1, F_o)$, $(D_o, \phi_o, F_o + 1)$ were formed, the D_o, ϕ_o and F_o having been suitably scaled. These four sets were regarded as the coordinates of four points in a 3-dimensional $D\phi F$ space with D_o, ϕ_o, F_o as the origin.

The value of $\sum_i (Y_i - F_i)^2$ was calculated for all four points and that point P_ℓ selected for which $\sum_i (Y_i - F_i)^2$ was largest. Using a set of geometric rules in $D\phi F$ space the orientation of the set of four points was determined, and the coordinates of a new point, P_ℓ' were calculated according to geometric rules, such that P_ℓ' would be at a position on the opposite side of the plane defined by the other 3 points. The exact position depended on the geometric orientation of the points. P_ℓ was discarded and P_ℓ' and the other three points formed the set of four points on which the procedure was repeated. The geometric rules were such that each point lay on a unit 3-dimensional grid in $D\phi F$ space.

The procedure terminated when it appeared that four points had been found which straddled a point where $\sum_i (Y_i - F_i)^2$ was a minimum.

The scale factors were increased by a factor of 10, the whole procedure being repeated on a finer scale in normal D, ϕ, and F units.

The output parameters from this procedure became the initial values for the least squares procedure.

Appendix 4D.

The Convolution Procedure for Initial Parameter Values.

In the case of erratic pulsars it was found that the method described in Appendix 4C was not reliable, possibly because the set A_K and ϕ were not completely orthogonal.

It was suggested by J. Sutton that one could sum the data along the path of the pulsar through the total power fan beams for different assumed values of declination, weighting each data point by the expected beam shape at that point. This sum is a maximum when the declination chosen coincides with the declination of the pulsar. This procedure is essentially a convolution of the data by the beamshape of the aerial. The principle was extended to provide initial values of ϕ and F as well as D.

The procedure was as follows:--

Consider the function $C_{\iota K}$ defined by

$$\underset{\iota=1,\ldots,5}{C_{\iota K}} = \frac{\sum_{c} Y_{cK} G_{cK}}{\sum_{c} G_{cK}^2} \qquad \begin{matrix} c = 5(\iota-1)+1,\ 5(\iota-1)+2,\ \ldots \\ \ldots,\ 5(\iota-1)+5. \\ K = 1, \ldots, 400. \end{matrix}$$

Where G_{cK} is the beamshape defined in Appendix 4B.

The subscript ι is defined to be the integer part of $\frac{c}{5}$ and is the phase index of the channel

$$\text{ie} \quad \phi_c = \phi + \frac{2\pi(\iota-1)}{10}$$

Clearly the summations in the expression for $C_{\iota K}$ are over channels which have the same phase, but different declinations.

If the Fourier transform of the set $C_{\iota K}$ for each ι is examined, it is clear that the following statements will be true:

1) If a pulsar signal is present a peak will occur in the transform at the frequency corresponding to the beat frequency.
2) The amplitude of the peak will be proportional to the signal strength in the set $C_{\iota K}$.

3) The phase of the signal at the peak in the transform will be related to the phase of the pulsar signal.

4) If the procedure is repeated using different values of D in the calculation of G_{CK}, the peak in the transform will be highest for that value of D which is closest to the actual D for the pulsar.

If the value of phase derived from the transform of C_{LK} is ϕ_L then the calculated phase for channel $L = 1$ based on ϕ_L is

$$\Phi_L = \phi_L - \frac{2\pi(L-1)}{10}$$

The mean pulsar phase, averaged over all the data, will then be

$$\phi = \frac{1}{5} \sum_{L=1}^{5} \Phi_L$$

This gives an initial value ϕ_o for the pulsar signal phase for later analysis. F_o is obtained from the position of the peak in the transform, and D_o from 4) above.

A sample of the output from this programme is shown in Figure 4.10. Values for D, ϕ, F, obtained from this output were input to the least squares procedure.

Figure 4.10 A sample of output from the convolution procedure for initial parameter values. Initial values for pulsar phase and beat frequency are indicated. This is repeated for different values of declination until the response is greatest. The declination number is also indicated.

42958 16 2 1973 0

DEC 71660.000 ← D_o

P

FREQ	PERIOD		PHI 1		PHI 2		PHI 3		PHI 4		PHI 5		FINAL
0.0000000000			0.000		0.000		0.000		0.000		0.000		0.000
0.0003063937	3263.8	4.70	74.922	4.12	20.913	3.50	16.530	2.91	27.578	2.23	37.754	3.49	177.698
0.0006127874	1631.9	4.68	88.323	4.16	23.619	3.56	20.697	3.02	34.307	2.26	46.012	3.53	212.957
0.0009191811	1087.9	4.63	37.262	4.26	7.682	3.71	11.482	3.28	18.591	2.30	22.420	3.64	97.436
0.0012255748	815.9	1.60	24.572	0.99	10.525	5.62	3.019	5.26	7.426	5.40	8.205	3.77	53.747
0.0015319685	652.8	1.54	43.314	1.08	15.047	0.11	6.900	5.98	14.443	5.48	19.494	2.84	99.198
0.0018383622	544.0	1.52	15.802	1.24	5.874	0.02	2.507	0.00	7.242	5.55	7.785	1.67	39.210
0.0021447559	466.3	4.66	17.820	4.06	4.514	3.67	4.170	2.87	4.551	2.40	8.952	3.53	40.006
0.0024511496	408.0	4.66	22.469	4.19	5.327	3.71	5.332	3.33	8.348	2.52	12.767	3.68	54.243
0.0027575433	362.6	5.30	2.535	1.76	1.287	4.54	1.143	4.18	5.101	3.13	3.940	3.78	14.006
0.0030639370	326.4	1.29	14.602	1.57	5.504	0.38	4.256	5.57	5.135	5.27	6.789	2.82	36.286
0.0033703307	296.7	1.17	9.722	2.26	3.936	0.68	4.934	0.17	4.038	5.49	5.620	1.96	28.249
0.0036767244	272.0	4.79	6.125	3.71	5.115	1.39	2.726	1.82	3.484	2.29	2.063	2.80	19.514
0.0039831181	251.1	4.51	11.316	4.25	5.867	2.63	2.458	2.68	4.312	2.48	5.808	3.31	29.761
0.0042895117	233.1	4.01	3.125	5.04	2.949	3.19	2.046	3.92	2.480	2.86	1.731	3.80	12.330
0.0045959054	217.6	1.51	6.119	0.17	2.566	4.14	0.958	5.28	3.966	5.59	4.361	3.34	17.970
0.0049022991	204.0	1.13	3.904	0.52	0.999	4.91	1.237	5.92	3.158	5.84	4.556	3.66	13.853
0.0052086928	192.0	4.87	4.577	3.99	2.110	4.64	1.591	1.48	2.349	1.69	1.258	3.33	11.884
0.0055150865	181.3	4.63	5.458	4.12	2.273	4.52	1.788	2.20	4.028	2.71	4.473	3.64	18.020
0.0058214802	171.8	1.34	3.030	0.68	1.151	4.88	1.461	2.72	2.146	3.59	3.154	2.64	10.943
0.0061278739	163.2	1.23	10.547	0.98	3.759	5.63	1.142	4.79	1.854	5.15	4.848	3.56	22.149
0.0064342676	155.4	0.94	7.996	1.31	2.242	0.15	0.899	5.20	1.953	5.76	5.784	2.67	18.874
0.0067406613	148.4	5.31	4.187	3.71	2.182	0.88	0.974	1.82	1.200	0.62	3.696	2.47	12.239
0.0070470550	141.9	4.52	8.441	4.08	3.679	0.82	1.520	1.90	3.925	1.83	5.453	2.63	23.018
0.0073534487	136.0	3.92	4.881	4.81	1.264	0.56	2.347	1.68	3.358	2.41	4.856	2.68	16.706
0.0076598424	130.6	1.97	4.656	0.62	2.928	0.50	2.412	0.56	1.363	3.70	2.534	1.47	13.893
0.0079662361	125.5	1.41	6.420	0.88	3.031	0.84	1.077	5.30	1.479	4.82	3.185	2.65	15.193
0.0082726298	120.9	0.89	3.146	3.03	1.027	2.86	1.033	3.59	1.634	5.75	1.090	3.22	7.929
0.0085790235	116.6	5.17	1.325	3.71	4.278	3.22	1.047	2.78	3.234	1.69	2.855	3.31	12.739
0.0088854172	112.5	4.13	1.445	3.77	4.305	6.25	0.857	2.26	2.454	2.06	2.968	3.70	12.029
0.0091918109	108.8	4.25	0.467	3.95	1.454	0.19	2.769	0.40	1.841	3.85	1.420	2.53	7.951
0.0094982046	105.3	5.44	2.379	0.02	1.648	0.51	2.785	6.05	3.311	4.63	3.256	3.33	13.378
0.0098045983	102.0	5.36	3.894	6.24	2.879	1.44	2.001	5.74	1.442	4.65	1.074	4.69	11.290
0.0101109920	98.9	5.84	1.507	6.13	2.751	2.17	2.305	2.94	2.219	1.60	3.441	3.74	12.224
0.0104173857	96.0	1.55	3.930	0.08	1.971	1.93	1.102	2.95	3.443	1.46	5.085	1.59	15.531
0.0107237794	93.3	1.53	4.592	0.88	1.429	0.00	2.140	3.90	1.574	0.81	2.215	1.42	11.950
0.0110301731	90.7	5.90	1.226	1.96	1.694	6.25	3.633	5.37	3.672	5.10	3.431	4.92	13.656
0.0113365668	88.2	4.91	4.684	2.48	3.189	0.42	2.828	5.77	4.116	4.55	3.804	3.63	18.620
0.0116429605	85.9	3.76	1.476	2.48	4.837	1.48	2.742	0.60	2.664	2.82	2.397	2.23	14.117
0.0119493542	83.7	2.01	7.947	2.36	4.906	1.89	2.377	1.53	3.596	1.81	4.837	1.92	23.662
0.0122557478	81.6	1.97	7.801	2.98	1.493	5.12	2.125	4.39	0.311	0.49	3.252	2.99	14.981
0.0125621415	79.6	4.74	7.304	4.88	7.881	5.12	9.679	4.89	10.090	5.35	11.341	5.00	46.295
0.0128685352	77.7	4.85	26.653	4.92	16.860	5.10	16.041	4.92	19.679	5.08	21.233	4.97	100.465
0.0131749289	75.9	4.86	32.638	4.91	19.391	5.10	17.284	4.95	21.667	4.93	22.678	4.95	113.658
0.0134813226	74.2	4.84	18.831	4.91	12.362	5.14	12.913	5.00	14.221	4.82	13.994	4.94	72.321
0.0137877163	72.5	1.86	1.752	4.75	0.578	5.34	6.314	5.42	3.024	4.43	1.631	4.36	13.298
0.0140941100	71.0	1.69	10.361	1.83	7.122	6.12	2.210	1.57	5.111	1.71	6.134	2.58	30.939
0.0144005037	69.4	1.32	2.762	1.92	6.106	0.53	0.887	1.75	5.184	1.73	5.507	1.45	20.447
0.0147068974	68.0	5.05	8.909	3.44	1.037	4.38	1.192	2.33	0.905	2.81	1.075	3.60	13.117
0.0150132911	66.6	5.01	9.502	4.74	3.896	4.27	2.243	4.79	2.630	4.51	2.892	4.66	21.163

F_o → 0.0131749289

Φ_o ↙ 4.95

Appendix 4E.

The Least Squares Iterative Procedure.

Notation.

F_i Fitted Function

Y_i Data

α_j Minimization Parameters

The procedure minimizes $\sum_i (Y_i - F_i)^2$

That is, the derivatives of of $\sum_i (Y_i - F_i)^2$ with respect to the α_j are all zero.

$$\text{ie.} \sum_i (Y_i - F_i)\frac{\partial F_i}{\partial \alpha_j} = 0 \text{ for all } j \qquad (1)$$

F_i may be expanded in a Taylor Series

$$F_i = F_i^{\,0} + \sum_j \frac{\partial F_i^{\circ}}{\partial \alpha_j}(\alpha_j - \alpha_j^{\circ}) + \cdots\cdots \qquad (2)$$

where the superscript zero denotes an initial value.

The derivative may also be expanded

$$\frac{\partial F_i}{\partial \alpha_j} = \frac{\partial F_i^{\circ}}{\partial \alpha_j}_{\circ} + \sum_\ell \frac{\partial^2 F_i^{\circ}}{\partial \alpha_j \partial \alpha_\ell}(\alpha_\ell - \alpha_\ell^{\circ}) + \cdots \qquad (3)$$

$$\doteq \frac{\partial F_i^{\circ}}{\partial \alpha_j} \quad \text{— a first order approximation}$$

Equation (1) may be rewritten as

$$\sum_i (Y_i - F_i^{\circ})\frac{\partial F_i^{\circ}}{\partial \alpha_j} = \sum_\ell \left[\sum_i \frac{\partial F_i^{\circ}}{\partial \alpha_j}\frac{\partial F_i^{\circ}}{\partial \alpha_\ell}\right](\alpha_\ell - \alpha_\ell^{\circ})$$

$$\text{or } \sum_i \overline{(Y_i - F_i^{\circ})\frac{\partial F_i^{\circ}}{\partial \alpha_j}} = \sum_\ell \left[\sum_i \overline{\frac{\partial F_i^{\circ}}{\partial \alpha_j}\frac{\partial F_i^{\circ}}{\partial \alpha_\ell}}\right](\alpha_\ell - \alpha_\ell^{\circ}) \qquad (4)$$

where $\sum(\overline{\quad})$ means normalization over all data points (division by 10,000)

The matrices $\underline{a}$, $\underline{R}$ and $\underline{\underline{S}}$ are defined as follows:

$$a_j - a_j^{\circ} = \alpha_j - \alpha_j^{\circ} \quad \text{(column vector)}$$

$$R_j = \sum_i \overline{(Y_i - F_i^{\,0})\frac{\partial F_i^{\circ}}{\partial \alpha_j}} \quad \text{(column vector)}$$

$$S_{\ell j} = \sum_i \overline{\frac{\partial F_i^{\circ}}{\partial \alpha_\ell}\frac{\partial F_i^{\circ}}{\partial \alpha_j}} \quad \text{(symmetric square matrix)}$$

Equation (4) becomes

$$\underline{R} = \underline{\underline{S}}\,(\underline{a} - \underline{a}^{\circ}) \qquad (5)$$

Hence $$\underline{a} - \underline{a}^{\circ} = \underline{\underline{S}}^{-1}\underline{R} \qquad (6)$$

that is $$\alpha_j - \alpha_j^{\circ} = \left[\underline{\underline{S}}^{-1}\underline{R}\right]_j \qquad (7)$$

The α_j derived from (7) are used to recompute the F and derivatives, and the procedure is repeated.

Formal Standard Errors of Iterated Parameters.

Define
$$\underline{\Delta a} = \underline{a} - \underline{a}^0 \qquad \text{col vector}$$
$$[\underline{\Delta Y}]_i = Y_i - F_i^0 \qquad \text{col vector}$$
$$\frac{\partial F_i^\circ}{\partial \alpha_j} = \left[\frac{\partial F^\circ}{\partial a}\right]_{ji} \qquad j \text{ rows } 1 \text{ cols}$$
$$= \left[\frac{\partial F^\circ}{\partial a}\right]_{ij} \qquad 1 \text{ rows } j \text{ cols}$$
$$\therefore \underline{\underline{S}} = \overline{\left[\frac{\partial F^\circ}{\partial a}\right]\left[\frac{\partial F^\circ}{\partial a}\right]^T} \qquad j \text{ rows } j \text{ cols}$$
$$\underline{R} = \overline{\left[\frac{\partial F^\circ}{\partial a}\right]^T \underline{\Delta Y}}$$

Now
$$\underline{\Delta a} = \underline{\underline{S}}^{-1}\underline{R}$$
$$= \underline{\underline{S}}^{-1}\left[\frac{\partial F}{\partial a}\right]^T \underline{\Delta Y}$$

$$[\Delta a]^T = \Delta Y^T \left[\frac{\partial F}{\partial a}\right] \underline{\underline{S}}^{-1} \qquad \underline{\underline{S}} \text{ symmetric}$$

Now
$$\underline{\Delta a}\cdot\underline{\Delta a}^T = \underline{\underline{S}}^{-1}\overline{\left[\frac{\partial F}{\partial a}\right]^T \Delta Y\ \Delta Y^T\left[\frac{\partial F}{\partial a}\right]}\ \underline{\underline{S}}^{-1}$$
$$\langle \underline{\Delta a}\cdot\underline{\Delta a}^T\rangle = \underline{\underline{S}}^{-1}\left[\frac{\partial F}{\partial a}\right]^T \langle \Delta Y\, \Delta Y^T\rangle \left[\frac{\partial F}{\partial a}\right] \underline{\underline{S}}^{-1}$$
$$= \sigma_y^2\, \underline{\underline{S}}^{-1}\frac{1}{N}\underline{\underline{S}}^T\underline{\underline{S}}^{-1} \qquad \text{as } \langle \Delta Y\, \Delta Y^T\rangle = \sigma_y^2 \cdot \underline{\underline{I}}$$
$$= \frac{1}{N}\sigma_y^2\, S^{-1} \qquad \text{as } \underline{\underline{S}} \text{ is symmetric}$$
$$\text{where } \sigma_y^2 = \sum_i (Y_i - F_i)^2$$

Consider the diagonal elements only.

Then
$$\left\langle (\alpha_j - \alpha_j^\circ)(\alpha_j - \alpha_j^\circ)\right\rangle = \frac{1}{N}\sigma_y^2\left[\underline{\underline{S}}^{-1}\right]_{jj}$$

The R.H.S. of this equation is a reasonable estimate of $\sigma_{\alpha_j}^2$ since after several iterations the values of α_j ought to vary during the iterations by amounts of the order of σ_{α_j}.

Hence
$$\sigma_{\alpha_j}^2 = \frac{1}{N}\sigma_y^2\left[\underline{\underline{S}}^{-1}\right]_{jj}$$

This was the relationship used to derive the formal standard

deviations of the iterated parameters.

It should be noted that in this analysis no correlations between adjacent beams were allowed for. While this was not strictly true, the effect of including correlations would have been the reduction of the formal errors of the analysis, which was not a sufficiently significant improvement to justify the extra complications involved.

Initial values for D, ϕ, F were obtained by other iterative procedures (Appendices 4C and 4D). Initial values for B_c were determined as follows:

$$B_c^{\,0} = \frac{\sum_{k=1}^{400} Y_{ck}}{400} \qquad c = 1, \ldots, 25$$

Appendix 4F. The Analysis Programme.

The programme was written in Usercode, the machine language of the English Electric KDF-9 computer. The structure of the programme was as follows:

1. Main Control Programme.

2. Subroutines
   a) Generation of the expected waveform
   b) Computation of initial background levels
   c) Generation of amplitude function
   d) Generation of the S matrix
   e) Generation of the R matrix
   f) Computation of the time of each sample
   g) Read the data tape and store the data
   h) Computation of the calibration factors for each data channel
   i) Simplex iterative procedure
   j) Fourier transform declination search programme
   k) Convolution method for obtaining initial values
   l) Fetch a data sample from magnetic tape
   m) Precession to 1950.0 coordinates

3. Library subroutines
   a) function subroutines eg. sin, cos, $\sqrt{\ }$, etc.
   b) matrix subroutines eg. store allocation, multiplication, inversion, etc.
   c) fast Fourier transform
   d) diagnostic routines for programme development.

It should be noted that subroutines 2(l) and 2(m) were

written by Dr. D. F. Crawford.

The sequence of operations during the least squares iterative procedure is illustrated by the flow diagram in Fig. 4.11. The use of the programme in modes other than this, eg. for declination searching or initial value measurements, occurred by means of the specific subroutines as listed above as well as the basic input and output subroutines.

Data

The data recorded on magnetic tape for a typical pulsar transit consisted of

1) ~ 3 minutes introductory recording during which equipment and control settings were checked
2) ~ 3 minutes recording with the calibration signal on
3) ~ 3 minutes recording with the calibration signal off (to provide a reference level).
4) ~ 20 minutes of pulsar transit.

See Fig. 4.8 for an analogue record illustrating these steps.

Control Data.

The control data input on paper tape contained the following information:

α Right ascension of pulsar in seconds.

δ Approximate declination of pulsar in 0.01 deg.

P Approximate pulsar period in 0.1 m sec.

w_p Observed pulse width (m sec).

D_{BN} Declination number of the northernmost beam.

D_o Initial value for declination number (10^{-2} dec. no.)

ϕ_o Initial value for pulsar phase (10^{-2} rad)

Figure 4.11 A Flow Diagram for the main analysis programme being used to carry out the Least Squares Iterative Procedure.

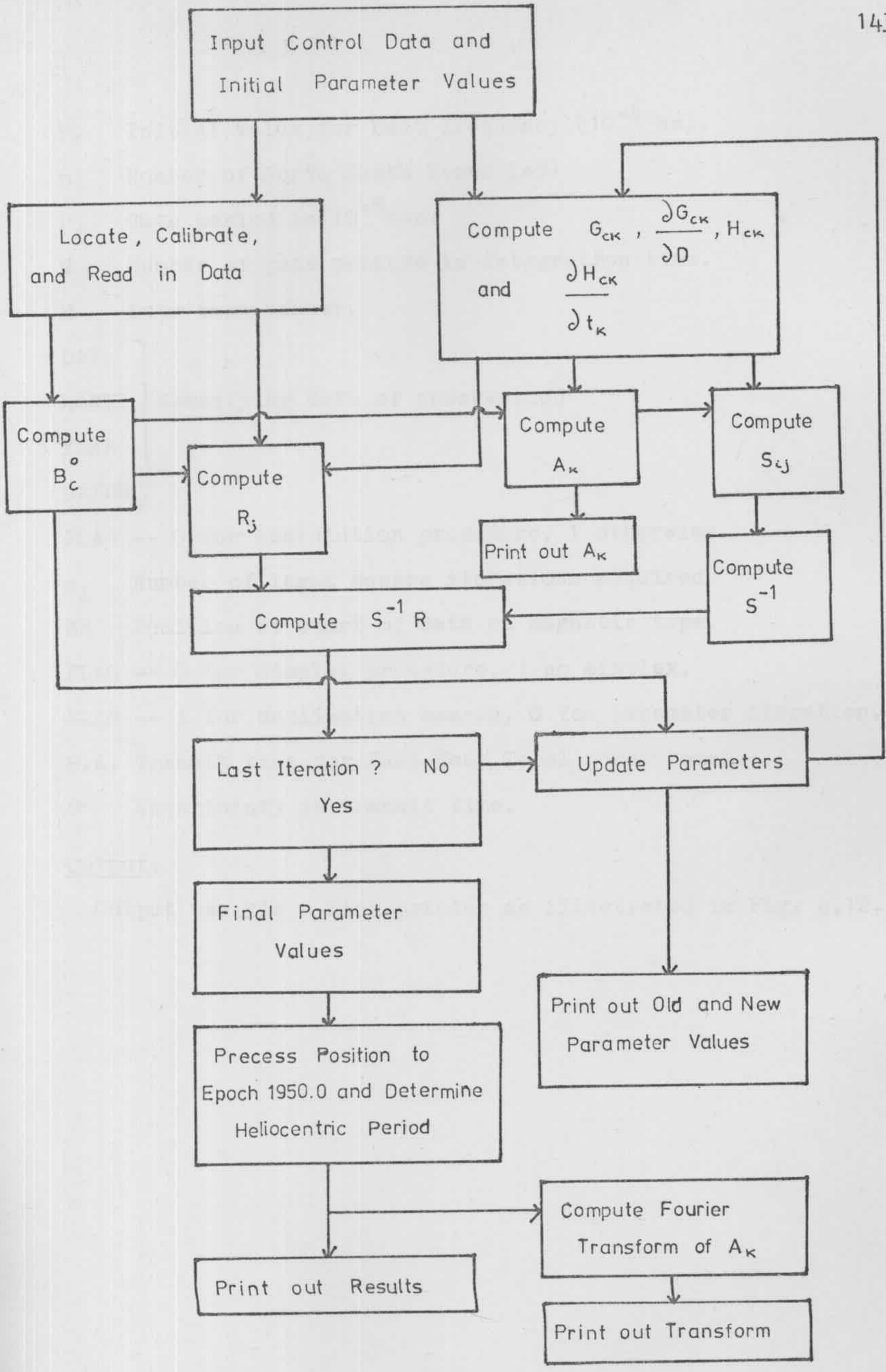
Input Control Data and Initial Parameter Values
Locate, Calibrate, and Read in Data
Compute G_{ck}, $\frac{\partial G_{ck}}{\partial D}$, H_{ck} and $\frac{\partial H_{ck}}{\partial t_k}$
Compute B_c^o
Compute R_j
Compute A_k
Compute S_{ij}
Print out A_k
Compute S^{-1}
Compute $S^{-1}R$
Last Iteration ? No Yes
Update Parameters
Final Parameter Values
Print out Old and New Parameter Values
Precess Position to Epoch 1950.0 and Determine Heliocentric Period
Compute Fourier Transform of A_k
Print out Results
Print out Transform

F_o Initial value for beat frequency (10^{-4} Hz).

n Number of North South beams (=5)

P_g Gate period in 10^{-5}sec.

N Number of gate periods in integration time.

M Data tape number.

DAY
MONTH } Specifying date of observation
YEAR
DE/DB

FLAG -- 0 for convolution procedure, 1 otherwise.

n_i Number of least square iterations required.

BN Position of start of data on magnetic tape.

FLAG -- 0 for Simplex procedure, 1 no simplex.

FLAG -- 1 for declination search, 0 for parameter iteration.

R.A. Transit time for East-West Total power beams.

σ Uncertainty in transit time.

Output.

Output was via a line printer as illustrated in Fig. 4.12.

Figure 4.12 A sample of the output from the Least Squares Iterative procedure programme. Not shown are the complete amplitude function and its Fourier transform.

15 2 1973 0

PRESENT R.A. HOURS	MINUTES	SECONDS	S.D. SECONDS	PRESENT DEC DEGREES	MINUTES	SECONDS	S.D. SECONDS
8	37	29	2.0000	-41	29	42.4852	1.5123

GEOCENTR PERIOD SECONDS	S.D. SECONDS	HELIOCEN PERIOD SECONDS	S.D. SECONDS	PHI	S.D.
0.7516150027495314	0.0000013860597512	0.7516182142608159	0.0000013860656821	1.8740	0.0053

1950 R.A. HOURS	MINUTES	SECONDS	S.D. SECONDS	1950 DEC DEGREES	MINUTES	SECONDS	S.D. SECONDS
8	35	33.8489	2.0000	-41	24	39.8362	1.5123

MEAN AMPLITUDE	S.D.
6.563	0.310

DATA TAPE

30986	-4150	7650	41	5498	55017	187	133	5	75919	
4	427	15	2	1973	0	1	10	2112	1	
0										

Chapter 5

ACCURATE PULSAR POSITIONS.

5.1 Introduction.

Because of the beamshape of the East-West fan beam (Table 2.1), the uncertainties in the right ascensions of pulsars discovered at Molonglo were generally about $\pm 2^s$ ($\leqslant 30$ arc sec) on discovery, later being reduced to about $\pm 1^s$ for most pulsars. On the other hand, for the same reason, the uncertainty in declination was generally about $\pm 2^o$ on discovery. For this reason greater emphasis was given to improving the precision of declination measurements rather than obtaining more precise right ascensions. Moreover, the long transit time of a pulsar in the fan beams of the North-South arm resulted, with the use of the BPI technique, in higher signal to noise ratios for declination measurements than could be obtained for right ascension measurements using the more sensitive East-West arm.

Hence only a few pulsar right ascensions were measured precisely, as described in 2.4.1.1. The results are given in 5.2.

The high sensitivity of the BPI technique on the North-South fan beams, led to its modification for use in searching for pulsars in declination when the declination uncertainties were large. Rather than search for individual pulses in the outputs of the fan beams, full fan beam transits were recorded as described in 4.2 at declination settings covering the pulsar position. Instead of applying the least squares fitting procedure to all the data, however, a Fourier transform procedure was applied to the data from each of the five adjacent fan beams. The transform for each fan beam was output as shown in Figure 5.1. If the pulsar declination lay within the range of the five fan

Figure 5.1 A sample of the output from the Fourier Transform declination search procedure. Note the peak in the transform indicating that the pulsar was lying between the North-South fan beams numbered -2 and -3, -2 being the closest.

MP1706 27/2/71 DE

PSR1706-16

D = 344

D = 344

P

FREQ	PERIOD	B1 (0)	B2 (-1)	B3 (-2)	B4 (-3)	B5 (-4)
0.0000000000		0.000	0.000	0.000	0.000	0.000
0.0003005964	3326.7	934.875	979.170	303.354	730.591	849.953
0.0006011928	1663.4	1395.504	1487.921	369.369	1242.372	1321.400
0.0009017891	1108.9	373.489	422.190	59.080	502.751	425.361
0.0012023855	831.7	9.851	10.274	193.495	12.127	15.239
0.0015029819	665.3	90.551	100.691	275.299	54.432	52.725
0.0018035783	554.5	0.210	1.360	85.241	38.774	15.313
0.0021041747	475.2	80.667	73.103	67.235	40.197	89.493
0.0024047711	415.8	40.676	49.942	53.282	27.432	35.597
0.0027053674	369.6	17.026	44.199	10.347	3.062	16.940
0.0030059638	332.7	90.383	157.377	33.916	19.926	75.666
0.0033065602	302.4	21.876	76.103	59.019	2.037	14.677
0.0036071566	277.2	26.264	1.696	159.318	29.804	41.704
0.0039077530	255.9	55.701	17.277	203.307	51.062	74.252
0.0042083494	237.6	15.933	2.280	101.536	6.566	14.883
0.0045089457	221.8	29.453	5.067	25.119	11.292	6.550
0.0048095421	207.9	24.751	1.907	7.341	22.528	6.215
0.0051101385	195.7	9.230	4.826	7.622	11.354	9.769
0.0054107349	184.8	11.120	8.597	2.634	29.419	20.972
0.0057113313	175.1	3.513	1.792	9.035	42.523	12.911
0.0060119277	166.3	10.982	17.813	43.737	30.731	16.000
0.0063125240	158.4	8.808	12.497	28.367	5.082	8.256
0.0066131204	151.2	5.023	0.441	6.026	7.958	8.596
0.0069137168	144.6	8.310	2.591	47.584	17.822	17.821
0.0072143132	138.6	17.714	3.040	127.235	1.563	9.391
0.0075149096	133.1	30.705	16.954	263.125	74.276	10.024
0.0078155060	128.0	10.871	21.021	→ 336.528	163.376	7.687
0.0081161023	123.2	1.931	24.515	218.893	95.117	6.878
0.0084166987	118.8	9.666	24.886	66.612	8.371	8.507
0.0087172951	114.7	4.391	3.527	17.456	4.208	0.037
0.0090178915	110.9	16.621	8.958	16.378	2.140	11.621
0.0093184879	107.3	13.842	19.746	8.575	2.106	19.831

beams a peak was apparent at the frequency of the beat between the pulsar and the gating signal. Once the pulsar declination had been found approximately by this method, further transits were recorded, with the pulsar near the centre beam of the five fan beams, to obtain a precise declination by the least squares procedure.

The usefulness of this method of searching in declination was emphasised in the measurement of preliminary precise declinations (±1 arc min) for PSR1154-62 and PSR1240-64. Because of dispersion broadening in the 4MHz passband of the telescope, individual pulses from these pulsars are almost undetectable in the outputs from the East-West fan beams. Despite a slightly narrower passband (2.5MHz) the pulses are completely undetectable in the outputs of the fan beams of the less sensitive North-South arm. However by the use of the above technique a signal to noise ratio of about 15:1 was obtained for PSR1154-62, and slightly less for PSR1240-64, at the peaks of the respective Fourier spectra. As a result, precise declinations (±1 arc min) were obtained for both pulsars[1], and it was this measurement which led to the suggested association of PSR1154-62 with a supernova remnant[2](7.2).

Precise declinations for 30 pulsars, obtained by the BPI technique, are given in 5.3.

5.2 Results of Right Ascension Measurements.

5.2.1 Table of Results.

The results of right ascension measurements are given in Table 5.1. The uncertainties quoted are those derived as described in 5.2.3.

Table 5.1

Pulsar	No. Transits	1950 Right Ascension	Stand. Error
0031-07	1	$00^h31^m35^s.1$	$0^s.3$
0450-18	1	04 50 20.7	0.5
0834+06	1	08 34 26.0	0.4
0959-54	5	09 59 50.9	0.2
1530-53	1	15 30 18.1	0.3
1706-16	1	17 06 32.2	0.2
1747-46	1	17 47 55.0	0.4
1749-28	1	17 49 48.4	0.2
1818-04	2	18 18 12.7	0.3
1857-26	3	18 57 40.9	0.3
1911-04	1	19 11 14.2	0.2

5.2.2 Calibration of Right Ascensions.

The calibration of the East-West arm in right ascension was obtained by observing standard sources of known position. If $\Delta\alpha_i$ represents the discrepancy between the observed right ascension of a calibration source and its standard position, then, for each day's observation, the mean value of the quantity $\Delta\alpha_i \cos\delta_i$ averaged over about ten sources gave the pointing correction for the aerial (δ_i is declination of calibration source i). For a given pulsar, at declination δ_p the correction applied to its observed right ascension was then

$$\Delta\alpha_p = (\overline{\Delta\alpha_i \cos\delta_i}) \sec\delta_p$$

seconds of time.

5.2.3 Discussion of Uncertainties.

As mentioned in 2.4.1.1. two different methods were applied to analyse pulses received in the early, centre and late beams of the East-West arm. The values for right ascension obtained by the two methods differed by up to $0^s.8$ for individual pulsars, while the formal standard errors for the procedures varied from $0^s.03$ to $0^s.14$ for the method using all pulses and from $0^s.16$ to $0^s.49$ for the method using only pulses occurring simultaneously in overlapping beams. (In Table 5.1 the right ascensions quoted are obtained by the second method when there is only one transit and from the mean of results from the first method for more than one transit).

The uncertainties due to calibration errors vary from $0^s.08$ to $0^s.3$ and represent the standard deviation of the pointing corrections in each observing session transferred to the declination of the pulsar.

The final uncertainties quoted for single observations or used to find weights for each of a set of observations of a pulsar are derived by adding the squares of the calibration uncertainties and the fitting procedure standard errors. For those pulsars with more than one observation the uncertainties quoted are derived from the scatter about the weighted mean of the observations.

5.3 Results of Declination Measurements.

5.3.1 Table of Results.

Results of declination measurements on 30 pulsars using the BPI technique are listed in Table 5.2.

Table 5.2

Pulsar	No. Transits	1950 Declination	Standard Error
0031-07	3	-07° 38' 15"	3"
0450-18	5	-18° 04' 18"	2"
0628-28	3	-28° 34' 03"	2"
0736-40	4	-40° 35' 47"	2"
0740-28	1	-28° 15' 34"	5"
0818-13	1	-13° 41' 04"	5"
0833-45	6	-45° 00' 08"	2"
0835-41	2	-41° 24' 42"	3"
0950+08	2	08° 09' 55"	4"
1055-52	2	-52° 10' 46"	3"
1154-62	6	-62° 08' 23"	2"
1240-64	6	-64° 06' 51"	2"
1426-66	1	-66° 10' 06"	5"
1449-64	3	-64° 01' 01"	3"
1451-68	2	-68° 31' 33"	4"
1530-53	3	-53° 24' 17"	3"
1541+09	1	09° 38' 46"	6"
1556-44	4	-44° 30' 12"	2"
1642-03	2	-03° 12' 29"	4"
1706-16	2	-16° 37' 02"	3"
1727-47	4	-47° 42' 22"	2"
1747-46	3	-46° 56' 42"	3"
1749-28	4	-28° 06' 00"	2"
1818-04	2	-04° 28' 55"	4"
1845-01	2	-01° 27' 30"	4"
1857-26	6	-26° 04' 54"	2"
1911-04	2	-04° 45' 46"	5"
1933+16	2	16° 10' 13"	5"
1944+17	1	17° 58' 26"	8"
2045-16	2	-16° 27' 41"	3"

5.3.2 Calibration of Declinations.

The calibration of the pointing of the aerial was complicated by the discovery, after all the observations were completed, that phase variations had been occurring along the local oscillator lines of the aerial because of water vapour condensation in the open lines. This precluded the generation of calibration curves averaged over whole observing sessions which is the usual practice at Molonglo. Instead, as described below, calibration curves were generated showing the pointing of the aerial as a function of time throughout the observing sessions. A diurnal pointing variation was allowed for, since it was indicated by phase measurements on the aerial.

The complete form of the pointing correction was assumed to be $\Delta\delta = A \sec z + B \sec^2 z \tan z$ arc sec [3], where z is the angle from the zenith of the telescope. The first term is due to phase errors along the aerial, and the second term arises from the spherical component of ionispheric refraction.

Based on past experience [4] a fixed value for B of ~ 2 arc sec was assumed for simplicity.

The quantity

$$A = \Delta\delta \cos z - 2 \sec z \tan z$$

for calibration sources was plotted as a function of time and an empirical curve was fitted as shown in Figure 5.2.

Hence for a given pulsar a value of A could be obtained, and the declination correction $\Delta\delta$ calculated.

5.3.3 Discussion of Uncertainties.

As with the right ascension measurements the two sources of uncertainty in the declination measurements are the fitting errors

Figure 5.2 An empirical declination correction curve covering an observing session. The points represent declination errors for calibration sources. The diurnal variation was suggested by phase variations observed along the aerial.

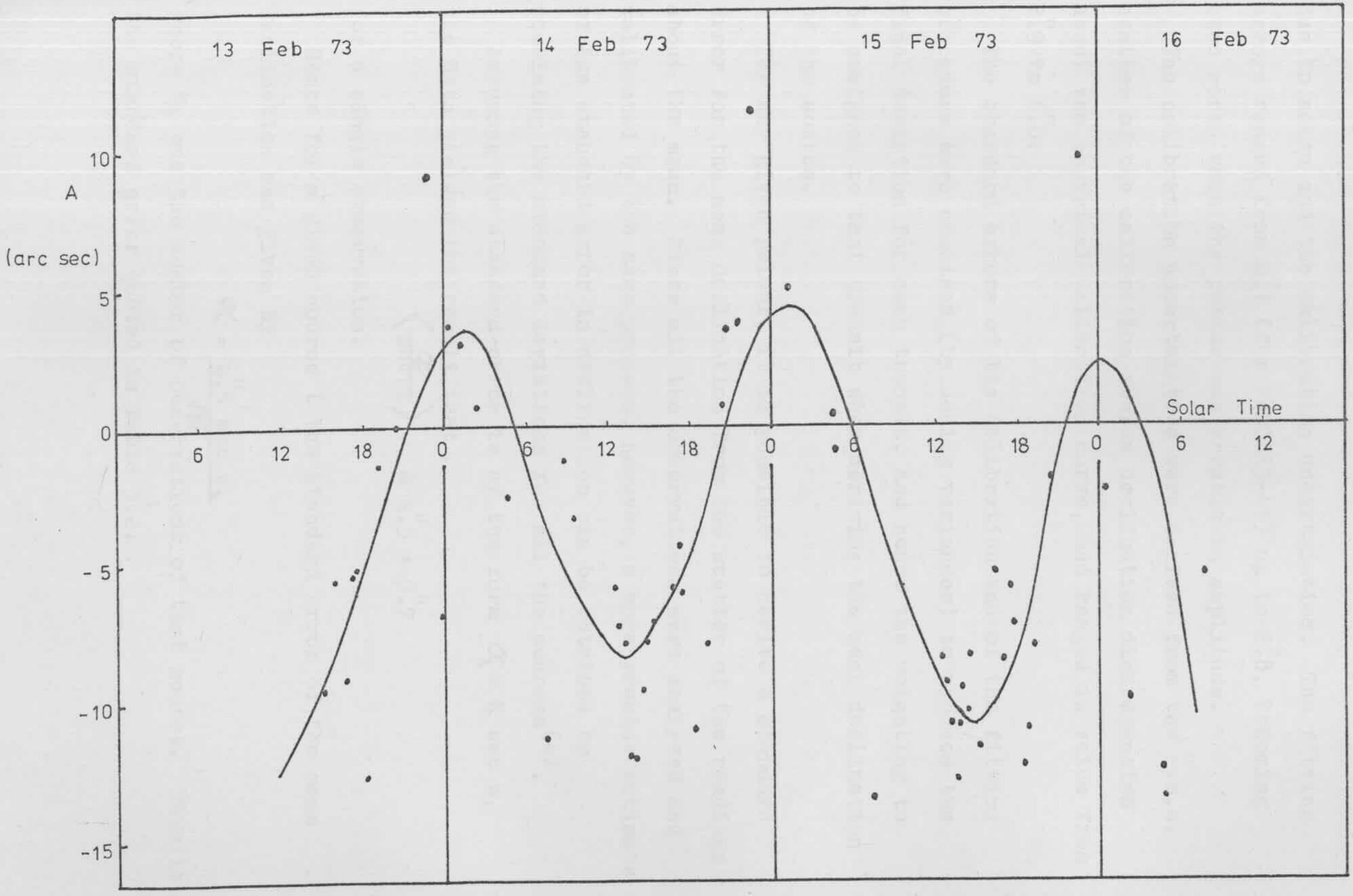
13 Feb 73
14 Feb 73
15 Feb 73
16 Feb 73
A
(arc sec)
10
5
0
-5
-10
-15
6
12
18
0
Solar Time

due to noise and the calibration uncertainties. The fitting errors ranged from $0''.1$ (for PSR0833-45) up to $2''.8$, becoming even worse when the pulsar was erratic in amplitude.

The calibration uncertainties were derived from the r.m.s. scatter of the calibration source declination discrepancies about the empirical calibration curve, and ranged in value from $2''.9$ to $6''.0$.

The standard errors of the calibration and of the fitting procedure were combined (by adding variances) to produce the final deviation for each transit, and hence the weighting to be assigned to that transit when deriving the mean declination of the source.

For any given pulsar, it is possible to derive a standard error for the mean declination from the scatter of the readings about the mean. Since all the observations were analysed and calibrated by the same process, however, a more precise estimate of the standard error in declination can be obtained by combining the standard deviations for all the sources[4].

Assuming the standard error is of the form $\sigma_s = K \sec z$, the data yielded the result that

$$\left\langle \frac{\sigma_s}{\sec z} \right\rangle = 4''.5 \pm 0''.7$$

for a single observation.

Hence for a given source i the standard error of the mean declination was given by

$$\sigma_i = \frac{4''.5 \sec z_i}{\sqrt{N_i}}$$

where N_i was the number of observations of that source. This is the standard error quoted in Table 5.2.

5.4 Comparisons with Other Observations.

5.4.1 Right Ascensions.

To enable direct comparisons of Molonglo right ascension measurements with other pulsar right ascension measurements, the Molonglo results are listed in Table 5.3, together with the most precise measurements available from other observatories or previous Molonglo measurements.

Table 5.3

Pulsar	Molonglo R. A.	Previous R. A. result	Ref.
0031-07	$00^h31^m35^s.1\pm0.3$	$00^h31^m36^s.4\ \pm1^s.1$	5
0450-18	04 50 20.7±0.5	04 50 22 ±2	6
0834+06	08 34 26.0±0.4	08 34 26.15±0.03	5
0959-54	09 59 50.9±0.2	09 59 51 ±3	6
1530-53	15 30 18.1±0.3	15 30 23 ±1	6
1706-16	17 06 32.2±0.2	17 06 33.23±0.05	5
1747-46	17 47 55.0±0.4	17 47 58 ±1	6
1749-28	17 49 48.4±0.2	17 49 49.27±0.07	7
1818-04	18 18 12.7±0.3	18 18 13.61±0.02	5
1857-26	18 57 40.9±0.3	18 57 44 ±2	8
1911-04	19 11 14.2±0.2	19 11 15.14±0.02	5

It can be seen that in 5 cases the differences between the measurements are significant compared to the combined uncertainties of the two measurements. It should be noted that in all these cases only one measurement was used to establish the Molonglo right ascension. Clearly further measurements are required to resolve the discrepancies. They were not undertaken during this programme because of the lower

priority of right ascension measurements in comparison to declination measurements.

5.4.2 Declinations.

Molonglo pulsar declination measurements are listed in Table 5.4 together with the most precise previous measurements available. It can be seen that for those eleven pulsars whose declinations had previously been measured to a precision of the order of or greater than the precision of the corresponding Molonglo measurement, the difference between the two is within three times the standard error of the Molonglo measurement, except for PSR0818-13. In the case of PSR1706-16, this is only true if one allows for the precision of the previous measurement. It should also be noted that the Molonglo declination measurement for PSR0818-13 is based on only one observation.

Based on these comparisons it can be said that for those pulsars for which the previous measurements were not precise, the precise Molonglo declinations are accurate to within three times the quoted standard errors, except possibly for those measurements based on one observation, where the uncertainty may be larger than 3 standard errors.

Table 5.4

Pulsar	Molonglo Declination	Previous Measurement	Ref.
0031-07	-07°38'15"±3"	-07°38'26" ±32"	5
0450-18	-18°04'18"±2"	-18°04'14" ±20"	9
0628-28	-28°34'03"±2"	-28°34'08".1± 1".5	7
0736-40	-40°35'47"±2"	-40°35'20" ±60"	1
0740-28	-28°15'34"±5"	-28°15'16" ±20"	9
0818-13	-13°41'04"±5"	-13°41'22".8± 0".2	10
0833-45	-45°00'08"±2"	-45°00'05".3± 0".2	11
0835-41	-41°24'42"±3"	-41°24'54" ±42"	1
0950+08	08°09'55"±4"	08°09'44".5± 1".5	7
1055-52	-52°10'46"±3"	-51°40' ±30'	12
1154-62	-62°08'23"±2"	-62°08'36" ±60"	1
1240-64	-64°06'51"±2"	-64°07'12" ±60"	1
1426-66	-66°10'06"±5"	-66°09'54" ±60"	1
1449-64	-64°01'01"±3"	-64°02' ± 5'	13
1451-68	-68°31'33"±4"	-68°32' ± 1'	14
1530-53	-53°24'17"±3"	-53°30' ±10'	6
1541+09	09°38'46"±6"	09°38'29" ±20"	9
1556-44	-44°30'12"±2"	-44°31'30" ±42"	12
1642-03	-03°12'29"±4"	-03°12'31".1± 0".3	5
1706-16	-16°37'02"±3"	-16°37'11".7± 2".7	5
1727-47	-47°42'22"±2"	-47°42'18" ±60"	1
1747-46	-46°56'42"±3"	-46°56'12" ±60"	1
1749-28	-28°06'00"±2"	-28°06'01" ± 4"	7
1818-04	-04°28'55"±4"	-04°29'03".3± 0".3	5
1845-01	-01°27'30"±4"	-01°27' ± 1'	15

Table 5.4 (contd.)

Pulsar	Molonglo Declination	Previous Measurement	Ref.
1857-26	$-26^{\circ}04'54''\pm2''$	$-26^{\circ}04'49''\pm20''$	9
1911-04	$-04^{\circ}45'46''\pm5''$	$-04^{\circ}45'59''.4\pm0''.6$	5
1933+16	$16^{\circ}10'13''\pm5''$	$16^{\circ}09'58''.8\pm0''.1$	16
1944+17	$17^{\circ}58'26''\pm8''$	$17^{\circ}58'44''\pm20''$	9
2045-16	$-16^{\circ}27'41''\pm3''$	$-16^{\circ}27'47''.6\pm8''.4$	5

5.5 References.

1. Vaughan, A. E., and Large, M. I., Mon. Not. R. astr. Soc., 156, 25P (1972).

2. Large, M. I., and Vaughan, A. E., Nature Physical Science, 236, 117 (1972).

3. Hunstead, R. W., Proc. Astron. Soc. Austral., 1, 231 (1969).

4. Hunstead, R. W., Mon. Not. R. astr. Soc., 157, 367 (1972).

5. Manchester, R. N., and Peters, W. L., Ap. J., 173, 224 (1972).

6. Morris, D., Schwartz, U. J., and Slee, O. B., Astrophys. Lett., 5, 187 (1970).

7. Hunt, G. C., Mon. Not. R. astr. Soc., 153, 119 (1971).

8. Vaughan, A. E., and Large, M. I., Nature, 225, 167 (1970).

9. Krishnan Mohan S., Balasubramanian, V., and Swarup, G., Nature Physical Science, 234, 151 (1971).

10. Manchester, R. N., Taylor, J. H., and Huguenin, G. R., Nature Physical Science, 240, 74 (1972).

11. Huguenin, G. R., Taylor, J. H., Hjellming, R. M., and Wade, C. M., Nature Physical Science, 234, 50 (1971).

12. Vaughan, A. E., and Large, M. I., Mon. Not. R. astr. Soc., 156, 27P (1972).

13. Ables, J. G., Private Communication.

14. Large, M. I., Vaughan, A. E., and Wielebinski, R., Astrophys. Lett., 3, 123 (1969).

15. Swarup, G., Mohanty, D. K., and Balasubramanian, V., I. A. U. Circ. No. 2356 (1971).

16. Reichley, P. E., Downs, G. S., and Morris, G. A., Ap. J. Letters, 159, L35 (1970).

Chapter 6

OTHER MEASUREMENTS USING BPI.

6.1 Introduction.

In the Least Squares Fitting procedure, the major parameters apart from the declination are the pulsar phase and the beat frequency. A subsidiary set of parameters is the amplitude function. These parameters were used to derive further properties of the pulsars apart from their declinations.

The beat frequency gave values for the observed periods of the pulsars, since it arises from the difference between the pulsar repetition frequency and the known gate frequency. The amplitude function was used to derive the mean flux density of the pulsars and also give an indication of variations in the pulsar flux densities on time scales between 6 seconds and about 10 minutes. Lastly a measurement of pulsar phase, determined, not by the fitting procedure, but from Fourier transforms of data from different radio frequency bands, led to the approximate measurement of the dispersion measures of several pulsars.

6.2 Period Measurements.

6.2.1 Table of Results.

The pulsar period P_p was derived from the beat frequency F via the relationship

$$P_p = \frac{P_g}{1 - F P_g}$$ where P_g is the gating period.

After correction for the motion of the earth (see 6.2.2) the results were combined to produce mean periods for the pulsars observed. The results are listed in Table 6.1 together with several alternate estimates of the period uncertainty, the derivations of which are given in 6.2.3.

Table 6.1

Pulsar	Period	σ_m	$\langle\sigma\rangle_m$	No. Observations
0031-07	0.942 92	1	2	3
0450-18	0.548 941 5	7	43	4*
0628-28	1.244 409	1	8	3
0736-40	0.374 921	1	1	4
0740-28	0.166 741 3	-	3	1
0818-13	1.237 71	-	7	1
0833-45	0.089 224 400**	7	4	6
0835-41	0.751 621	3	5	2
0950+08	0.253 064 80	5	5	2
1055-52	0.197 107 9	2	6	2
1154-62	0.400 521	1	1	6*
1240-64	0.388 479	2	1	6
1426-66	0.785 457	6	6	2
1449-64	0.179 483 53	7	1	3
1451-68	0.263 376 6	3	9	2
1530-53	1.368 85	2	3	3
1541+09	0.748 52	-	3	1
1556-44	0.257 061	4	1	4
1642-03	0.387 688 2	1	4	2
1706-16	0.653 06	2	1	2
1727-47	0.829 701	1	4	3*
1747-46	0.742 357	5	12	2*
1749-28	0.562 554	7	1	3*
1818-04	0.598 080	4	3	2
1845-01	0.659 432	6	1	2
1857-26	0.612 203	3	3	6

Table 6.1 (contd.)

Pulsar	Period	σ_m	$\langle\sigma\rangle_m$	No. Observations
1911-04	0.825 957	-	14	1
1919+21	1.337 33	-	2	1
1933+16	0.358 737	-	1	1
1944+17	0.440 609	-	-	1
2045-16	1.961 59	1	2	2

*One or two transits from this sample were outside the Chauvenet Limits[1] for the sample and were hence excluded. The number indicates how many transits were used in this analysis.

**The period quoted here is that measured on 16th Feb.,1973. For a fuller discussion of PSR0833-45 period measurements see 6.2.5.

6.2.2 Correction for the Motion of the Earth.

The periods measured using B.P.I. were corrected for the Doppler shift due to the motion of the earth about the sun. No corrections for the rotation of the earth on its axis were necessary, since the observations were carried out near the meridian transit of the source. Because of the lack of a suitable ephemeris, corrections to the barycentre of the solar system were not possible. However the differences between the barycentric and heliocentric periods are insignificant in comparison to the uncertainties of the period measurements themselves.

The heliocentric correction was applied as follows

$$\frac{P_{HELIO}}{P_{GEO}} = \frac{1 + \frac{v}{c}\cos\theta}{\sqrt{1 - \frac{v^2}{c^2}}}$$

where P_{HELIO} = heliocentric pulsar period

P_{GEO} = observed geocentric period

c = speed of light

and $v \cos\theta$ = component of the earth's orbital motion in the direction of the pulsar.

See Appendix 6A for a derivation of this correction.

The term $\frac{v}{c}\cos\theta$ was computed as

$$\frac{1}{|r|c}(\underset{\sim}{v}.\underset{\sim}{r}) = \frac{1}{|r|c}(v_x X + v_y Y + v_z Z)$$

where $\underset{\sim}{v}$ represents the velocity of the earth,

v_x, v_y, v_z the components of $\underset{\sim}{v}$ in heliocentric equatorial coordinates,

$\underset{\sim}{r}$ the position vector of the pulsar,

and X, Y, Z the components of $\underset{\sim}{r}$ in heliocentric equatorial coordinates (approximately equal to the geocentric equatorial coordinates).

The quantities $\frac{V_x}{c}$, $\frac{V_y}{c}$, $\frac{V_z}{c}$ were obtained from the precession sub-routine used in the fitting procedure, which was written by Dr. D. F. Crawford.

The position components were calculated as follows

$$\frac{X}{|r|} = \cos\alpha \cos\delta$$

$$\frac{Y}{|r|} = \sin\alpha \cos\delta$$

$$\frac{Z}{|r|} = \sin\delta$$

Finally the term $\sqrt{1 - \frac{V^2}{c^2}}$ was calculated using

$$\frac{v^2}{c^2} = \left(\frac{V_x}{c}\right)^2 + \left(\frac{V_y}{c}\right)^2 + \left(\frac{V_z}{c}\right)^2$$

6.2.3 Discussion of Uncertainties.

The uncertainties quoted under σ_m in Table 6.1 are standard errors on the mean period derived from the scatter in the measured values about the mean. It can be seen that they range from 7×10^{-9}sec to 2×10^{-5}sec, ie over 3.5 orders of magnitude. Since all the periods were measured by the same process, the uncertainties should all be consistent, and in fact can all be used to derive a better estimate of the period uncertainty for each pulsar.

To determine this it is first necessary to derive the functional dependence of the period uncertainties on the parameters of the pulsar. This can be done as follows

$$P_p = \frac{P_g}{1 - F P_g}$$

P_p = Pulsar Period
P_g = Gate Period
F = Beat Frequency

$$\frac{\partial P}{\partial F} = P_p^2$$

$$\sigma_p = P_p^2 \sigma_F$$

where σ_p & σ_F are uncertainties in P and F.

Now $\sigma_F \propto \frac{1}{\bar{S}}$ where $\bar{S}$ is the mean flux density, assuming constant receiver noise. This assumes that the uncertainty in F is not affected very much by the shape of the beat waveform, ie. by w_p, but mainly by its amplitude (more strictly, by the signal to noise ratio).

Hence $\sigma_p \propto \frac{P_p^2}{\bar{S}}$

Therefore the statistic which is normalized to all pulsars is $\frac{\sigma_p \bar{S}}{P_p^2}$.

Using the same method as in 5.3.3 (2), and eliminating two pulsars with abnormally high scatter in period the following result was obtained

$$\left\langle \frac{\sigma_p \bar{S}}{P_p^2} \right\rangle = (2.1 \pm 0.3) \times 10^{-6}$$

where σ_p is in sec., $\bar{S}$ in flux units, and P_p in seconds.

The relatively small scatter in this result supports the view that

a) the functional dependence of σ_p was correct, and

b) the period uncertainties are consistent.

The period uncertainty derived from the above quantity is a better estimate than that derived from the scatter of values, and can also be applied where only one observation was made.

It is derived as follows

$$\langle \sigma \rangle_m = 2.1 \times 10^{-6} \cdot \frac{P_p^2}{\sqrt{n}\,\bar{S}} \quad \text{seconds}$$

where n is the number of observations of a given pulsar of period P_p and mean flux density $\bar{S}$.

This is the quantity listed under $\langle \sigma \rangle_m$ in Table 6.1.

A simple check on the validity of the quantity $\left\langle \frac{\sigma_p \bar{S}}{P_p^2} \right\rangle$ can be made by estimating the uncertainty in the period of a pulsar which is derived from the times of arrival of two pulses,

one at the beginning of a North South Total power transit and one at the end.

The r.f. bandwidth B is 2.5 MHz and post detector time constant τ is taken to be 10^{-3} seconds.

The r.m.s. ripple is

$$\frac{S_o}{\sqrt{B\tau}}$$ where S_o is the total detected signal, taken to be 150 flux units approximately.

Whence

r.m.s. ripple = 0.3 f.u.

Consider a pulse just over 3 x r.m.s., say 1 f.u. peak height.

Then the timing uncertainty for a single pulse is

$\sigma \sim 0.5\ W_p$ say, where W_p is the observed pulse width.

Whence the uncertainty for a peak height of S_p would be

$$\sim 0.5\ \frac{W_p}{S_p}$$

The uncertainty in time interval over N pulse periods (occupying a total time T = 1200 seconds) would then be $\sim \frac{W_p}{S_p}$ and the period uncertainty

$$\sigma_p \sim \frac{W_p}{S_p N}$$

If we assume $\frac{W_p}{P} \sim \frac{1}{20}$, then

$$\sigma_p \sim \frac{1}{20}\,\frac{P}{S_p} \cdot \frac{1}{N}$$

$$\sim \frac{1}{400}\,\frac{P}{\bar{S}}\,\frac{1}{N} \quad \text{as } \bar{S} = \frac{W_p S_p}{P}$$

$$\sim 2.1 \times 10^{-6}\,\frac{P^2}{\bar{S}} \quad \text{as } N = \frac{1200}{P}$$

or $\frac{\sigma_p \bar{S}}{P^2} \sim 2.1 \times 10^{-6}$.

Hence the uncertainty $\langle\sigma\rangle_m$ is of the correct order of magnitude for a pulsar observation using the fan beams of

the North-South arm.

6.2.4 Comparison with other Measurements.

For comparison the results of the period measurements are listed in Table 6.2 along with precise periods obtained by other observers.

It can be seen that out of the 31 pulsars, in 19 cases the periods agree within $2\langle\sigma\rangle_m$, and in 25 the periods agree within $3\langle\sigma\rangle_m$. One pulsar has no uncertainty quoted because of the lack of a suitable flux density measurement. The remaining 5 have differences greater than $3\langle\sigma\rangle_m$.

Hence it can be said that in general the technique of period measurement using B.P.I. is successful, and is mainly limited by the transit time in the fan beams of the North-South arm. A corollary of this is that the case for the accuracy of the other important parameter in the fitting procedure, the declination, is strengthened.

6.2.5 Period Measurements for PSR0833-45.

Period measurements of PSR0833-45 are of particular interest since the first time derivative of the period is large enough to produce noticeable changes in period over a short time interval. This is of course enhanced by the high mean flux density and short period of the pulsar.

6.2.5.1 Period and $\dot{P}$ Measurement by Timing over a short interval.

The arrival times of 3 pulses from PSR0833-45 were measured from recordings of East-West total power transits on 29/5/72, 30/5/72 and 1/6/72, one pulse being measured for each day.

If we call the time of arrival of the second pulse T_o then

Table 6.2

Pulsar	Molonglo Period Measurement	Other Measurement*	Ref.
0031-07	0.942 92 ± 1	0.942 951	3
0450-18	0.548 942 ± 4	0.548 935	4
0628-28	1.244 409 ± 8	1.244 415	5
0736-40	0.374 921 ± 1	0.374 918 6	6
0740-28	0.166 741 3 ± 3	0.166 751	6
0818-13	1.237 71 ±7	1.238 1	7
0833-45	0.089 224 400 ± 4	---**	
0835-41	0.751 621 ± 5	0.751 621	6
0950+08	0.253 064 80 ± 5	0.253 065 04	3
1055-52	0.197 107 9 ± 6	0.197 106 5	6
1154-62	0.400 521 ± 1	0.400 520 3	6
1240-64	0.388 479 ± 1	0.388 479 0	6
1426-66	0.785 457 ± 6	0.785 442 5	6
1449-64	0.179 483 53 ± 1	0.179 483 5	6
1451-68	0.263 376 6 ± 9	0.263 376 8	6
1530-53	1.368 85 ± 3	1.368 881	6
1541+09	0.748 52 ± 3	0.748 448	8
1556-44	0.257 061 ± 1	0.257 055 3	6
1642-03	0.387 688 2 ± 4	0.387 688 8	3
1706-16	0.653 06 ± 1	0.653 050	3
1727-47	0.829 701 ± 4	0.829 699	6
1747-46	0.742 36 ± 1	0.742 351	6
1749-28	0.562 554 ± 1	0.562 553	5
1818-04	0.598 080 ± 3	0.598 073	3
1845-01	0.659 432 ± 1	0.659 428	9

Table 6.2 (contd.)

Pulsar	Molonglo Period Measurement	Other Measurement*	Ref.
1857-26	0.612 203 ± 3	0.612 209	9
1911-04	0.825 96 ± 1	0.825 934	3
1919+21	1.337 33 ± 2	1.337 301	3
1933+16	0.358 737 ± 1	0.358 735	3
1944+17	0.440 609	0.440 618	9
2045-16	1.961 59 ± 1	1.961 567	3

* Uncertainties not quoted. These results have been quoted to sufficient accuracy to establish their differences from the Molonglo results.

** See 6.2.5. No result is quoted here because of the high value of $\dot{P}$ for this pulsar.

the times of arrival of the pulses on the other days

are $T = T_o + N (P_o + \Delta P_o + \dot{P}N)$

where N is the number of pulsar pulse periods between the measurements

P_o the period measured by BPI on 30/5/72.

ΔP_o the amount by which P_o is in error

$\dot{P}$ the period change per period.

It is convenient to define an expected time of arrival by

$$T_E = T_o + N P_o$$

Whence $T - T_E = \dot{P} N^2 + \Delta P_o N.$

The values of N for each pulse (= 0 for the second) could be estimated approximately from the expression for T_E and only needed to be known to about ± 500.

The quantity $T - T_E$ was that interval of time less than one period which remained after an exact number N of periods P_o were subtracted from $T - T_o$. It was measured to ± 0.1 m sec.

From the expression for $T - T_E$ it can be seen that a least squares fit of a parabola to the data will yield values for $\dot{P}$ and ΔP_o.

The following were the results of this calculation

$\Delta P_o = 7$ n sec.

$\dot{P} = 3.14 \times 10^{-15}$ sec/period.

$\equiv 3$ n sec/day.

The change in the Doppler period correction was found to be - 8 n sec/day at the time of the observations.

∴ The true value of $\dot{P}$ for the pulsar was 11 n sec/day, close to the result[10] of more precise measurements.

6.2.5.2 Period and $\dot{P}$ Measurement from Period Measurements over a long interval.

Six independent measurements of the period of PSR0833-45 using BPI were made over a period of about 520 days. The results are listed in Table 6.3.

Table 6.3

Date	Period	
16/9/71	0.089 218 836	
3/12/71	0.089 219 713	
30/5/72	0.089 221 638	± 7
1/6/ 72	0.089 221 652	
19/7/72	0.089 222 163	
16/2/73	0.089 224 400	

Assuming the period is of the form

$$P(t) = P(t_o) + \dot{P}(t - t_o),$$

a least squares fit to the data in Table 6.3 yielded the following result

$$P(t_o) = 0.089\,216\,611 \pm 8 \text{ sec}$$

$$t_o = \text{JD2441000}$$

$$\dot{P} = 10.71 \pm 0.05 \text{ n sec/day.}$$

The value for $\dot{P}$ is within 3σ of the result from more precise measurements.[10]

6.3 Flux Density Measurements.

6.3.1 Table of Results.

Pulsar mean flux densities derived from observations and analysis using B.P.I. are listed in Table 6.3.

Table 6.3

Pulsar	Mean Flux Density (m.f.u.)*	Uncertainty(m.f.u.)
0031-07	78	7
0450-18	81	7
0628-28	185	41
0736-40	152	(1)**
0740-28	170	9
0818-13	37	13
0833-45	1577	250
0835-41	155	16
0950+08	1732	825
1055-52	100	49
1154-62	175	16
1240-64	137	21
1449-65	269	10
1451-68	125	57
1530-53	89	12
1541+09	71	13
1556-44	79	13
1642-03	610	84
1706-16	81	9
1727-47	181	32
1747-46	72	44
1749-28	556	43

Table 6.3 (contd.)

Pulsar	Mean Flux Density (m.f.u.)*	Uncertainty(m.f.u.)*
1818-03	175	(3)**
1845-01	70	8
1857-26	120	17
1911-04	102	11
1919+21	116	31
1933+16	425	86
2045-16	204	(2)**

* 1 m.f.u. = 1 milli flux unit
= 10^{-29} Wm^{-2} Hz^{-1}

** Probably an underestimate. The uncertainties are formal errors and may not reflect the real uncertainties.

6.3.2 Discussion of Amplitude Function and Derivation of Mean Flux Density.

The amplitude function A_K, described in Appendix 4A, was used to compute the mean flux density as follows,

Let $\overline{S}$ be the mean flux density, w_p the observed pulse width and P the pulsar period ($\approx P_g$ the gate period). Also let the integration period be $T = NP_g$

The energy per pulse = $\overline{S}$. P

The energy per integration period = N. $\overline{S}$. P.

$= \overline{S}\ T$

Now the amplitude function A_K is proportional to the energy received in each integration time

$$A_K \propto \overline{S}\ T$$

$$\overline{S} \propto \frac{A_K}{T}$$

The constant of proportionality

$$= K\ C$$

where C is the term which gives the sensitivity of the aerial as a function of declination. The constant K was set by comparing results with other pulsar mean flux density measurements as described in 6.3.3.

For those pulsars for which $w_p > \frac{P}{10}$ the value for the mean flux density was computed as

$$\bar{S} = K\ C\ \frac{A_K}{T} \cdot \frac{10 w_p}{P}$$

This was necessary since for pulsars with large values of w_p, only the fraction $\frac{P}{10 w_p}$ of the total pulse energy was received in any one channel.

As mentioned in 4.5.3 a Fourier transform was computed for the final set A_K for each pulsar observation. These transforms were inspected for evidence of periodic flux density variations on time scales between 6 seconds and ten minutes. No well defined periodicities were observed but the results of these inspections are given in Table 6.4 for completeness.

Table 6.4

a) No features in Power Spectrum of Pulsar Amplitude

0031-07, 0450-18, 0736-40, 0740-28, 0833-45, 0835-41, 1055-52, 1154-62, 1240-64, 1426-66, 1449-65, 1451-68, 1530-53, 1541+09. 1556-44, 1706-16, 1727-47, 1818-03, 1845-01, 1857-26, 1911-04, 1919+21, 1933+16, 1944+17,

b) Some long term variability ~2 - 10 minutes

0628-28, 1642-03, 1747-46, 2045-16

c) Erratic or variable over whole spectrum

0818-13, 0950+08, 1749-28.

6.3.3 Discussion of Results.

The uncertainties quoted in Table 6.3 are derived from the observed variations in mean flux density either during a single transit, or from observation to observation. Each observational value was derived after about twenty minutes of integration. On the basis of the results of Rickett[11] it is clear that the decorrelation bandwidths of the Molonglo pulsars will be considerably less than 2.5 MHz at 408MHz because their dispersion measures are in general higher than those in his sample. Hence, with an observing bandwidth of 2.5 MHz at 408 MHz, the uncertainties reflect the effects of noise, or variations in flux density which are intrinsic to the pulsar, except where the dispersion measure is very low.

The flux values quoted in Table 6.3 are uncalibrated both internally with respect to each other, and externally with respect to some absolute flux standard.

The lack of internal calibration is not regarded as serious since the sensitivity of the aerial was essentially constant over the time of the observations, and any changes which did occur would in most cases have been averaged out by repeated observations. It should be noted that the sensitivity of the aerial does vary with declination as discussed in 2.4.1.2, and 6.3.2, and this effect was taken into account in deriving the mean flux densities.

Since no standard pulsar flux scale is available, the Molonglo values were roughly calibrated by comparing them with flux density values obtained at other observatories, as well as earlier Molonglo measurements, for about twenty pulsars[4,9,12-18].

The results are illustrated in Figure 6.1 and indicate that the flux scale for the Molonglo measurements can be defined within about ± 3dB.

Hence it can be seen that while the uncertainties listed in Table 6.3 are those derived from the observations, the real uncertainties which should be attached to the results are of the order of ± 3dB. This reflects the need for observations to be made which not only lead to well calibrated values for mean flux densities but also give some indication of the pulse amplitude statistics.

6.4 Determination of Dispersion Measures using BPI.

6.4.1 Reasons for Measurement.

As discussed in 2.4.2.2, early measurements of dispersion measure made at Molonglo were inaccurate. In fact, in most cases, the results were systematically low due to inaccurate knowledge of the observing bandwidths, with large random uncertainties due to the small time delays to be measured, and the effects of fine structure in the pulsar spectrum.

The problems were increased for highly dispersed pulsars where the signal to noise ratio was low because of the dispersion broadening of the pulse. In particular, for PSR1154-62, individual pulses were almost undetectable in the noise when observed through a 2 MHz bandwidth on the East-West arm of the telescope. Because of the possible association of PSR1154-62 with the Crux supernova remnant[19] an attempt was made to redetermine the dispersion measure of the pulsar to enable comparison of the distances of the pulsar and the supernova remnant from the earth.

Figure 6.1 A comparison of Molonglo pulsar mean flux densities obtained using BPI with values obtained at other observatories or from previous Molonglo measurements. Points joined by a line are discrepant values in the literature. Lines illustrating a ±3dB uncertainty have been drawn about the line equating both sets of measurements. The units denoted (f.u.)* for the Molonglo values were established from this curve rather than absolutely from a standard calibration.

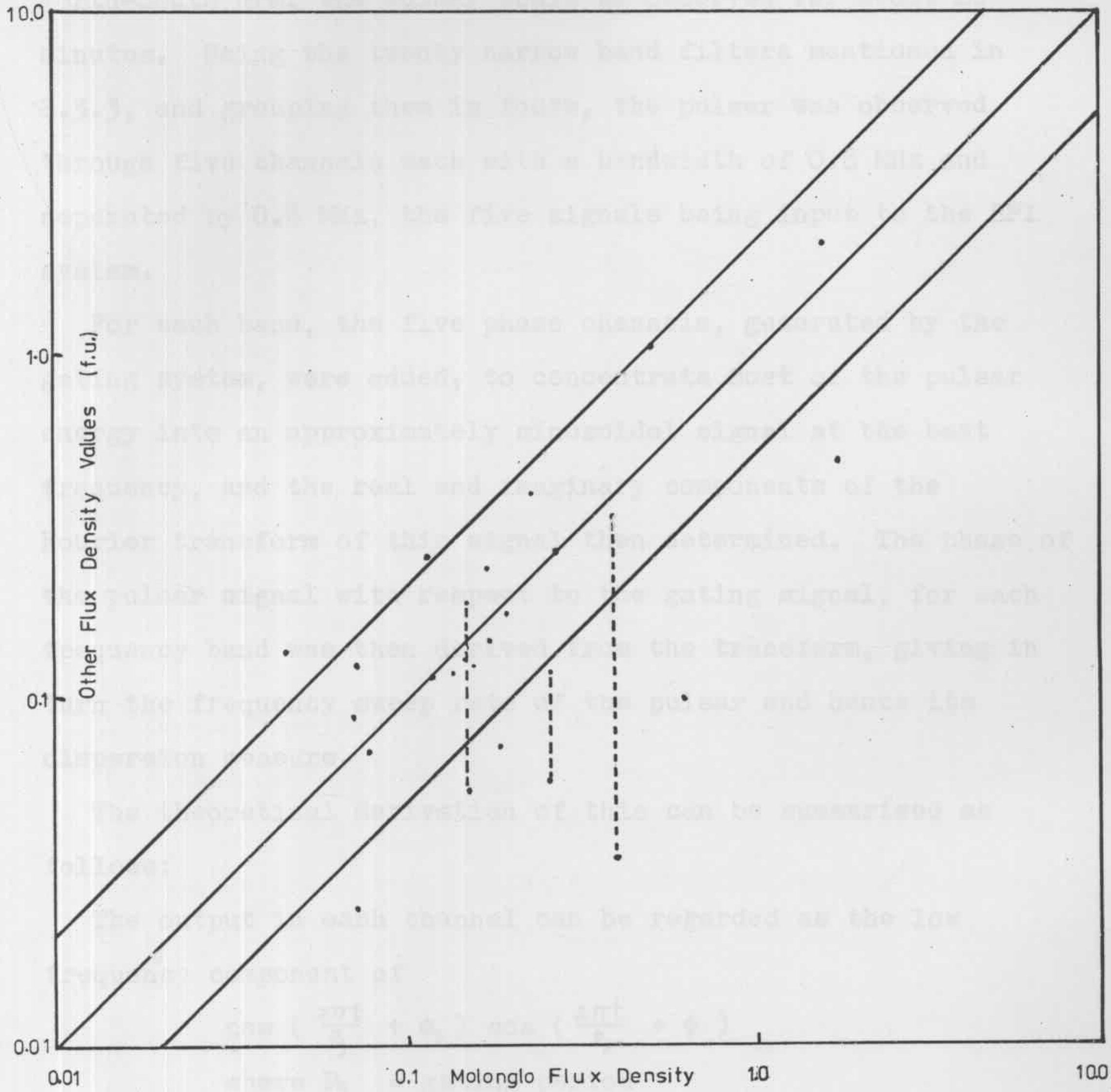
10.0
1·0
0·1
0·01
Other Flux Density Values (f.u.)
0.01
0.1
1.0
10.0
Molonglo Flux Density (f.u.)

6.4.2 Method Used for Determination of Dispersion Measure.

Since the declination of PSR1154-62 had been measured precisely enough to place it in a particular fan beam of the North-South arm, the pulsar could be observed for about 20 minutes. Using the twenty narrow band filters mentioned in 2.3.3, and grouping them in fours, the pulsar was observed through five channels each with a bandwidth of 0.8 MHz and separated by 0.8 MHz, the five signals being input to the BPI system.

For each band, the five phase channels, generated by the gating system, were added, to concentrate most of the pulsar energy into an approximately sinusoidal signal at the beat frequency, and the real and imaginary components of the Fourier transform of this signal then determined. The phase of the pulsar signal with respect to the gating signal, for each frequency band was then derived from the transform, giving in turn the frequency sweep rate of the pulsar and hence its dispersion measure.

The theoretical derivation of this can be summarised as follows:

The output in each channel can be regarded as the low frequency component of

$$\cos\left(\frac{2\pi t}{P_g} + \phi_g\right) \cos\left(\frac{2\pi t}{P_p} + \phi\right)$$

where P_g = gating period

P_p = pulsar period

ϕ_g = gate phase

ϕ_p = pulsar phase

ie. the output can be written as

$$\cos\left[2\pi t\left(\frac{1}{P_g} - \frac{1}{P_p}\right) + (\phi_g - \phi_p)\right]$$

If the signal which is transformed has phase ϕ_s then

$$\phi_s = \phi_g - \phi_p$$

or $$\Delta\phi_p = -\Delta\phi_s$$

Now at 408 MHz

$$dm = -\frac{8180}{\dot{\nu}_{408}}$$

where $\dot{\nu}_{408}$ is the pulsar frequency sweep rate at 408 MHz

See Appendix 6B for the derivation of this relationship.

ie. $$dm = -8180\,\frac{\Delta t}{\Delta B_{408}}$$

$$= -8180 \cdot \frac{1}{2\pi} \cdot \frac{P_p \Delta\phi_p}{\Delta B_{408}}$$

$$= 8180\,\frac{P_p}{2\pi}\,\frac{\Delta\phi_s}{\Delta B_{408}}$$

Now $\Delta B_{408} = -\Delta B_{I.F.}$ (because the 5.5 MHz I.F. is a lower sideband)

Whence $$dm = -8180\,\frac{P_p}{2\pi}\,\frac{\Delta\phi_s}{\Delta B_{I.F.}}$$

The pulsar PSR1933+16 was used to calibrate the system.

This technique is only useful where the uncertainties in ϕ_s are small compared to the change in ϕ_s across the band, ie. for strong pulsars, or pulsars with large dispersion measures.

An expression for the uncertainties in each value of ϕ_s as determined from the components of the Fourier transform is derived in Appendix 6C.

6.4.3 Results.

Using PSR1933+16 as a calibrator, the dispersion measure for PSR1154-62 was found to be 320 $\pm$30cm^{-3}pc compared to the previous measurement at Molonglo of 270 $\pm$35cm^{-3}pc. A more recent determination[6], however, yielded the result 267 $\pm$2cm^{-3}pc.

No clear explanation is apparent for the inaccuracy of the BPI technique for dispersion measure, except perhaps the poor signal to noise ratios in the outer bands, due to the overall bandwidth of the North-South arm being about 2.5 MHz rather than 4 MHz as it is for the East-West arm. Despite the poor result, the method is mentioned here because, for very highly dispersed pulsars, useful results could be obtained if no other methods were available.

6.5 References.

1. Parrat, L. G., "Probability and Experimental Errors in Science" p176. John Wiley and Sons, Inc., New York (1961).

2. Hunstead, R. W., Mon. Not. R. astr. Soc., 157, 367 (1972).

3. Manchester, R. N., and Peters, W. L., Ap. J., 173, 224 (1972).

4. Krishnan, Mohan S., Balasubramanian, V., and Swarup, G., Nature Physical Science, 234, 151 (1971).

5. Hunt, G. C., Mon. Not. R. astr. Soc., 153, 119 (1971).

6. McCulloch, P. M., Komesaroff, M. M., Ables, J. G., Hamilton, P. A., Rankin, J. M., Astrophys. Letters, 14, 169 (1973).

7. Manchester, R. N., Taylor, J. H., Huguenin, G. R., Nature Physical Science, 240, 74 (1972).

8. Lyne, A. G., and Smith, F. G., Mon. Not. R. astr. Soc., 157, 15 P (1972).

9. Jodrell Bank Data (Unpublished).

10. Radhakrishnan, V., and Manchester, R. N., Nature, 222, 228 (1969).

11. Rickett, B. J., Mon. Not. R. astr. Soc., 150, 67 (1970).

12. Goldstein, S. J. Jr., and James, J. T., Ap. J. Letters, 158, L179 (1969).

13. Huguenin, G. R., Taylor, J. H., Hjellming, R. M., and Wade, C. M., Nature Physical Science, 234, 50 (1971).

14. Manchester, R. N., Ap. J. Suppl., 23,283 (1971).

15. Morris, D., Schwartz, U. J., and Slee, O. B., Astrophys. Letters, 10, 67 (1972).

16. Large, M. I., Vaughan, A. E., and Wielebinski, R., Nature Physical Science, 220, 753 (1968).

17. Large, M. I., Vaughan, A. E., and Wielebinski, R., Astrophys. Letters, 3, 123 (1969).

18. Large, M. I., Vaughan, A. E., and Wielebinski, R., Nature, 223, 1249 (1969).

19. Large, M. I., and Vaughan, A. E., Nature Physical Science, 236, 117 (1972).

20. Panofsky, W. K. H., and Phillips, M., "Classical Electricity and Magnetism", p.413. Addison-Wesley Publishing Company, Inc., (1962).

21. Drake, F. D., Gunderman, E. J., Jauncey, D. L., Comella, J. M., Zeissig, G. A., Craft, H. D. Jr., Science, 160, 503 (1968).

Appendix 6A Relativistic Doppler Correction.

Following the methods illustrated in R. K. Wangsness, "Introductory Topics in Theoretical Physics", pp25-27., the relativistic Doppler correction is derived as follows.

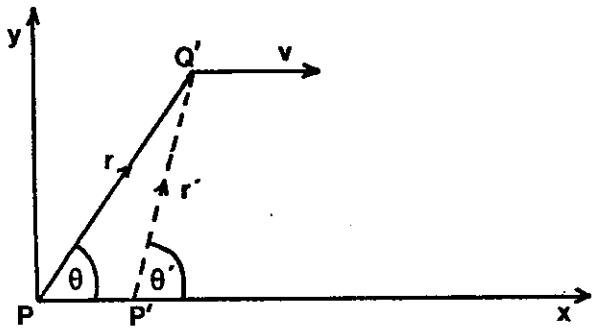

P = Pulsar

Q'= Observer

In the pulsar rest frame (≡ rest frame of the sun for this discussion) the radiation travels from P along r to Q' where r is at an angle such that $-v\cos\theta$ is the component of the earth's velocity in the direction of the pulsar.

In this frame the observed wave can be written as

$$U = \frac{U_o}{r} e^{-i(kr - \omega t)}$$

The observer at Q' however interprets the wave as having the form

$$U = \frac{U_o}{r'} e^{-i(k'r' - \omega' t')}$$

where the primed coordinates refer to the observer's rest frame.

Since phase number is invariant under a Lorentz transformation

$$(k'r' - \omega' t') = (kr - \omega t.)$$

Now $r = x\cos\theta + y\sin\theta$

and $r' = x'\cos\theta' + y'\sin\theta'$

Also $x' = \gamma(x - \beta ct)$

$y' = y$

$t' = \gamma(t - \frac{\beta x}{c})$

Lorentz transformation formulae

Whence, using $k = \frac{\omega}{c} = 2\pi \frac{\nu}{c}$

$$\nu\left(\frac{x\cos\theta + y\sin\theta}{c} - t\right) = \nu'\left(\frac{\gamma(x-\beta ct)\cos\theta' + y\sin\theta'}{c} - \gamma\left(t - \frac{\beta x}{c}\right)\right).$$

This is true for all x, y, t, so the coefficients of these quantities are separately equal

Whence $\nu = \nu'\gamma\ (1 + \beta\cos\theta')$

and $\cos\theta' = \dfrac{\cos\theta - \beta}{1 - \beta\cos\theta}$

So $\nu = \dfrac{\nu'}{\gamma} \cdot \dfrac{1}{1 - \beta\cos\theta}$

This gives the Doppler correction for the frequencies. Since the proof is not dependent on the nature of the wave it is also true for a train of pulses, and in particular

$$P = P'\gamma\ (1 - \beta\cos\theta).$$

Where P = heliocentric pulsar period

P' = geocentric pulsar period

$$\frac{P_{HELIO}}{P_{GEO}} = \frac{1 - \frac{v}{c}\cos\theta}{\sqrt{1 - \frac{v^2}{c^2}}}$$

where $-v\cos\theta$ is the component of v in the direction of the pulsar, or,

$$\frac{P_{HELIO}}{P_{GEO}} = \frac{1 + \frac{v}{c}\cos\theta}{\sqrt{1 - \frac{v^2}{c^2}}}$$

where $v\cos\theta$ is the component of the earth's velocity in the direction of the pulsar.

Appendix 6B Relationship between Dispersion Measure and Frequency Sweep Rate.

Consider a plane wave travelling towards an observer at the origin through a medium of refractive index n

The wave will be of the form

$$U = U_o \, e^{i(\omega t + n k r)}$$

where k is the wave number in free space.

The refractive index n is of the form

$$n = \sqrt{1 - \frac{Ne^2}{\varepsilon_o m \omega^2}} = \sqrt{1 - \frac{\nu_p^2}{\nu^2}} \qquad (20)$$

where ν_p is the free electron plasma frequency,

$$= 8.98 \times 10^{-3} N^{\frac{1}{2}} \qquad (21)$$

The phase term in the expression for the wave is

$$\phi = \omega t + n k r$$

$$= 2\pi\nu t + 2\pi\nu \frac{L}{c}\left(1 - \frac{\nu_p^2}{2\nu^2}\right)$$

where L is the distance from the source to the observer.

To determine the frequency drift rate we set the phase equal to some arbitrary constant, say zero, and see how the time of arrival of the wave varies with frequency.

$$t = -\frac{L}{c}\left(1 - \frac{\nu_p^2}{2\nu^2}\right)$$

$$\frac{\partial t}{\partial \nu} = -\frac{L}{c} \frac{\nu_p^2}{\nu^3}$$

$$\text{or} \quad \dot{\nu} = -\frac{c}{L} \frac{\nu^3}{\nu_p^2}$$

At 408 MHz this reduces to

$$\dot{\nu}_{408} = -\frac{8180}{N L}$$

for N = no. electrons in cm^{-3}

L = distance in parsecs

or dispersion measure = $-\frac{8180}{\dot{\nu}}$

Appendix 6C Uncertainties in a Phase Measurement derived from Fourier Components.

Let the real component of the transform be X

Let the imaginary component be Y

Let the phase be θ

Define σ_x, σ_Y, σ_θ and σ_r as the uncertainties in X, Y, θ and $r = \sqrt{X^2+Y^2}$, the power spectrum.

From $\theta = \sin^{-1} \frac{Y}{\sqrt{X^2+Y^2}}$

we obtain $\frac{\partial\theta}{\partial Y} = \frac{X}{X^2+Y^2}$, $\frac{\partial\theta}{\partial X} = \frac{-Y}{X^2+Y^2}$

From $r = \sqrt{X^2+Y^2}$

we obtain $\frac{\partial r}{\partial X} = \frac{X}{\sqrt{X^2+Y^2}}$, $\frac{\partial r}{\partial Y} = \frac{Y}{\sqrt{X^2+Y^2}}$

Now $\sigma_r^2 = \left(\frac{\partial r}{\partial X}\right)^2 \sigma_x^2 + \left(\frac{\partial r}{\partial Y}\right)^2 \sigma_Y^2$

$= \frac{X^2\sigma_x^2 + Y^2\sigma_Y^2}{X^2+Y^2}$

Similarly $\sigma_\theta^2 = \left(\frac{\partial\theta}{\partial x}\right)^2 \sigma_x^2 + \left(\frac{\partial\theta}{\partial Y}\right)^2 \sigma_Y^2$

$= \frac{Y^2\sigma_x^2 + X^2\sigma_Y^2}{(X^2+Y^2)^2}$

$= \frac{\sigma_r^2}{r^2}$ as $\sigma_x^2 = \sigma_Y^2$ since the noise will have a completely random phase angle.

Whence $\sigma_\theta = \frac{\sigma_r}{r}$

That is, the uncertainty in phase (in radians) is equal to the noise/signal ratio of the power spectrum.

Chapter 7

PULSAR - SUPERNOVA ASSOCIATIONS.

7.1 Introduction.

Associations of astronomical objects are important clues for theories concerning the origins and histories of the objects. The early suggestion that pulsars might be neutron stars[1] was supported by tentative association of PSR0833-45 with the Vela supernova remnant[2] since it has been shown[3] that neutron stars could be formed when stars of mass greater than 4.0 times the solar mass undergo a supernova explosion. At present there is only one completely certain pulsar-supernova association, that of PSR0532+21 with the Crab Nebula. The other associations are plausible if pulsars have high velocities $\sim 100 - 400$ km s^{-1}. Velocities of this order have been observed for pulsar scintillation patterns[4], which can be interpreted as pulsar motion, and also directly, as pulsar proper motion[5].

7.2 The Crux Supernova.

During observations at Molonglo to determine the declination of PSR1154-62, the extended galactic source G296.8-0.3 was discovered and investigated[6]. By comparisons of the flux of G296.8-0.3 at other frequencies, obtained from 85 MHz, 1420 MHz and 2700 MHz surveys of the region[7,8,9], a spectral index of -0.7 ± 0.2 was obtained, indicating a non-thermal source of radiation. Coupled with the size, position, and shape of the source, the spectrum indicated that G296.8-0.3 is a supernova remnant. 408 MHz isophotes for G296.8-0.3 are shown in Figure 7.1.

Using the relationships derived by Milne[10], the distance to the remnant was estimated to be about 4.1 kpc and its age about

Figure 7.1 Isophotes of the Galactic radio source G296.8-0.3 obtained with the Molonglo Cross at 408MHz. The isophote interval is 43 K brightness temperature. Isophote 1 is 21 K above the local background temperature. The positions of the pulsar and the centroid of the radio source are marked. The single closed isophote at the position of the pulsar is consistent with a Cross observation of the mean power of the pulsar. The uncertainty in declination shown for the pulsar is that derived from the declination search procedure (see 5.1). The uncertainty has since been reduced (see 5.4.2).

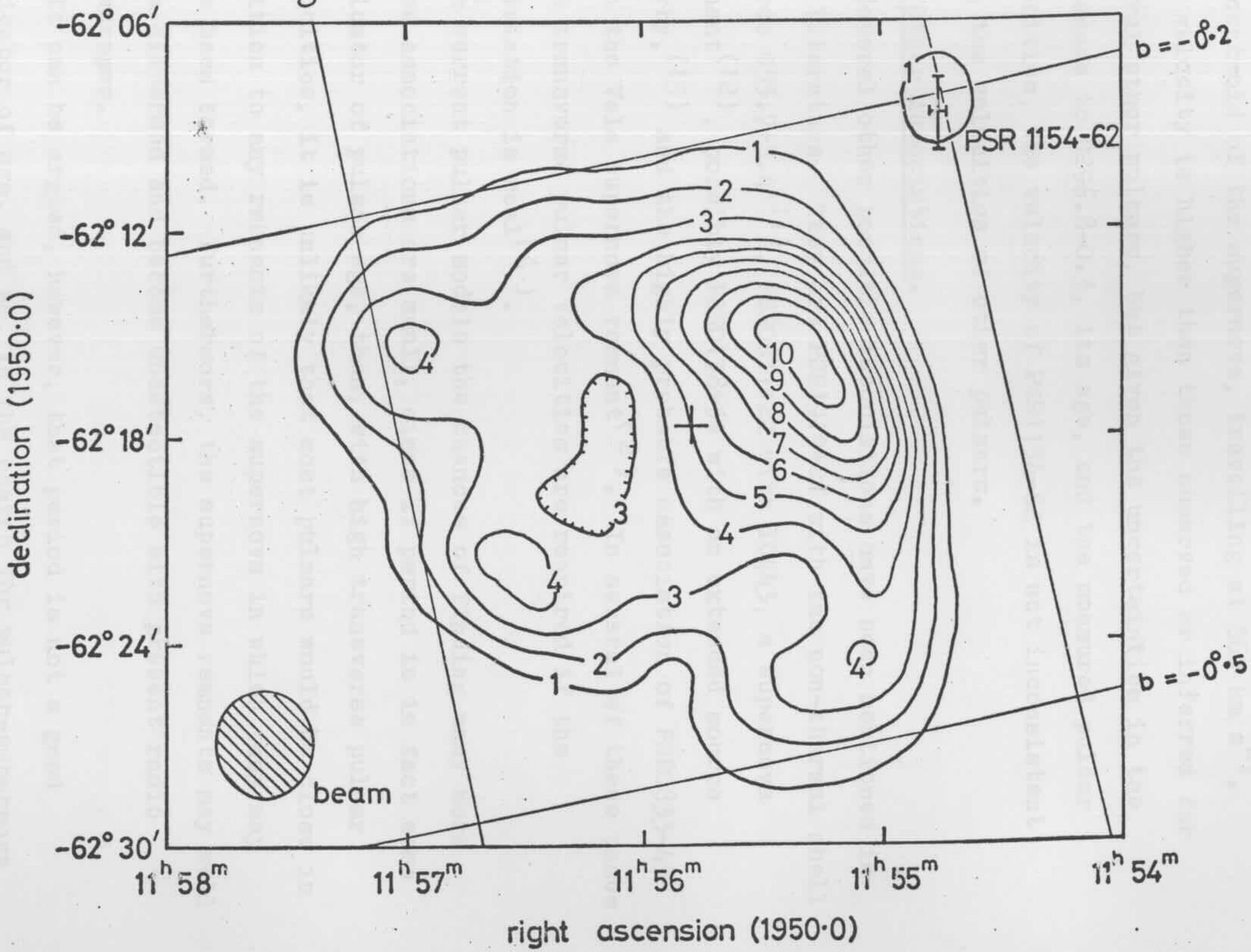
l = 297°.0
l = 296°.7
-62° 06′
-62° 12′
-62° 18′
-62° 24′
-62° 30′
b = -0°.2
b = -0°.5
PSR 1154-62
beam
declination (1950·0)
11h 58m
11h 57m
11h 56m
11h 55m
11h 54m
right ascension (1950·0)

25,000 years. On this model the pulsar is about 14 pc from the centroid of the supernova, travelling at 560 km s^{-1}. This velocity is higher than those observed or inferred for several other pulsars, but given the uncertainties in the distances to G296.8-0.3, its age, and the measured pulsar velocities, the velocity of PSR1154-62 is not inconsistent with the velocities of other pulsars.

7.3 Other Associations.

Several other possible associations have been mentioned in the literature. They are PSR1919+21 with the non-thermal shell source G55.7+3.4[11], PSR0611+22 with IC443, a supernova remnant[12], possibly PSR0138+59 with an extended source nearby,[13] and the highly probable association of PSR0833-45 with the Vela supernova remnant[2]. In several of these cases high transverse pulsar velocities are required if the association is real[6].

On current pulsar models the chances of finding many more close associations are small, since if period is in fact some indicator of pulsar age, then, with high transverse pulsar velocities, it is unlikely that most pulsars would be close in position to any remnants of the supernova in which they may have been formed. Furthermore, the supernova remnants may well have dispersed and become undetectible with present radio telescopes.

It can be argued, however, that period is not a good indicator of age, and so, in the search for pulsar-supernova remnant associations emphasis is needed on finding many weak supernova remnants, and on measuring pulsar proper motions, to

try to project the present pulsar position back to where it may have been in the past--possibly near some supernova remnant.

7.4 The Crab Nebula Pulsar.

The one certain association is that of PSR0531+21 with the Crab Nebula, the remnant of a supernova explosion in 1054 A.D. Assuming a velocity ~ 120 km s^{-1}[14] the pulsar, seen optically as well as over the rest of the spectrum, coincided in 1054 A.D. with the site of the explosion which formed the remnant. The pulsar also provides the answer to the problem the Crab Nebula posed by its X-ray and ultraviolet emission[15]. The decay times of the electrons giving rise to this radiation are $\sim$ 100 years, so some energy source must be present to have enabled the radiation to have continued to the present. The energy radiated by the pulsar is sufficient for this, and also sufficient to explain the outward acceleration of the expanding shell due to radiation pressure. Finally, it is possible that wisps of excited gases near the centre of the nebula may be related to discontinuous period changes in the pulsar when large bursts of energy were radiated[16].

Given the large amount of data that has been collected on the Crab pulsar, as well as the interest it provides by radiating over almost the whole electromagnetic spectrum (30 MHz—γrays), and being clearly associated with the Crab Nebula, it is not surprising that for many people it is almost the only pulsar that exists, and that many empirical and theoretical relationships in pulsar work are inevitably normalised to fit it. The pitfalls in this are apparent since

the Crab pulsar may be as singular within the total pulsar population as the Crab Nebula is among the population of similar objects in the Galaxy.

7.5 References

1. Hewish, A., Bell, S. J., Pilkington, J. D. H., Scott, P. F., and Collins, R. A., Nature, 217, 709 (1968).

2. Large, M. I., Vaughan, A. E., and Mills, B. Y., Nature, 220, 340 (1968).

3. Ostriker, J. P., and Gunn, J. E., Ap. J. Letters, 164, L 95 (1971).

4. Galt, J., and Lyne, A. G., Mon. Not. R. astr. Soc., 158, 281 (1972).

5. Manchester, R. N., Talk given at Stanford Pulsar Conference, (Feb. 1974).

6. Large, M. I., and Vaughan, A. E., Nature Physical Science, 236, 117 (1972).

7. Hill, E. R., Slee, O. B., and Mills, B. Y., Austral. J. Phys., 11, 530 (1958).

8. Hill, E. R., Austral. J. Phys., 21, 735 (1968).

9. Thomas, B. MacA., and Day, G. A., Austral. J. Phys. Astrophys. Supp., No. 11, 1 (1969).

10. Milne, D. K., Austral. J. Phys., 23, 425 (1970).

11. Caswell, J. L., and Goss, W. M., Astrophys. Letters, 7, 141 (1970).

12. Davies, J. G., Lyne, A. G., and Seiradakis, J. H., Nature, 240, 229 (1972).

13. Schönhardt, R. E., Nature Physical Science, 243, 62 (1973).

14. Trimble, V., I. A. U. Symposium, No. 46., 12 (1971).

15. Smith, F. G., (Review paper) Rep. Prog. Phys., 35, 399 (1972).

16. Scargle, J. D., and Harlan, E. A., Ap. J. Letters, 159, L143 (1970).

Chapter 8

THE OPTICAL FIELDS OF RADIO PULSARS.

8.1 Introduction.

Just as there have been several attempts to find associations between pulsars and supernova remnants (see Chapter 7), so there has been some interest in trying to discover optical objects which may either be the pulsars or be associated with them. This work depends initially on precise radio positions being determined for the pulsar and optical photographic plates being searched for possible candidates. The final stage is time resolved photometry observations of the possible candidates to determine if the optical emission is pulsed.

The search for optical pulsars was encouraged by the discovery of the pulsed optical emission of the Crab pulsar, but the lack of pulsed optical emission from any of the candidate objects near PSR0833-45, the Vela pulsar, has decreased the likelihood that pulsed optical emission will be observed for any other known pulsars. This has indeed been borne out for those pulsars for which time resolved optical measurements have been made[1].

8.2 Previous Observations of Pulsar Fields.

Soon after the discovery of pulsars was announced, and their positions measured, the optical fields were examined[2,3]. The rich field of PSR1919+21 makes it very likely that the suggested association[2] with an 18^m blue star is probably a chance association. A tentative candidate for PSR0950+08[3] was ruled out by later more precise position measurements[4,5], including measurements at Molonglo carried out by the author and Dr. A. J. Turtle. For PSR1133+16 a very faint candidate

was suggested[4,5], while no candidate for PSR0834+06 was found[5].

Several early attempts were made to detect optical pulsations [6,7] but without success. With the exception of the Crab Nebula[8] this situation has remained to the present.

8.3 The Field of the Vela Pulsar PSR0833-45.

Since, of all pulsars, PSR0833-45 has properties most similar to the Crab pulsar, much attention was given to searches for optical pulses from objects in the field of this pulsar. The time averaged limiting magnitude for pulsed optical emission was initially set at about 21.5[9] for several objects in the field, being later reduced to about 22.1[10], and then to about 25[11].

The major problem at the moment is the determination of the radio position of the pulsar. Several measurements[12,13,14] exist but they do not agree with each other, although two of them are consistent within the stated uncertainties. The various radio positions are illustrated in Figure 8.1 together with optical objects in the field. It should be noted that the position as derived by BPI is different to that previously published[14], as a result of further measurements and better calibration. Clearly the difference between the Molonglo position and that derived from pulsar timing needs to be resolved. It should be noted, in this respect, that the positional discrepancy is almost entirely in ecliptic longitude, one of the coordinates obtained in the timing position measurement.

Several searches have already been carried out in blank fields within the error boxes of pulsar positions to time

Figure 8.1 The optical field of PSR0833-45. The objects are labelled A to L in conformity with Figure 1 of ref. 18. The circles indicating the optical magnitude show the diameter of the star image on the deep plate of ref. 15. Error rectangles of 1 standard deviation are given for the three radio position measurements. A line of constant ecliptic latitude is drawn through the pulsar timing position.

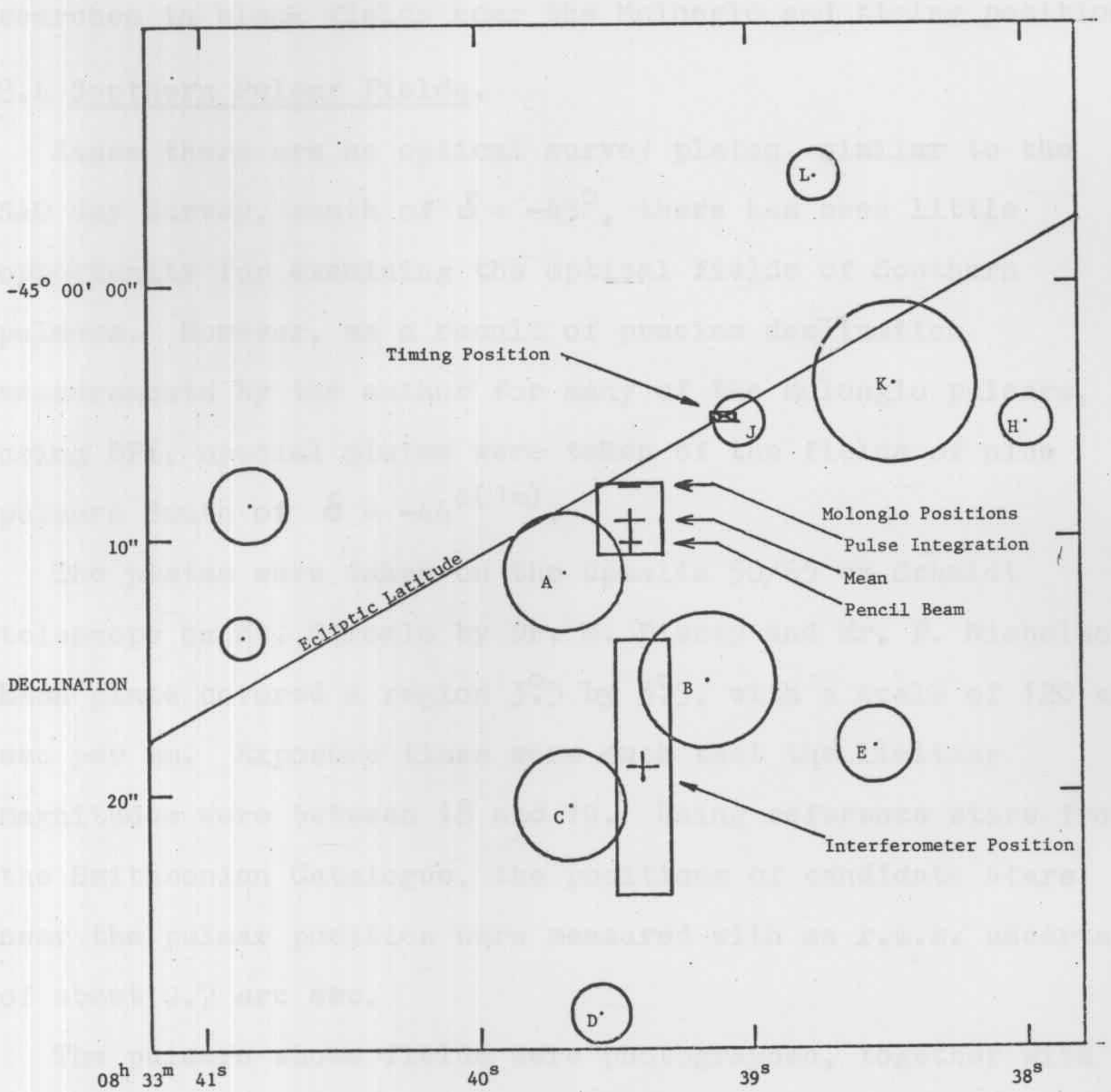
-45° 00' 00"
10"
20"
DECLINATION
Timing Position
Ecliptic Latitude
L
K
J
H
A
B
C
D
E
Molonglo Positions
Pulse Integration
Mean
Pencil Beam
Interferometer Position
08h 33m 41s
40s
39s
38s
RIGHT ASCENSION

averaged limiting magnitudes of about 27[15]. To reach these limits very small diaphragms need to be used, so the positional uncertainties need to be small to reduce the observing time required for the search. At the present there is a need for searches in blank fields near the Molonglo and timing positions.

8.4 Southern Pulsar Fields.

Since there are no optical survey plates, similar to the SAO Sky Survey, south of $\delta = -45^{\circ}$, there has been little opportunity for examining the optical fields of Southern pulsars. However, as a result of precise declination measurements by the author for many of the Molonglo pulsars, using BPI, special plates were taken of the fields of nine pulsars South of $\delta = -44^{\circ}$[16].

The plates were taken on the Upsalla 50/65 cm Schmidt telescope on Mt. Stromlo by Dr. M. Disney and Mr. P. Nicholson. Each plate covered a region $3^{\circ}.5$ by $3^{\circ}.5$, with a scale of 120 arc sec per mm. Exposure times were such that the limiting magnitudes were between 18 and 19. Using reference stars from the Smithsonian Catalogue, the positions of candidate stars near the pulsar position were measured with an r.m.s. uncertainty of about 0.7 arc sec.

The pulsars whose fields were photographed, together with the pulsar positions adopted for the examination of the fields, are given in Table 8.1.

The pulsar fields themselves, with the pulsar position indicated by 3σ error boxes, are illustrated in Figures 8.2, 8.3 and 8.4. The scales in these photographs are ~2 arc sec per mm. The positions of six stars close to the radio position

Figure 8.2 The optical fields of PSR1055-52, PSR1154-62 and PSR1240-64. 3σ error boxes around the radio positions are shown. Also listed are the positions of the stars numbered on each field, to allow further measurements on the field.

1055−52

Pulsar Position
$10^h55^m49^s\pm1^s$ $-52^\circ10'46''\pm3''$

Star Positions

1.	$10^h55^m45^s.2$	$-52^\circ10'04''$
2.	10 55 47.3	-52 10 50
3.	10 55 47.4	-52 10 27
4.	10 55 48.6	-52 10 47
5.	10 55 50.0	-52 11 51
6.	10 55 52.3	-52 10 46

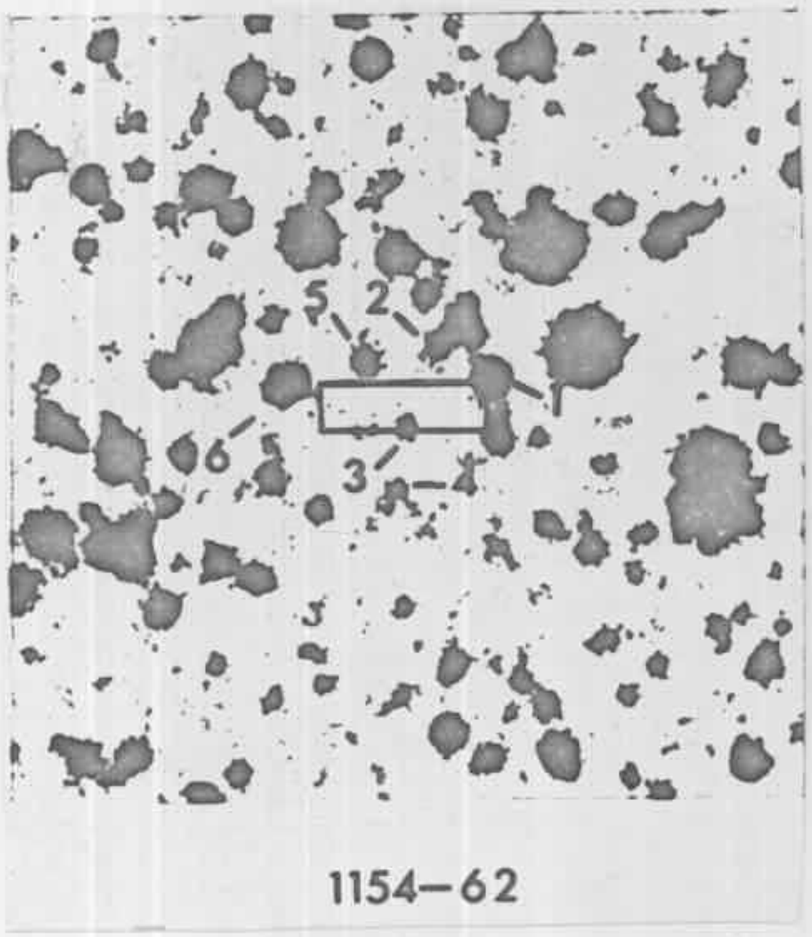

1154−62

Pulsar Position
$11^h54^m45^s\pm1^s$ $-62^\circ08'23''\pm2''$

Star Positions

1.	$11^h54^m41^s.8$	$-62^\circ08'17''$
2.	11 54 43.7	-62 08 09
3.	11 54 44.9	-62 08 28
4.	11 54 45.3	-62 08 45
5.	11 54 46.4	-62 08 12
6.	11 54 49.2	-62 08 18

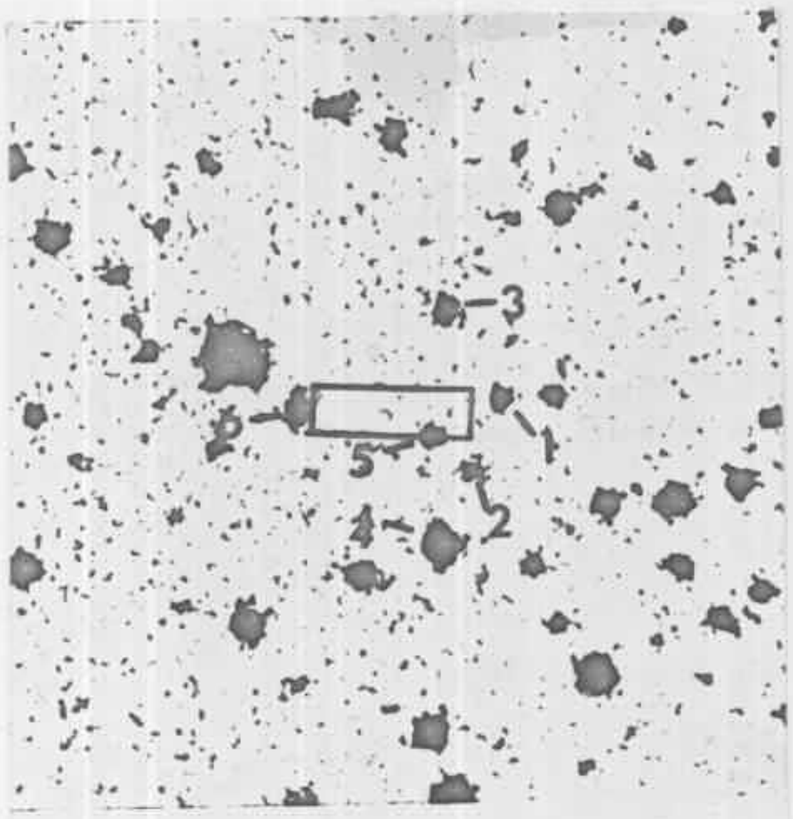

1240−64

Pulsar Position
$12^h40^m20^s\pm1^s$ $-64^\circ06'51''\pm2''$

Star Positions

1.	$12^h40^m15^s.8$	$-64^\circ06'48''$
2.	12 40 17.0	-64 07 06
3.	12 40 17.9	-64 06 26
4.	12 40 18.2	-64 07 26
5.	12 40 18.5	-64 06 57
6.	12 40 23.9	-64 06 51

Figure 8.3 The optical fields of PSR1449-64, PSR1451-68 and PSR1530-53. 3σ error boxes around the radio positions are shown. Also listed are the positions of the stars numbered on each field, to allow further measurements on the field.

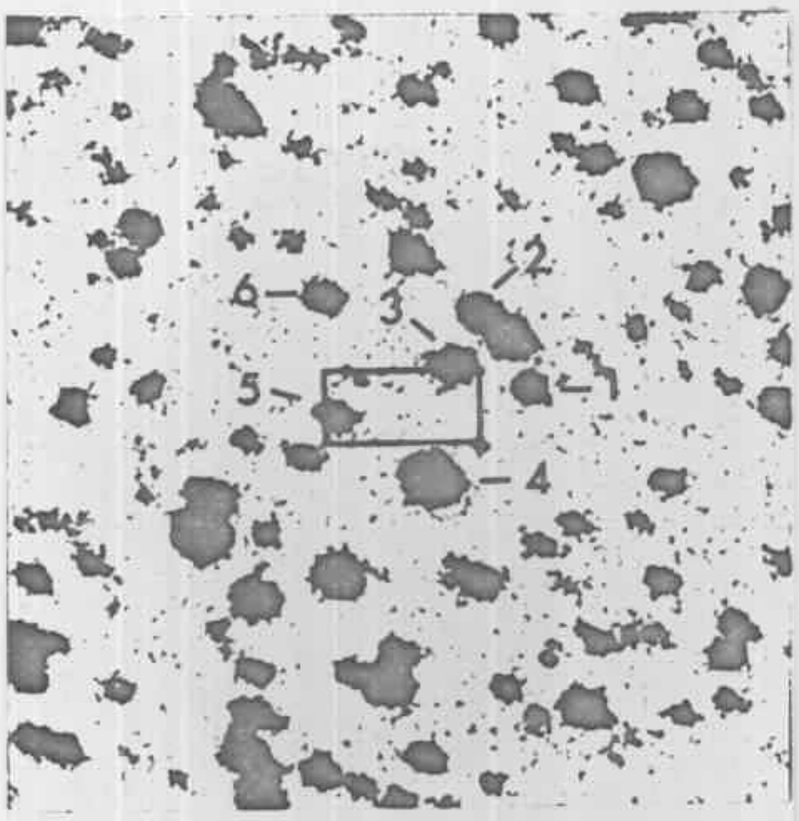

1449−64

Pulsar Position
$14^h49^m22^s \pm 1^s$ $-64^\circ01'01'' \pm 3''$

Star Positions

1.	$14^h49^m17^s.2$	$-64^\circ00'57''$
2.	14 49 19.1	-64 00 37
3.	14 49 20.0	-64 00 51
4.	14 49 21.0	-64 01 20
5.	14 49 24.6	-64 01 02
6.	14 49 24.9	-64 00 32

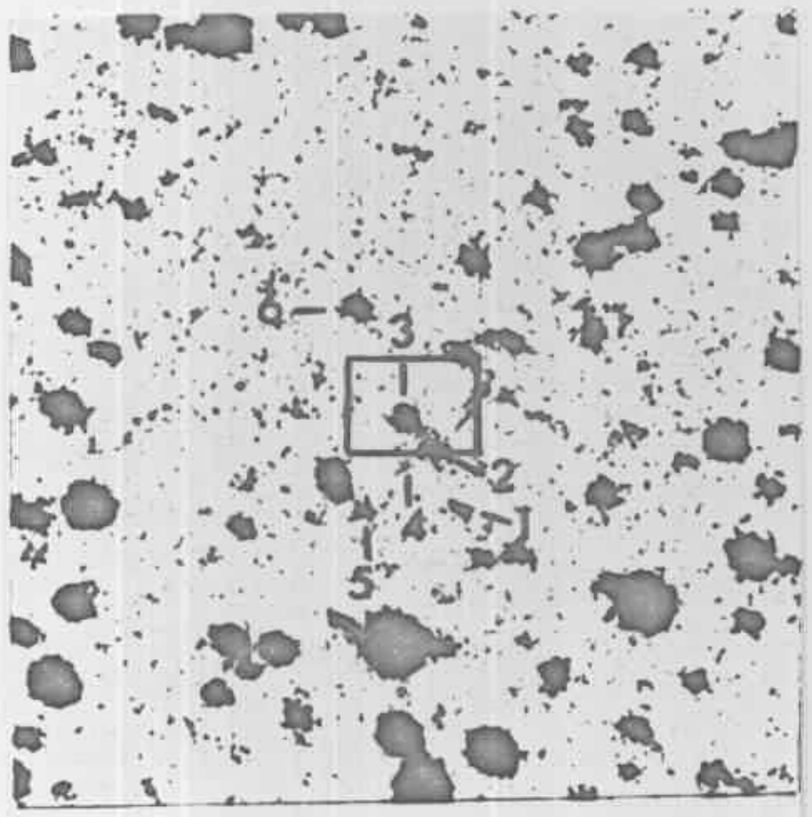

1451−68

Pulsar Position
$14^h51^m29^s \pm 1^s$ $-68^\circ31'33'' \pm 4''$

Star Positions

1.	$14^h51^m26^s.9$	$-68^\circ31'55''$
2.	14 51 27.9	-68 31 39
3.	14 51 29.2	-68 31 31
4.	14 51 29.2	-68 31 43
5.	14 51 31.1	-68 31 54
6.	14 51 31.5	-68 31 04

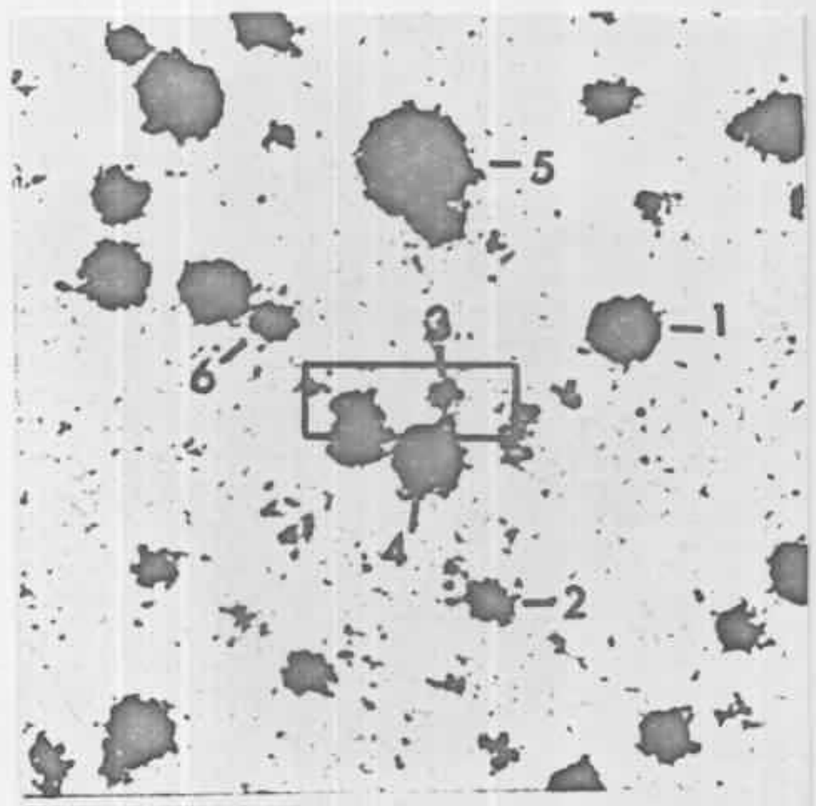

1530−53

Pulsar Position
$15^h30^m23^s \pm 1^s$ $-53^\circ24'17'' \pm 3''$

Star Positions

1.	$15^h30^m17^s.4$	$-53^\circ24'01''$
2.	15 30 21.1	-53 25 09
3.	15 30 22.3	-53 24 17
4.	15 30 22.9	-53 24 34
5.	15 30 23.3	-53 23 20
6.	15 30 27.2	-53 23 59

Figure 8.4 The optical fields of PSR1556-44, PSR1727-47 and PSR1747-46. 3σ error boxes around the radio positions are shown. Also listed are the positions of the stars numbered on each field, to allow further measurements on the field.

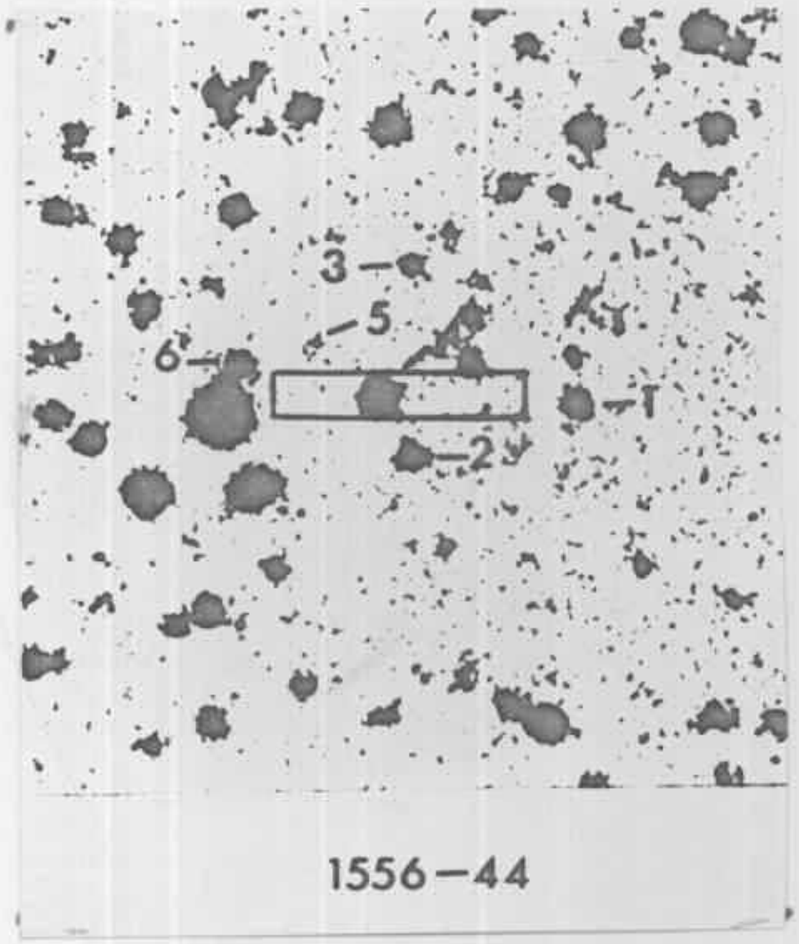

Pulsar Position
$15^h56^m12^s\pm1^s$ $-44^\circ30'12''\pm2''$

Star Positions

1.	$15^h56^m07^s.9$	$-44^\circ30'14''$
2.	15 56 11.8	-44 30 27
3.	15 56 11.9	-44 29 39
4.	15 56 12.6	-44 30 12
5.	15 56 13.8	-44 29 59
6.	15 56 15.9	-44 30 05

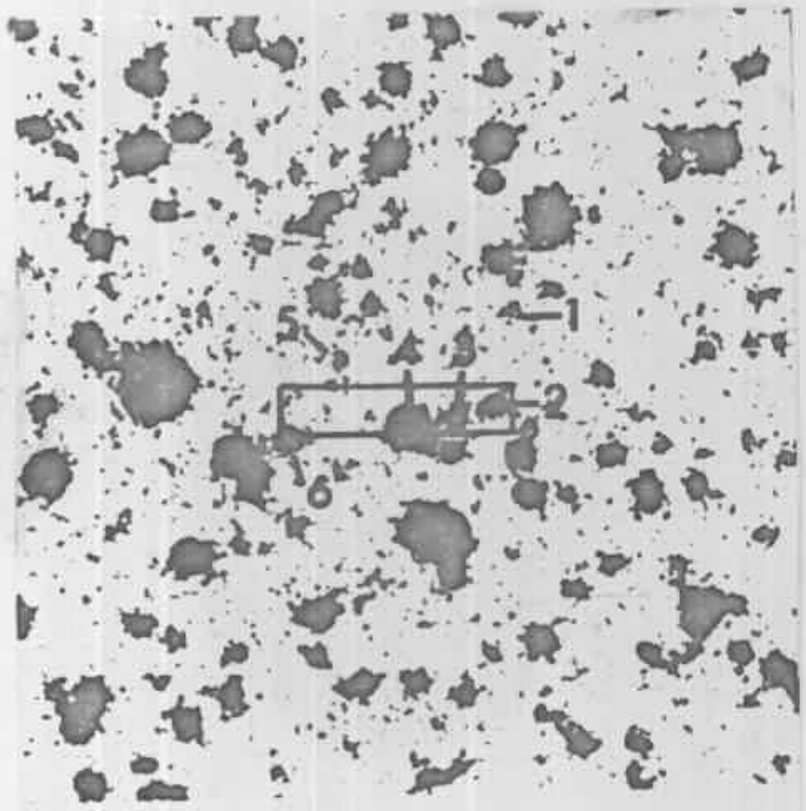

Pulsar Position
$17^h27^m56^s\pm1^s$ $-47^\circ42'22''\pm2''$

Star Positions

1.	$17^h27^m53^s.5$	$-47^\circ41'59''$
2.	17 27 54.0	-47 42 23
3.	17 27 55.0	-47 42 26
4.	17 27 56.1	-47 42 28
5.	17 27 57.8	-47 42 11
6.	17 27 59.1	-47 42 30

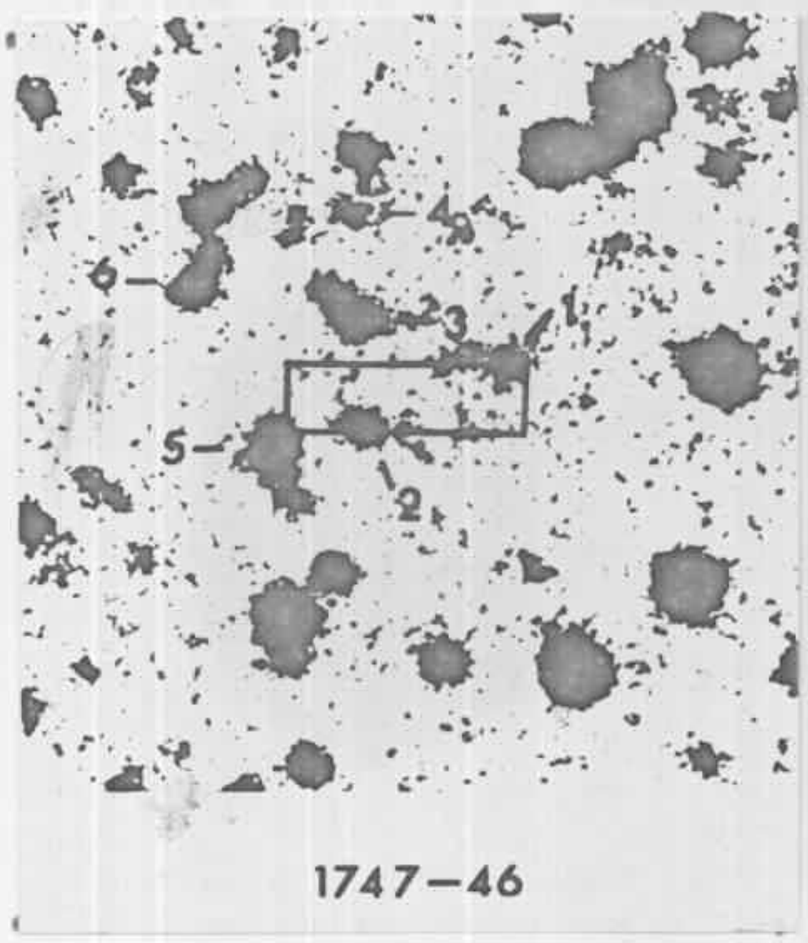

Pulsar Position
$17^h47^m58^s\pm1^s$ $-46^\circ56'42''\pm3''$

Star Positions

1.	$17^h47^m55^s.7$	$-46^\circ56'33''$
2.	17 47 59.2	-46 56 49
3.	17 47 59.3	-46 56 22
4.	17 47 59.4	-46 55 55
5.	17 48 01.3	-46 56 52
6.	17 48 03.3	-46 56 14

Table 8.1

Pulsar	α(1950)	δ(1950)
PSR1055-52	$10^h\ 55^m\ 49^s \pm 1^s$	$-52^\circ\ 10'\ 46'' \pm 3''$
PSR1154-62	11 54 45 ±1	-62 08 23 ±2
PSR1240-64	12 40 20 ±1	-64 06 51 ±2
PSR1449-64	14 49 22 ±1	-64 01 01 ±3
PSR1451-68	14 51 29 ±1	-68 31 33 ±4
PSR1530-53	15 30 23 ±1	-53 24 17 ±3
PSR1556-44	15 56 12 ±1	-44 30 12 ±2
PSR1727-47	17 27 56 ±1	-47 42 22 ±2
PSR1747-46	17 47 58 ±1	-46 56 42 ±3

and symmetrical about it, are given for each plate. This was done because the present uncertainties in the radio positions do not allow the choice of a unique optical candidate for each pulsar. Hence from these plates further examination can be carried out when more precise pulsar positions are available.

It should be noted that no obvious supernovae remnants were found near the pulsar positions.

After ranking the nine pulsars in order of estimated visual magnitude using a simple expression for the optical luminosity and normalising to the Crab pulsar[16], the pulsars 1055-52, 1449-64, 1451-68 and 1556-44 were chosen to be searched for possible pulsed optical emission using a 1P21 phototube at the f/18 offset cassegrain focus on the Mt. Stromlo 30 inch telescope.

PSR1055-52 was missed because of bad weather, but successful observations were carried out (by Dr. M. Disney and

Mr. P. Nicholson) on the other three. The output from the telescope was cycled through 100 bins in a PDP-8 computer such that several complete pulsar periods were covered by the bins. The contents of the bins were examined for pulses but none were observed.

Because of uncertainties in the pulsar positions, since removed, a diaphragm of 40 arc sec diameter was used in most cases, with integration times between 10 minutes and 1 hr. The resulting time averaged limiting magnitudes for pulsed optical emission, assuming a duty cycle of 10% and a detection level of 3σ or more, are listed in Table 8.2.

Table 8.2

Pulsar	Diaphragm (arc sec)	Integration time (sec)	Limiting m
PSR1451-68	40	3700	20.4
PSR1449-64	40	3750	20.4
PSR1449-64	8	640	21.3
PSR1556-44	40	1900	20.1

Clearly further searches are needed with small diaphragms to increase the sensitivity. Furthermore, there is a need for examination of the field of PSR1055-52, particularly since it has a general pulse shape and interpulse reminiscent of the Crab pulsar[17].

8.5 References.

1. Horowitz, P., Papaliolios, C., and Carleton, N. P., Ap. J. Letters, 163, L 5 (1971).
2. Ryle, M., and Bailey, J. A., Nature, 217, 907 (1968).
3. Bailey, J. A., and Mackay, C. D., Nature, 218, 129 (1968).
4. Mackay, C. D., Elsmore, B., and Bailey, J. A., Nature, 219, 21 (1968).
5. Turtle, A. J., and Vaughan, A. E., Nature, 219, 846 (1968).
6. Borgman, J., and Koornneef, J., Nature, 218,531 (1968).
7. Jelley, J. V., and Willstrop, R. V., Nature, 218, 753 (1968).
8. Cocke, W. J., Disney, M. J., and Taylor, D. J., Nature, 221, 525 (1969).
9. Warner, B., and Nather, R. E., Nature, 222, 254 (1969).
10. Willstrop, R. V., Nature, 223, 281 (1969).
11. Chiu, H. Y., Lynds, R., and Maran, S. P., Ap. J. Letters, 162, L 99 (1970).
12. Reichley, P. E., and Downs, G. S., Quoted in ref. 13.
13. Huguenin, G. R., Taylor, J. H., Hjellming, R. M., and Wade, C. M., Nature, 234, 50 (1971).
14. Vaughan, A. E., and McAdam, W. B., Nature, 241, 138 (1973).
15. Lasker, B. M., Bracker, S. B., and Saá, O., Ap. J. Letters, 176, L 65 (1972).

16. Vaughan, A. E., Disney, M. J., and Nicholson, P., Mon. Not. R. astr. Soc., (in the press) (1974).

17. McCulloch, P. M., Talk delivered at Stanford Pulsar Conference, (Feb. 1974).

18. Cocke, W. J., Disney, M. J., and Westerlund, B. E., Nature, 222, 359 (1969).

Chapter 9

DISTRIBUTION FUNCTIONS FOR THE LUMINOSITY, PERIOD AND Z-DISTANCE OF PULSARS.

9.1 Introduction.

In order to determine the precise nature of pulsars it is necessary to analyse the radiation from individual objects and interpret it in terms pf physical models, hoping to find a model which accounts for all properties of all pulsars.

It is also possible, however, to consider the distribution functions for certain pulsar properties, rather than the properties of individual pulsars, and obtain information about the general nature of pulsars. Furthermore, by considering distribution function data and making several a priori assumptions, one can make statements relevant to non-static (ie. evolutionary) models of pulsars.

Of the pulsar properties which could be analysed, a convenient, and physically significant , set is the luminosity, the pulse period, and the distance of the pulsar from the galactic plane (z-distance). Other parameters include flux density, galactic longitude (or distance from the galactic centre), $\dot{P}$ (or $P/\dot{P}$). However, flux density is not only related to the pulsar but also to its distance from the earth, the galactic longitude or the distance from the galactic centre will display irregularities due to the irregular radial density function for the galaxy, while $\dot{P}$ has not been measured for many Molonglo pulsars. On the other hand, the luminosity is a measure of the total radio energy flux from the pulsar, the period is an apparently basic physical property of the pulsar, while the population of pulsars as a function of z-distance, will probably be a smooth

function since it is orthogonal to the radial galactic matter distribution and because the z-distance distributions for other galactic objects eg. supernovae remnants, are smooth.

This chapter presents several analyses of distributions in these parameters, each analysis attempting to accommodate problems inherent to the preceding analysis.

9.2 Simplified Approach to Luminosity and z-distance Distributions.

In order to obtain an impression of the shape of the distributions in luminosity and z-distance, it is possible to carry out a simple analysis by essentially choosing data in which firstly the z-distance is restricted, to give a luminosity function, and then the distance of the pulsar from the earth, projected along the Galactic plane, is restricted, to give the z-distance distribution.

This analysis, suggested by Professor B. Y. Mills, was carried out in 1970 on the 40 pulsars then known.

The procedure was as follows:

Define

$\rho_1(z)\,\rho_2(L)\,dL$ = no. of pulsars per unit volume, at z above the plane, with luminosity between L and L + dL.

(Note: $\rho_2(L)$ assumed independent of z).

Also $\int_0^\infty \rho_2(L)\,dL = 1$

Assume:

1. Dispersion measure a fair distance indicator
2. $\rho_1(z)$ and $\rho_2(L)$ independent of position in the Galaxy, ie. that a disc distribution can be assumed (for a given z).

3. That there is a lower limit to observable pulsar flux densities, S, a constant.

a) Determination of $\rho_2(L)$

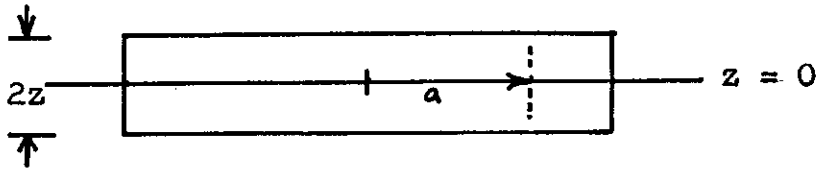

Consider a thin disc centred on the earth and 2z thick.

A pulsar of luminosity L can be seen out to a distance (radius) a given by

$$a = \left(\frac{L}{4\pi S}\right)^{\frac{1}{2}}$$

Now the number of pulsars with luminosity between L and L + dL with z distances less than $|z|$ (small) is

$$dn = \rho_1(0)\,\rho_2(L)\,dL\,\pi a^2 \cdot 2z$$

$$= \rho_1(0)\,\rho_2(L)\,\frac{L\,z}{2\,S}\,dL$$

so $$\rho_1(0)\,\rho_2(L) = \frac{2\,S}{L\,z}\,\frac{\partial n}{\partial L}$$

Now $$\rho_1(0) = \int_0^\infty \rho_1(0)\,\rho_2(L)\,dL$$

$$= \frac{2\,S}{z}\int_0^\infty \frac{1}{L}\cdot\frac{\partial n}{\partial L}\,dL.$$

$$= \frac{2\,S}{z}\sum\frac{1}{L}$$ where the sum is over all pulsars within z of the plane.

Whence $$\rho_2(L) = \frac{1}{L\sum\frac{1}{L}}\,\frac{\partial n}{\partial L}$$

$$\propto \frac{1}{L}\cdot\frac{\partial n}{\partial L}$$ as $\sum\frac{1}{L}$ is a constant.

By deriving $\frac{\partial n}{\partial L}$ from the curve of the integral count n as a function of L, and dividing by L, the form of $\rho_2(L)$ was found to be

$$\rho_2(L) \propto L^{-2}$$ within the uncertainties.

b) Determination of $\rho_1(z)$

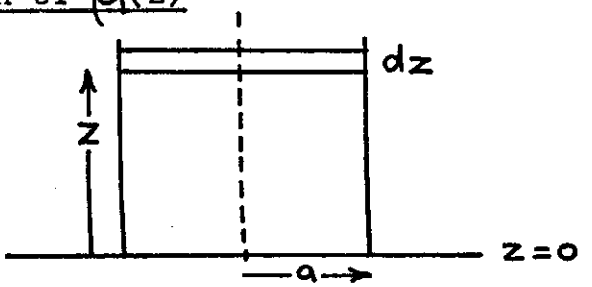

Consider a cylinder as shown with radius a small enough to ensure that all pulsars within the cylinder will have been found.

ie. $a << \left(\frac{Lmin}{4\pi S}\right)^{\frac{1}{2}}$ where Lmin is the minimum Luminosity so far observed.

The number of pulsars between z and z + dz is

$$dn = dz\,\pi a^2 \frac{\rho_1(z)}{\rho_1(0)} \rho_1(0) \left(1 - \int_0^{L=4\pi S z^2} \rho_2(L)\,dL\right)$$

Where the integral represents that fraction of pulsars below the limit of detection.

$$\therefore \frac{\rho_1(z)}{\rho_1(0)} = \frac{\partial n}{\partial z} \cdot \frac{1}{\pi a^2 \left(1 - \int_0^{4\pi S z^2} \rho_2(L)\,dL\right)}$$

Now $\frac{\partial n}{\partial z}$ can be measured from the curve of the integral count n as a function of z. It is observed to be approximately exponential in form with a $\frac{1}{e}$ -width of ~ 5 $cm^{-3}pc$. The term in brackets in the denominator will vary significantly with z, approaching zero as z becomes very large.

As a result, without carrying out the specific calculations, the form of $\rho_1(z)$ is thus seen to be similar but wider than an exponential of width ~ 5 $cm^{-3}pc.$, probably with an elongated tail on the distribution.

This simple approach is only able to give an impression of the distributions. It has the following disadvantages:

1) The minimum observable mean flux density is assumed independent of any other parameters, such as period, whereas

by experiment this is known to be false.

2) In deriving each separate distribution, the restrictions imposed result in the use of only a small number of pulsars. As a result the statistical uncertainties in the derived distributions are large.

3) The two distributions considered are assumed to be orthogonal, which may not necessarily be the case.

4) The slopes of integral counts are not necessarily good estimates of the differential distribution.

9.3 The Effects of Search Sensitivities.

9.3.1 The 'Range of the Search'.

The sensitivity curves for the Molonglo search given in Figure 3.10 are repeated here as Figure 9.1. They show the sensitivity, for a 50% chance of detection, as a function of pulsar period and dispersion measure. On the same graph, the observed flux density as a function of dispersion measure, for pulsars of different luminosity, appears as a series of parallel lines of slope 2. This of course assumes that dispersion measure is a good distance estimator, and in particular that $L = (dm)^2 S$. By observing the points of intersection of these straight lines with the sensitivity curves it is possible to derive the range out to which a pulsar of given period and luminosity would be visible. Hence it is possible to estimate the range of the search, $R(L, P)$, in units of $cm^{-3}pc$.

The function $R(L, P)$ is plotted against period, for different values of luminosity in Figure 9.2. The feature near the top of the diagram arises from the selectivity of

Figure 9.1 Experimentally derived sensitivity curves for the search of the Galactic Plane. S_o was 100 x 10^{-26} Wm^{-2} Hz^{-1} on the plane and about 75 x 10^{-26} Wm^{-2} Hz^{-1} away from the plane. It was assumed constant at 75 x 10^{-26} Wm^{-2} Hz^{-1} in the analysis using these curves. The parameter on each curve is the period in seconds.


35
30
25
20
15
Sensitivity dB below S_o
10
100
1000
10000
Dispersion Measure (cm^{-3} pc)
·015
·03
·06
·03
·06
·13
·25
·5
1
2
4
8

Figure 9.2 The range of the Molonglo search as a function of luminosity and period. The range is given in units of dispersion measure.

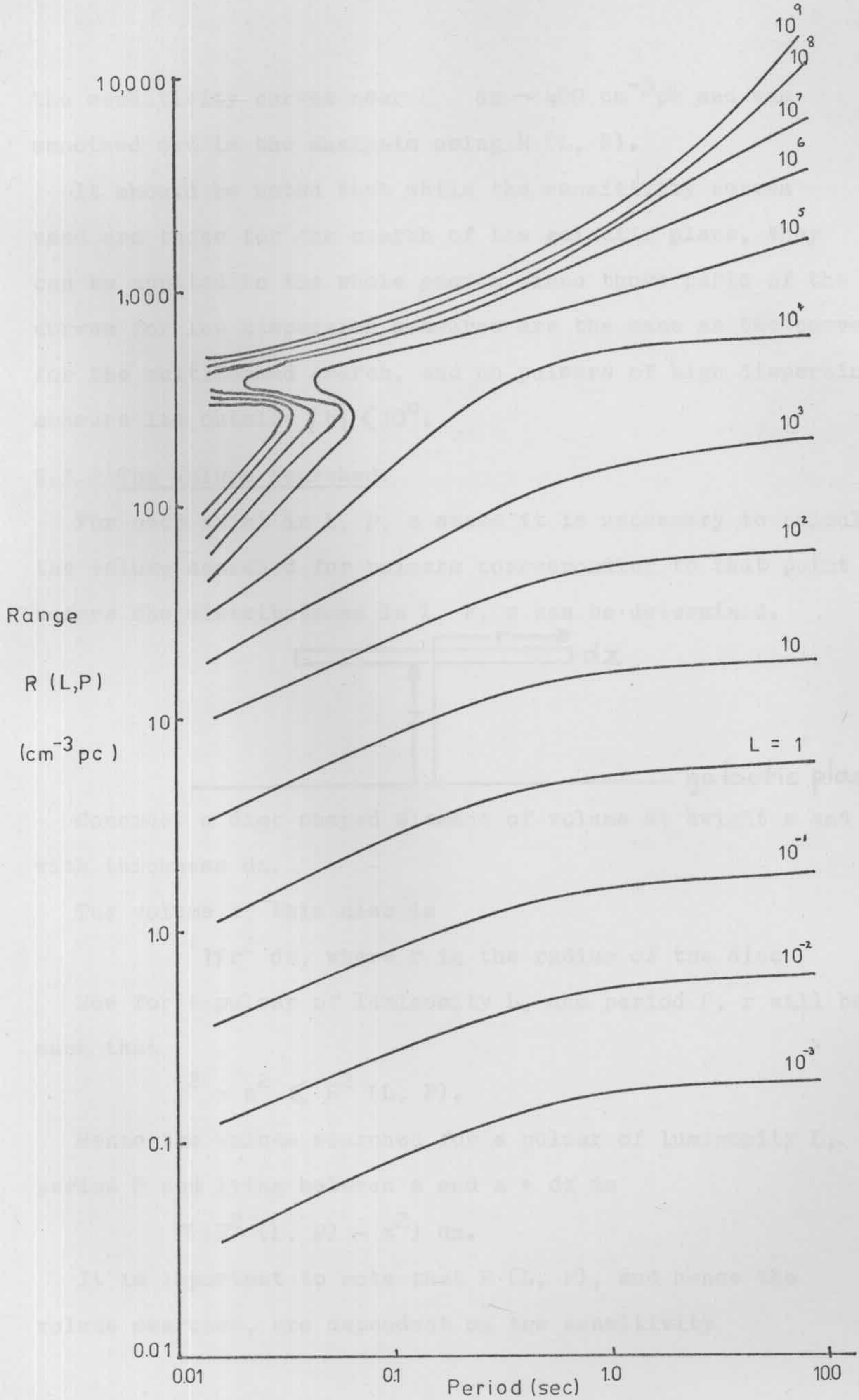
10,000
1,000
100
10
1.0
0.1
0.01
Range
R (L,P)
(cm⁻³ pc)
10⁹
10⁸
10⁷
10⁶
10⁵
10⁴
10³
10²
10
L = 1
10⁻¹
10⁻²
10⁻³
0.01
0.1
1.0
10.0
Period (sec)

the sensitivity curves near dm $\sim$ 400 $cm^{-3}pc$ and was smoothed out in the analysis using R (L, P).

It should be noted that while the sensitivity curves used are those for the search of the galactic plane, they can be applied to the whole search since those parts of the curves for low dispersion measures are the same as the curves for the multibeamed search, and no pulsars of high dispersion measure lie outside $|b| < 10^{\circ}$.

9.3.2 The Volume Searched.

For each point in L, P, z space it is necessary to calculate the volume searched for pulsars corresponding to that point before the distributions in L, P, z can be determined.

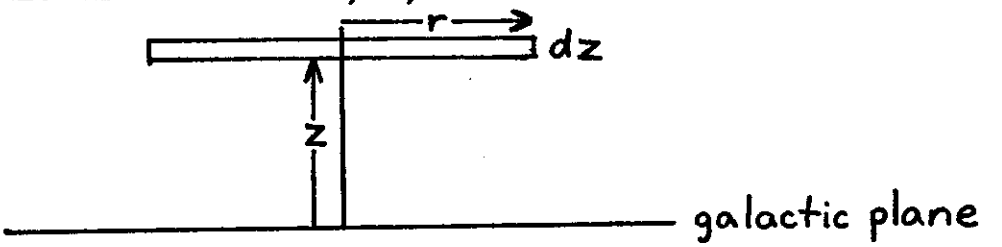

Consider a disc shaped element of volume at height z and with thickness dz.

The volume of this disc is

πr^2 dz, where r is the radius of the disc

Now for a pulsar of luminosity L, and period P, r will be such that

$$r^2 + z^2 \leqslant R^2 (L, P).$$

Hence the volume searched for a pulsar of luminosity L, period P and lying between z and z + dz is

$$\pi (R^2 (L, P) - z^2)\, dz.$$

It is important to note that R (L, P), and hence the volume searched, are dependent on the sensitivity

characteristics of the search system. Unless these are the same for different searches, or the effects of their differences are taken into account, only the data from the particular search to which R (L, P) applies can be used to derive the distribution functions.

9.4 Previous Analysis of L, P, z distributions.

There have been several attempts to derive distribution functions for pulsars in L, P, z[1-5]. In all cases except the last, no account was taken of observational selection effects. Furthermore, in several cases, assumptions were made about the relationship between period and luminosity which are not necessarily supported by the data.

Large[5], however, in his analysis, made the assumption that the period-luminosity correlation is small and has a negligible effect on the derivation of the pulsar distribution functions. There was some criticism of this (see discussion following ref. 5), and the analysis to be presented in this chapter seeks to extend Large's analysis to cover any possible correlations between the pulsar parameters.

The method of analysis given by Large is as follows:

The number of pulsars observed in ranges dL, dP, dz of luminosity, period and z-distance can be written as

$$N(L, P, z)\, dL\, dP\, dz = A(L, P, z)\, \rho(L, P, z)\, dL dP dz$$

where A (L, P, z) dz is the volume of space searched (see 9.3.2) for pulsars of luminosity L, period P, and lying between z and z + dz, and ρ(L, P, z) is the pulsar spatial density function to be determined.

Using the assumption that L, P, z are uncorrelated, one can separate the variables of $\rho(L, P, z)$ writing it as

$$\rho(L, P, z) = \rho_0 \rho_1(L) \rho_2(P) \rho_3(z)$$

Whence

$$\rho_1(L) \propto \frac{\iint N(L, P, z)\, dP\, dz}{\iint A(L, P, z) \rho_2(P) \rho_3(z)\, dP\, dz}$$

and similarly for $\rho_2(P)$ and $\rho_3(z)$.

These equations were solved iteratively using the Molonglo pulsars as data.

The results indicated that the luminosity function could be represented by

$$\rho_1(L)\, dL \propto L^{-x}\, dL$$

where x varies from ~ 1.5 at L = 1 fu(dm)^2 to ~ 3 at L = 10^4 fu(dm)^2.

The period distribution peaked at about P = 0.5 seconds and fell off rapidly at P = 2 seconds.

The distribution in z distance could be adequately represented by an exponential with scale height ~ 7 cm^{-3}pc.

9.5 Factor Analysis of Pulsar Distributions.

9.5.1 New Data -- Observed Distributions.

Since 1971, when the analysis by Large was carried out on the Molonglo pulsars, more recent observations have led to the measurement of mean flux densities for a large number of pulsars (see 6.3). These improved values have been used in the analysis presented here. However where new values have not been measured the previously adopted value was retained.

The observed distributions are illustrated in Figures 9.3,

Figure 9.3 The observed distribution in luminosity, defined as (Flux density) x (dispersion measure)^2, for the Molonglo pulsars.

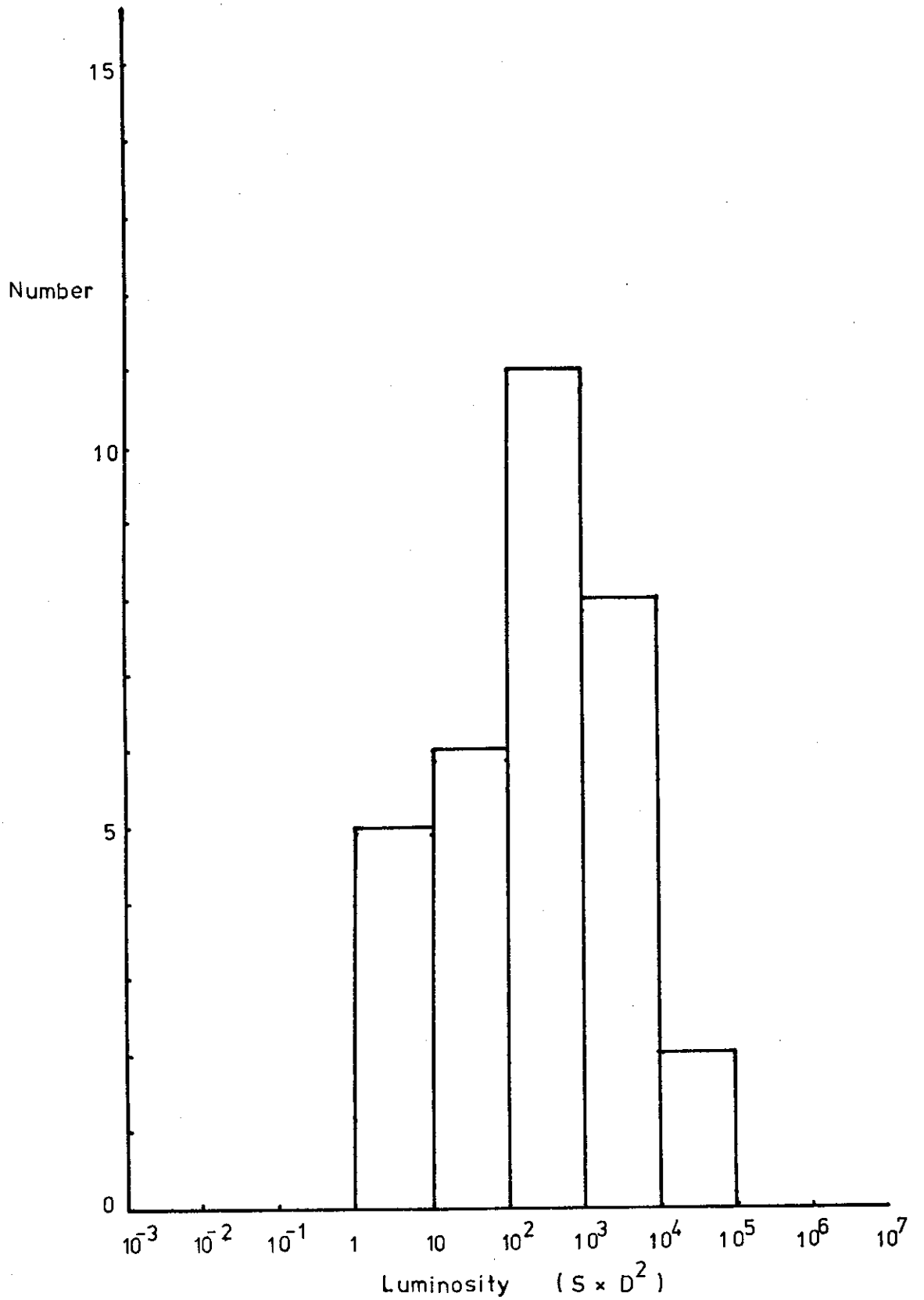
15
10
5
0
Number
10^{-3}
10^{-2}
10^{-1}
1
10
10^{2}
10^{3}
10^{4}
10^{5}
10^{6}
10^{7}
Luminosity (S × D^{2})

Figure 9.4 The observed distribution in period for the Molonglo pulsars.

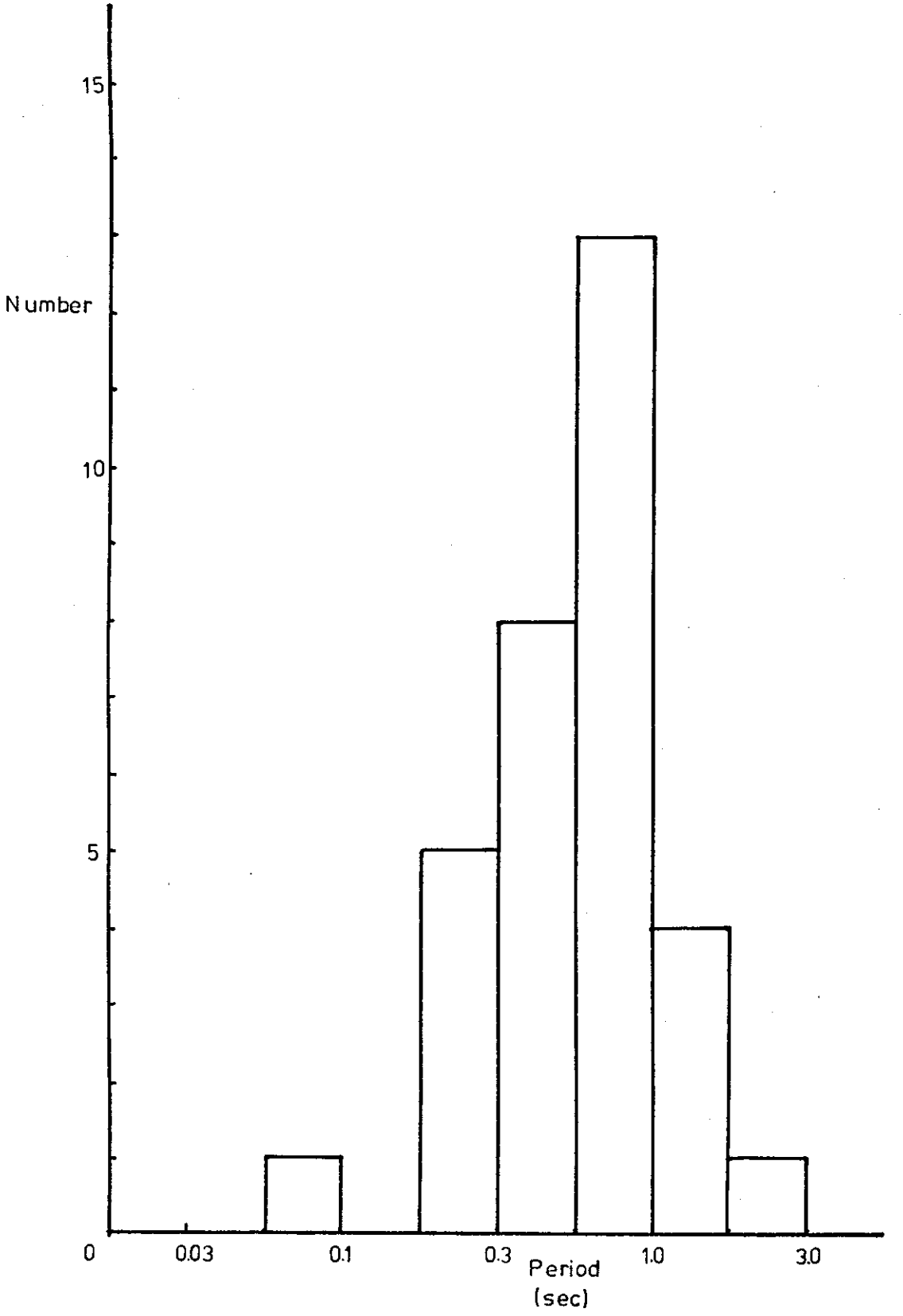
15
10
5
0
Number
0.03
0.1
0.3
1.0
3.0
Period
(sec)

Figure 9.5 The observed z-distance distribution for the Molonglo pulsars.

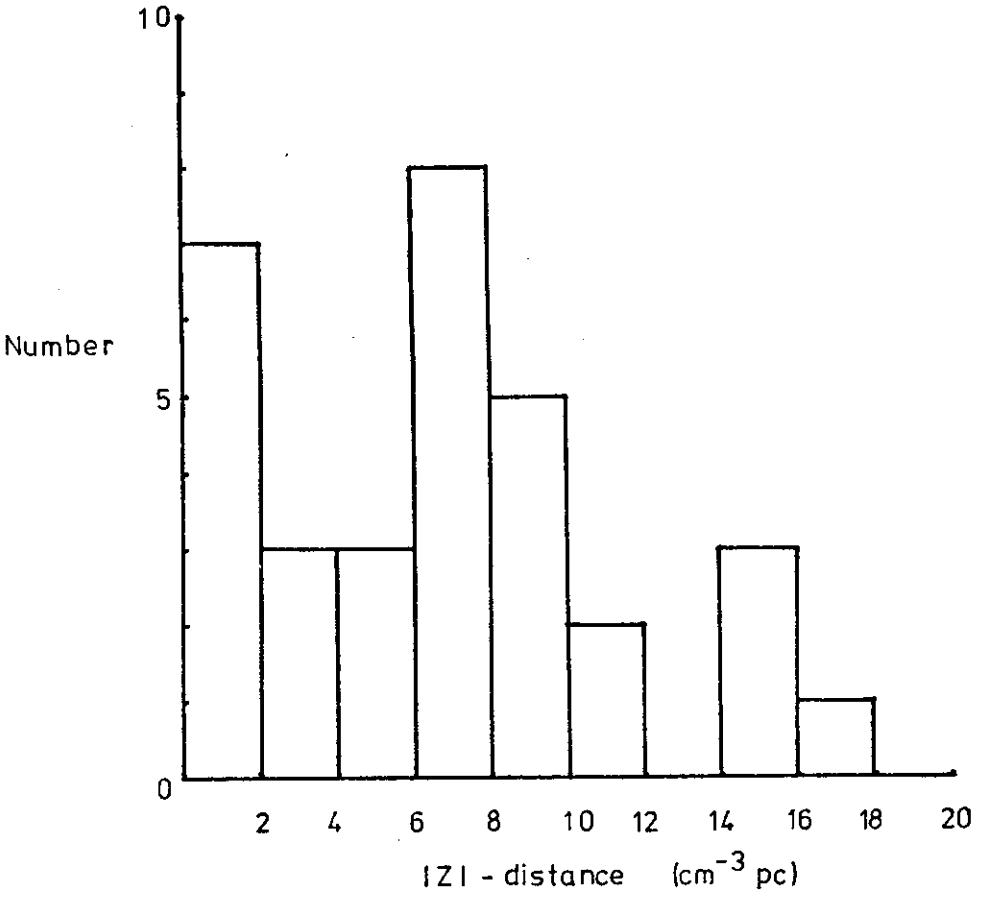
10
5
0
Number
2
4
6
8
10
12
14
16
18
20
|Z| - distance (cm^{-3} pc)

9.4 and 9.5, based on the pulsar properties listed in Table 9.1.

Table 9.1

Pulsar	b^{II} (degrees)	P (S)	dm ($cm^{-3}pc$)	$\overline{S}_{408}$ (m.f.u.)
0031-07	-69.8	0.943	10.9	72
0254-54	-54.9	0.448	10	100
0450-18	-34.1	0.549	25	74
0628-28	-16.8	1.244	34.4	228
0736-40	- 9.2	0.375	100	150
0818-13	12.6	1.238	40.9	45
0833-45	- 2.8	0.089	63	1593
0835-41	- 0.3	0.767	120	157
0940-56	- 2.1	0.664	172	150
0959-54	0.3	1.437	90	100
1055-52	6.6	0.197	40	98
1154-62	- 0.2	0.401	320	186
1240-64	- 1.5	0.389	270	141
1359-50	11.0	0.690	20	100
1426-66	- 5.4	0.787	60	150
1449-65	- 4.4	0.179	90	272
1451-68	- 8.6	0.263	8.6	120
1530-53	1.9	1.369	20	80
1556-44	6.3	0.257	58.8	81
1604-00	35.5	0.413	10.7	50
1642-03	26.1	0.388	35.7	629
1700-18	14.0	0.802	40	100

Table 9.1 (contd.).

Pulsar	b^{II} (degrees)	P (S)	dm ($cm^{-3}pc$)	$\overline{S}_{408}$ (m.f.u.)
1706-16	13.7	0.653	25	50
1727-47	- 7.7	0.830	121	199
1747-46	-10.2	0.742	40	71
1749-28	- 1.0	0.563	50.9	519
1818-04	4.7	0.598	84.5	175
1857-26	-13.5	0.612	35	121
1911-04	- 7.1	0.826	89.4	100
1929+10	- 3.9	0.227	3.2	500
1944+17	- 3.5	0.441	35	200
2045-16	-33.1	1.962	11.5	262

Note 1) More precise values for dm have been published since this analysis was carried out.

2) These values for $\overline{S}_{408}$ are slightly different to values given in Table 6.3 due to the omission of the factor T_{int} in their derivation. The effect on the distributions is not significant.

9.5.2 Observed Correlations.

The luminosity of a pulsar was defined as

$$L = \overline{S}_{408} \times (dm)^2$$

and the z distance as

$$z = dm \sin|b^{II}|$$

The correlation coefficients between L,P and z were measured to allow estimation of their possible significance.

They are listed in Table 9.2

Table 9.2.

Corrln. Coeff.	L v. P	$-0.24\begin{pmatrix}+0.13\\-0.54\end{pmatrix}$	*
" "	P v. z	$+0.02\begin{pmatrix}+0.35\\-0.35\end{pmatrix}$	*
" "	z v. L	$-0.17\begin{pmatrix}+0.17\\-0.50\end{pmatrix}$	*

* 95% Confidence limits for 32 pulsars.

From this data it can be seen that only ρ_{LP} is possibly significant, and even this has a 20% chance of being zero.

Because of the large spread of values of L it was decided to conduct the analysis using the logarithms of L, P, z as the variables. A second effect of this was to linearize any quadratic or higher order correlations between L and P.

The correlations between these variables are given in Table 9.3.

Table 9.3.

Corrln. Coeff.	Log L v. Log P	$-0.17\begin{pmatrix}+0.17\\-0.50\end{pmatrix}$	*
" "	Log P v. Log z	$+0.08\begin{pmatrix}+0.35\\-0.35\end{pmatrix}$	*
" "	Log z v. Log L	$+0.06\begin{pmatrix}+0.35\\-0.35\end{pmatrix}$	*

* 95% Confidence limits for 32 pulsars.

As a result of this change to the logarithms, the z distance distribution becomes as shown in Figure 9.6.

9.5.3 The Factor Analysis Procedure.

The aim of this procedure was to make it possible to derive smoothed distributions which took into account any correlations which may or may not have been present.

Figure 9.6 The observed z-distance distribution using equal intervals of log z.

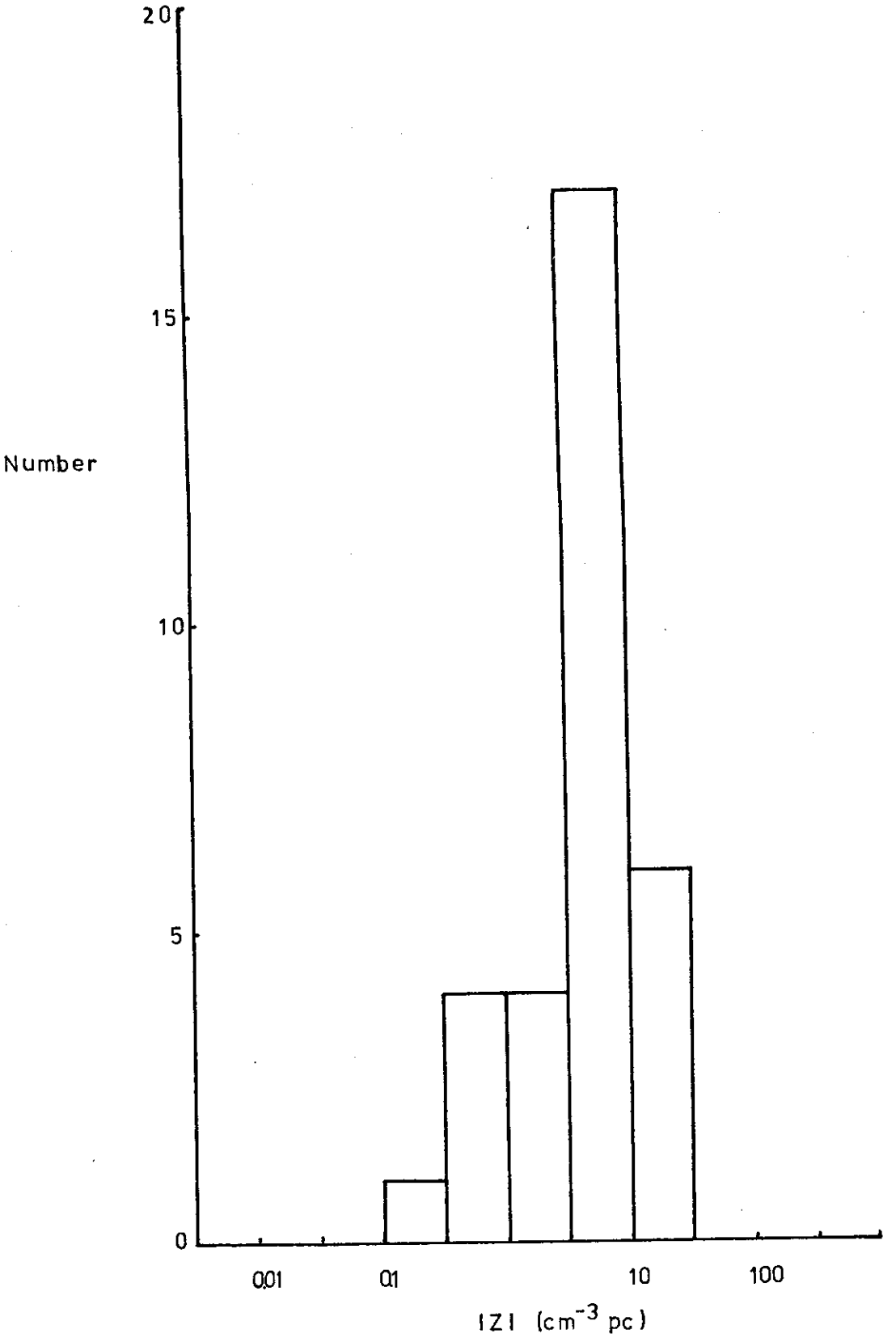
20
15
10
5
0
Number
0.01
0.1
10
100
|Z| (cm^{-3} pc)

Briefly the procedure was as follows:

a) From the observed distribution of the parameters (their logarithms in fact) form the variance-covariance matrix for the data.

b) Derive the eigenvectors of the variance-covariance matrix and use them to transform the data into statistically uncorrelated variables as described in Appendix 9A.

c) Each of the distribution functions in the modified variables can be smoothed without reference to the others since they are independent.

d) Since the distributions are in terms of uncorrelated variables, the complete distribution can now be written as the product of the three independent distribution functions in each of these new variables.

e) Calculate the actual distribution by transforming, point by point, the product of these distribution functions back into the original coordinates, at the same time dividing by the volume searched for each point in L, P, z space.

f) Display the final distribution functions as families of curves, each function having one of the other two variables as parameters.

This can be summarised as follows:

Let n (L, P, z) be the observed distribution of pulsars in the original coordinates.

This transforms to $n'(L',P',z')$ in the new coordinates, which can be written as

$$n_0 f_1'(L') f_2'(P') f_3'(z')$$

since L', P', z' are independent.

Now if the real distribution per unit volume is $\rho(L,P,z)$ then

$$\rho(L, P, z) = \frac{n(L,P,z)}{V(L,P,z)}$$

$$= \frac{n_0 f_1'(L') f_2'(P') f_3'(z')}{V(L,P,z)}$$

where $(L', P', z') \Leftrightarrow (L,P,z)$.

The displays then have the form

$$\rho_{1i}(L, P_i, \bar{z}), \rho_{2i}(L_i, P, \bar{z})$$

$$\rho_3(\Sigma L, \Sigma P, z)$$

The important step in this procedure is the smoothing of f_1', f_2', and f_3' as independent functions, so that the effects of any correlations on the final distributions can be seen.

9.5.4 The Modified Distributions.

Since the observed correlations are quite small the modified distributions are in fact similar to the original distributions.

They are illustrated in Figures 9.7, 9.8 and 9.9. The main effect has been a slight narrowing compared to the original distributions as might be expected. Also shown in each diagram is the smooth curve drawn through the histogram. The error bars arise from uncertainties in the measured flux densities and are described in 9.5.6.

Figure 9.7 The modified luminosity distribution. The points with error bars represent the means and standard errors for the numbers in each class as the flux densities are randomly altered by 0, ±3dB. The smoothed distribution is also shown.

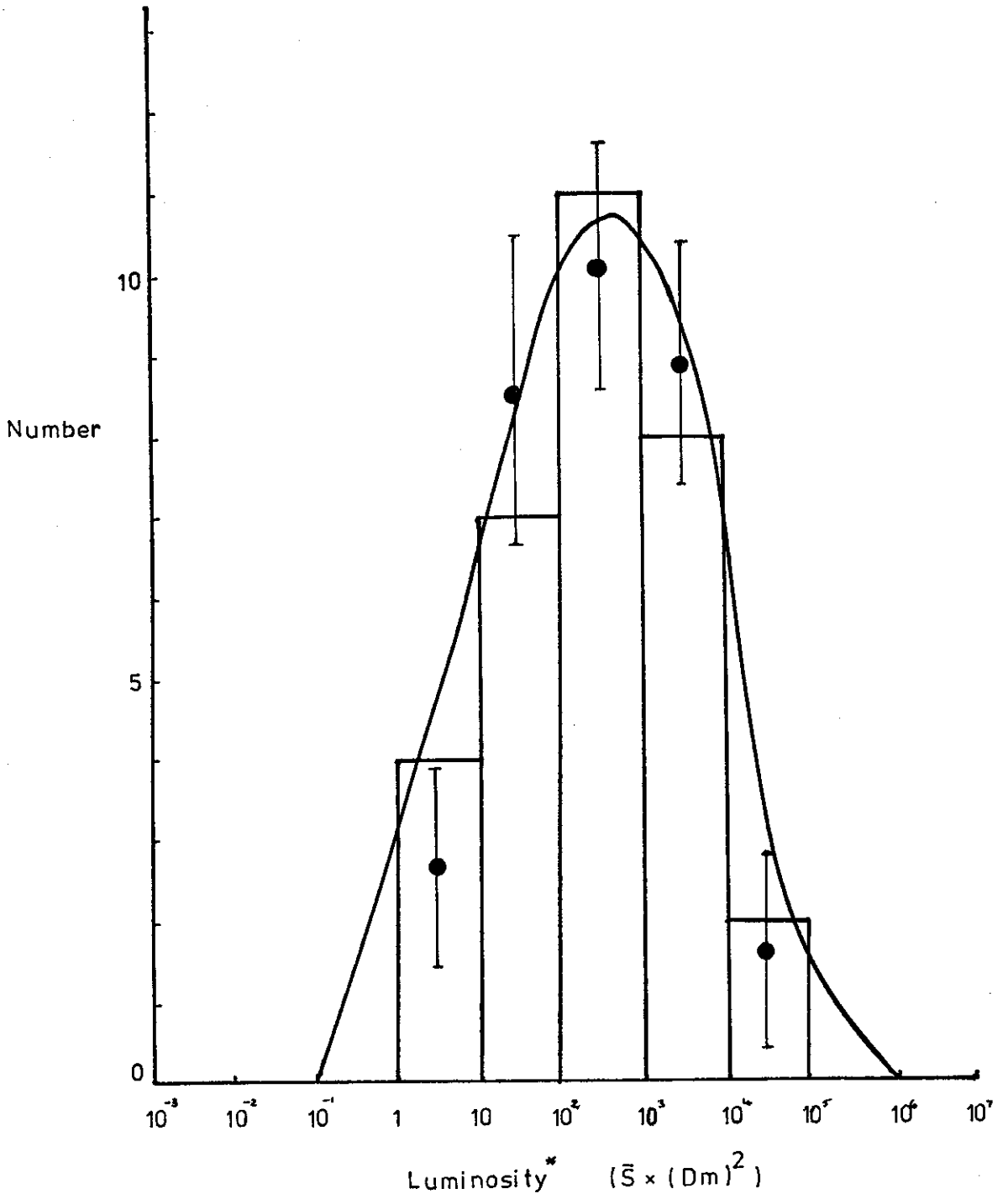
Number
10
5
0
10^{-3}
10^{-2}
10^{-1}
1
10
10^{2}
10^{3}
10^{4}
10^{5}
10^{6}
10^{7}
Luminosity* $(\bar{S} \times (Dm)^2)$

Figure 9.8 The modified period distribution. The points with error bars have the same meaning as in Figure 9.7. The smoothed distribution is also shown.

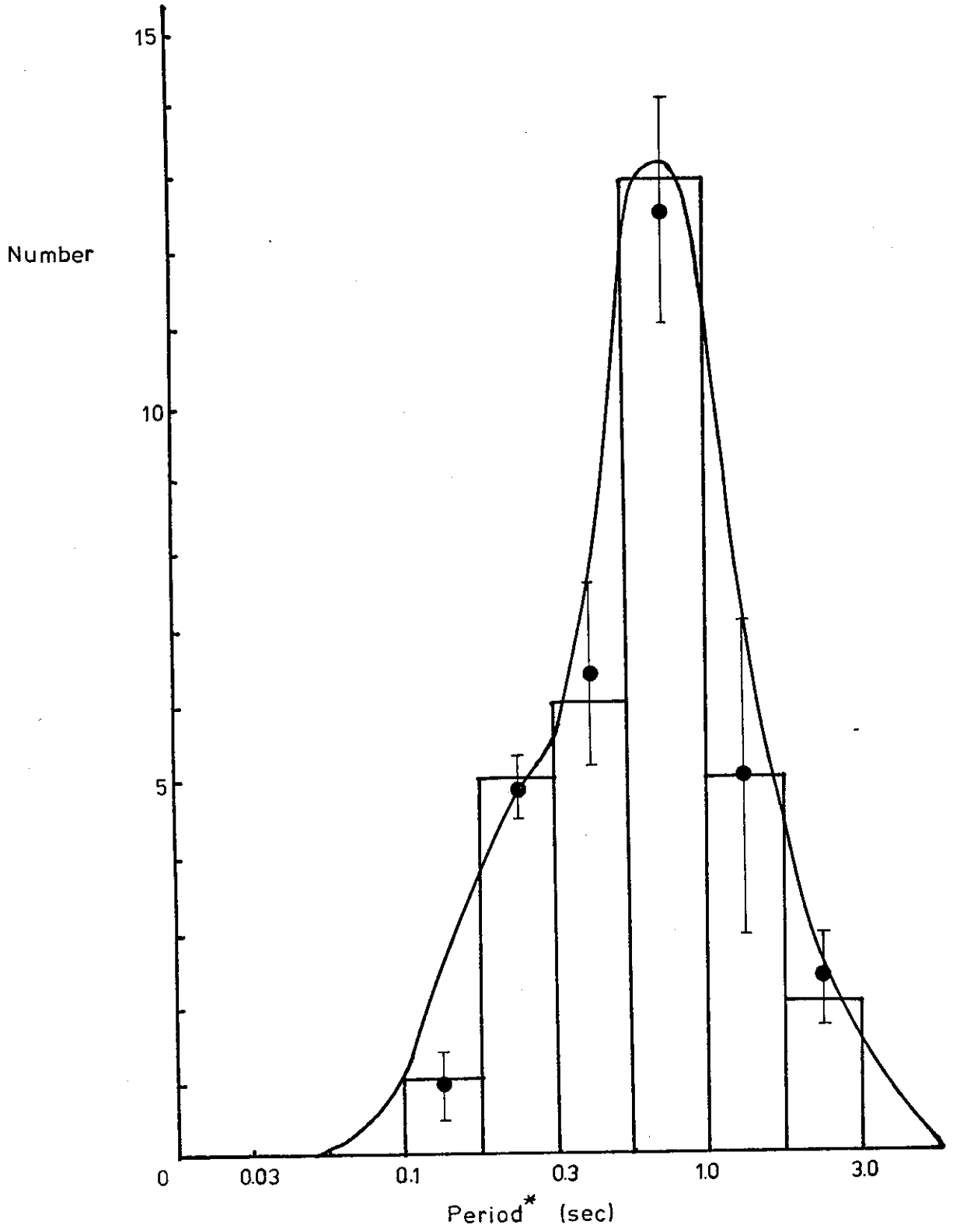
Number
15
10
5
0
0.03
0.1
0.3
1.0
3.0
Period* (sec)

Figure 9.9 The modified z-distance distribution. The points with error bars have the same meaning as in Figure 9.7. The smoothed distribution is also shown.

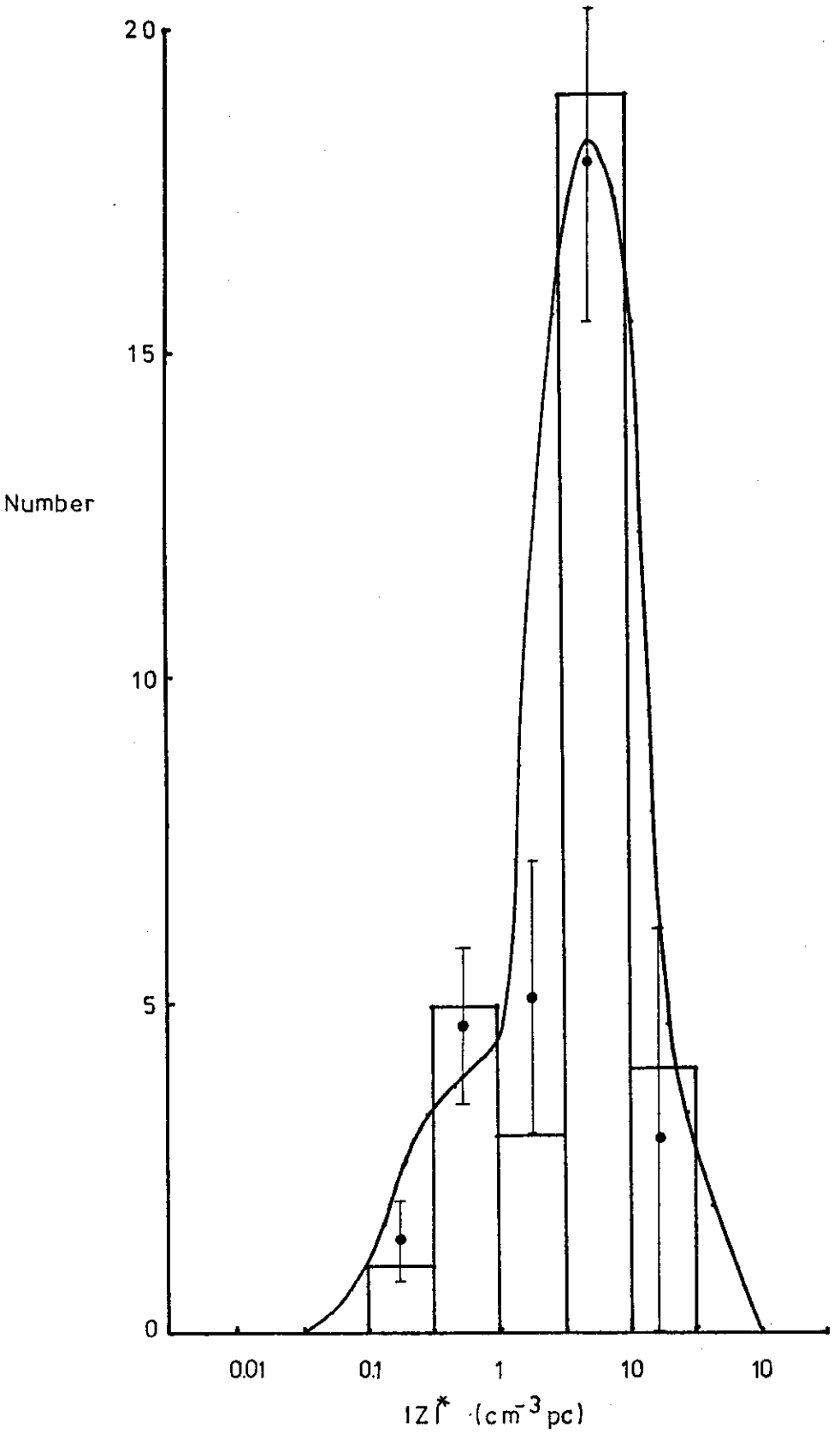
20
15
10
5
0
Number
0.01
0.1
1
10
10
IZf* (cm⁻³ pc)

9.5.5 Uncertainties due to Statistical Fluctuations.

Because of the small numbers in the observed distribution, it is likely that statistical uncertainties are present. To estimate the possible magnitude of these one may proceed as follows:

a) assume that the number of pulsars in each class is Poisson distributed.

If there ar x_0 pulsars in the class,

b) to find the upper limit, find the mean of the Poisson distribution which gives a 0.25 probability for points lying at or below x_0, ie. for which there is 0.75 probability for points $x_0 + 1$ or above.

ie. find m for $\sum_{x=x_0+1}^{\infty} \frac{e^{-m} m^x}{x!} = 0.75$

c) to find the lower limit, find the mean of the Poisson distribution which gives a 0.25 probability for points at or above x_0.

ie. find m for $\sum_{x=x_0}^{\infty} \frac{e^{-m} m^x}{x!} = 0.25$

These values of m, found from tables of the summed Poisson distribution, give reasonable estimates of the bounds of statistical uncertainty about x_0 within that particular class.

As a first order approximation, these uncertainties in the observed distributions may be transferred directly to the actual distributions with the appropriate scaling factors.

9.5.6 Uncertainties due to Flux Density Uncertainties.

As described in 6.3.3, the Molonglo pulsar flux density scale can only be specified to within about ±3dB. Until better measurements are made, it is clear that any distributions

involving flux density will have uncertainties because of this. In an attempt to discover the magnitude of the uncertainties due to flux density uncertainties, the transformation to modified coordinates was carried out seven times with flux densities produced by randomly altering the actual values by 0, ±3dB. The results of this Monte Carlo process are shown in Figures 9.10, 9.11 and 9.12 which illustrate the modified distributions both for the actual data and the seven trials. The points with error bars in Figures 9.7, 9.8 and 9.9 represent the means for each class derived from the seven trials, together with the standard errors of the means. These standard errors were taken as giving an estimate of the uncertainties in the distributions and were carried through to the actual distributions where they were found to be comparable to the uncertainties due to statistical fluctuations in the observed distributions.

Hence while better measurements are required for pulsar flux densities, the present uncertainties do not affect the errors in the distribution functions by more than a factor of about $\sqrt{2}$.

9.5.7 The Relationship between Dispersion Measure and Distance.

An assumption which has been made throughout this analysis is that the dispersion measure is a reasonable statistical indicator of distance. This assumption was also made in the analysis carried out by Large and was the subject of some discussion[5].

Two questions need to be considered. They are the width of the dispersing layer relative to the z-distance distribution

Figure 9.10 The modified luminosity distributions arising from the actual data and the seven Monte Carlo trials produced by randomly altering the flux densities by 0, ±3dB.

Luminosity*

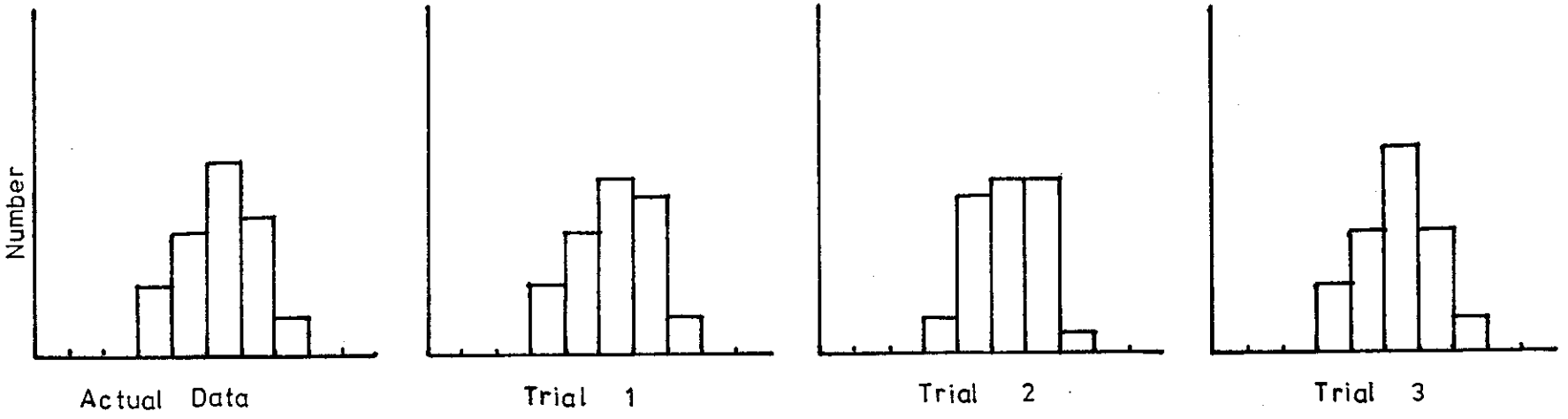
Number
Actual Data
Trial 1
Trial 2
Trial 3

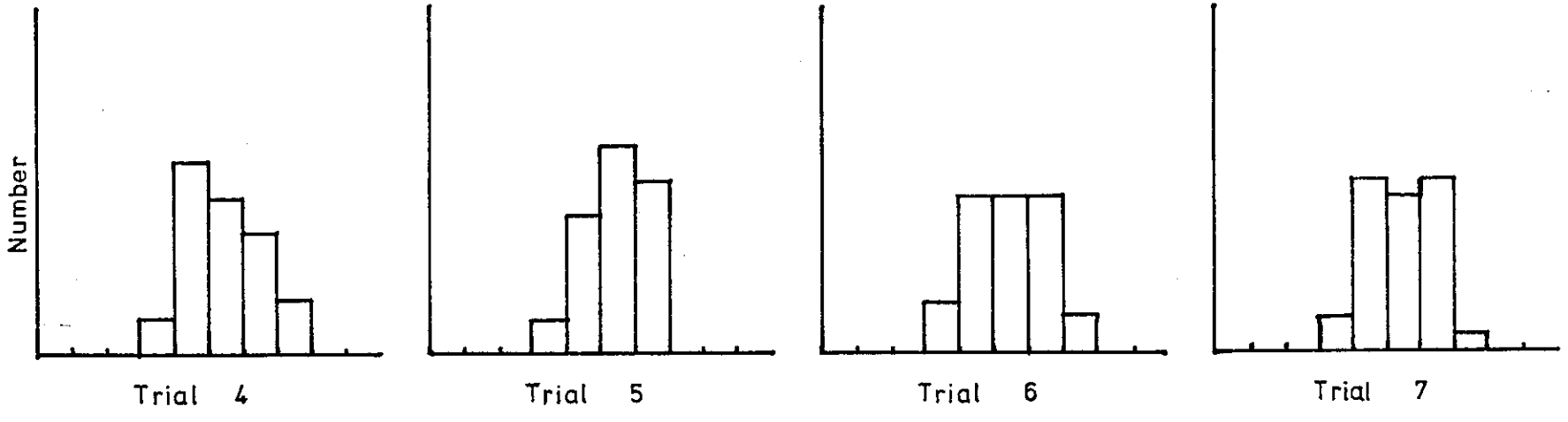
Number
Trial 4
Trial 5
Trial 6
Trial 7

Figure 9.11 The modified period distributions arising from the actual data and the seven Monte Carlo trials produced by randomly altering the flux densities by 0, ±3dB.

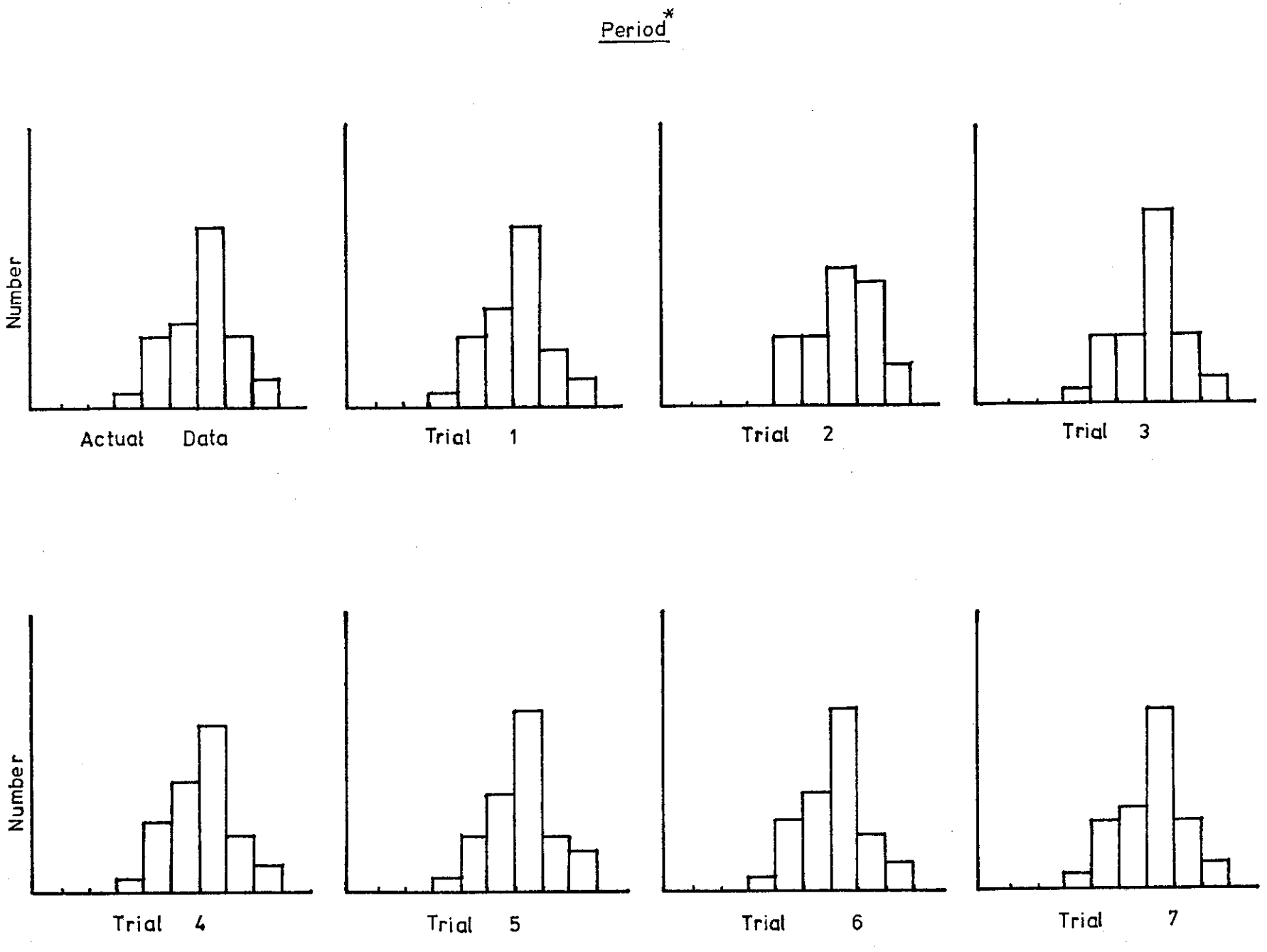
Period*
Number
Actual Data
Trial 1
Trial 2
Trial 3
Number
Trial 4
Trial 5
Trial 6
Trial 7

Figure 9.12 The modified z-distance distributions arising from the actual data and the seven Monte Carlo trials produced by randomly altering the flux densities by 0, ±3dB.

$|Z|^*$ – distance

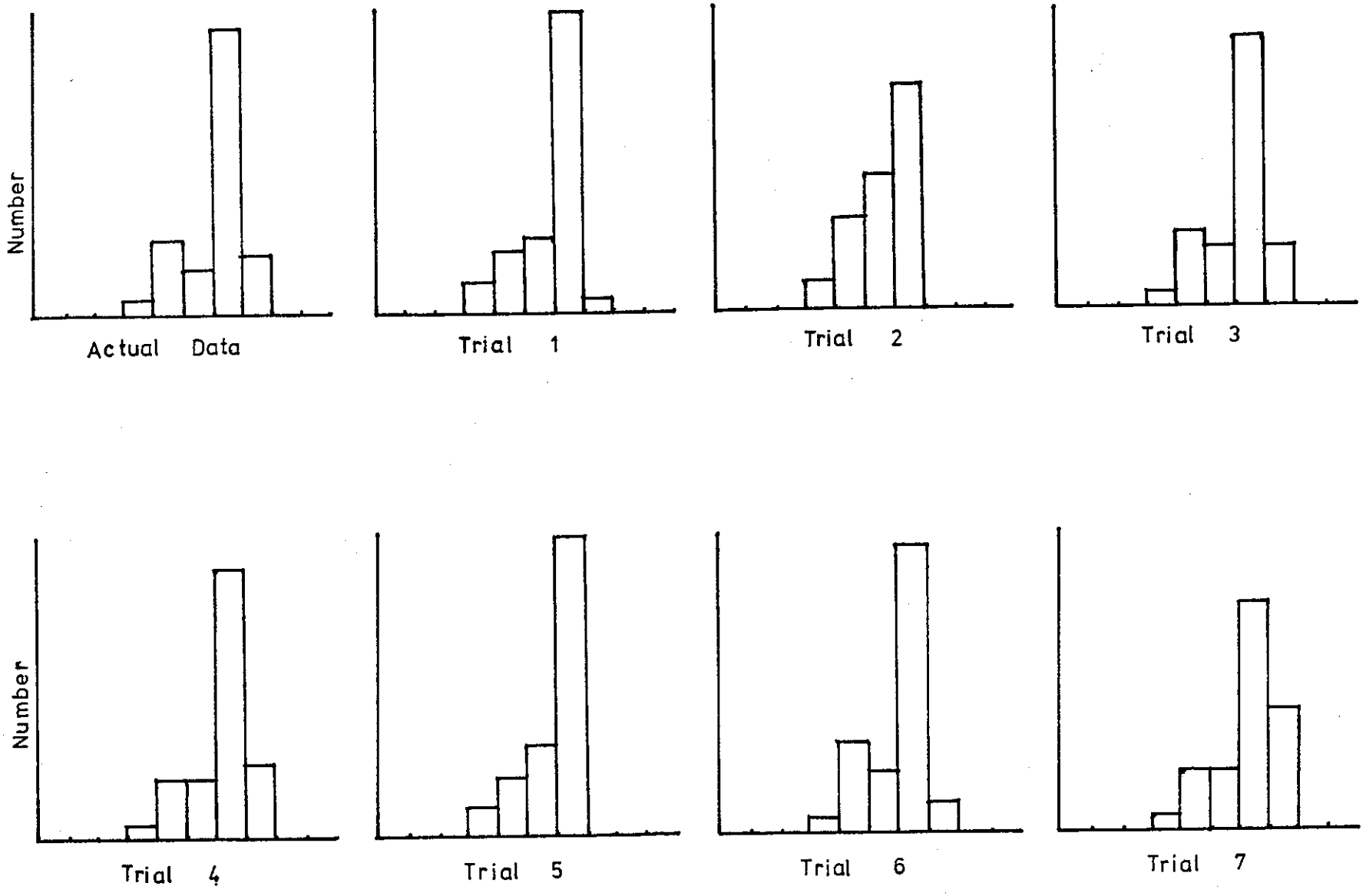
Number
Actual Data
Trial 1
Trial 2
Trial 3
Number
Trial 4
Trial 5
Trial 6
Trial 7

of pulsars, and the effects of H11 regions around hot stars on observed dispersion measures.

Mills,[6] assuming an electron density of the form

$$n(z) = \frac{n_0}{1 + \left(\frac{z}{a}\right)^2}$$

found that $n_0 a \sim 10$ cm^{-3}pc. It can be seen from Figure 9.5, that this means that most pulsars lie well within the dispersing layer and that the effect of assuming that the layer is uniform will not be statistically significant.

Several investigators[7,8,9] have considered the effects of clumps of ionized hydrogen on pulsar dispersion measures, and on the basis of the positions and sizes of known H11 regions near the sun, have computed pulsar distances allowing for these regions. Using these distances, a histogram for the quantity (Distance)÷(Dispersion measure) is shown in Figure 9.13. The mean value of this quantity is 21cm^3, and the standard deviation for an individual pulsar is 11cm^3. Distances based on this model suggest that there is a strong possibility of individual pulsar distances being wrong by more than a factor of 2 using the simple model. However, the use of the dispersion measure as a statistical distance indicator is still valid as shown by the shape of the histogram. The overall effect on the luminosity function of the spread in distance would be comparable to the uncertainties already present.

Other workers support the view that most of the dispersion measure is due to the interstellar medium rather than H11 regions. This is indicated to a certain extent by the studies

Figure 9.13 A histogram of the quantity (Distance)÷(Dispersion measure), the distances being derived taking into account models for H11 regions about hot stars, which lie near the paths to the pulsars.

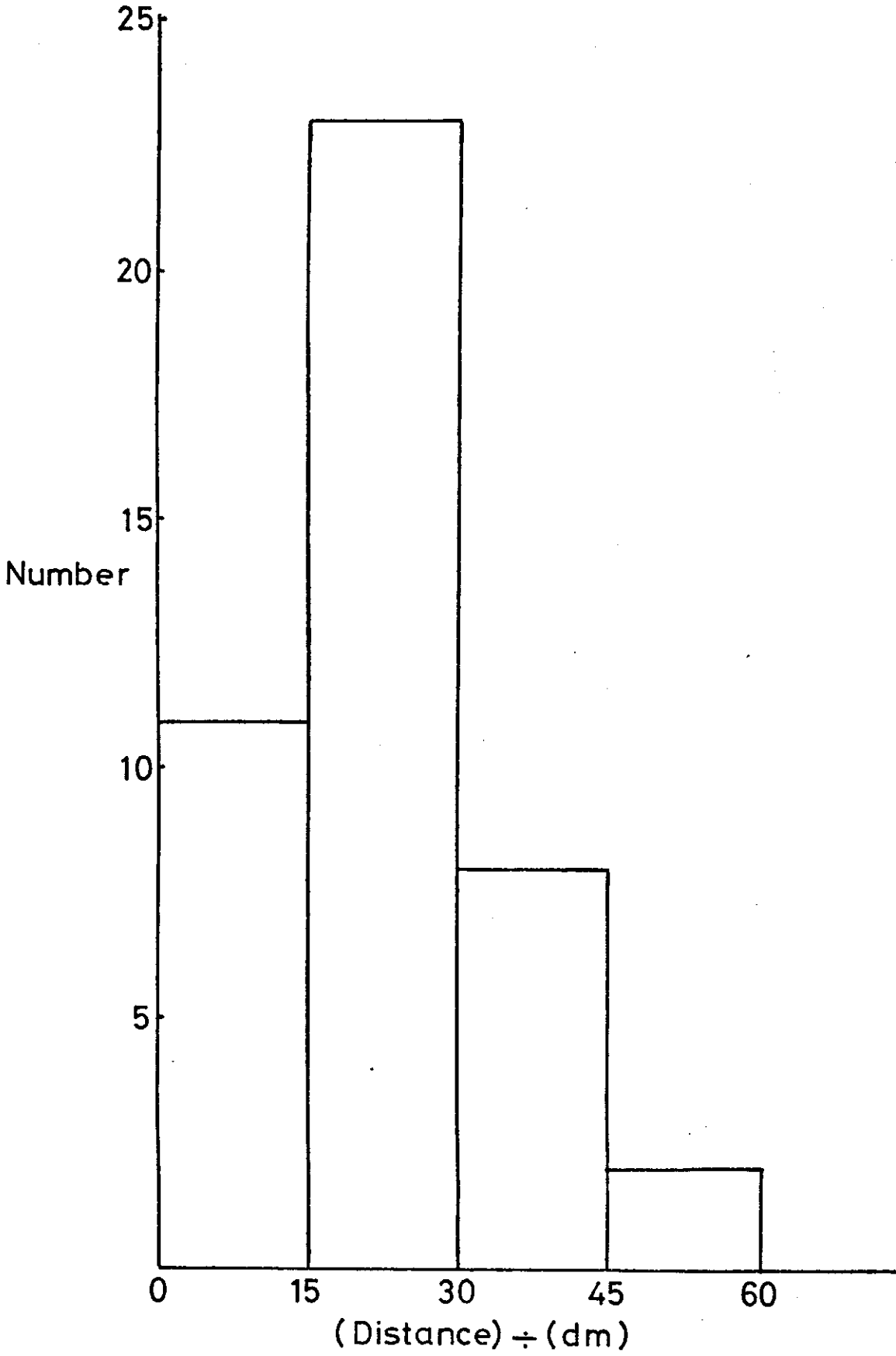
25
20
15
Number
10
5
0
15
30
45
60
(Distance) ÷ (dm)

by Rickett[10] of the causes of pulsar intensity variations. He found that this arose from scattering by small electron density irregularities along the line of sight to the pulsar and that it was related to the dispersion measure, which was presumably arising from the same electrons.

Lyne,[11] on the other hand, has shown that the mean value of $|z|$, defined by $|z| = dm \sin |b|$, is essentially independent of the dispersion measure, so that, assuming that the z-distance distribution will not depend on distance from the sun, the dispersion measure is again seen to be a good statistical distance estimator.

Making the assumption of a uniform dispersing layer, Mills[12] was led to comment on the possible association of several pulsars with features in local galactic structure, further strengthening the case for the use of dispersion measure to give estimates of pulsar distances with good statistical reliability.

9.5.8 Computed Pulsar Distribution functions for Luminosity, Period, and z-distance.

The final distributions were computed as follows:

For given values of log L, log P and log $|z|$, the corresponding modified coordinates were computed using the transformation matrix as described in Appendix 9A. For these modified coordinates, the values for the smoothed modified distributions shown in Figures 9.7, 9.8 and 9.9 were obtained, normalised (ie. $\div 32$) and multiplied together. This result was multiplied by n_o (32) and divided by the volume searched for

the particular L, P and z. This result was then multiplied by $\frac{8}{4\pi}$ since the Molonglo searches only covered 8 steradians of the sky.

The results were then plotted as the series of parametric curves shown in Figures 9.14, 9.15 and 9.16. The uncertainties in Figures 9.14, 9.15 and 9.16 are the result of combining the statistical uncertainties in the observed distributions with the uncertainties in the modified distributions due to ±3dB uncertainties in pulsar flux densities.

The luminosity distributions shown in Figure 9.14 give the number of pulsars per $(dm)^3$ in each logarithmic interval of luminosity. The three curves plotted are the distributions for pulsars with periods of about $1^s.0$, that for pulsars with periods of about $0^s.1$, and that for pulsars of all periods. The distributions have been averaged over all z-distances. The first two illustrate the slight correlation that exists between period and luminosity, but the error bars indicate that the correlation ought not to be regarded as very significant. Of the three curves, only the short period distribution shows any significant curvature. There is some curvature present at the extremes of the other distributions but, with the error bars, a straight line fit is sufficient.

Summed over all periods the distribution can be written as

$$(L)\ dL = L^{-x}\ dL$$

where $x = 2$, with slight changes to $x = 1.75$ at $L = 1$, and $x = 2.5$ at $L = 10^5$. This is similar to the results obtained by Large[5] though with less curvature.

Figure 9.14 The actual distribution of pulsars in luminosity. The top curve is averaged over all values of z-distance and summed over all periods. Shown also are the curves for pulsars with periods around $0^{s}.1$ and for those with periods around $1^{s}.0$. The error bars combine the uncertainties due to statistical fluctuations in the observed distributions and errors due to flux density uncertainties.

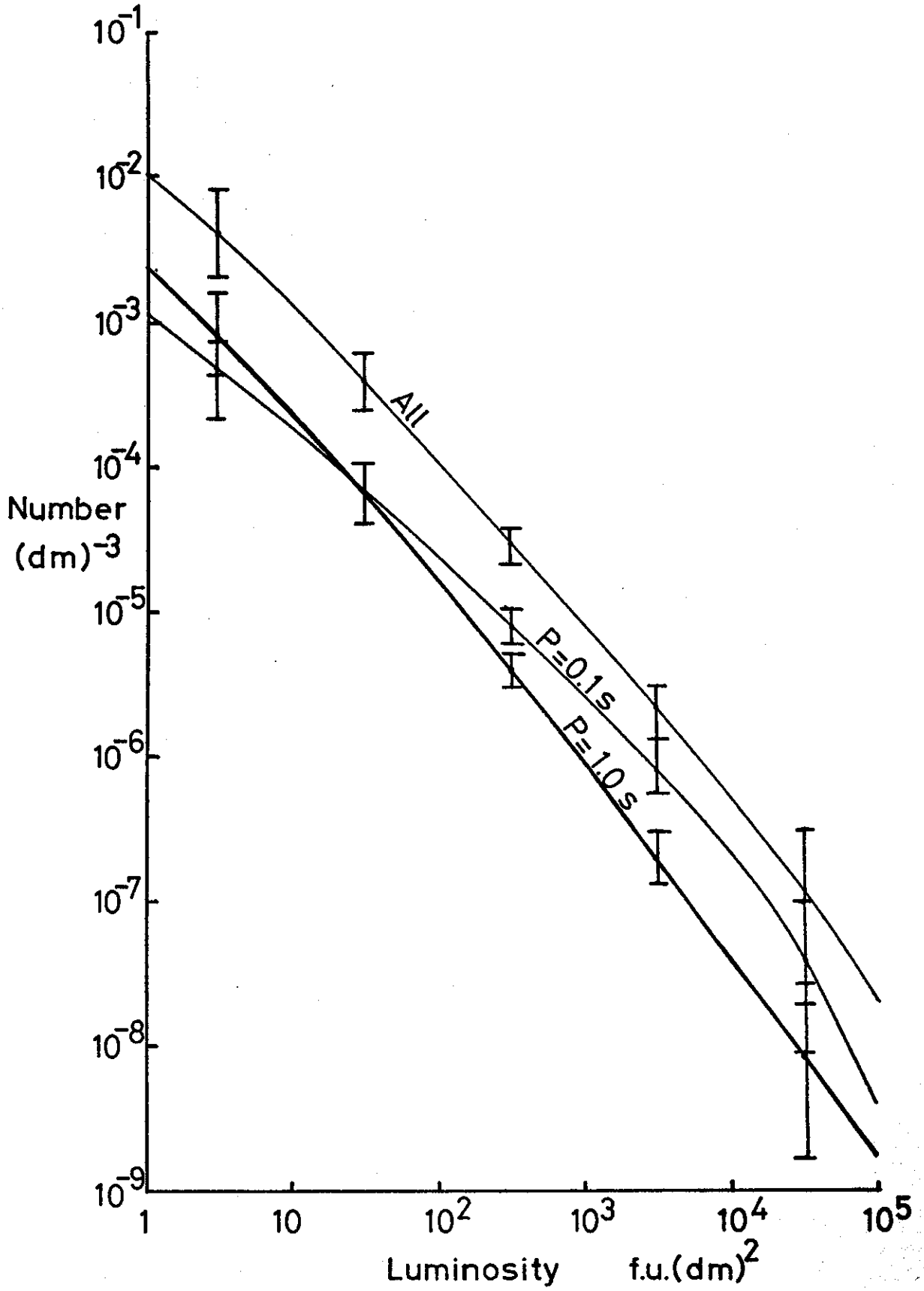
10^{-1}
10^{-2}
10^{-3}
10^{-4}
10^{-5}
10^{-6}
10^{-7}
10^{-8}
10^{-9}
Number
$(dm)^{-3}$
All
P=0.1s
P=1.0s
1
10
10^2
10^3
10^4
10^5
Luminosity f.u.$(dm)^2$

Figure 9.15 The actual distribution of pulsars in period. Both curves have been averaged over all values of z-distance. Shown is the period distribution for low luminosity pulsars, and the normalised curve for high luminosity pulsars. The error bars have the same meaning as those in Figure 9.14.

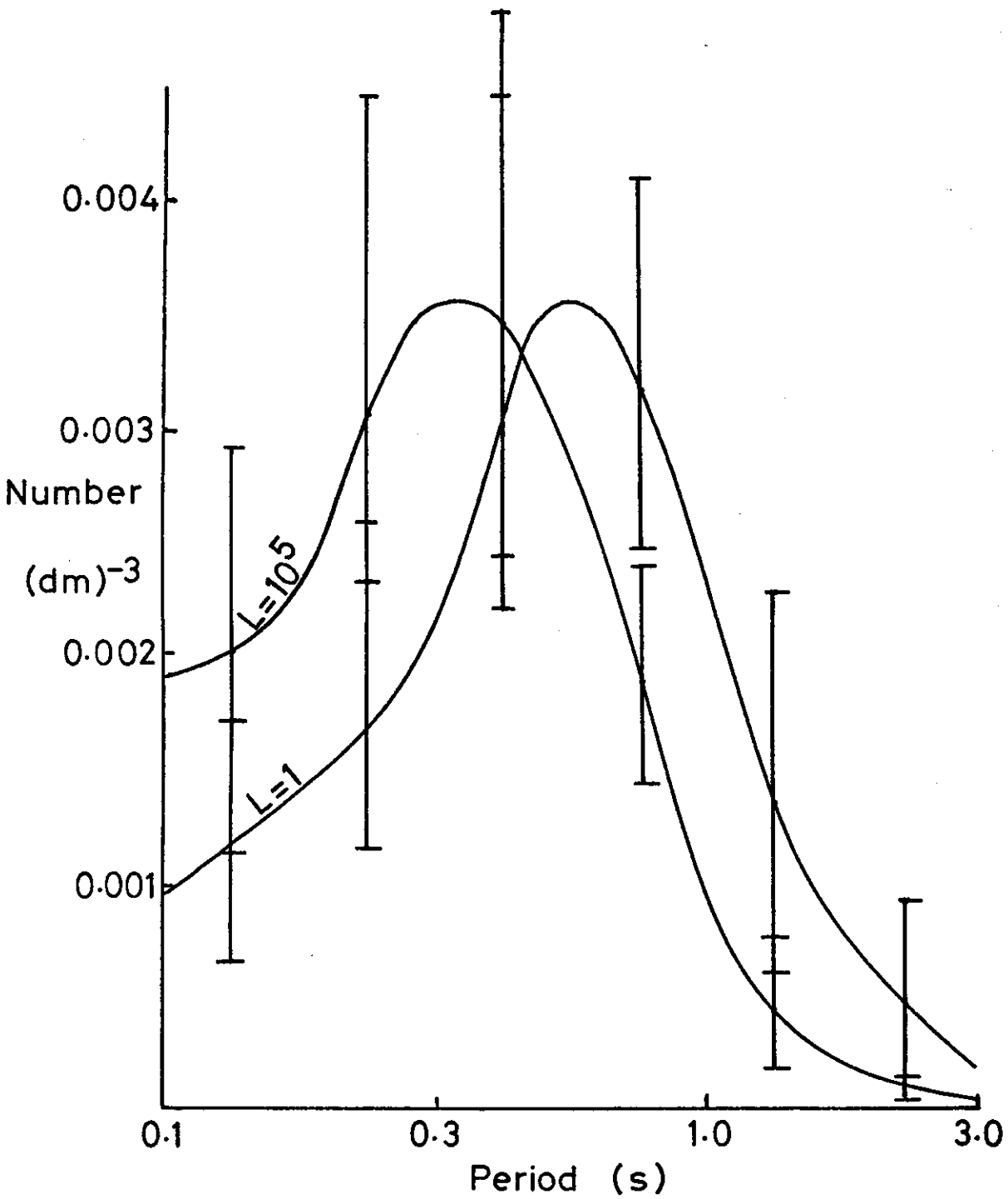
0·004
0·003
Number
(dm)⁻³
0·002
0·001
L=10⁵
L=1
0·1
0·3
1·0
3·0
Period (s)

Figure 9.16 The actual distribution of pulsars in z-distance. The curves have been summed over all values of period. Shown is the z-distance distribution for all pulsars and the curves for pulsars of luminosity L = 1, L = 10^3, L = 10^5 (with arbitrary scaling in the case of the last two). The peak in the curve for all L and for L = 1 is probably spurious as is indicated by the smooth dashed curve through the error bars.

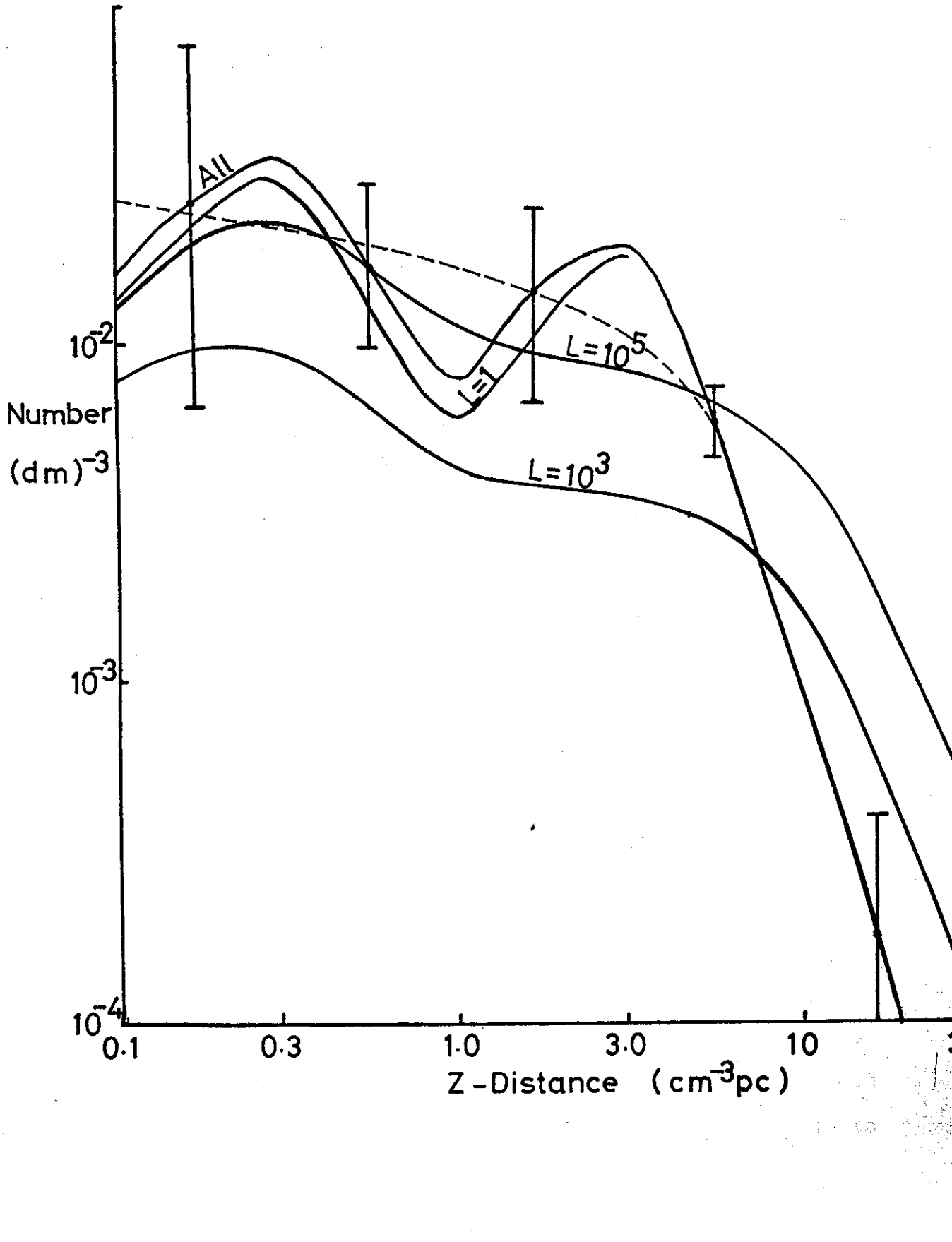
All
L=10^5
L=1
L=10^3
10^-2
10^-3
10^-4
Number
(dm)^-3
0.1
0.3
1.0
3.0
10
Z-Distance (cm^-3pc)

The period distribution shown in Figure 9.15, gives the number of pulsars per $(dm)^3$ in each logarithmic interval of period. The distribution has been summed over all values of luminosity, though because of the luminosity distribution, the shape of the distribution is set by the period distribution for L = 1. For comparison, the normalized period distribution for $L = 10^5$ has been inserted to illustrate again the slight correlation of period with luminosity, though clearly it is not significant.

There are several interesting features of this distribution. Firstly it is apparent that a significant number of short period pulsars may exist, but are being missed by present searches. Secondly, the sharp cut off for periods over about 2 seconds is clearly real, and must be significant in terms of pulsar mechanisms.

The pulsar distribution in z-distance is not very easily interpreted from this analysis. The distribution curve shown in Figure 9.16 for pulsars of all periods and luminosities, shows a peak at z = 3 $cm^{-3}pc$. This is probably spurious since, because of the luminosity distribution, it is due mainly to the z-distance distribution for L = 1, for which the range R (L,P) was only 3 $cm^{-3}pc$. A smooth curve through the error bars is shown as a dashed line in the diagram. The distributions in z for $L = 10^3$ and $L = 10^5$ are also shown (appropriately scaled), and these show no significant peaks. The most noticeable characteristic is that the density of pulsars above z = 10—20 $cm^{-3}pc$ is very small. The actual shape of the distribution cannot be determined unambiguously. The difference between this result and that obtained by Large[5] is probably due to two factors.

Firstly, as a result of improved position measurements, the observed distributions in z-distance are different, and secondly, the use of the logarithms of z-distance has tended to make the shape of the distribution difficult to determine.

9.6 Discussion.

9.6.1 Implications of the Distributions for Further Pulsar Searches.

The z-distance distribution, together with the range function R (L,P) indicates that at the present, pulsars with luminosities equal to 10 fu(dm)^2 or less are not being found much outside a sphere bounded by the edges of the pulsar z-distance distribution. Hence for pulsars weaker than this the increase in the volume searched as search sensitivities are increased, follows a spherical geometry.

ie.

$$\text{Volume searched} = \frac{4\pi}{3} R^3$$

where R is the range.

Now if one defines S_{min} as the minimum observable mean flux density of a pulsar in a given search, then R may be defined as

$$R = \left(\frac{L}{S_{min}}\right)^{\frac{1}{2}},$$

assuming R is independent of pulsar period. Hence the volume searched is approximately

$$\frac{4\pi}{3} \left(\frac{L}{S_{min}}\right)^{\frac{3}{2}}$$

From this the number of pulsars in each interval dL which might be expected to be found will be

$$\propto S_{min}^{-\frac{3}{2}} L^{\frac{3}{2}} L^{-2} \, dL$$

$$\propto S_{min}^{-\frac{3}{2}} L^{-\frac{1}{2}} dL$$

or the number of pulsars in logarithmic intervals will be proportional to

$$S_{min}^{-\frac{3}{2}} L^{\frac{1}{2}} \, d(\log L).$$

On the other hand, for higher values of L, the range will exceed the width of the pulsar z-distribution and the increase in the volume searched, with increasing search sensitivity, will follow a cylindrical geometry

ie. Volume searched = $2a\pi R^2$

where a = 10 $cm^{-3}pc$ is the width of the pulsar distribution. By the same method as before, the number of pulsars in logarithmic intervals will be proportional to $S_{min}^{-1} \, d(\log L)$, changing possibly at higher values of L ($\sim 10^5$) to being proportional to $S_{min}^{-1} L^{-0.5} \, d(\log L)$.

Hence it can be seen that at the present, increases in search sensitivity, S_{min}^{-1}, will favour the discovery of pulsars of low luminosity compared to pulsars of high luminosity. However this increase of the numbers of low luminosity pulsars discovered will only be a slow function of the increase in search sensitivity. For increases in search sensitivity up to a factor of about 20, the shape of the observed luminosity distribution will be essentially unchanged. Figure 3.5 illustrates this well, showing the luminosity distribution for pulsars missed by the Molonglo searches but found by the more sensitive Jodrell Bank search.

This situation might be altered if high sensitivity searches

were carried out at low frequencies, ($\sim$100MHz) since several pulsars have a steep spectrum with a maximum at frequencies somewhat lower than 408MHz. Naturally the effects of dispersion would limit this search to close pulsars, but these are the very pulsars which may have a low luminosity at 408MHz.

It is clear from the range function, and from the period distribution function, that relatively small volumes were searched for short period pulsars. Searches sensitive at periods as short as 10 m sec would alter this situation and determine more precisely the short period end of the distribution in periods. Also more short period pulsars would show whether or not there was a significant correlation between period and luminosity, particularly if the searches were carried out at relatively high frequencies, where dispersion and scintillation broadening are less serious, so that distant pulsars might be found, possibly with high luminosities.

9.6.2 Implications of the Distributions for Theoretical Work on Pulsars.

The narrow z-distance distribution, together with the recent announcement[13] of a high proper motion having been found for a long period pulsar, puts the assumption that the period of a pulsar is some measure of its age, in jeopardy. The linear velocity implied from the proper motion is such that the pulsar would have left the galaxy in a time much less than the so called "age" of the pulsar $P/\dot{P}$. Other pulsars are believed to have high velocities also[Chapter 7], and it may

be a general property of pulsars. The restricted distribution of pulsars above the galactic plane is therefore contradictory to the assumption that $P/\dot{P}$ is even related to the age. It rather suggests that pulsars are much younger than is presently believed, and that they have been created with virtually the period distribution presently observed.

The lack of a clear correlation between period and luminosity may be significant in terms of the coupling between the mechanically rotating star and the radio emission mechanism. Clearly this coupling must be loose, and the radio emission must represent only a small amount of the total energy lost from the pulsar.

While these conclusions based on the distributions can only be stated in general terms, they are fundamentally important, not only for models of pulsars themselves, but also for theories concerning their association with supernovae remnants. Clearly more searches, and combination of results from various searches may lead to more precise statements as to the general nature of pulsars and their relationship to the universe around them.

9.6.3 Conclusion.

This analysis has answered the major criticisms of previous analyses and in particular, dealt with the problem of correlations between the parameters. It is relatively insensitive to statistical distance errors involved in using the dispersion measure for distances, and to statistical errors in the flux densities, and the uncertainties in the final results are such that the luminosity and period distributions can be considered as well defined. From this analysis the

extent of the z distribution of pulsars is also clearly defined, though its shape not determined unambiguously.

While the implications of this work for theoretical studies are of a general nature, they cannot, however, be ignored.

On the question of further observations, the implications for new searches are specific and important and need to be considered in planning future pulsar surveys.

9.7 References.

1. Large, M. I., Vaughan, A. E., and Wielebinski, R., Astrophys. Lett., 3, 123 (1969).

2. Hirth, W., and v. Reinhardt, M., Astrophys. Lett., 3, 169 (1969).

3. Notni, P., Oleak, H., and Schmidt, K. H., Astrophys. Lett., 6, 61 (1970).

4. Ostriker, J. P., and Gunn, J. E., Nature, 223, 813 (1969).

5. Large, M. I., I. A. U. Symposium No. 46. Edited by Davies & Smith (1971).

6. Mills, B. Y., Proc. Astron. Soc. Austral., 5, 176 (1969).

7. Prentice, A. J. R., and ter Haar, D., Nature, 222, 964 (1969).

8. Prentice, A. J. R., and ter Haar, D., Mon. Not. R. astr. Soc., 146, 423 (1969).

9. Prentice, A. J. R., Buckee, J. W., and ter Haar, D., Nature, 228, 452 (1970).

10. Rickett, B. J., Mon. Not. R. astr. Soc., 150, 67 (1970).

11. Lyne, A. G., Paper given at I. A. U. Symposium on the Galaxy, Australia (1973).

12. Mills, B. Y., Nature, 224, 504 (1969).

13. Manchester, R. N., Talk given at Stanford Pulsar Conference (Feb. 1974).

Appendix 9A. The Derivation of Uncorrelated Distributions by Modifying (Rotating) the Coordinate System.

Consider a matrix Q operating on a vector x in a given set of coordinates. $Qx = K$ where K is a vector.

Consider a linear transformation of coordinate systems such that

$$x' = A\,x$$

defines the same vector x in the new coordinate system.

Then

$$K' = A\,K.$$

and

$$Qx = Q\,A^{-1}\,x' = A^{-1}\,K'$$

or

$$(A\,Q\,A^{-1})\,x' = K'$$

Hence the matrix $A\,Q\,A^{-1}$ (similar to Q for nonsingular A) has the same effect in the new coordinate system as Q has in the original system and so represents Q in the new system.

Consider now the variance-covariance matrix of a distribution in the original coordinate system, defined as

$$V = \begin{pmatrix} \sigma_x^2 & \sigma_{xy}^2 & \sigma_{xz}^2 \\ \sigma_{xy}^2 & \sigma_y^2 & \sigma_{yz}^2 \\ \sigma_{zx}^2 & \sigma_{yz}^2 & \sigma_z^2 \end{pmatrix}$$

where $\sigma_x^2 = \sum_i (x_i - \bar{x})^2$ etc.,

and $\sigma_{xy}^2 = \sum_i (x_i - \bar{x})(y_i - \bar{y})$ etc.,

where $\bar{x} = \frac{1}{n}\sum_{i=1}^{n} x_i$

Then in a new coordinate system V is represented by $A\,V\,A^{-1}$ where A is the transformation matrix (ie. for a vector p, $p' = Ap$).

The modified coordinate system is defined by the fact that the correlation coefficients of the distributions in this system are zero. This implies that the variance covariance matrix is diagonal.

ie. $A\ V\ A^{-1} = \lambda$

where $$\lambda = \begin{pmatrix} \lambda_1 & 0 & 0 \\ 0 & \lambda_2 & 0 \\ 0 & 0 & \lambda_3 \end{pmatrix}$$

or, defining $B = A^{-1}$ $(= A^T$ as $A\ A^T = 1)$

$$V\ B = B\lambda$$

Now write $B = (B_1, B_2, B_3)$ where the B_i are column vectors.

Then $V\ B_i = B_i\ \lambda_i$

ie. the B_i are the eigenvectors of V (with eigenvalues λ_i) and the required transformation matrix is

$$A = B^T.$$